NAVAL FACILITIES ENGINEERING SERVICE CENTER
Port Hueneme, California 93043-4370

Technical Report
TR-2082-SHR

NUMERICAL METHODS FOR IMPLEMENTING THE BOUNDING SURFACE PLASTICITY MODEL FOR CLAYS

by

Thomas Joseph Holland, Ph. D.
University of California, Davis

September 1997

19971021 141

REPORT DOCUMENTATION PAGE

Public reporting burden for this collection of information is estimated to average 1 hour per response, including the time for reviewing instructions, searching existing data sources, gathering and maintaining the data needed, and completing and reviewing the collection of information. Send comments regarding this burden estimate or any other aspect of this collection information, including suggestions for reducing this burden, to Washington Headquarters Services, Directorate for Information and Reports, 1215 Jefferson Davis Highway, Suite 1204, Arlington, VA 22202-4302, and to the Office of Management and Budget, Paperwork Reduction Project (0704-0188), Washington, DC 20503.

1. AGENCY USE ONLY (Leave blank)	2. REPORT DATE	3. REPORT TYPE AND DATES COVERED
	September 1997	Final; October 1994 through August 1997

4. TITLE AND SUBTITLE NUMERICAL METHODS FOR IMPLEMENTING THE BOUNDING SURFACE PLASTICITY MODEL FOR CLAYS

5. FUNDING NUMBERS

6. AUTHOR(S)

Thomas Joseph Holland, Ph. D.

7. PERFORMING ORGANIZATION NAME(S) AND ADDRESSE(S)

University of California, Davis
Davis, CA

8. PERFORMING ORGANIZATION REPORT NUMBER

TR-2082-SHR

9. SPONSORING/MONITORING AGENCY NAME(S) AND ADDRESSES

Naval Facilities Engineering Service Center
1100 23rd Avenue
Port Hueneme, CA 93043-4370

10. SPONSORING/MONITORING AGENCY REPORT NUMBER

11. SUPPLEMENTARY NOTES

12a. DISTRIBUTION/AVAILABILITY STATEMENT

Approved for public release; distribution is unlimited.

12b. DISTRIBUTION CODE

13. ABSTRACT *(Maximum 200 words)*

Previous work on the development and numerical implementation of the bound surface plasticity model for clays is discussed. Modifications were made to the hardening relationship to improve the numerical performance in the tensile range. A rate equation for the loading surface was developed. Modifications were made to the invariant description of the bounding surface to avoid numerical difficulties in evaluating the derivatives.

The closest point projection method is described for simple and general internal variable plasticity models. The method was developed within the classical plasticity framework and uses the Newton-Raphson method to satisfy the implicit integration of the rate equations and the consistency condition. An explicit treatment of the internal variables is discussed. Application of this method for the bounding surface plasticity model for clays was developed by adding an internal variable and using the rate equation for the loading surface.

A new algorithm "the reduced Newton method" was developed for the bounding surface plasticity model for clays. It involved mapping the stress rate equations, internal variable rate equations and the consistency condition into two nonlinear equations and integrating them with a backwards Euler formula using Newton-Raphson iteration.

Comparisons of predictions for a number of sample problems was made using the trapezoidal integration, closest point and reduced Newton methods. "Exact" solutions for stress points that start on the bounding surface were developed by assigning an arbitrary stress path and calculating the corresponding strains using numerical integration with a tight tolerance. The "exact" solutions were used to evaluate the effectiveness of the proposed general numerical implementation of the bounding surface method.

A standard effective stress interface is proposed for finite element programs that use the Newton-Raphson method. The reduced Newton model is implemented within the DYSAC2 finite element program and is used to analyze an earth embankment subjected to earthquake and shock loads.

14. SUBJECT TERMS

Computational plasticity, soil plasticity, bounding surface plasticity model, finite element, DYSAC2 finite element program, Newton-Raphson method, earthquake and shock loads

15. NUMBER OF PAGES
196

16. PRICE CODE

17. SECURITY CLASSIFICATION OF REPORT	18. SECURITY CLASSIFICATION OF THIS PAGE	19. SECURITY CLASSIFICATION OF ABSTRACT	20. LIMITATION OF ABSTRACT
Unclassified	Unclassified	Unclassified	UL

EXECUTIVE SUMMARY

Previous work on the development and numerical implementation of the Bounding Surface Plasticity model for clays is discussed. Modifications are made to the hardening relationship to improve the numerical performance in the tensile range. A rate equation for the loading surface is developed. Modifications are made to the invariant description of the bounding surface to avoid numerical difficulties in evaluating the derivatives.

The Closest Point Projection method is described for simple and general internal variable plasticity models. The method is developed within the classical plasticity framework and uses the Newton-Raphson method to satisfy the implicit integration of the rate equations and the consistency condition. An explicit treatment of the internal variables is discussed. Application of this method for the Bounding Surface Plasticity model for clays is developed by adding an internal variable and using the rate equation for the loading surface.

A new algorithm coined "the Reduced Newton method" is developed for the Bounding Surface Plasticity model for clays. It involves mapping the stress rate equations, internal variable rate equations and the consistency condition into two nonlinear equations and integrating them with a backwards Euler formula using Newton-Raphson iteration.

Comparison of predictions for a number of sample problems is made using the trapezoidal integration, Closest Point and Reduced Newton methods. "Exact" solutions for stress points that start on the bounding surface are developed by assigning an arbitrary stress path and calculating the corresponding strains using numerical integration with a tight tolerance. These "exact" solutions are used to evaluate the effectiveness of the proposed general numerical implementation of the Bounding Surface model.

A standard effective stress interface is proposed for finite element programs that use the Newton-Raphson method. The Reduced Newton model is implemented within the

DYSAC2 finite element program and is used to analyze an earth embankment subjected to earthquake and shock loads.

TABLE OF CONTENTS

0. Numerical Methods for Implementing the Bounding Surface Plasticity Model for Clays

In most structural or geotechnical engineering studies, the behavior of the object being designed is the focus. The object is loaded externally with known and unknown forces (e.g., deadweight, wind, soil, vehicles, support reactions, etc.) and the observed behavior is in displacements (e.g., deformation under load) and, to some degree, appearance (e.g., concrete turning to rubble). To analyze this behavior mathematically, the following sets of equations must be satisfied:

    1) the equations of equilibrium (equations of motion for dynamic problems),

    2) the equations of compatibility (kinematics), and

    3) the constitutive equations.

For quasistatic problems the equilibrium equations relate the forces (internal and external) to the stresses. The compatibility equations provide the kinematic relationship between the displacements and the strains. The constitutive equations are dependent on the type of material and relate the stresses to the strains. The relationships among these equations are shown in Figure 0.0-1.

The focus of this study is on the constitutive equations and their numerical implementation using the Finite Element Method (FEM). It is assumed that the finite element program is nonlinear, implicit and has already addressed the equilibrium and compatibility equations. The FEM is generally a displacement-based formulation which implies that the constitutive equations are given strains and expected to return stresses and the tangent moduli to the global solution iteration procedure.

The constitutive equations are developed to model the behavior of the material with a given set of measurable parameters obtained from laboratory tests. To develop these constitutive equations the following issues must be addressed:

1) development of the constitutive model to match the material behavior under consideration, and

2) implementation of the model within an appropriate solution algorithm (usually numerical).

In the evolution of the constitutive model, a great deal of effort is spent comparing experimental data with numerical results to validate and develop confidence in the model. Important physical and geometric parameters such as void ratio for soils are incorporated into the model. These physical parameters allow the model to have general application to a family of material types (e.g., clays and silts). The constitutive model used in this study is the Bounding Surface Plasticity model for clays.

The Bounding Surface Plasticity concept was developed at the University of California at Berkeley in the mid 1970's and it promised to be computationally efficient. The concept provided for a gradual transition from elastic to plastic material behavior and was originally developed for metals. It became especially useful for materials that have no distinct yield points (e.g., soils, concrete, etc.). Bounding Surface Plasticity was applied to clay soils at the University of California at Davis during the mid 1980's and was validated using traditional laboratory and geotechnical centrifuge soils tests.

The subject for this study is the numerical implementation of the single ellipse, Bounding Surface model for geotechnical analysis of clay soils. The implementation

addresses two issues:

1) efficiency, and

2) accuracy.

The importance of efficiency lies in the structure of the solution algorithm of a typical nonlinear, implicit finite element program as illustrated by the nested loops shown in Figure 0.0-2. Evaluation of the constitutive equations occurs within the innermost loop. Thus, efficiency of the constitutive model evaluation significantly impacts the performance of the global analysis of a geotechnical structure.

Accurate tangent moduli can enhance the performance of the global solution algorithm by helping to provide an optimal direction (when multiplied by the residual vector) for the iteration which will improve the global convergence. Also, implied with the issue of accuracy is robustness. Even for calculations that involve small solution time steps in the outer loop, the global iteration method can sometimes generate large trial strains during the iteration process even though the eventual incremental strains may be small. These large strains are provided as input to the constitutive model and reasonable stresses and tangent moduli are expected to be returned from the material properties algorithm. A constitutive model and its numerical implementation that cannot provide reasonable values for large strain increments may be useless even for calculations that involve small time steps.

One approach for dealing with the accuracy/robustness issue is the use of a uniform substepping method at the material model level. Given a set of incremental strains from the global iteration, the predicted stresses and tangent moduli can be compared using different numbers of substeps across the increment. If the stresses from one substep level are within a given tolerance of the previous level (e.g., one step versus two substeps) then the finer

solution is accepted. In the global analysis, this assures that the stresses and tangent moduli of neighboring elements are obtained within the same degree of accuracy in stress space. The uniform substepping approach also has the added advantage of seeking the correct answer when Newton-Raphson-based methods, which cannot distinguish the correct solution from extraneous solutions of a nonlinear problem.

The original numerical implementation of the Bounding Surface model uses trapezoidal integration, which is second order accurate and relatively stable. It requires information at the beginning and at the end of the step and thus needs to iterate. The implementation also includes substepping to enhance accuracy and robustness. Difficulties arise in certain analyses where the consistency condition is not exactly satisfied at the end of the increment, that is, where the computed stress point falls outside the bounding surface in stress space. This study looks at alternative numerical implementations that would prevent this behavior and promote greater efficiency and accuracy.

0.1 Report Layout

Section 1 briefly describes the theoretical aspects of the single ellipse Bounding Surface model for clays. It also describes theoretical and numerical modifications that were made to improve the original model and develops relationships that are used in its numerical implementation.

Section 2 describes the Closest Point Projection algorithm and its application to the implementation of the Bounding Surface model. The Closest Point method is a general three dimensional methodology for implementing constitutive models and was originally developed in nonlinear optimization theory.

The Reduced Newton algorithm is described in Section 3. It is a specific Newton-Raphson-based method applied to the Bounding Surface model and reduces the number of differential equations to be solved at the innermost iteration level.

Section 4 compares both the Closest Point and Reduced Newton methods as well as the original trapezoidal implementation to numerically "exact" solutions of the constitutive equations. Exact solutions include stress paths that both start on and within the bounding surface and highlights the behavior of the solution methods.

Section 5 describes the implementation of the Reduced Newton model into the DYSAC2 finite element computer program. Implementation issues are discussed. The resulting code is then applied to the solution of a realistic geotechnical engineering problem.

Conclusions and recommendations are given in Section 6.
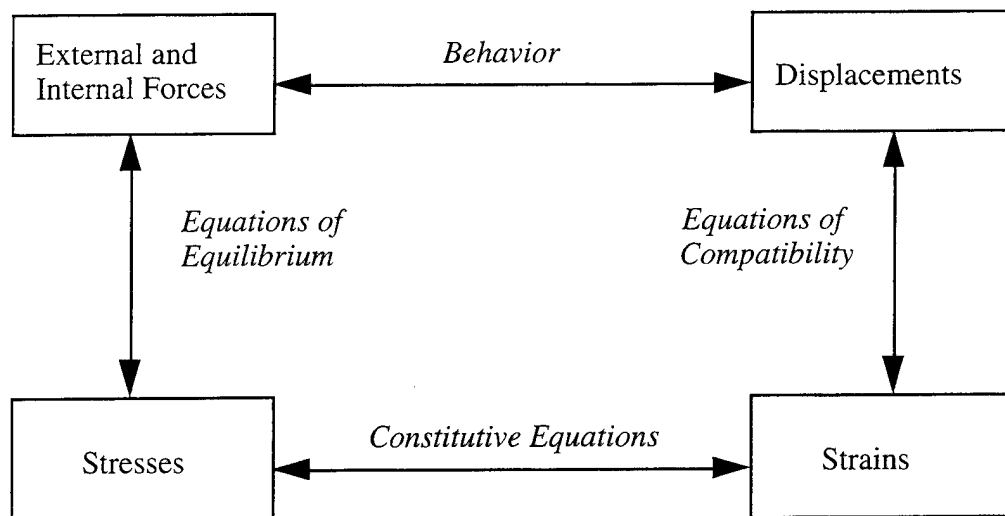
Figure 0.0-1. Relationship of Engineering Mechanics Equations.
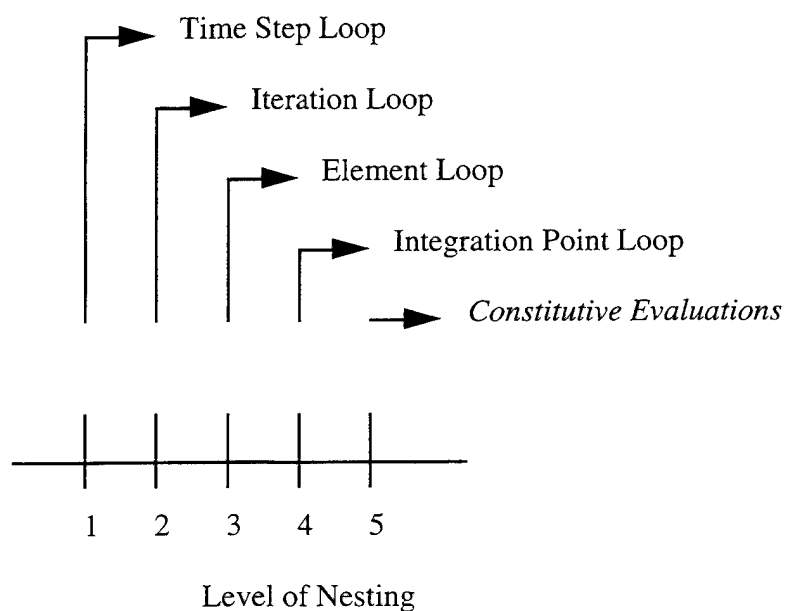
Figure 0.0-2. Nesting Levels of a Typical Implicit Finite Element Program.

1. Bounding Surface Plasticity Model for Clays

The Bounding Surface plasticity concept was first introduced for modeling metals at the University of California at Berkeley (UCB) in the mid 1970's [Dafalias and Popov, 1975]. The concept was applied to clays at the University of California at Davis (UCD) in the early 1980's [Dafalias and Herrmann, 1980a; Dafalias et. al. 1980b; Dafalias et. al., 1980c; Dafalias 1980d; Dafalias and Herrmann, 1980e; Dafalias et. al., 1981; Herrmann, et. al., 1982; DeNatale, et. al. 1983; Herrmann, et. al. 1983a; Herrmann and Mish, 1983b; Herrmann, et. al. 1983c; Herrmann and Mish, 1983d; Herrmann and Mish, 1983e; Herrmann, et. al., 1985; Kaliakin, 1985; Shen, et. al., 1986; Dafalias and Herrmann, 1986; Herrmann, et. al., 1987]. A single ellipse model with an associated plastic flow was developed for clays in the mid 1980's [Kaliakin, 1985; Herrmann, et. al.; 1985; Herrmann, et. al., 1987]. The model was validated using traditional soils tests and centrifuge tests conducted at UCD [Herrmann, et. al., 1982; Herrmann, et. al., 1987]

The following sections describe the Bounding Surface model and the plasticity framework in which it resides. Section 1.1 briefly lays out the classical plasticity framework for associative flow. Section 1.2 discusses the Bounding Surface Plasticity concept. Section 1.3 describes the nonlinear elastic volumetric relationship, Section 1.4 presents the single ellipse Bounding Surface, Section 1.5 details the hardening function and Section 1.6 describes the plastic modulus. This work was developed at UCD for clays [Kaliakin, 1985] and is provided for reference. A small modification is made in the hardening function to avoid numerical difficulties in Section 1.5. A new relationship for the loading surface is given in Section 1.7 that lays out the Bounding Surface model in a more conventional classical plasticity framework. Finally, a modification to improve the invariant form description of the model [Kaliakin, 1985] is described in Section 1.8.

1.1 Classical Plasticity Framework for Associative Plasticity

Before introducing the Bounding Surface Plasticity model, the classical plasticity framework using the associative flow rule [Dafalias, 1990] is presented in this section. Classical plasticity assumes that the material has a region of elastic behavior within which loading followed by unloading returns to the original state. During loading, however, if the stress reaches a defined stress state, known as the yield surface, the material begins to yield or permanently deform. This yield surface in one dimension consists of two points and is shown on a simple stress-strain diagram in Figure 1.1-1. Unloading after yielding does not return to the initial state, but leaves a permanent deformation and possibly residual stresses. The process of yielding can also redefine the size, shape and/or location of the yield surface, as shown in Figure 1.1-1. In this case, the change in the surface is a result of the yielding and is a function of the stress and/or strain history. The history of the change in the surface at a particular material point is described by the values of one or more internal variables. The yield surface can also be described by a number of external variables that are functions of temperature, humidity, age and other conditions. The mathematical framework for this classical plasticity model will be described below.

The yield function for a classical plasticity model is shown as a one-dimensional surface in Figure 1.1-1. For more complex analyses (two- and three-dimensional) the yield function is described in stress space as a multi-dimensional surface (see Figure 1.1-2). The internal variables not only describe how the surface grows, but how it translates, changes shape and/or orientation. The yield surface is a function of both the stresses and the

internal variables, and is given as:

$$f(\sigma, q) = 0 \qquad (1.1\text{-}1)$$

where f = yield function

σ = vector of stresses, $\left[\sigma_x, \sigma_y, \sigma_z, \tau_{xy}, \cdots\right]^T$

q = vector of internal variables, $\left[q_1, q_2, \cdots\right]^T$.

Definition of the yield surface places some restrictions on the stresses. Stress states can lie within the surface (elastic region) or on the surface itself (plastic or, if unloading, elastic). They cannot, however, exist outside of the surface. This can be easily seen from Figure 1.1-1.

The strains are assumed to decompose into elastic and plastic portions. This kinematic assumption describing the additive nature of the elastic and plastic strain rates is given as:

$$\dot{\varepsilon} = \dot{\varepsilon}^e + \dot{\varepsilon}^p \qquad (1.1\text{-}2)$$

where $\dot{\varepsilon}$ = vector of total strain rates, $\left[\dot{\varepsilon}_x, \dot{\varepsilon}_y, \dot{\varepsilon}_z, \dot{\gamma}_{xy}, \ldots\right]^T$

$\dot{\varepsilon}^e$ = vector of elastic strain rates

$\dot{\varepsilon}^p$ = vector of plastic strain rates.

The strains are described in terms of rate equations (i.e., they evolve over time) because time incorporates the history of the plasticity. Time can also allow for a viscous behavior although this is not included in this study. The stress rate is a function of the

elastic strain rates only and is given as:

$$\dot{\sigma} = C \, \dot{\varepsilon}^e = C(\dot{\varepsilon} - \dot{\varepsilon}^p) \qquad\qquad (1.1\text{-}3)$$

where $\dot{\sigma}$ = vector of stress rates

C = elastic constitutive matrix, $\begin{bmatrix} C_{xx} & C_{xy} & \\ C_{yx} & C_{yy} & \cdots \\ \vdots & & \ddots \end{bmatrix}$.

Equation 1.1-3 describes how the stress rates are proportional to the elastic strain rates. As in the one dimensional case, elastic loading and then unloading will return to the same state. When the stresses reach the yield state (Equation 1.1-1), plastic flow commences (i.e., plastic straining begins). Plastic flow is described by the increase in the plastic strains and is given by the following rate equation:

$$\dot{\varepsilon}^p = \gamma \, N(\sigma, q) \qquad\qquad (1.1\text{-}4)$$

where γ = plasticity parameter; $\gamma > 0$, for plastic flow ($f = 0$), and

$\gamma = 0$, for elastic loading or unloading ($f \leq 0$)

$N(\sigma, q)$ = a function describing the plastic strain directions.

The associative flow rule assumes that the direction of plastic flow is perpendicular to the yield surface which is described in stress space (Equation 1.1-1). The rate equations for the plastic strains are therefore a function of the yield surface and are given as:

$$\dot{\varepsilon}^p = \gamma \, \frac{\partial f}{\partial \sigma} \qquad\qquad (1.1\text{-}5)$$

where $\dfrac{\partial f}{\partial \sigma}$ = vector of yield function derivatives $\left(\text{i.e.,} \left[\dfrac{\partial f}{\partial \sigma_x}, \dfrac{\partial f}{\partial \sigma_y}, \cdots \right]^T \right)$.

The change in the internal variables can be described in terms of rate equations which are given as:

$$\dot{q} = \gamma \, h(\sigma, q) \qquad (1.1\text{-}6)$$

where $h(\sigma, q) =$ direction of internal variable rates.

Because of the restriction that the stress state cannot exist outside the yield surface (Equation 1.1-1), during plastic flow the stress point must remain on the surface. This is described mathematically as the consistency condition and is given as:

$$\dot{f} = 0 \qquad (1.1\text{-}7)$$

Applying the consistency condition to the yield state (Equation 1.1-1) and applying the chain rule results in:

$$\frac{\partial f}{\partial \sigma} \, \dot{\sigma} + \frac{\partial f}{\partial q} \, \dot{q} = 0 \qquad (1.1\text{-}8)$$

Substituting in Equation 1.1-6 into Equation 1.1-8 results in and expression for the plasticity parameter in terms of the stress rates and is given as:

$$\gamma = \frac{1}{K_p} \left(\frac{\partial f}{\partial \sigma} \, \dot{\sigma} \right) \qquad (1.1\text{-}9)$$

where $K_p = $ plastic modulus $= -\left(\dfrac{\partial f}{\partial q} \right) h.$

The plasticity parameter can be expressed in terms of the strains by substituting Equations 1.1-3 and 1.1-5 into Equation 1.1-9. This is given as:

$$\gamma = \frac{\left(\dfrac{\partial f}{\partial \sigma} \right) C \, \dot{\varepsilon}}{K_p + \left(\dfrac{\partial f}{\partial \sigma} \right) C \left(\dfrac{\partial f}{\partial \sigma} \right)} \qquad (1.1\text{-}10)$$

Combining Equations 1.1-3, 1.1-5 and 1.1-10 results in the expression for the plastic constitutive matrix. This is given as:

$$\dot{\sigma} = \left[C + H(\gamma) \frac{C\left(\dfrac{\partial f}{\partial \sigma}\right)\left(\dfrac{\partial f}{\partial \sigma}\right)C}{K_p + \left(\dfrac{\partial f}{\partial \sigma}\right)C\left(\dfrac{\partial f}{\partial \sigma}\right)} \right] \dot{\varepsilon} \qquad (1.1\text{-}11)$$

where $H(\gamma)$ = Heavyside function; $H(\gamma) = 0$, $\gamma \leq 0$ and $H(\gamma) = 1$, $\gamma > 0$.

In classical plasticity, a plastic step occurs (for a stress point starting on the yield surface) when a strain increment produces an elastic stress state outside of the yield surface. This is mathematically given by a positive plasticity parameter (Equation 1.1-10). The plastic step requires integration of Equation 1.1-11 (note that the rate equations for the plastic strains and internal variables were used in the derivation of this equation). Numerical integration techniques, such as the backward and forward Euler and the trapezoidal methods, provide approximations for these integrations. The consistency condition (i.e., enforcing the stress point to remain on the surface) is satisfied indirectly through the plasticity parameter and an accurate integration. Since the integration is an approximation, the resulting integration error often fails to satisfy the consistency condition exactly.

1.2 Bounding Surface Plasticity Concept

The Bounding Surface Plasticity concept was introduced at the University of California, Berkeley in the 1970's [Dafalias and Popov, 1975]. The motivation for the concept was the observation that for most materials any stress-strain curve (including reversals) eventually converged to well defined "bounds" in stress-strain space. These bounds cannot be crossed but can change position during loading. An additional observation was that the rate of convergence of the stress-strain curve to the bound appeared to be a function of the distance of the current state from the bound. This concept

can be described with a typical uniaxial stress-plastic strain response shown in Figure 1.2-1. As the stress approaches the bound, its rate of convergence or its uniaxial plastic modulus (E^p) decreases until it becomes tangent with the bound. The modulus is therefore a function of the distance between the current stress state (σ) and the "image" stress ($\bar{\sigma}$) on the bound.

The bounding surface in multiaxial stress space is described in a similar manner to a yield surface in "classical" plasticity (i.e., stress points can exist on and within, but not outside the bounding surface). The unique feature of the bounding surface concept is that there is a gradual transition from elasticity to plasticity (i.e., plasticity can occur within the surface), unlike traditional yield surface models where plasticity occurs only when the stress point is on the surface. To accomplish this, the theory incorporates particular features that allow it to operate within the classical incremental plasticity framework. These features will be discussed in the following paragraphs.

Bounding Surface Plasticity was developed at UCB [Dafalias and Popov, 1975] as a means for introducing a gradual transition from elasticity to plasticity. The bounding surface is defined in stress space and is given as:

$$F(\bar{\sigma}, q) = 0 \qquad (1.2\text{-}1)$$

where F = bounding surface function

$\bar{\sigma}$ = vector of "image" stresses.

The bounding surface can also have an elastic nucleus defined within it. The current stress point defines another surface known as the loading surface. These surfaces are shown in Figure 1.2-2.

For "classical" associative plasticity, the plastic strain rates are a function of the plasticity parameter and are perpendicular to the yield surface at the stress point (Equation 1.1-5). For stress points within the bounding surface this information is defined by

drawing a line from a projection center (α) through the current stress point and projecting this to a point on the bounding surface (see Figure 1.2-2). This is known as the mapping rule. The normal for the plastic strain rate is taken at this "image" stress point on the bounding surface. The strain rate is defined as:

$$\dot{\varepsilon}^p = \gamma \frac{\partial F}{\partial \overline{\sigma}} \tag{1.2-2}$$

The mapping rule defines how the current stress is related to the "image" stress. It is defined as:

$$\overline{\sigma} = b(\sigma - \alpha) + \alpha \tag{1.2-3}$$

where b = measure of distance between stress point and surface

α = projection center.

Note that b ranges from 1 (when the current and "image" stress point coincide) to ∞ (at the projection center). This parameter also implicitly defines the location of the loading surface. The evolution of the loading surface is discussed in Section 1.7.

The plasticity parameter is defined by applying the consistency condition to the image stress points on the surface. For points within the bounding surface an equivalent relationship is defined [Kaliakin, 1985] and is given as:

$$\gamma = \frac{1}{\overline{K}_p}\left(\frac{\partial F}{\partial \overline{\sigma}} \dot{\overline{\sigma}}\right) = \frac{1}{K_p}\left(\frac{\partial F}{\partial \overline{\sigma}} \dot{\sigma}\right) \tag{1.2-4}$$

where $\overline{K}_p = -\frac{\partial F}{\partial q} h$ = plastic modulus at the image stress point

$\dot{\overline{\sigma}}$ = image stress rate

K_p = plastic modulus at the current stress point

$\dot{\sigma}$ = current stress rate.

Equation 1.2-2 is the crux of Bounding Surface Plasticity. It describes how the plasticity (via the hardening modulus) occurs within the bound. The plastic modulus at the image stress point $\left(\overline{K}_p\right)$ is defined via the consistency condition, as in classical plasticity, with Equation 1.1-9. The plastic modulus at the current stress point (K_p), within the bounding surface, is a function of $\overline{K}_p$ (i.e., $K_p = \overline{K}_p$ for stress points on the bound) and the distance to the bounding surface (b). This is defined in more detail in Section 1.6.

The following sections describe various aspects and modifications made to the Bounding Surface Plasticity concept for clays [Kaliakin, 1985; Herrmann, et. al., 1985].

1.3 Development of Nonlinear Elastic Volumetric Relationship

The relationship of the elastic change in the void ratio (e) and the volumetric stress (I) for unloading-reloading (URL) is modeled as a straight line in log-linear space [Kaliakin, 1985]. This is shown as the κ line in Figure 1.3-1. Because of problems associated with I near zero in log space, a limiting value of the volumetric stress (I_l) is given where the relationship is changed from log to linear. This is given as:

$$\frac{dI}{de^e} = -\frac{\langle I - I_l \rangle + I_l}{\kappa} \qquad (1.3-1)$$

where I = volumetric stress $(\sigma_1 + \sigma_2 + \sigma_3)$ (i.e., the first stress invariant)

de^e = elastic change in the void ratio

I_l = limiting value of I

κ = slope of unloading - reloading line.

The Macaulay brackets $\left(\langle\ \rangle\right)$ imply that $\langle n \rangle = n$ if $n > 0$ and $\langle n \rangle = 0$ if $n < 0$.

This defines two separate mathematical regions:

    1) the region of log-linear relationship between the void ratio and the volumetric stress $(I > I_l)$, and

    2) the region of a linear-linear relationship $(I < I_l)$.

For this section, equations where $I > I_l$ are denoted as the "a" equations and $I < I_l$ are denoted as the "b" equations. The elastic void ratio differentials for the respective regions are defined as:

$$de^e = -\frac{\kappa}{I}dI \qquad\qquad (I > I_l) \qquad (1.3\text{-}2a)$$

$$de^e = -\frac{\kappa}{I_l}dI \qquad\qquad (I < I_l) \qquad (1.3\text{-}2b)$$

The definition of specific volume (v) is defined as:

$$v = 1 + e \qquad\qquad (1.3\text{-}3)$$

Differentiating Equation 1.3-3 results in:

$$dv = de \qquad\qquad (1.3\text{-}4)$$

Equations 1.3-2 now can be written as the elastic increment in specific volume:

$$dv^e = -\frac{\kappa}{I}dI \qquad\qquad (1.3\text{-}5a)$$

$$dv^e = -\frac{\kappa}{I_l}dI \qquad\qquad (1.3\text{-}5b)$$

    where dv^e = elastic change in specific volume.

The increment in volumetric strain can be expressed in terms of the specific volume for small strains as:

$$d\theta^e = -\frac{dv^e}{v_0}$$

(1.3-6)

where $d\theta^e$ = elastic change in volumetric strain

v_o = initial specific volume.

Substituting the increments of specific volume (Equations 1.3-5) into Equation 1.3-6, the elastic increment of volumetric strain is given in terms of the volumetric stress increment:

$$d\theta^e = \frac{\kappa}{v_0 I} \, dI$$

(1.3-7a)

$$d\theta^e = \frac{\kappa}{v_0 I_l} \, dI$$

(1.3-7b)

These relationships can be integrated from times t_n to t_{n+1} to give the volumetric stress (I) in terms of the elastic volumetric strain (θ^e):

$$I_{n+1} = I_n \, e^{\beta\left(\theta^e_{n+1} - \theta^e_n\right)}$$

(1.3-8a)

$$I_{n+1} = \beta \, I_l\left(\theta^e_{n+1} - \theta^e_n\right) + I_n$$

(1.3-8b)

where $\beta = \dfrac{v_0}{\kappa}$

1.4 Single Ellipse Bounding Function for Clays

The Bounding Surface plasticity concept was developed for clays at the University of California at Davis (UCD) in the early 1980's [Dafalias and Herrmann, 1980a; Dafalias

et. al. 1980b; Dafalias et. al., 1980c; Dafalias 1980d; Dafalias and Herrmann, 1980e; Dafalias et. al., 1981; Herrmann, et. al., 1982; DeNatale, et. al. 1983; Herrmann, et. al. 1983a; Herrmann and Mish, 1983b; Herrmann, et. al. 1983c; Herrmann and Mish, 1983d; Herrmann and Mish, 1983e; Herrmann, et. al., 1985; Kaliakin, 1985; Shen, et. al., 1986; Dafalias and Herrmann, 1986; Herrmann, et. al., 1987]. A single ellipse model with associated plastic flow (Section 1.6) was developed for clays in the mid 1980's [Kaliakin, 1985; Herrmann, et. al., 1985; Herrmann, et. al., 1987]. The model was validated using traditional soils tests and centrifuge tests conducted at UCD.

The single ellipse bounding surface function is expressed in terms of stress invariants and is given as:

$$F = \bar{I}^2 + (R-1)^2 \left(\frac{\bar{J}}{N}\right)^2 - \frac{2}{R}I_o\bar{I} + \frac{2-R}{R}I_o^2 \tag{1.4-1}$$

where F = bounding function

$\bar{I} = b(I - I_c) + I_c$

I = first stress invariant ($\sigma_{11} + \sigma_{22} + \sigma_{33}$)

$I_c = CI_o$

C = material constant defining the projection center location

I_o = bound size (i.e., intersection of bound with volumetric axis)

$\bar{J} = bJ$

J = second stress invariant = $\sqrt{\frac{1}{2} s_{ij} s_{ij}}$

$$N = \frac{2N_e}{1 + N_{ec} - (1 - N_{ec})\sin(3\alpha)}$$

$$\alpha = \text{lode angle} = \tfrac{1}{3}\sin^{-1}\left[\frac{3\sqrt{3}}{2}\left(\frac{S}{J}\right)^{3}\right]$$

$$S = \text{third stress invariant} = \sqrt[3]{\tfrac{1}{3}s_{ij}s_{jk}s_{ki}}$$

$$N_{cc} = \frac{N_e}{N_c}$$

N_e = slope of critical state line in extension (*I-J* space)

N_c = slope of critical state line in compression (*I-J* space)

R = a parameter defining the shape of the ellipsoid.

The bounding surface for clays is shown in Figure 1.4-1

1.5 Development of the Bounding Surface Hardening Relationship

The form of the relationship for the normal consolidation line [Kaliakin, 1985] is similar to the elastic relationship (Equation 1.3-1) and is given as:

$$\frac{dI_0}{de} = -\frac{\langle I_0 - I_l \rangle + I_l}{\lambda} \tag{1.5-1}$$

where I_o = bounding surface size

e = void ratio

λ = slope of normal consolidation line.

This is shown in Figure 1.3-1 as the λ line. The change in the void ratio can be decomposed into an elastic and plastic portion:

$$de = de^e + de^p \tag{1.5-2}$$

where de^p = plastic change in void ratio.

Combining Equation 1.5-1 with Equation 1.3-1 (note that Equation 1.3-1 is valid for $I = I_o$) results in a relationship between the bounding surface size and the plastic void ratio and is:

$$\frac{dI_0}{de^p} = -\frac{\langle I_0 - I_l \rangle + I_l}{\lambda - \kappa}$$

(1.5-3)

In previous work [Kaliakin, 1985] the plastic void ratio is used as the internal variable. The relationship describing its evolution is based upon an associative flow rule [Kaliakin, 1985] and is given as:

$$de^p = -3v_0 \gamma \frac{\partial F}{\partial \bar{I}}$$

(1.5-4)

where v_o = initial specific volume = $(1 + e_o)$

$\bar{I}$ = volumetric image stress.

Equation 1.2-1 can be rewritten in terms of volumetric stress and strain as:

$$d\theta^p = \gamma \frac{\partial F}{\partial \bar{I}}$$

(1.5-5)

Combining Equations 1.5-3, 1.5-4 and 1.5-5 results in an expression relating the plastic volumetric strains to the bounding surface size. This is given in differential form as:

$$dI_0 = 3v_0 \frac{\langle I_0 - I_l \rangle + I_l}{\lambda - \kappa} d\theta^p$$

(1.5-6)

Once again, the Macaulay brackets indicate two possible integrations, where $I > I_l$ and $I < I_l$. However, when finding exact solutions (i.e., given a change in I_0 and calculating the plastic volumetric strains, see Appendix C), it was noted that when $I_0 < I_l$ the magnitude of the tensile volumetric strains could not exceed a given value. This is a result of the mathematics and not an observed phenomena. Therefore, for this study the Macaulay brackets are eliminated in Equation 1.5-6 (this is consistent with the Closest

Point Projection application to the Cam-Clay model [Simo and Meschke, 1993]). (While this step may seem arbitrary or approximate, it must be remembered that the introduction of I_l was itself quite arbitrary). The differential of the bounding surface is now defined as:

$$dI_0 = 3I_0\xi \, d\theta^p \tag{1.5-7}$$

where $\quad \xi = \dfrac{v_0}{\lambda - \kappa}.$

Integrating Equation 1.5-7 between times t_n and t_{n+1} results in an expression for the bound size in terms of the plastic volumetric strain:

$$I_{0_{n+1}} = I_{0_n} e^{\xi\left(\theta^p_{n+1} - \theta^p_n\right)} \tag{1.5-8}$$

1.6 Plastic Modulus for Single Ellipse Bounding Function

In classical plasticity the plastic modulus is determined for a stress point on the yield surface via the consistency condition (Equation 1.2-3). This is facilitated by the fact that the stress point is on the surface and the yield function derivatives can be defined directly by enforcing the consistency condition. In Bounding Surface plasticity the plastic modulus must be defined within the bounding surface and can not be directly obtained. The behavior of the modulus can be described by considering a line from the projection center to the bounding surface. The modulus is a function of the distance from the bound. It becomes infinite at the elastic nucleus (and within) and approaches the classical plastic modulus definition at the bounding surface. The general expression for the plastic modulus $\left(\overline{K}_p\right)$ on the bound, at the "image" stress point, is given by Equation 1.2-4 and can be expressed in terms of the internal variable I_0 as:

$$\overline{K}_p = -\frac{\partial F}{\partial I_0} h \tag{1.6-1}$$

The variable h is defined by the rate equation of the internal variable, (see Equation 1.1-6). Substitute Equation 1.5-5 into 1.5-7 and noting the form of the rate equation for the internal variable (Equation 1.1-6), h is given as:

$$h = -3 \, I_0 \xi \, \frac{\partial F}{\partial \bar{I}} \qquad (1.6\text{-}2)$$

Combining Equations 1.6-1 and 1.6-2, the plastic modulus at the "image" stress can be expressed as:

$$\bar{K}_p = 3 \, I_0 \xi \, \frac{\partial F}{\partial \bar{I}} \frac{\partial F}{\partial I_0} \qquad (1.6\text{-}3)$$

The plastic modulus (K_p) for points inside the bounding surface was developed for the single ellipse form of the Bounding Surface model for clays by [Kaliakin, 1985]. The modulus is a function of the plastic modulus at the image stress point $\left(\bar{K}_p \right)$ and the distance to the bound (b). It is defined as:

$$K_p = \bar{K}_p + \xi \, p_{atm} \left[z^m h_1 + \left(1 - z^m \right) h_2 \right] \left[\tfrac{1}{2} \left(a + \mathrm{sign}(n_p) \sqrt[w]{|n_p|} \right) \right]$$
$$\left[9 \left(\frac{\partial F}{\partial \bar{I}} \right)^2 + \tfrac{1}{3} \left(\frac{\partial F}{\partial \bar{J}} \right)^2 \right] \frac{(b-1)}{\langle b - (b-1) s_p \rangle} \qquad (1.6\text{-}4)$$

where p_{atm} = atmospheric pressure

$$z = \frac{J \, R}{N \, I_o}$$

m = positive material constant

$$h_1(\alpha) = \frac{2\eta}{1 + \eta - (1 - \eta) \sin(3\alpha)} h_c$$

$$\eta = \frac{h_e}{h_c}$$

$h_c = h_1\left(\frac{\pi}{6}\right) =$ value of h_1 in triaxial compression

$h_e = h_1\left(-\frac{\pi}{6}\right) =$ value of h_1 in triaxial extension

$n_p =$ p-direction component of unit outward normal in triax space

$h_2 =$ shape hardening parameter for states near the volumetric axis

$s_p =$ parameter defining the elastic nucleus $\left(s_p \geq 1\right)$.

On the bounding surface (i.e., $b = 1$) the plastic modulus is the same as the image modulus (i.e., $K_p = \overline{K}_p$). As one moves toward the projection center (i.e., $b \to \infty$) the value of the term in the Macaulay brackets $\left(\langle\ \rangle\right)$ goes through zero and then negative (if $s_p > 1$). Recalling the convention for the Macaulay brackets, the plastic modulus becomes infinite as b approaches the projection center or the edge of elastic nucleus. The elastic nucleus is defined by s_p and is given in terms of the distance to the bound by:

$$b_{elastic} = \frac{s_p}{s_p - 1} \tag{1.6-5}$$

where $\quad b_{elastic} =$ defines the edge of the elastic nucleus.

For stress points within the elastic nucleus, use of the Macaulay brackets assures that the plastic modulus remains at infinity.

This form of the plastic modulus was defined to capture overconsolidated clay behavior and to give appropriate behavior near the critical state line. For further discussion on the development of this expression, the reader is directed to previous work on the single ellipse Bounding Surface model [Kaliakin, 1985].

1.7 Development of Rate Equation for Loading Surface

The loading surface is the surface on which the stress point resides inside the bounding surface. The loading surface has not been explicitly defined in the bounding

surface literature but is required for any return method algorithm. The development of the rate equation for the loading surface begins with the definition of the image stress in invariant space:

$$\bar{I} = b(I - I_c) + I_c \tag{1.7-1}$$

where $\quad I_c = C\, I_o$

C = projection center constant

b = measure of distance from the loading surface to the bounding surface.

$$\bar{J} = bJ \tag{1.7-2}$$

$$\bar{\alpha} = \alpha \tag{1.7-3}$$

Differentiating the image stress invariants with respect to time yields:

$$\dot{\bar{I}} = \dot{b}(I - I_c) + b(\dot{I} - \dot{I}_c) + \dot{I}_c \tag{1.7-4}$$

$$\dot{\bar{J}} = \dot{b}(J) + b(\dot{J}) \tag{1.7-5}$$

$$\dot{\bar{\alpha}} = \dot{\alpha} \tag{1.7-6}$$

where $\quad \dot{I}_c = C(\dot{I}_o)$.

The plasticity parameter (Equation 1.2-4) can be expressed in terms of the invariants as:

$$\gamma = \frac{1}{\bar{K}_p}\left(\frac{\partial F}{\partial \bar{I}}\,\dot{\bar{I}} + \frac{\partial F}{\partial \bar{J}}\,\dot{\bar{J}} + \frac{\partial F}{\partial \alpha}\,\dot{\bar{\alpha}}\right) = \frac{1}{K_p}\left(\frac{\partial F}{\partial \bar{I}}\,\dot{I} + \frac{\partial F}{\partial \bar{J}}\,\dot{J} + \frac{1}{b}\frac{\partial F}{\partial \alpha}\,\dot{\alpha}\right) \tag{1.7-7}$$

Substituting Equations 1.7-4, 1.7-5 and 1.7-6 into the first part of Equation 1.7-7 yields:

$$\overline{K}_p \gamma = b\left(\frac{\partial F}{\partial \overline{I}}(I - I_c) + \frac{\partial F}{\partial \overline{J}} J\right) + b\left(\frac{\partial F}{\partial \overline{I}} \dot{I} + \frac{\partial F}{\partial \overline{J}} \dot{J} + \frac{1}{b}\frac{\partial F}{\partial \alpha} \dot{\alpha}\right) + (1-b)\frac{\partial F}{\partial \overline{I}} \dot{I}_c \quad (1.7\text{-}8)$$

The terms in the second parentheses (multiplied by b) is recognized to be the plasticity parameter times the hardening modulus (i.e., the second term of Equation 1.7-7) which simplifies Equation 1.7-8 to:

$$\overline{K}_p \gamma = b\left(\frac{\partial F}{\partial \overline{I}}(I - I_c) + \frac{\partial F}{\partial \overline{J}} J\right) + \gamma\, K_p + (1-b)\frac{\partial F}{\partial \overline{I}} \dot{I}_c \quad (1.7\text{-}9)$$

Recall that the projection center was defined in Equation 1.7-1 as $I_c = CI_0$. Combining Equations 1.5-5 and 1.5-7 (written in rate form) with Equation 1.7-1 results in the expression for the rate of the projection center parameter:

$$\dot{I}_c = 3\,\gamma\,C\,v_0\,\frac{I_0}{\lambda - \kappa}\,\frac{\partial F}{\partial \overline{I}} \quad (1.7\text{-}10)$$

Substituting Equation 1.7-10 into 1.7-9 the rate of the loading surface (b) is obtained as:

$$\dot{b} = \gamma\,\frac{\overline{K}_p - bK_p - 3Cv_o(1-b)\dfrac{I_o}{\lambda - \kappa}\left(\dfrac{\partial F}{\partial \overline{I}}\right)^2}{(I - I_c)\dfrac{\partial F}{\partial \overline{I}} + J\dfrac{\partial F}{\partial \overline{J}}} \quad (1.7\text{-}11)$$

1.8 Improved Invariant Form

The model uses the associative flow rule in which the strain direction is given as the perpendicular to the bounding surface (i.e., the first derivative of the bounding function with respect to the image stress). Since the bounding function is given in terms of stress

invariants, this derivative is given via the application of the chain rule:

$$\frac{\partial F}{\partial \overline{\sigma}_{ij}} = \frac{\partial F}{\partial \overline{I}}\frac{\partial \overline{I}}{\partial \overline{\sigma}_{ij}} + \frac{\partial F}{\partial \overline{J}}\frac{\partial \overline{J}}{\partial \overline{\sigma}_{ij}} + \frac{\partial F}{\partial \alpha}\frac{\partial \alpha}{\partial \overline{\sigma}_{ij}}$$

(1.8-1)

The lode angle (α) was used for the third invariant in previous work on Bounding

Surface plasticity [Herrmann, et. al., 1985; Kaliakin, 1985] and Cam-Clay [ABAQUS,

1994] because of its easy visualization in the π-plane. The partial derivatives of the

bounding function (F) with respect to the invariants can be expressed as:

$$\frac{\partial F}{\partial \overline{I}} = 2\overline{I} - \frac{2}{R}I_o$$

(1.8-2)

$$\frac{\partial F}{\partial \overline{J}} = 2(R-1)^2 \frac{\overline{J}}{N^2}$$

(1.8-3)

$$\frac{\partial F}{\partial \alpha} = \frac{\partial F}{\partial N}\frac{\partial N}{\partial \alpha} = 3(R-1)^2 \frac{\overline{J}^2}{N}\left[\frac{(1-N_{ec})\cos(3\alpha)}{N_e}\right]$$

(1.8-4)

The partial derivatives of the invariants with respect to the image stresses are given

as:

$$\frac{\partial \overline{I}}{\partial \overline{\sigma}_{ij}} = \delta_{ij}$$

(1.8-5)

$$\frac{\partial \overline{J}}{\partial \overline{\sigma}_{ij}} = \frac{s_{ij}}{2J}$$

(1.8-6)

$$\frac{\partial \alpha}{\partial \overline{\sigma}_{ij}} = \frac{\sqrt{3}}{2J\cos(3\alpha)}\left[\frac{1}{J^2}\left(s_{ik}s_{kj} - \frac{3}{2}\frac{S^3}{J^2}s_{ij}\right) - \frac{2}{3}\delta_{ij}\right]$$

(1.8-7)

where $-\frac{\pi}{6} \leq \alpha \leq \frac{\pi}{6}$

Numerical difficulties occur at the endpoints of the lode angle (i.e., $\alpha = \pm\frac{\pi}{6}$)

because the term, $\cos(3\alpha) = 0$. The value of the derivatives associated with the lode angle

at the endpoints are:

$$\frac{\partial F}{\partial \alpha} = 0 \qquad (1.8\text{-}8)$$

$$\frac{\partial \alpha}{\partial \overline{\sigma}_{ij}} = \infty \qquad (1.8\text{-}9)$$

The problem lies in the fact that α is discontinuous at these endpoints. This can be

resolved for the first derivative by realizing that the cosine term cancels out when Equations

1.8-8 and 1.8-9 are multiplied together. Second derivative terms (as required by the

Closest Point algorithm), however, do not have this obvious fix. Another approach to this

problem is noting that α is not used directly in the functional but is used within

trigonometric functions which are continuous. A new variable is defined as:

$$\mu = \sin(3\alpha) \qquad (1.8\text{-}10)$$

Equation 1.8-1 can now be written in terms of this new variable as:

$$\frac{\partial F}{\partial \overline{\sigma}_{ij}} = \frac{\partial F}{\partial \overline{I}}\frac{\partial \overline{I}}{\partial \overline{\sigma}_{ij}} + \frac{\partial F}{\partial \overline{J}}\frac{\partial \overline{J}}{\partial \overline{\sigma}_{ij}} + \frac{\partial F}{\partial \mu}\frac{\partial \mu}{\partial \overline{\sigma}_{ij}} \qquad (1.8\text{-}11)$$

The derivatives associated with the third invariant (Equations 1.8-4 and 1.8-7) can now be written as:

$$\frac{\partial F}{\partial \mu} = (R-1)^2 \frac{\bar{J}^2}{N} \left(\frac{1-N_{ec}}{N_e} \right) \qquad (1.8\text{-}12)$$

$$\frac{\partial \mu}{\partial \bar{\sigma}_{ij}} = \frac{\sqrt{3}}{2J} \left[\frac{1}{J^2} \left(s_{ik}s_{kj} - \frac{3}{2}\frac{S^3}{J^2}s_{ij} \right) - \frac{2}{3}\delta_{ij} \right] \qquad (1.8\text{-}13)$$

This form eliminates the $\cos(3\alpha)$ term in the first derivatives and thus avoids

division by zero. It also has the added benefit of eliminating the $\cos(3\alpha)$ term in the second
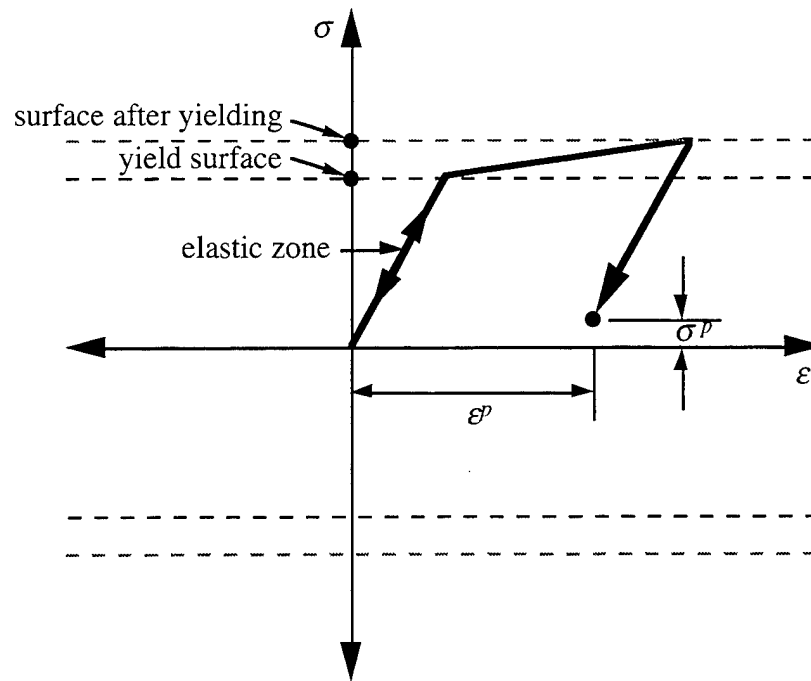
derivatives (see Appendix A).

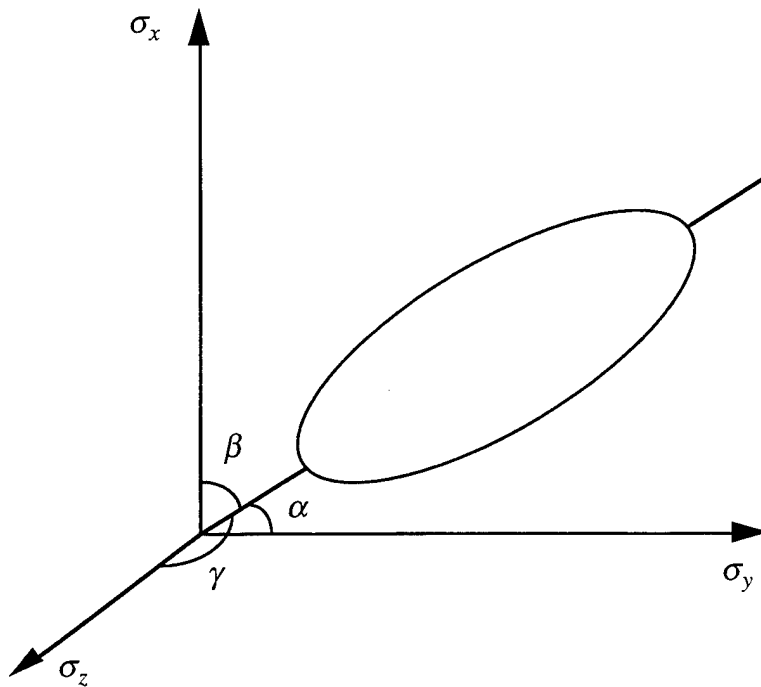Figure 1.1-1. Plastic Stress-Strain Diagram.

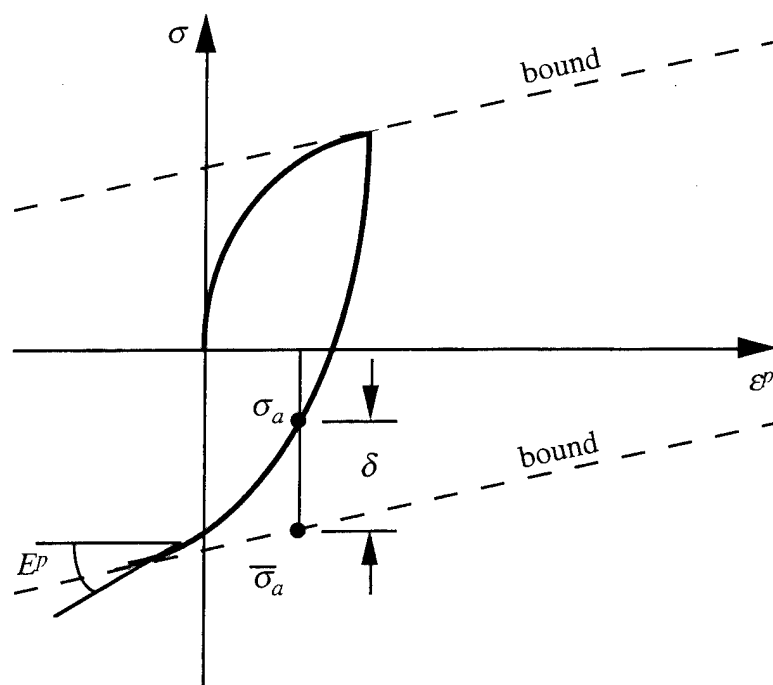Figure 1.1-2. Yield Surface in Principal Stress Space.

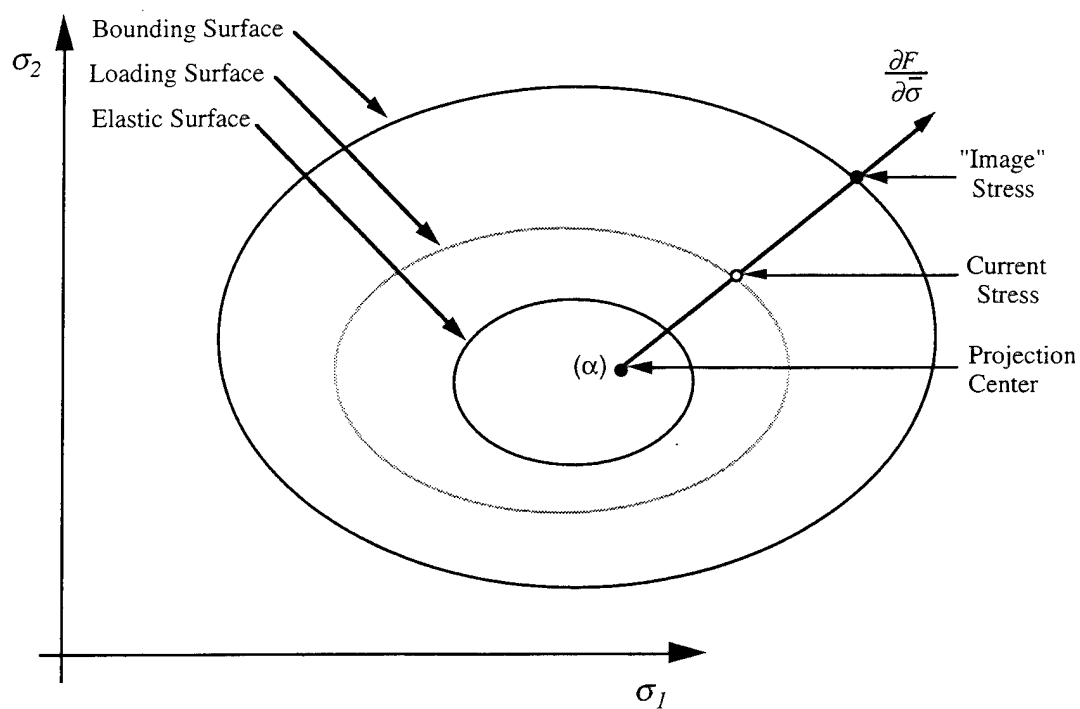Figure 1.2-1. Uniaxial Bounding Surface Plasticity.

Figure 1.2-2. Bounding Surface Concept.
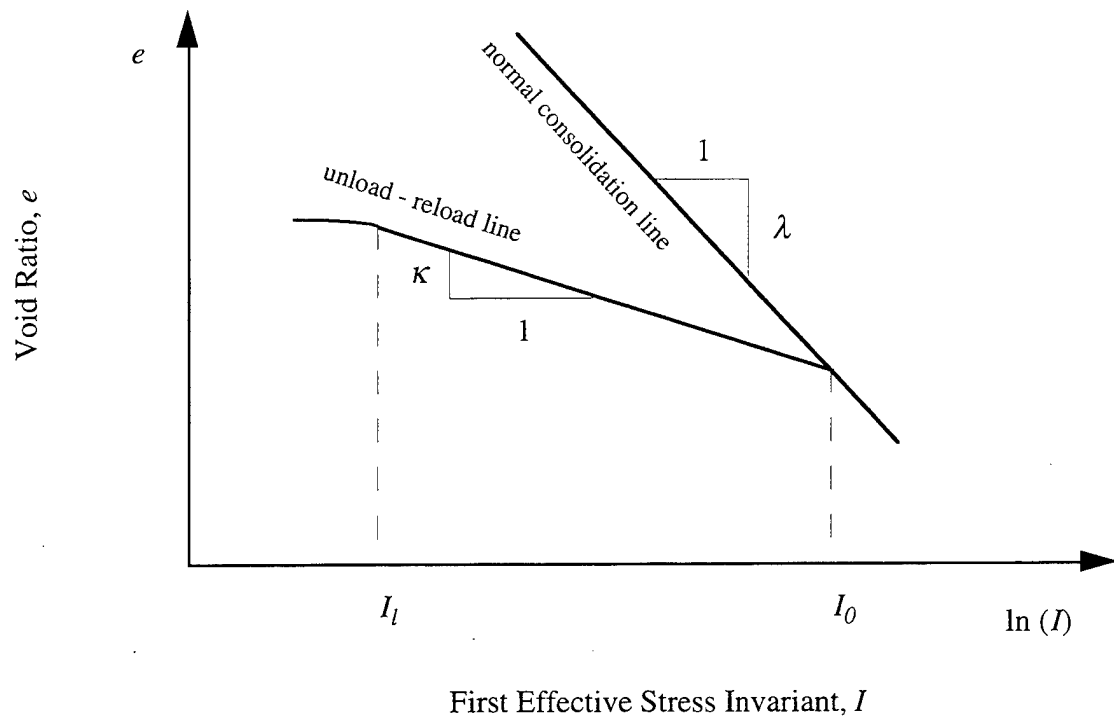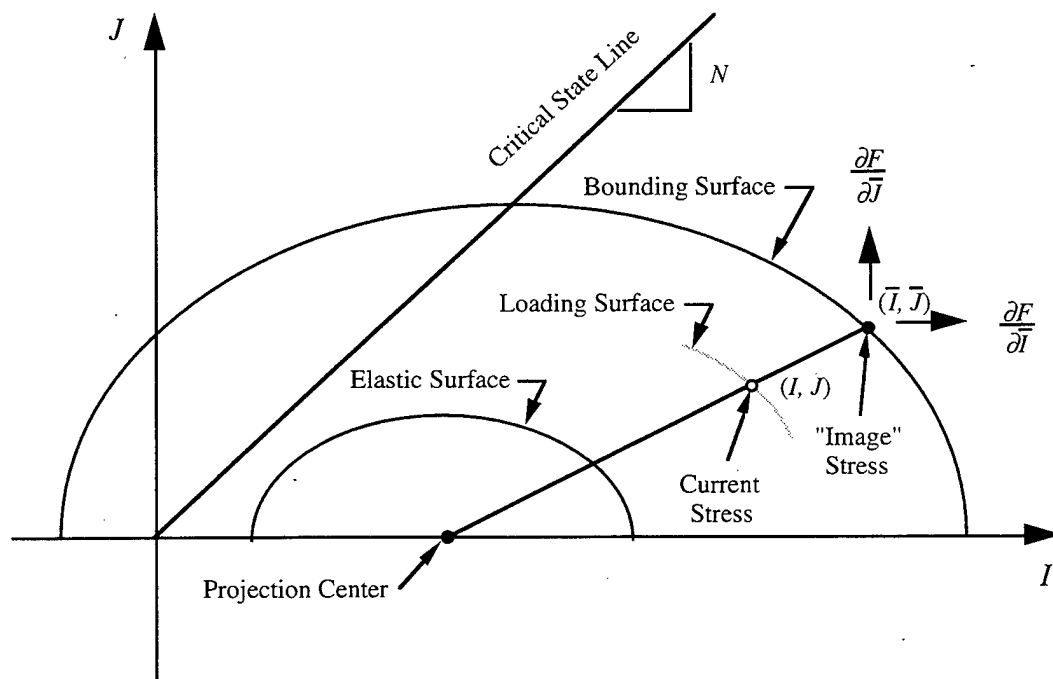
Figure 1.3-1. Void Ratio-Volumetric Stress Relationship.

Figure 1.4-1. Single Ellipse Bounding Surface Model for Clays.

2. Closest Point Projection Method

The Closest Point Projection method was introduced to computational plasticity by the late Professor Juan Simo of Stanford University in the early 1990's [Simo and Hughes, 1990, Simo and Meschke, 1993]. The method was developed within the classical plasticity framework and uses the Newton-Raphson method in the implicit integration of the rate equations and the satisfaction of the consistency condition. As with any Newton-Raphson method, a guess in the "neighborhood" generally results in quadratic convergence. The method has proven to be extremely fast in J2 Flow models [Simo and Hughes, 1990].

In order to employ the Newton-Raphson method, the algorithm requires that the yield function be twice differentiable and the internal variable rate equations be differentiable. Creation of this local "Jacobian" requires additional calculations, but improves the convergence. The local "Jacobian" also provides the framework for developing the algorithmically consistent tangent moduli [Simo and Taylor, 1985] that improves global convergence.

To remain consistent with Professor Simo's work, the differential form of the equations is used instead of the rate form (dI instead of $\dot{I}$) throughout this section. Sections 2.1 and 2.2 lay out the framework for the stress point algorithm and the consistent moduli, respectively, for a simple elastic-plastic model. Sections 2.3 and 2.4 describe the stress point algorithm and the consistent moduli for a general plastic model with internal variables. Section 2.5 extends the general model using explicit-implicit integration. Finally, in Section 2.6, application is made of the Closest Point method to the Bounding Surface Clay model.

2.1 Derivation of Closest Point Stress Point Algorithm (simple model)

To lay out the framework for the Closest Point method, a simple elastic-perfectly-plastic model with an associative flow rule will be used. This will provide insight and

facilitate the application to more complex models such as the Bounding Surface Clay model.

The yield function for the simple model is a function of the stresses only and is given as:

$$f = f(\sigma) = 0 \tag{2.1-1}$$

where f = yield function

σ = stress vector.

The associative flow rule assumes that upon plastic flow the strains flow in a direction perpendicular to the yield surface [Dafalias, 1990] which is described in stress space. Thus, the rate equations for the plastic strains are a function of the yield surface (see Equation 1.1-5) and are given as:

$$\dot{\varepsilon}^p = \gamma \, \frac{\partial f}{\partial \sigma} \tag{2.1-2}$$

where γ = plasticity parameter

$\dfrac{\partial f}{\partial \sigma}$ = vector of yield function derivatives.

The desired result of a constitutive algorithm is the stresses at the end of the step (σ_{n+1}) given a set of strains (ε_{n+1}). The stresses are a function of only the elastic strains for this simple model and are written as:

$$\sigma_{n+1} = C \, \varepsilon^e_{n+1} = C \left(\varepsilon_{n+1} - \varepsilon^p_{n+1} \right) \tag{2.1-3}$$

where σ = vector of stresses (i.e., [σ_x, σ_y, σ_z, τ_{xy}, ...]^T).

Beside the stresses at time t_{n+1}, the plastic strains are unknown. In order to determine these, the rate equations (Equations 2.1-2) are integrated between times t_n and

t_{n+1} using a backwards Euler approximation. Backwards Euler was chosen because it involves the end point values (i.e., at t_{n+1}) of the various terms (e.g., plasticity parameter, gradients, etc.). This facilitates a simple derivation of the Closest Point Projection method. The approximation for the plastic strains is given as:

$$\varepsilon_{n+1}^p = \varepsilon_n^p + \gamma_{n+1} \left(\frac{\partial f}{\partial \sigma} \right)_{n+1} \tag{2.1-4}$$

Note that γ_{n+1} will be used for clarity throughout this section instead of the more

appropriate $\Delta t\, \gamma|_{n+1}$.

By adding and subtracting the plastic strains at the beginning of the step (ε_n^p) to the

strain terms in the parenthesis of Equation 2.1-3 and substituting in the right hand side of Equation 2.1-4, the stress equations are given in terms of a "trial" stress and the unknown plasticity parameter. The stress equations are given as:

$$\sigma_{n+1} = \sigma^{trial} - \gamma_{n+1}\, C \left(\frac{\partial f}{\partial \sigma} \right)_{n+1} \tag{2.1-5}$$

$$\text{where} \quad \sigma^{trial} = C \left(\varepsilon_{n+1} - \varepsilon_n^p \right).$$

Since the total strains at time t_{n+1} are given and the plastic strains at time t_n are known from the previous calculation, the "trial" stresses are in terms of known quantities and can be viewed as an elastic prediction. The concept of the Closest Point Projection method is to return the stresses back to the surface via the "closest projection." This is shown in Figure 2.1-1.

Since the backwards Euler method needs terms evaluated at time t_{n+1}, it requires iteration. The Closest Point Projection method incorporates Newton-Raphson iteration not only to solve the stress equations (Equation 2.1-3), but to enforce the consistency condition

directly. This is accomplished by first defining local residuals using the stress equations. The local residuals are defined as:

$$R_{n+1} = \sigma_{n+1} - \sigma^{trial} + \gamma_{n+1} \ C\left(\frac{\partial f}{\partial \sigma}\right)_{n+1} = 0 \qquad (2.1\text{-}6)$$

These residuals are differentiated at time t_{n+1} (implying that values at time t_n are constants) to give an infinitesimal increment of the residual. Note that the strains are known at times t_n and t_{n+1} and therefore do not vary. Recall, also, that the yield equation in this simple model (Equation 2.1-1) is a function of stresses only, and the plasticity parameter is also a variable. The resulting differentiation is given as:

$$dR_{n+1} = d\sigma_{n+1} + d\gamma_{n+1}C\left(\frac{\partial f}{\partial \sigma}\right)_{n+1} + \gamma_{n+1}C\left(\frac{\partial^2 f}{\partial \sigma^2}\right)_{n+1} d\sigma_{n+1} \qquad (2.1\text{-}7)$$

The yield function (Equation 2.1-1) can also be differentiated at time t_{n+1}. By setting this equation to zero, a discrete form of the consistency condition ($\dot{f} = 0$) is established [Simo and Hughes, 1990]. This is equivalent to satisfying the consistency condition at a finite difference point using a backward difference formula for the first derivative. The yield function differential is given as:

$$df_{n+1} = \left(\frac{\partial f}{\partial \sigma}\right)_{n+1} d\sigma_{n+1} = 0 \qquad (2.1\text{-}8)$$

At this point the iteration counter k is introduced. Values at $k = 1$ are given as:

$$\sigma_{n+1}^{(k)} = \sigma_n^{trial} \qquad (2.1\text{-}9)$$

$$f^{(k)} = f\left(\sigma_{n+1}^{(k)}\right) \qquad (2.1\text{-}10)$$

$$\gamma_{n+1}^{(k)} = 0 \qquad (2.1\text{-}11)$$

$$R_{n+1}^{(k)} = \sigma_{n+1}^{(k)} - \sigma_n^{trial} + \gamma_{n+1}^{(k)} \, C \left(\frac{\partial f}{\partial \sigma} \right)_{n+1}^{(k)} \qquad (2.1\text{-}12)$$

For elastic steps, the yield function (Equation 2.1-10) would be less than or equal to zero and the trial stress would be substituted as the new stress. If the yield function were greater than zero the Newton-Raphson iteration would be required to drive the yield function (Equation 2.1-10) and residuals (Equation 2.1-12) to zero. It is interesting to note that for the first iteration the local residuals are all zero except for the yield condition (f) which is not satisfied.

A Taylor series expansion is made on the residuals and yield condition (Equations 2.1-12 and 2.1-10) at time t_{n+1} and truncated at the linear term. This step amounts to a derivation of the Newton-Raphson nonlinear solution algorithm. Both approximations are set to zero:

$$R_{n+1}^{(k)} + dR_{n+1}^{(k)} = 0 \qquad (2.1\text{-}13)$$

$$f_{n+1}^{(k)} + df_{n+1}^{(k)} = 0 \qquad (2.1\text{-}14)$$

To obtain accurate results, it is assumed that the step sizes are sufficiently small that the differentials can be approximated with finite increments (i.e., $\Delta R_{n+1}^{(k)} \approx dR_{n+1}^{(k)}$ and $\Delta f_{n+1}^{(k)} \approx df_{n+1}^{(k)}$). This is required to assure accuracy of the finite difference approximations. In addition, care must be taken in assuring that the global step sizes (and the step sizes used in the local Newton-Raphson iteration) are small enough so that there is convergence at the local level. This is often accomplished by including substepping at the local level.

Equations 2.1-7 and 2.1-8 are substituted into Equations 2.1-13 and 2.1-14, respectively, and Equation 2.1-13 is multiplied by C^{-1} (assuming it exists). The resulting

equations are given in incremental form as:

$$C^{-1}R_{n+1}^{(k)} + \Xi_{n+1}^{(k)}\,\Delta\sigma_{n+1}^{(k)} + \Delta\gamma_{n+1}^{(k)}\left(\frac{\partial f}{\partial\sigma}\right)_{n+1}^{(k)} = 0 \tag{2.1-15}$$

$$\text{where}\quad \Xi_{n+1}^{(k)} = \left[C^{-1} + \gamma_{n+1}^{(k)}\left(\frac{\partial^2 f}{\partial\sigma^2}\right)_{n+1}^{(k)}\right]^{-1}.$$

$$f_{n+1}^{(k)} + \left(\frac{\partial f}{\partial\sigma}\right)_{n+1}^{(k)}\Delta\sigma_{n+1}^{(k)} = 0 \tag{2.1-16}$$

Note that the Ξ matrix is shown as an inverse matrix for clarity purposes in this section. However, in the coding of the algorithm, standard matrix factorization and substitution is usually used.

Equation 2.1-15 can be rewritten to solve for the unknown increment in stresses given an increment in the plasticity parameter. The stress increments are given as:

$$\Delta\sigma_{n+1}^{(k)} = -\Xi_{n+1}^{(k)}\left[C^{-1}R_{n+1}^{(k)} + \Delta\gamma_{n+1}^{(k)}\left(\frac{\partial f}{\partial\sigma}\right)_{n+1}^{(k)}\right] \tag{2.1-17}$$

The increment in stresses of Equation 2.1-17 can be substituted into Equation 2.1-16 yielding:

$$f_{n+1}^{(k)} - \left(\frac{\partial f}{\partial\sigma}\right)_{n+1}^{(k)}\Xi_{n+1}^{(k)}\left[C^{-1}R_{n+1}^{(k)} + \Delta\gamma_{n+1}^{(k)}\left(\frac{\partial f}{\partial\sigma}\right)_{n+1}^{(k)}\right] = 0 \tag{2.1-18}$$

Finally, Equation 2.1-18 can be rewritten to solve for the increment in the plasticity

parameter as:

$$\Delta\gamma_{n+1}^{(k)} = \frac{f_{n+1}^{(k)} - \left(\dfrac{\partial f}{\partial\sigma}\right)_{n+1}^{(k)} \Xi_{n+1}^{(k)} \, C^{-1} \, R_{n+1}^{(k)}}{\left(\dfrac{\partial f}{\partial\sigma}\right)_{n+1}^{(k)} \Xi_{n+1}^{(k)} \left(\dfrac{\partial f}{\partial\sigma}\right)_{n+1}^{(k)}} \qquad (2.1\text{-}19)$$

The Closest Point method begins by calculating the "trial" elastic stress (Equations

2.1-5 and 2.1-9). This is tantamount to the first Newton-Raphson iteration starting with an

initial guess of an elastic step (i.e., $\Delta\sigma_{n+1}^{(0)} = \Delta\sigma_{elastic}$). If the yield function is greater than

zero, this stress point is taken as the first iterate. The yield function, derivatives and

residuals are then calculated at this stress point. These values are then inserted into

Equation (2.1-19) and the increment in the plasticity parameter is determined. The

plasticity parameter increment is inserted into Equation 2.1-17 to solve for the stress

increments. The unknown plasticity parameter and stresses are then updated via:

$$\gamma_{n+1}^{(k+1)} = \gamma_{n+1}^{(k)} + \Delta\gamma_{n+1}^{(k)} \qquad (2.1\text{-}20)$$

$$\sigma_{n+1}^{(k+1)} = \sigma_{n+1}^{(k)} + \Delta\sigma_{n+1}^{(k)} \qquad (2.1\text{-}21)$$

The new stress point and plasticity parameter are used for the next iteration with the

process continuing until the yield function and stress residuals are within some tolerance of

zero. Recall (from Equation 2.1-4) that the plasticity parameter (γ_{n+1}) shown here is, in

fact, $\Delta t \, \gamma|_{n+1}$. The Closest Point stress point algorithm is described in Box 2.1-1 and the

behavior during iteration is shown Figure 2.1-2.

Box 2.1-1. Fully Implicit Closest Point Stress Point Algorithm (simple model).

---

1. Given: $\qquad \varepsilon_{n+1}, \varepsilon_n^p, C$

2. Initialize: $\qquad k = 1, \quad \gamma_{n+1}^{(1)} = 0, \quad \varepsilon_{n+1}^{p^{(1)}} = \varepsilon_n^p$

3. Calculate elastic prediction: $\sigma^{trial} = C\left(\varepsilon_{n+1} - \varepsilon_n^p\right)$

4. Calculate yield function and local residuals:

$$f_{n+1}^{(k)} = f\left(\sigma_{n+1}^{(k)}\right) \qquad R_{n+1}^{(k)} = \sigma_{n+1}^{(k)} - \sigma^{trial} + \gamma_{n+1}^{(k)} \, C \left(\frac{\partial f}{\partial \sigma}\right)_{n+1}^{(k)}$$

5. Test for convergence: IF $\left(f_{n+1}^{(k)} < \text{TOLER}_f \quad \text{AND} \quad \left\| R_{n+1}^{(k)} \right\| < \text{TOLER}_R \right) \qquad$ EXIT

6. Compute the derivatives and assemble matrices:

$$\left(\frac{\partial f}{\partial \sigma}\right)_{n+1}^{(k)} = \frac{\partial f\left(\sigma_{n+1}^{(k)}\right)}{\partial \sigma_{n+1}^{(k)}} \qquad \Xi_{n+1}^{(k)} = \left[C^{-1} + \gamma_{n+1}^{(k)}\left(\frac{\partial^2 f}{\partial \sigma^2}\right)_{n+1}^{(k)} \right]^{-1}$$

7. Obtain increment in plasticity parameter:

$$\Delta\gamma_{n+1}^{(k)} = \frac{f_{n+1}^{(k)} - \left(\dfrac{\partial f}{\partial \sigma}\right)_{n+1}^{(k)} \Xi_{n+1}^{(k)} \, C^{-1} \, R_{n+1}^{(k)}}{\left(\dfrac{\partial f}{\partial \sigma}\right)_{n+1}^{(k)} \Xi_{n+1}^{(k)} \left(\dfrac{\partial f}{\partial \sigma}\right)_{n+1}^{(k)}}$$

8. Obtain increment in stresses:

$$\Delta\sigma_{n+1}^{(k)} = -\Xi_{n+1}^{(k)} \left[C^{-1} R_{n+1}^{(k)} + \Delta\gamma_{n+1}^{(k)}\left(\frac{\partial f}{\partial \sigma}\right)_{n+1}^{(k)} \right]$$

9. Update: $\quad \gamma_{n+1}^{(k+1)} = \gamma_{n+1}^{(k)} + \Delta\gamma_{n+1}^{(k)}, \quad \sigma_{n+1}^{(k+1)} = \sigma_{n+1}^{(k)} + \Delta\sigma_{n+1}^{(k)}$

10. Set: $\quad k \leftarrow k + 1$, Go to step 4

2.2 Derivation of Consistent Tangent Moduli (simple model)

When the Newton-Raphson algorithm is used to solve the global nonlinear problem, a global Jacobian matrix is required. This global Jacobian matrix is an assembly of element Jacobian matrices which, in turn, are composed of Jacobian matrices constructed at the quadrature points. The accurate construction of the Jacobian matrix at the quadrature point requires a matrix of derivatives of the stress component relative to the assumed strain increments. This matrix is given the name "consistent tangent stiffness matrix" [Simo and Taylor, 1985] and must be supplied by the material routine. Recall, however, that an "exact" Jacobian is not necessarily required for convergence, although it generally improves the rate of convergence.

Derivation of the consistent tangent moduli will follow a framework similar to the Closest Point stress point algorithm. For eventual comparison to the classical continuum developed moduli, indicial notation is introduced in this section. The stress equations (Equation 2.1-5) are given in indicial notation as:

$$\sigma_{ij_{n+1}} = \sigma_{ij}^{trial} - \gamma_{n+1} \, C_{ijkl} \left(\frac{\partial f}{\partial \sigma_{kl}} \right)_{n+1} \tag{2.2-1}$$

where $\sigma_{ij}^{trial} = C_{ijkl} \left(\varepsilon_{kl_{n+1}} - \varepsilon_{kl_n}^{p} \right)$.

As with the stress point algorithm, the stress equations are differentiated at time t_{n+1}. However, since the tangent moduli $\left(\dfrac{\partial \sigma_{ij}}{\partial \varepsilon_{kl}} \right)_{n+1}$ are the variation in stresses given a variation in strains, the strain at time t_{n+1} is not fixed. The differentiated stress equations can now be given as:

$$d\sigma_{ij_{n+1}} = C_{ijkl} \, d\varepsilon_{kl_{n+1}} - d\gamma_{n+1} \, C_{ijkl} \left(\frac{\partial f}{\partial \sigma_{kl}} \right)_{n+1} - \gamma_{n+1} \, C_{ijkl} \left(\frac{\partial^2 f}{\partial \sigma_{kl} \partial \sigma_{mn}} \right)_{n+1} d\sigma_{mn_{n+1}} \tag{2.2-2}$$

Both sides are multiplied by C^{-1} and rearranged to solve for the increment in stresses. The stress increments are given in terms of the increment in strains and plasticity parameter and are:

$$d\sigma_{ij_{n+1}} = \Xi_{ijkl}\left[d\varepsilon_{kl_{n+1}} - d\gamma_{n+1}\left(\frac{\partial f}{\partial\sigma_{kl}}\right)_{n+1}\right] \tag{2.2-3}$$

where $\quad \Xi_{ijkl} = \left[C_{ijkl}^{-1} + \gamma_{n+1}\left(\frac{\partial^2 f}{\partial\sigma_{kl}\partial\sigma_{mn}}\right)_{n+1}\right]^{-1}.$

The increment in stresses is inserted into the discrete consistency condition (Equation 2.1-8). The resulting expression for the increment in the plasticity parameter $(d\gamma_{n+1})$ can now be given in terms of the increment in strains. This is given as:

$$d\gamma_{n+1} = \frac{\left(\dfrac{\partial f}{\partial\sigma_{mn}}\right)_{n+1}\Xi_{mnop}\,d\varepsilon_{op_{n+1}}}{\left(\dfrac{\partial f}{\partial\sigma_{ab}}\right)_{n+1}\Xi_{abcd}\left(\dfrac{\partial f}{\partial\sigma_{cd}}\right)_{n+1}} \tag{2.2-4}$$

Equation 2.2-4 is substituted into Equation 2.2-3 which now puts the stress increments in terms of the strain increments:

$$d\sigma_{ij_{n+1}} = \Xi_{ijkl}\left[d\varepsilon_{kl_{n+1}} - \frac{\left(\dfrac{\partial f}{\partial\sigma_{mn}}\right)_{n+1}\Xi_{mnop}\,d\varepsilon_{op_{n+1}}}{\left(\dfrac{\partial f}{\partial\sigma_{ab}}\right)_{n+1}\Xi_{abcd}\left(\dfrac{\partial f}{\partial\sigma_{cd}}\right)_{n+1}}\left(\frac{\partial f}{\partial\sigma_{kl}}\right)_{n+1}\right] \tag{2.2-5}$$

The consistent tangent moduli are determined by differentiating the stress

increments by the strain increments at time t_{n+1}. The moduli are given as:

$$\left(\frac{\partial \sigma_{ij}}{\partial \varepsilon_{kl}}\right)_{n+1} = \Xi_{ijkl} - \frac{\Xi_{ijmn}\left(\dfrac{\partial f}{\partial \sigma_{mn}}\right)_{n+1}\left(\dfrac{\partial f}{\partial \sigma_{op}}\right)_{n+1}\Xi_{opkl}}{\left(\dfrac{\partial f}{\partial \sigma_{ab}}\right)_{n+1}\Xi_{abcd}\left(\dfrac{\partial f}{\partial \sigma_{cd}}\right)_{n+1}} \qquad (2.2\text{-}6)$$

$$\text{where} \qquad \Xi_{ijkl} = \left[C_{ijkl}^{-1} + \gamma_{n+1}\left(\frac{\partial^2 f}{\partial \sigma_{kl}\partial \sigma_{mn}}\right)_{n+1}\right]^{-1}.$$

The tangent moduli for the associative flow rule and elastic-perfectly-plastic material are derived using the classical continuum approach [Dafalias, 1990] independent of any particular stress point algorithm. The resulting moduli are given as:

$$D_{ijkl} = C_{ijkl} - \frac{C_{ijmn}\left(\dfrac{\partial f}{\partial \sigma_{mn}}\right)\left(\dfrac{\partial f}{\partial \sigma_{op}}\right)C_{opkl}}{\left(\dfrac{\partial f}{\partial \sigma_{ab}}\right)C_{abcd}\left(\dfrac{\partial f}{\partial \sigma_{cd}}\right)} \qquad (2.2\text{-}7)$$

$$\text{where} \qquad D_{ijkl} = \text{tangent moduli derived from continuum plasticity.}$$

The consistent tangent moduli developed by the Closest Point algorithm (Equation 2.2-6) results in terms that are consistent with the method used to integrate the stress point algorithm. Upon comparing the moduli it is seen that the difference between the two approaches for this simple model lies in the use of the Ξ matrix instead of the elastic constants. The Ξ matrix depends not only upon the elastic moduli but also the plasticity parameter and the second derivative terms of the yield function. Earlier literature has shown that consistent tangent moduli usually result in faster global convergence [Simo and Taylor, 1985] because they create an exact global Jacobian (unless other approximations are made). Reduction in global calculations can result in significant cost savings if the increased local calculations are not overwhelming.

2.3 Derivation of Closest Point Algorithm (general model)

Classical plasticity includes internal variables that describe the changes in shape, size and location of the yield surface as plastic straining occurs. The general formulation of the Closest Point algorithm was developed with the internal variables expressed in rate form [Simo and Hughes, 1990]. The yield function for the general formulation is now described in terms of the stresses and internal variables and is given as:

$$f = f(\sigma, q) = 0 \qquad (2.3\text{-}1)$$

where q = internal variables.

The rate equations for the plastic strains with non-associative flow and internal variables are given in a general form as:

$$\dot{\varepsilon}^p = \gamma\, N \qquad (2.3\text{-}2)$$

$$\dot{q} = \gamma\, h \qquad (2.3\text{-}3)$$

where $N = N(\sigma, q)$ = direction of plastic strains

$h = h(\sigma, q)$ = direction of internal variables.

The plastic strain and internal variable directions are shown as functions of both stresses and internal variables, although they can be a function of just one of these characteristics.

The rate equations for both the strains and internal variables are approximated between times t_n and t_{n+1} using a backwards Euler scheme and are given as:

$$\varepsilon_{n+1}^p = \varepsilon_n^p + \gamma_{n+1} N_{n+1} \tag{2.3-4}$$

$$q_{n+1} = q_n + \gamma_{n+1} h_{n+1} \tag{2.3-5}$$

where $\quad N_{n+1} = N(\sigma_{n+1}, q_{n+1})$

$$h_{n+1} = h(\sigma_{n+1}, q_{n+1}).$$

As in the stress point algorithm (Section 2.1), the plastic strains at time t_n $\left(\varepsilon_n^p\right)$ are added and subtracted in the stress equation (Equation 2.1-3) and use is made of Equation 2.3-4. The resulting equation for stress is in terms of the "trial" stress (elastic prediction) and is given as:

$$\sigma_{n+1} = \sigma^{trial} - \gamma_{n+1} C N_{n+1} \tag{2.3-6}$$

where $\quad \sigma^{trial} = C\left(\varepsilon_{n+1} - \varepsilon_n^p\right).$

The set of nonlinear equations to be solved consists of the stress equations (Equation 2.3-6) and the internal variable equations (Equation 2.3-5). The local residual vector for these equations is defined as:

$$R_{n+1} = \begin{bmatrix} \sigma_{n+1} - \sigma^{trial} + \gamma_{n+1} C N_{n+1} \\ q_{n+1} - q_n - \gamma_{n+1} h_{n+1} \end{bmatrix} = 0 \tag{2.3-7}$$

The local residuals are differentiated at time t_{n+1} to give the local Jacobian matrix. Recall that the strain rates and internal variable rates can be functions of both stress and internal variables. Again, since the strains are given for the stress point algorithm they are

fixed at time t_{n+1}. The differentiated residuals are given as:

$$dR_{n+1} = \begin{bmatrix} d\sigma_{n+1} + d\gamma_{n+1} C N_{n+1} + \gamma_{n+1} C \left(\dfrac{\partial N}{\partial \sigma}\right)_{n+1} d\sigma_{n+1} + \gamma_{n+1} C \left(\dfrac{\partial N}{\partial q}\right)_{n+1} dq_{n+1} \\ dq_{n+1} - d\gamma_{n+1} h_{n+1} - \gamma_{n+1} \left(\dfrac{dh}{d\sigma}\right)_{n+1} d\sigma_{n+1} - \gamma_{n+1} \left(\dfrac{dh}{dq}\right)_{n+1} dq_{n+1} \end{bmatrix} = 0 \qquad (2.3\text{-}8)$$

The yield function is differentiated at time t_{n+1} and now includes the contributions of both stress and internal variables. The discrete consistency condition is now given as:

$$df_{n+1} = \left(\frac{\partial f}{\partial \sigma}\right)_{n+1} d\sigma_{n+1} + \left(\frac{\partial f}{\partial q}\right)_{n+1} dq_{n+1} = 0 \qquad (2.3\text{-}9)$$

To facilitate the general algorithm development, a number of matrices and vectors are defined:

$$G = \begin{bmatrix} C & 0 \\ 0 & -I \end{bmatrix} \qquad \Sigma = \begin{bmatrix} \sigma \\ q \end{bmatrix} \qquad Z = \begin{bmatrix} N \\ h \end{bmatrix}$$

$$\nabla f = \begin{bmatrix} \dfrac{\partial f}{\partial \sigma} \\ \dfrac{\partial f}{\partial q} \end{bmatrix} \qquad Y = \begin{bmatrix} \dfrac{\partial N}{\partial \sigma} & \dfrac{\partial N}{\partial q} \\ \dfrac{\partial h}{\partial \sigma} & \dfrac{\partial h}{\partial q} \end{bmatrix} \qquad I = \begin{bmatrix} 1 & 0 & \\ 0 & 1 & \cdots \\ & \vdots & \ddots \end{bmatrix} \qquad (2.3\text{-}10)$$

Equations 2.3-8 and 2.3-9 can now be written in matrix form as:

$$d\Sigma_{n+1}^{(k)} + d\gamma_{n+1}^{(k)} G Z_{n+1}^{(k)} + \gamma_{n+1}^{(k)} G Y_{n+1}^{(k)} d\Sigma_{n+1}^{(k)} = 0 \qquad (2.3\text{-}11)$$

$$\nabla f_{n+1}^{(k)} d\Sigma_{n+1}^{(k)} = 0 \qquad (2.3\text{-}12)$$

Substituting Equations 2.3-11 and 2.3-12 into the linear portion of the Taylor series expansion and assuming a finite increment for the differentials (Equations 2.1-15 and

2.1-16) results in:

$$R_{n+1}^{(k)} + \Delta\Sigma_{n+1}^{(k)} + \Delta\gamma_{n+1}^{(k)} \, G \, Z_{n+1}^{(k)} + \gamma_{n+1}^{(k)} \, G \, Y_{n+1}^{(k)} \, \Delta\Sigma_{n+1}^{(k)} = 0 \qquad (2.3\text{-}13)$$

$$f_{n+1}^{(k)} + \nabla f_{n+1}^{(k)} \, \Delta\Sigma_{n+1}^{(k)} = 0 \qquad (2.3\text{-}14)$$

Equation 2.3-13 can be solved for the increment in stresses and internal variables

yielding:

$$\Delta\Sigma_{n+1}^{(k)} = -\Xi_{n+1}^{(k)} \left[G^{-1} R_{n+1}^{(k)} + \Delta\gamma_{n+1}^{(k)} \, Z_{n+1}^{(k)} \right] \qquad (2.3\text{-}15)$$

$$\text{where} \quad \Xi = \left[G^{-1} + \gamma_{n+1}^{(k)} \, Y_{n+1}^{(k)} \right]^{-1}.$$

As noted in Section 2.1, the inverse of the Ξ matrix is shown for clarity, however,

standard matrix factorization and substitution would generally be used in the algorithm.

Finally, the increment in the plasticity parameter is determined by substituting Equation

2.3-15 into Equation 2.3-14 and is given as:

$$\Delta\gamma_{n+1}^{(k)} = \frac{f_{n+1}^{(k)} - \nabla f_{n+1}^{(k)} \, \Xi \, G^{-1} \, R_{n+1}^{(k)}}{\nabla f_{n+1}^{(k)} \, \Xi \, Z_{n+1}^{(k)}} \qquad (2.3\text{-}16)$$

As before, the Closest Point algorithm begins with the calculation of the "trial"

stresses (Equation 2.3-6). If the yield condition is positive, the derivatives and residuals

are calculated at this stress point. The increment in the plasticity parameter (Equation 2.3-

16) is evaluated, then the increment in stresses and internal variables are calculated from

Equation 2.3-15. The plasticity parameter, stresses and internal variables are then updated

via:

$$\gamma_{n+1}^{(k+1)} = \gamma_{n+1}^{(k)} + \Delta\gamma_{n+1}^{(k)} \qquad (2.3\text{-}17)$$

$$\Sigma_{n+1}^{(k+1)} = \Sigma_{n+1}^{(k)} + \Delta\Sigma_{n+1}^{(k)} \qquad (2.3\text{-}18)$$

The new stress point, internal variables and plasticity parameter are used for the next iteration with the process continuing until the yield function and the local residuals are within some tolerance of zero. The general stress point algorithm is described in Box 2.3-1 and shown graphically in Figure 2.3-1.

Box 2.3-1. Fully Implicit Closest Point Algorithm with Internal Variables

---

1. Given: $\quad \varepsilon_{n+1}, \varepsilon_n^p, C$

2. Initialize: $\quad k = 1, \quad \gamma_{n+1}^{(1)} = 0, \quad \varepsilon_{n+1}^{p^{(1)}} = \varepsilon_n^p, \quad q_{n+1}^{(1)} = q_n$

3. Calculate elastic prediction: $\sigma^{trial} = C\left(\varepsilon_{n+1} - \varepsilon_n^p\right)$

4. Calculate yield function and local residuals:

$$f = f(\sigma, q) \qquad R_{n+1} = \begin{bmatrix} \sigma_{n+1} - \sigma^{trial} + \gamma_{n+1} C\, N_{n+1} \\ q_{n+1} - q_n - \gamma_{n+1} h_{n+1} \end{bmatrix}$$

5. Test for convergence: IF $\left(f_{n+1}^{(k)} < TOLER_f \quad AND \quad \left\| R_{n+1}^{(k)} \right\| < TOLER_R \right) \quad$ EXIT

6. Compute derivatives and assemble matrices:

$$\Xi_{n+1}^{(k)} = \left[G^{-1} + \gamma_{n+1}^{(k)} \; Y_{n+1}^{(k)} \right]^{-1}$$

7. Obtain increment in plasticity parameter:

$$\Delta\gamma_{n+1}^{(k)} = \frac{f_{n+1}^{(k)} - \nabla f_{n+1}^{(k)} \; \Xi_{n+1}^{(k)} \; G^{-1} \; R_{n+1}^{(k)}}{\nabla f_{n+1}^{(k)} \; \Xi_{n+1}^{(k)} \; Z_{n+1}^{(k)}}$$

8. Obtain increment in stresses and internal variables:

$$\Delta\Sigma_{n+1}^{(k)} = -\Xi_{n+1}^{(k)} \left[G^{-1} R_{n+1}^{(k)} + \Delta\gamma_{n+1}^{(k)} \; Z_{n+1}^{(k)} \right]$$

9. Update: $\quad \gamma_{n+1}^{(k+1)} = \gamma_{n+1}^{(k)} + \Delta\gamma_{n+1}^{(k)}, \quad \Sigma_{n+1}^{(k+1)} = \Sigma_{n+1}^{(k)} + \Delta\Sigma_{n+1}^{(k)}$

10. Set: $\quad k \leftarrow k + 1$, Go to step 4

2.4 Derivation of Consistent Tangent Moduli (general model)

Derivation of the consistent tangent moduli is somewhat more complicated because the internal variables are now included. The stress and internal variable approximations (Equations 2.3-6 and 2.3-5) are given as:

$$\sigma_{n+1} = \sigma^{trial} - \gamma_{n+1} \, C \, N_{n+1} \tag{2.4-1}$$

$$q_{n+1} = q_n + \gamma_{n+1} h_{n+1} \tag{2.4-2}$$

$$\text{where} \quad \sigma^{trial} = C\left(\varepsilon_{n+1} - \varepsilon_n^p\right).$$

Equations 2.4-1 and 2.4-2 are differentiated at time t_{n+1}. Recall that the tangent moduli are variations in stress with variations in strain and therefore the strains at time t_{n+1} are not fixed. The stress and internal variable differentials are now written as:

$$d\sigma_{n+1} = C \, d\varepsilon_{n+1} - d\gamma_{n+1} \, C \, N_{n+1} - \gamma_{n+1} \, C\left(\frac{\partial N}{\partial \sigma}\right)_{n+1} d\sigma_{n+1} - \gamma_{n+1} \, C\left(\frac{\partial N}{\partial q}\right)_{n+1} dq_{n+1} \tag{2.4-3}$$

$$dq_{n+1} = d\gamma_{n+1} \, h_{n+1} - \gamma_{n+1}\left(\frac{\partial h}{\partial \sigma}\right)_{n+1} d\sigma_{n+1} - \gamma_{n+1}\left(\frac{\partial h}{\partial q}\right)_{n+1} dq_{n+1} \tag{2.4-4}$$

Solving Equations 2.4-3 and 2.4-4 for the increments in stresses and internal variables and writing in matrix form results in:

$$d\Sigma_{n+1} = - \, \Xi_{n+1} \left[dX + d\gamma \, Z\right]_{n+1} \tag{2.4-5}$$

$$\text{where} \quad X = \begin{bmatrix} \varepsilon \\ \mathbf{0} \end{bmatrix}$$

$$\mathbf{0} = \begin{bmatrix} 0 \\ \vdots \end{bmatrix}.$$

Equation 2.4-5 can be substituted into the discrete consistency condition (Equation 2.3-12) and solved for the increment in the plasticity parameter as:

$$d\gamma_{n+1} = \frac{\nabla f_{n+1}\, \Xi_{n+1}\, X_{n+1}}{\nabla f_{n+1}\, \Xi_{n+1}\, Z_{n+1}} \qquad (2.4\text{-}6)$$

Substituting the plasticity parameter (Equation 2.4-6) into Equation 2.4-5 results in an expression for the increments in stress and internal variables in terms of strains. Differentiating this expression with respect to strains at time t_{n+1} provides the algorithmically consistent tangent moduli for the general model:

$$\left(\frac{\partial \sigma}{\partial \varepsilon}\right)_{n+1} = \Xi_{11} - \frac{\begin{bmatrix} \Xi_{11} \\ \Xi_{21} \end{bmatrix}_{n+1} \nabla f_{n+1}\, Z_{n+1} \begin{bmatrix} \Xi_{11} & \Xi_{12} \end{bmatrix}_{n+1}}{\nabla f_{n+1}\, \Xi_{n+1}\, Z_{n+1}} \qquad (2.4\text{-}7)$$

$$\text{where}\quad \Xi_{n+1} = \begin{bmatrix} C^{-1} + \gamma_{n+1}\left(\dfrac{\partial N}{\partial \sigma}\right)_{n+1} & \gamma_{n+1}\left(\dfrac{\partial N}{\partial q}\right)_{n+1} \\ \gamma_{n+1}\left(\dfrac{\partial h}{\partial \sigma}\right)_{n+1} & -I + \gamma_{n+1}\left(\dfrac{\partial h}{\partial q}\right)_{n+1} \end{bmatrix}^{-1} = \begin{bmatrix} \Xi_{11} & \Xi_{12} \\ \Xi_{21} & \Xi_{22} \end{bmatrix}.$$

Since the tangent moduli describe how the stress increment changes in relation to the strain increment, the Ξ matrix is partitioned (because it contains terms for both the stresses and internal variables). It is important to note that the tangent moduli are generally not symmetric since Ξ_{12} and Ξ_{21} are generally not equal. Because of the general lack of symmetry, the entire matrix needs to be available and nonsymmetric solution methods are required at the stress point algorithm level. It is worth noting that most "real world" problems (e.g., large-deformations, slide-surfaces, etc.) are nonsymmetric even if the constitutive relations are symmetric.

The unique case for symmetry comes when considering associative flow (for strains) and what is coined as "associative hardening" (for internal variables). These are

given respectively as:

$$N = \frac{\partial f}{\partial \sigma} \qquad h = \frac{\partial f}{\partial q} \qquad (2.4\text{-}8)$$

It must be noted that this symmetry is only possible when the elastic behavior is derivable from an elastic potential so that the C matrix is symmetric. This condition, in conjunction with Equation 2.4-8, results in a symmetric Ξ matrix, but introduces second derivatives of both the yield function and the internal variable rate equations. The symmetric Ξ matrix is given as:

$$\Xi_{n+1} = \begin{bmatrix} C^{-1} + \gamma_{n+1}\left(\dfrac{\partial^2 f}{\partial \sigma^2}\right)_{n+1} & \gamma_{n+1}\left(\dfrac{\partial^2 f}{\partial \sigma \partial q}\right)_{n+1} \\[4mm] \gamma_{n+1}\left(\dfrac{\partial^2 f}{\partial q \partial \sigma}\right)_{n+1} & -I + \gamma_{n+1}\left(\dfrac{\partial^2 f}{\partial q^2}\right)_{n+1} \end{bmatrix}^{-1} \qquad (2.4\text{-}9)$$

Substituting this matrix into the tangent moduli (Equation 2.4-7) results in symmetric tangent moduli. Most material models, however, rarely include this "associative hardening" and often, such as the case of the soil model considered here, do not have a symmetric elastic matrix (C).

The tangent moduli for the associative flow rule and elastic-perfectly -plastic material using the classical continuum approach [Dafalias, 1990] is given as:

$$D = C - \frac{C\left(\dfrac{\partial f}{\partial \sigma}\right)\left(\dfrac{\partial f}{\partial \sigma}\right)C}{K_p + \left(\dfrac{\partial f}{\partial \sigma}\right)C\left(\dfrac{\partial f}{\partial \sigma}\right)} \qquad (2.4\text{-}10)$$

$$\text{where} \qquad K_p = -\left(\frac{\partial f}{\partial q}\right)h.$$

The differences between Equations 2.4-7 and 2.4-10 for the more general model is not quite as simple as was the case in Section 2.2. The algorithmically consistent moduli

include additional derivatives from both the strain and internal variable rate equations. In the continuum approach, however, the internal variables enter into the moduli only through the hardening modulus (K_p) in the denominator; whereas in the consistent moduli, they appear in both the numerator and the denominator through the Ξ matrix and the Z vector.

An approach for creating symmetric tangent moduli is given in the following section.

2.5 Derivation of Closest Point Algorithm (implicit-explicit model)

An alternate formulation of the Closest Point algorithm is developed similar to the general model, but involves treating the internal variable rates in an explicit fashion. The rate equations for the plastic strains are approximated between times t_n to t_{n+1} as before using a backward Euler form:

$$\varepsilon_{n+1}^p = \varepsilon_n^p + \gamma_{n+1} N_{n+1} \tag{2.5-1}$$

$$\text{where} \quad N_{n+1} = N(\sigma_{n+1},\, q_{n+1}).$$

The internal variable rates, however, are approximated with the plasticity parameter evaluated at time t_{n+1} but the direction evaluated at time t_n. This is given as:

$$q_{n+1} = q_n + \gamma_{n+1} h_n \tag{2.5-2}$$

$$\text{where} \quad h_n = h(\sigma_n,\, q_n).$$

The local residual vector is defined as:

$$R_{n+1} = \begin{bmatrix} \sigma_{n+1} - \sigma^{trial} + \gamma_{n+1} C\, N_{n+1} \\ q_{n+1} - q_n - \gamma_{n+1} h_n \end{bmatrix} = 0 \tag{2.5-3}$$

The local residual is differentiated at time t_{n+1}. Recall that the internal variable rates are evaluated at time t_n and, therefore, have no contribution. The differentiated residuals are given as:

$$dR_{n+1} = \begin{bmatrix} d\sigma_{n+1} + d\gamma_{n+1} C\, N_{n+1} + \gamma_{n+1} C \left(\dfrac{\partial N}{\partial \sigma} \right)_{n+1} d\sigma_{n+1} + \gamma_{n+1} C \left(\dfrac{\partial N}{\partial q} \right)_{n+1} dq_{n+1} \\ dq_{n+1} - d\gamma_{n+1} h_n \end{bmatrix} = 0 \qquad (2.5\text{-}4)$$

Equation 2.5-4 is solved for the increment in stresses and internal variables (Equation 2.3-15) and substituted into the discrete consistency condition (Equation 2.3-9). The increment in stresses, internal variables and the plasticity parameter are given as:

$$\Delta\Sigma_{n+1}^{(k)} = -\Xi_{n+1}^{(k)} \left[G^{-1} R_{n+1}^{(k)} + \Delta\gamma_{n+1}^{(k)}\, Z_{n+1}^{(k)} \right] \qquad (2.5\text{-}5)$$

$$\Delta\gamma_{n+1}^{(k)} = \frac{f_{n+1}^{(k)} - \nabla f_{n+1}^{(k)}\, \Xi_{n+1}^{(k)}\, G^{-1}\, R_{n+1}^{(k)}}{\nabla f_{n+1}^{(k)}\, \Xi_{n+1}^{(k)}\, Z_{n+1}^{(k)}} \qquad (2.5\text{-}6)$$

$$\text{where} \quad \Xi = \left[G^{-1} + \gamma\; Y \right]^{-1}$$

$$Y = \begin{bmatrix} \dfrac{\partial N}{\partial \sigma} & 0 \\ 0 & 0 \end{bmatrix}.$$

The Y matrix with all the zeros is shown for discussion purposes. In the actual algorithm, only the nonzero submatix would be stored and the number of actual calculations would be reduced accordingly.

The consistent tangent moduli are obtained as in Section 2.4. Differentiating this

expression with respect to strains provides the consistent tangent moduli:

$$\left(\frac{\partial\sigma}{\partial\varepsilon}\right)_{n+1} = \Xi_{n+1} - \frac{\Xi_{n+1}\, N_{n+1}\left(\frac{\partial f}{\partial\sigma}\right)_{n+1}\Xi_{n+1}}{\left(\frac{\partial f}{\partial\sigma}\right)_{n+1}\Xi_{n+1}\, N_{n+1} - \left(\frac{\partial f}{\partial q}\right)_{n} h_{n}} \qquad (2.5\text{-}7)$$

$$\text{where} \quad \Xi = \left[C^{-1} + \gamma_{n+1}\left(\frac{\partial N}{\partial\sigma}\right)_{n+1}\right]^{-1}.$$

Symmetric tangent moduli are obtained when both the strain rate functions and the elastic moduli are symmetric $\left(\text{i.e., associative flow, } N = \frac{\partial f}{\partial\sigma}\right)$. Because the internal variables are evaluated at time t_{n}, "associative hardening" is not required for symmetry. Comparing these moduli to the continuum moduli provides an interesting insight. The continuum moduli for non-associative flow are defined as:

$$D = C - \frac{C\, N\left(\frac{\partial f}{\partial\sigma}\right)C}{\left(\frac{\partial f}{\partial\sigma}\right)C\, N + K_{p}} \qquad (2.5\text{-}8)$$

$$\text{where} \quad K_{p} = -\left(\frac{\partial f}{\partial q}\right)h.$$

The consistent moduli appear similar to the continuum derived moduli (Equation 2.5-8) except for the second derivative terms, which are included with the elastic terms of the consistent moduli. The contribution of the internal variables now appears in the denominator for both methods. The difference is that the hardening modulus (K_{p}) is defined at time t_{n+1} for the continuum moduli and at time t_{n} for the implicit-explicit consistent moduli.

An additional modification can be made by updating the directions that are evaluated

at time t_n by directions calculated using the previous iterate as:

$$N_{n+1}^* = N\left(\sigma_{n+1}^{(k)}, q_n^{(k-1)}\right) \tag{2.5-9}$$

$$h_n^* = h\left(\sigma_n^{(k-1)}, q_n^{(k-1)}\right) \tag{2.5-10}$$

2.6 Application of the Closest Point Method for Bounding Surface Plasticity

The Closest Point method was developed in the previous sections for typical plasticity models that are elastic within the yield surface. The Bounding Surface Plasticity model, however, uses the surface not as a yield surface, but as a bound. The complication in Bounding Surface Plasticity is that yielding can occur within the bound. With a clever choice of internal variables the model can be set up to resemble a classical yield model. This section will describe the establishment of the functions and their derivatives for the Bounding Surface Clay model.

The approach used for this development is to separate the volumetric and deviatoric components of the stress and strain relationships similar to the Cam-Clay model [Meschke and Simo, 1994]. This allows for developing the relationship between the volumetric stress (I) and the Bounding Surface size (I_0), which will reduce the number of nonlinear equations. The nonlinear elastic volumetric relationship is described in Section 1.3. Because of the Macaulay brackets in Equation 1.3-1, there are two elastic regions delineated by the transition volumetric stress (I_t). In order to remain consistent with Section 1.3, the equations in this section where $I > I_t$ are again denoted as the (a) equations, and the equations where $I < I_t$ are again denoted as the (b) equations. For this section, it is assumed that the steps that cross the transition volumetric stress are sufficiently small that the elastic relationships for each region will provide an adequate approximation for the step. Separate equations for steps crossing the transition stress are developed later in Section

3.2. Rewriting the differential relationships of the volumetric strain and stress (Equation 1.3-7) in terms of the total and plastic strains yields:

$$dI_{n+1} = I_{n+1} \, \beta \left(d\theta_{n+1} - d\theta_{n+1}^{p} \right) \tag{2.6-1a}$$

$$dI_{n+1} = I_{l} \, \beta \left(d\theta_{n+1} - d\theta_{n+1}^{p} \right) \tag{2.6-1b}$$

As described in the previous sections, to formulate the initial "trial" stress to start the Newton-Raphson iteration, an elastic prediction is made assuming no plasticity. During the plastic correction, the total volumetric strain is held constant. This results in the change in volumetric stress, during the plastic correction, being written in terms of only the plastic volumetric strain. This is given as:

$$dI_{n+1} = -K_{n+1} \, d\theta_{n+1}^{p} \tag{2.6-2}$$

$$\text{where} \quad K_{n+1} = -\beta \, I_{n+1} \qquad (I > I_{l})$$

$$K_{n+1} = -\beta \, I_{l} \qquad (I < I_{l}).$$

Because the total volumetric strain increment is fixed and applied in the first iteration, the correction which involves the developing plastic volumetric strain is negative. It must be noted that during the plastic iteration some plastic volumetric strain will be created and thus change the elastic prediction in the next iteration (see Box 2.6-1).

The relationship for the internal variable (I_0) of the Bounding Surface model is developed in Section 1.5. The differential relationship is given by Equation 1.5-7 and can be written at time t_{n+1} as:

$$dI_{o_{n+1}} = H_{n+1} \left(I_{o} \right) d\theta_{n+1}^{p} \tag{2.6-3}$$

$$\text{where} \quad H_{n+1} \left(I_{o} \right) = 3 \, I_{o_{n+1}} \, \xi \, .$$

Note that during the plastic iteration both the volumetric stress and Bounding Surface size are related to the plastic volumetric strain (Equations 2.6-2 and 2.6-3). Therefore, the differential in the Bounding Surface size can be written in terms of the differential in the volumetric stress during the plastic iteration as:

$$dI_{o_{n+1}} = -\frac{H_{n+1}}{K_{n+1}} dI_{n+1}$$ (2.6-4)

The plastic strain rates for the Bounding Surface model are defined in terms of the plasticity parameter and directions given by the "image" stresses (Equation 1.2-2). Rewriting these rates in terms of volumetric and deviatoric strains gives:

$$\dot{\theta}^p = \gamma \frac{\partial F}{\partial \bar{I}}$$ (2.6-5)

$$\dot{e}^p = \gamma \frac{\partial F}{\partial \bar{s}}$$ (2.6-6)

where $\dot{e}^p$ = plastic deviatoric strain tensor

$\bar{s} = b\,s$ = deviatoric "image" stress tensor.

The Bounding Surface function (F) used for this study is the single ellipse model [Kaliakin, 1985; Herrmann, et. al., 1985; Herrmann, et. al., 1987] as described in Section 1.4 (Equation 1.4-1).

As in the previous sections, the increments are approximated between times t_n and t_{n+1} with the backward Euler approximation, which results in:

$$\theta^p_{n+1} = \theta^p_n + \gamma_{n+1} \left(\frac{\partial F}{\partial \bar{I}} \right)_{n+1}$$ (2.6-7)

$$e^p_{n+1} = e^p_n + \gamma_{n+1} \left(\frac{\partial F}{\partial \bar{s}} \right)_{n+1}$$ (2.6-8)

Recall that the notation γ_{n+1} will be used instead of the more appropriate $\Delta t\ \gamma|_{n+1}$ for clarity.

The deviatoric stress rates are defined in terms of the deviatoric strain rates and the shear modulus (G) at time t_{n+1} and are given as:

$$\dot{s}_{n+1} = -2\,G_{n+1}\ \dot{e}^{p}_{n+1}$$
(2.6-9)

The rate equation for the loading surface (b) was developed in Section 1.7. For this formulation of the Closest Point algorithm, the variable b will be treated as an additional internal variable. From Equation 1.7-11, a backward Euler approximation yields:

$$b_{n+1} = b_n + \gamma_{n+1}\ g_{n+1}$$
(2.6-10)

$$\text{where} \quad g_{n+1} = \left(\frac{\overline{K}_p - bK_p - 3\,C\,v_o\,(1-b)\,\dfrac{I_o}{\lambda-\kappa}\left(\dfrac{\partial F}{\partial \overline{I}}\right)^2}{(I-I_c)\,\dfrac{\partial F}{\partial \overline{I}} + J\,\dfrac{\partial F}{\partial \overline{J}}} \right)_{n+1}.$$

The local residuals for the nonlinear equations are defined using the approximations of the plastic deviatoric strains (e), the plastic volumetric strain (θ) and the loading surface (b). Rewriting Equations 2.6-7, 2.6-8 and 2.6-10 gives:

$$\boldsymbol{R}_{n+1} = \boldsymbol{e}^{p}_{n+1} - \boldsymbol{e}^{p}_{n} - \gamma_{n+1}\left(\frac{\partial F}{\partial \boldsymbol{s}}\right)_{n+1}$$
(2.6-11a)

$$^{7}R_{n+1} = \theta^{p}_{n+1} - \theta^{p}_{n} - \gamma_{n+1}\left(\frac{\partial F}{\partial \overline{I}}\right)_{n+1}$$
(2.6-11b)

$$^{8}R_{n+1} = b_{n+1} - b_n - \gamma_{n+1}\ g_{n+1}$$
(2.6-11c)

where $\boldsymbol{R}$ = residual equations for the six deviatoric strain expressions

^{7}R = residual equation for the volumetric strain expression

^{8}R = residual equation for the loading surface (b) expression.

Since the internal variable for the Bounding Surface size (I_0) is expressed as a function of the plastic volumetric strain (Equation 2.6-3), it will be incorporated later in this section and will not be treated as a separate residual.

As in the general Closest Point framework, the residuals are differentiated at time t_{n+1}, noting that F is a function of the stresses I and s and the internal variables I_0 and b. The differentials of the residuals are given as:

$$dR_{n+1} = de^p_{n+1} - \gamma_{n+1}\left(\frac{\partial^2 F}{\partial s \partial s}\right)_{n+1} ds_{n+1} - \gamma_{n+1}\left(\frac{\partial^2 F}{\partial s \partial I}\right)_{n+1} dI_{n+1} - \gamma_{n+1}\left(\frac{\partial^2 F}{\partial s \partial I_o}\right)_{n+1} dI_{o_{n+1}}$$
$$- \gamma_{n+1}\left(\frac{\partial^2 F}{\partial s \partial b}\right)_{n+1} db_{n+1} - d\gamma_{n+1}\left(\frac{\partial F}{\partial s}\right)_{n+1} \tag{2.6-12a}$$

$$^7dR_{n+1} = d\theta^p_{n+1} - \gamma_{n+1}\left(\frac{\partial^2 F}{\partial \bar{I} \partial s}\right)_{n+1} ds_{n+1} - \gamma_{n+1}\left(\frac{\partial^2 F}{\partial \bar{I} \partial I}\right)_{n+1} dI_{n+1} - \gamma_{n+1}\left(\frac{\partial^2 F}{\partial \bar{I} \partial I_o}\right)_{n+1} dI_{o_{n+1}}$$
$$- \gamma_{n+1}\left(\frac{\partial^2 F}{\partial \bar{I} \partial b}\right)_{n+1} db_{n+1} - d\gamma_{n+1}\left(\frac{\partial F}{\partial \bar{I}}\right)_{n+1} \tag{2.6-12b}$$

$$^8dR_{n+1} = db_{n+1} - \gamma_{n+1}\left(\frac{\partial g}{\partial s}\right)_{n+1} ds_{n+1} - \gamma_{n+1}\left(\frac{\partial g}{\partial I}\right)_{n+1} dI_{n+1} - \gamma_{n+1}\left(\frac{\partial g}{\partial I_o}\right)_{n+1} dI_{o_{n+1}}$$
$$- \gamma_{n+1}\left(\frac{\partial g}{\partial b}\right)_{n+1} db_{n+1} - d\gamma_{n+1}\, g_{n+1} \tag{2.6-12c}$$

The differentials of the plastic volumetric and deviatoric strains (i.e., $de^p_{n+1}, d\theta^p_{n+1}$) can be expressed in terms of stresses by substituting Equation 2.6-2 and the differential form of Equation 2.6-9 into Equation 2.6-12. The internal variable I_0 is incorporated by substituting Equation 2.6-4 into Equation 2.6-12. The substitutions result in equations that

are expressed entirely in terms of stresses and internal variables and are given as:

$$dR_{n+1} = -\left(\frac{\mathbf{I}_{6x6}}{2G} + \gamma \frac{\partial^2 F}{\partial \mathbf{s}\, \partial \mathbf{s}}\right)_{n+1} d\mathbf{s}_{n+1} - \gamma_{n+1}\left(\frac{\partial^2 F}{\partial \mathbf{s}\, \partial I} - \frac{H}{K}\frac{\partial^2 F}{\partial \mathbf{s}\, \partial I_o}\right)_{n+1} dI_{n+1}$$

$$-\gamma_{n+1}\left(\frac{\partial^2 F}{\partial \mathbf{s}\, \partial b}\right)_{n+1} db_{n+1} - d\gamma_{n+1}\left(\frac{\partial F}{\partial \mathbf{s}}\right)_{n+1}$$

(2.6-13a)

$${}^7dR_{n+1} = -\gamma_{n+1}\left(\frac{\partial^2 F}{\partial \bar{I}\, \partial \mathbf{s}}\right)_{n+1} d\mathbf{s}_{n+1} - \left\{\frac{1}{K} + \gamma\left(\frac{\partial^2 F}{\partial \bar{I}\, \partial I} - \frac{H}{K}\frac{\partial^2 F}{\partial \bar{I}\, \partial I_o}\right)\right\}_{n+1} dI_{n+1}$$

$$-\gamma_{n+1}\left(\frac{\partial^2 F}{\partial \bar{I}\, \partial b}\right)_{n+1} db_{n+1} - d\gamma_{n+1}\left(\frac{\partial F}{\partial \bar{I}}\right)_{n+1}$$

(2.6-13b)

$${}^8dR_{n+1} = -\gamma_{n+1}\left(\frac{\partial g}{\partial \mathbf{s}}\right)_{n+1} d\mathbf{s}_{n+1} - \gamma_{n+1}\left(\frac{\partial g}{\partial I} - \frac{H}{K}\frac{\partial g}{\partial I_o}\right)_{n+1} dI_{n+1}$$

$$+\left(1 - \gamma\frac{\partial g}{\partial b}\right)_{n+1} db_{n+1} - d\gamma_{n+1}\, g_{n+1}$$

(2.6-13c)

The Bounding Surface function (F) is differentiated noting that it is a function of s, I, I_0 and b. This differentiation results in the discrete consistency condition which is given as:

$$dF = \left(\frac{\partial F}{\partial \mathbf{s}}\right)_{n+1} d\mathbf{s}_{n+1} + \left(\frac{\partial F}{\partial I}\right)_{n+1} dI_{n+1} + \left(\frac{\partial F}{\partial I_o}\right)_{n+1} dI_{o_{n+1}} + \left(\frac{\partial F}{\partial b}\right)_{n+1} db_{n+1} = 0$$

(2.6-14)

Recalling the relationship between I and I_0 (Equation 2.6-4). Equation 2.6-14 can be rewritten as:

$$dF = \left(\frac{\partial F}{\partial \mathbf{s}}\right)_{n+1} d\mathbf{s}_{n+1} + \left(\frac{\partial F}{\partial I} - \frac{H}{K}\frac{\partial F}{\partial I_o}\right)_{n+1} dI_{n+1} + \left(\frac{\partial F}{\partial b}\right)_{n+1} db_{n+1} = 0$$

(2.6-15)

The residual differentials and discrete consistency condition can be written in matrix form as:

$$dR_{n+1} = A_{n+1}^{-1} \, d\Sigma_{n+1} - d\gamma_{n+1} \, \mathbf{Z}_{n+1} \tag{2.6-16}$$

$$\nabla F_{n+1}^{(k)} \, d\Sigma_{n+1}^{(k)} = 0 \tag{2.6-17}$$

where $\quad \Sigma_{n+1} = \begin{bmatrix} s & I & B \end{bmatrix}_{n+1}^{T}$

$$\mathbf{Z}_{n+1} = \begin{bmatrix} \dfrac{\partial F}{\partial s} & \dfrac{\partial F}{\partial \bar{I}} & g \end{bmatrix}_{n+1}^{T}$$

$$\nabla F_{n+1}^{(k)} = \begin{bmatrix} \dfrac{\partial F}{\partial s} & \left(\dfrac{\partial F}{\partial I} - \dfrac{H}{K}\dfrac{\partial F}{\partial I_o} \right) & \dfrac{\partial F}{\partial b} \end{bmatrix}_{n+1}^{(k)}$$

$$A_{n+1}^{-1} = \begin{bmatrix} -\dfrac{\mathbf{I}_{6x6}}{2G} - \gamma\left(\dfrac{\partial^2 F}{\partial s\,\partial s}\right) & -\gamma\left(\dfrac{\partial^2 F}{\partial s\,\partial I} - \dfrac{H}{K}\dfrac{\partial^2 F}{\partial s\,\partial I_o}\right) & -\gamma\left(\dfrac{\partial^2 F}{\partial s\,\partial b}\right) \\[2ex] -\gamma\left(\dfrac{\partial^2 F}{\partial I\,\partial s}\right) & -\dfrac{1}{K} - \gamma\left(\dfrac{\partial^2 F}{\partial \bar{I}\,\partial I} - \dfrac{H}{K}\dfrac{\partial^2 F}{\partial \bar{I}\,\partial I_o}\right) & -\gamma\left(\dfrac{\partial^2 F}{\partial \bar{I}\,\partial b}\right) \\[2ex] -\gamma\left(\dfrac{\partial g}{\partial s}\right) & -\gamma\left(\dfrac{\partial g}{\partial I} - \dfrac{H}{K}\dfrac{\partial g}{\partial I_o}\right) & 1-\gamma\left(\dfrac{\partial g}{\partial b}\right) \end{bmatrix}_{n+1} .$$

The Jacobian matrix (A) can be simplified by noting that the second derivatives involving orthogonal directions (i.e., I and s or I_0 and s) are zero. The matrix is reduced to:

$$A_{n+1}^{-1} = \begin{bmatrix} -\dfrac{\mathbf{I}_{6x6}}{2G} - \gamma\left(\dfrac{\partial^2 F}{\partial s\,\partial s}\right) & 0 & -\gamma\left(\dfrac{\partial^2 F}{\partial s\,\partial b}\right) \\[2ex] 0 & -\dfrac{1}{K} - \gamma\left(\dfrac{\partial^2 F}{\partial \bar{I}\,\partial I} - \dfrac{H}{K}\dfrac{\partial^2 F}{\partial \bar{I}\,\partial I_o}\right) & -\gamma\left(\dfrac{\partial^2 F}{\partial \bar{I}\,\partial b}\right) \\[2ex] -\gamma\left(\dfrac{\partial g}{\partial s}\right) & -\gamma\left(\dfrac{\partial g}{\partial I} - \dfrac{H}{K}\dfrac{\partial g}{\partial I_o}\right) & 1-\gamma\left(\dfrac{\partial g}{\partial b}\right) \end{bmatrix}_{n+1} \tag{2.6-18}$$

The second derivatives of the Bounding Surface function (F) are derived in Appendix A. Because of the complex form of the b rate equation (Equation 2.6-10), the derivatives of g are approximated with finite difference formulas.

As in the previous sections, both the residuals and consistency condition are linearized (i.e., Taylor series expansion to the linear term) and set to zero. The assumption is made that step sizes are sufficiently small so that the differentials can be approximated with finite increments. The resulting equations, including an iteration counter (k), are given as:

$$R_{n+1}^{(k)} + \Delta R_{n+1}^{(k)} = R_{n+1}^{(k)} + \left(A^{-1}\right)_{n+1}^{(k)} \Delta \Sigma_{n+1}^{(k)} + \Delta \gamma_{n+1}^{(k)} \, Z_{n+1}^{(k)} = 0 \qquad (2.6\text{-}19)$$

$$F_{n+1}^{(k)} + \nabla F_{n+1}^{(k)} \, \Delta \Sigma_{n+1}^{(k)} = 0 \qquad (2.6\text{-}20)$$

Equation 2.6-19 is rearranged to solve for the unknown increments in s, I and b, and is given as:

$$\Delta \Sigma_{n+1}^{(k)} = -A_{n+1}^{(k)} \left[R + \Delta \gamma \, Z\right]_{n+1}^{(k)} \qquad (2.6\text{-}21)$$

Equation 2.6-21 is substituted into Equation 2.6-20 and solved for the increment in the plasticity parameter ($\Delta\gamma$), resulting in:

$$\Delta \gamma_{n+1}^{(k)} = \frac{F_{n+1}^{(k)} - \nabla F_{n+1}^{(k)} \, A_{n+1}^{(k)} \, R_{n+1}^{(k)}}{\nabla F_{n+1}^{(k)} \, A_{n+1}^{(k)} \, Z_{n+1}^{(k)}} \qquad (2.6\text{-}22)$$

Once the increment in the plasticity parameter is obtained, the increments in the stresses (s and I) and internal variables (b) are found with Equation 2.6-21. The internal variable (I_0) representing the Bounding Surface size is indirectly included via the plastic volumetric strain (Equation 2.6-3). The increments in plastic volumetric and deviatoric

strains are calculated using Equations 2.6-2 and 2.6-9 and are given as:

$$\begin{bmatrix} \Delta e^p \\ \Delta \theta^p \end{bmatrix}^{(k)}_{n+1} = -\begin{bmatrix} \dfrac{1}{2\,G} & \dfrac{1}{K} \end{bmatrix}^{(k)}_{n+1} \begin{bmatrix} \Delta s \\ \Delta I \end{bmatrix}^{(k)}_{n+1} \tag{2.6-23}$$

$$\text{where} \quad \mathbf{1} = \begin{bmatrix} 1 & 1 & 1 & 1 & 1 & 1 \end{bmatrix}.$$

The plastic strains and internal variable (b) are then updated during the iteration by:

$$e^{p^{(k+1)}}_{n+1} = e^{p^{(k)}}_{n+1} + \Delta e^{p^{(k)}}_{n+1} \tag{2.6-24a}$$

$$\theta^{p^{(k+1)}}_{n+1} = \theta^{p^{(k)}}_{n+1} + \Delta \theta^{p^{(k)}}_{n+1} \tag{2.6-24b}$$

$$b^{(k+1)}_{n+1} = b^{(k)}_{n+1} + \Delta b^{(k)}_{n+1} \tag{2.6-24c}$$

The elastic "trial" stress is calculated with the plastic strains initially set to the values at the end of the last global step. The values of I and I_o are calculated with Equations 1.3-8 and 1.5-8, respectively. The deviatoric stress (s) is calculated at time t_{n+1} by:

$$s_{n+1} = 2G_{n+1}\left(e_{n+1} - e^p_{n+1}\right) \tag{2.6-25}$$

The Bounding Surface function (F) is evaluated with the "trial" stresses and the internal variable (b) initialized with the value at time t_n. If F is less than or equal to zero, the step is elastic and the new stresses are sent back to the main routine. It is important to note that the internal variable (b) is a measure from the current stress point to the Bounding Surface and has to be recalculated elastically (not evolved), even for an elastic step. If F is greater than zero, the trial stress state is used as the initial guess for the plastic iteration. A case that is unique to the Bounding Surface model occurs when the elastic "trial" step is outside of the elastic bound but does not go outside of the Bounding Surface. Treating the stress measure (b) as an internal variable allows for proper evaluation of the consistency condition. Using the "trial" stresses and b evaluated at time t_n results in the image stress state $\left(\overline{\sigma}_{n+1}\right)$ being outside of the bound ($F > 0$), thus indicating plasticity. This is shown graphically in

Figure 2.6-1. The plastic iteration begins evolving the plastic strains and the internal variable (now using Equation 2.6-10) and continues until the value F is less than some tolerance associated with the Bounding Surface function and the norm of the residuals is less than some tolerance associated with the residuals. At convergence the image stress state coincides with the bounding surface. The plastic algorithm is shown in Box 2.6-1. The algorithmically consistent tangent moduli are the same as described in Section 2.4 (Equation 2.4-7).

Box 2.6-1. Fully Implicit Closest Point Algorithm for Bounding Surface Plasticity

1. **Given:** $\theta_{n+1}, e_{n+1}, \theta_n^p, e_n^p, b_n$

2. **Initialize:** $k = 0, \quad \gamma_{n+1}^{(0)} = 0, \quad \theta_{n+1}^{p^{(0)}} = \theta_n^p, \quad b_{n+1}^{(0)} = b_n, \quad e_{n+1}^{p^{(0)}} = e_n^p$

3. **Evaluate I, I_o, s and associated terms:**

$$I_{n+1} = I_n \, e^{\beta\left(\theta_{n+1}^e - \theta_n^e\right)} \qquad K_{n+1}^{(k)} = -\beta \, I_{n+1}^{(k)} \quad \left(I > I_l\right)$$

$$I_{n+1} = \beta \, I_l \left(\theta_{n+1}^e - \theta_n^e\right) \quad K_{n+1}^{(k)} = -\beta \, I_l \quad \left(I < I_l\right)$$

$$I_{o_{n+1}} = I_{o_n} \, e^{\xi\left(\theta_{n+1}^p - \theta_n^p\right)} \qquad H_{n+1}^{(k)} = 3\xi \, I_{o_{n+1}} \qquad s_{n+1} = 2\,G_{n+1}\left(e_{n+1} - e_{n+1}^p\right)$$

4. **Evaluate the functional and residuals:**

$$F_{n+1}^{(k)} = F\!\left(s_{n+1}^{(k)}, I_{n+1}^{(k)}, I_{o_{n+1}}^{(k)}, b_{n+1}^{(k)}\right) \qquad R_{n+1}^{(k)} = \begin{bmatrix} e_{n+1}^p - e_n^p \\ \theta_{n+1}^p - \theta_n^p \\ b_{n+1} - b_n \end{bmatrix}^{(k)} + \gamma_{n+1}^{(k)} \, Z_{n+1}^{(k)}$$

5. **Check convergence:** If $F_{n+1}^{(k)} \langle \text{tolerance}_F$ and $\left\| R_{n+1}^{(k)} \right\| \langle \text{tolerance}_R$ Then : EXIT

6. **Compute derivatives and assemble matrices (note, derivatives of g are estimated via finite difference):**

$$A_{n+1}^{-1} = \begin{bmatrix} -\dfrac{\mathbf{I}_{6x6}}{2G} - \gamma\left(\dfrac{\partial^2 F}{\partial s \partial s}\right) & 0 & -\gamma\left(\dfrac{\partial^2 F}{\partial s \partial b}\right) \\[2ex] 0 & -\dfrac{1}{K} - \gamma\left(\dfrac{\partial^2 F}{\partial I \partial I} - \dfrac{H}{K}\dfrac{\partial^2 F}{\partial I \partial I_o}\right) & -\gamma\left(\dfrac{\partial^2 F}{\partial I \partial b}\right) \\[2ex] -\gamma\left(\dfrac{\partial g}{\partial s}\right) & -\gamma\left(\dfrac{\partial g}{\partial I} - \dfrac{H}{K}\dfrac{\partial g}{\partial I_o}\right) & 1 - \gamma\left(\dfrac{\partial g}{\partial b}\right) \end{bmatrix}_{n+1}$$

7. **Solve for increment in stresses and internal variables,**

$$\Delta\gamma_{n+1}^{(k)} = \frac{F_{n+1}^{(k)} - \nabla F_{n+1}^{(k)} \, A_{n+1}^{(k)} \, R_{n+1}^{(k)}}{\nabla F_{n+1}^{(k)} \, A_{n+1}^{(k)} \, Z_{n+1}^{(k)}} \qquad \Delta\Sigma_{n+1}^{(k)} = -A_{n+1}^{(k)} \left[R + \Delta\gamma \, Z\right]_{n+1}^{(k)}$$

8. **Solve for plastic strains:** $\begin{bmatrix} \Delta e^p \\ \Delta\theta^p \end{bmatrix}_{n+1}^{(k)} = -\begin{bmatrix} \dfrac{1}{2\,G} & \dfrac{1}{K} \end{bmatrix}_{n+1}^{(k)} \begin{bmatrix} \Delta s \\ \Delta I \end{bmatrix}_{n+1}^{(k)}$

9. **Update:** $e_{n+1}^{p^{(k+1)}} = e_{n+1}^{p^{(k)}} + \Delta e_{n+1}^{p^{(k)}}; \; \theta_{n+1}^{p^{(k+1)}} = \theta_{n+1}^{p^{(k)}} + \Delta\theta_{n+1}^{p^{(k)}}; \; b_{n+1}^{(k+1)} = b_{n+1}^{(k)} + \Delta b_{n+1}^{(k)}; \; \gamma_{n+1}^{(k+1)} = \gamma_{n+1}^{(k)} + \Delta\gamma_{n+1}^{(k)}$

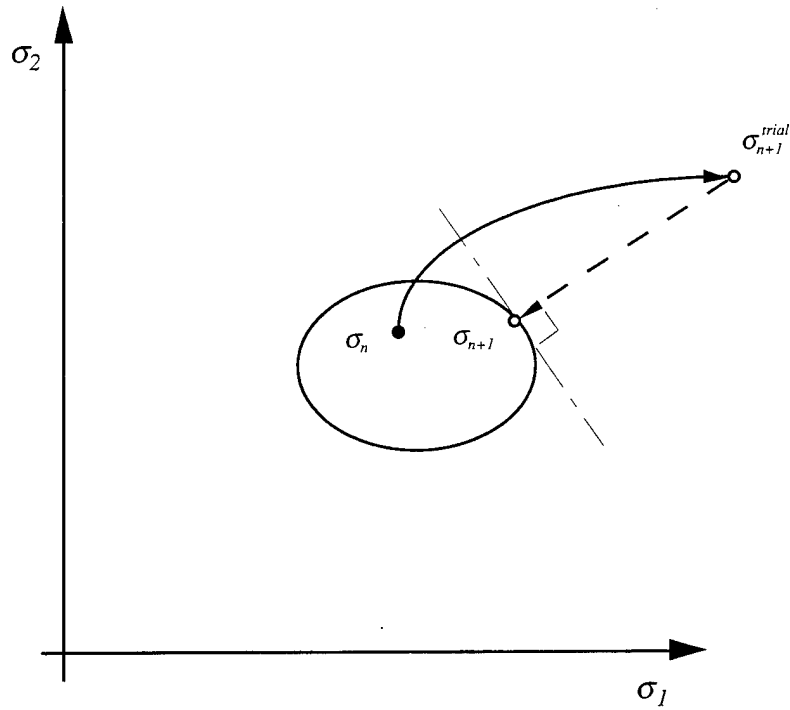10. **Set:** $k \leftarrow k+1$ and go to step 3.

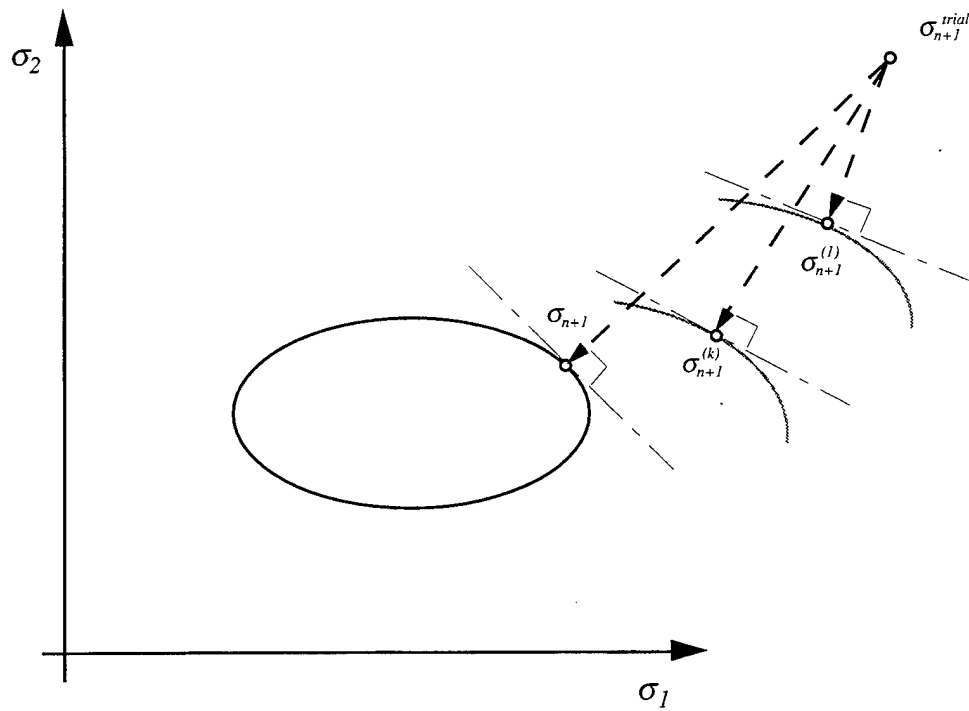Figure 2.1-1. Closest Point Projection - Simple Model.

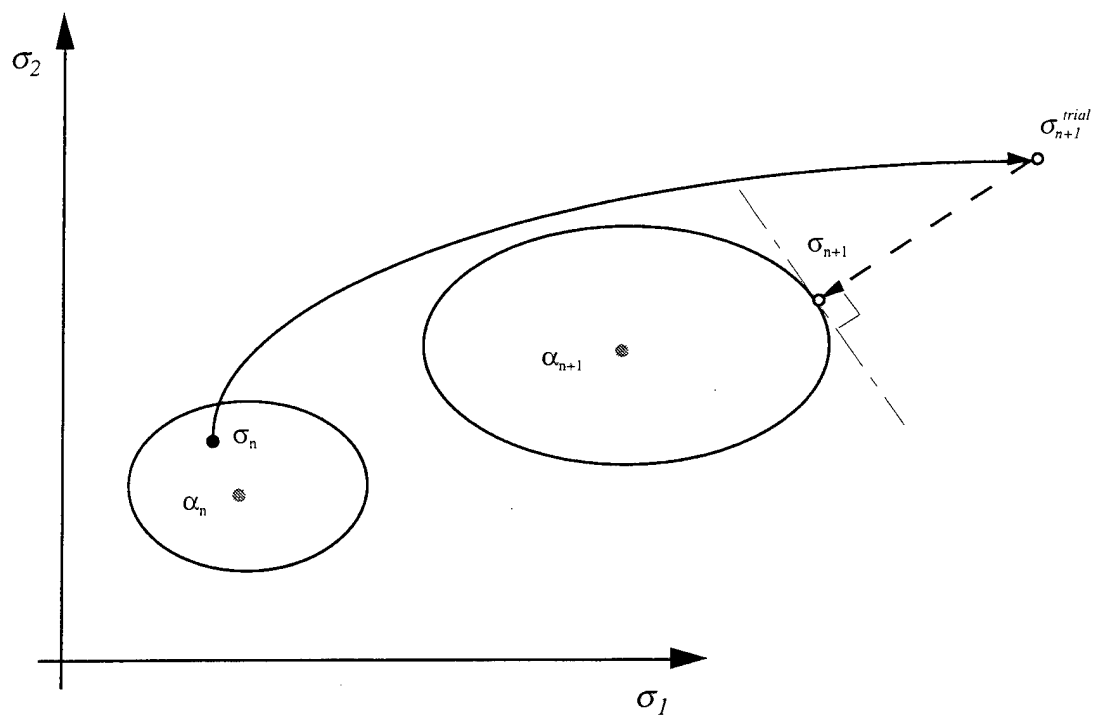Figure 2.1-2. Plastic Iteration in Closest Point Projection Method.

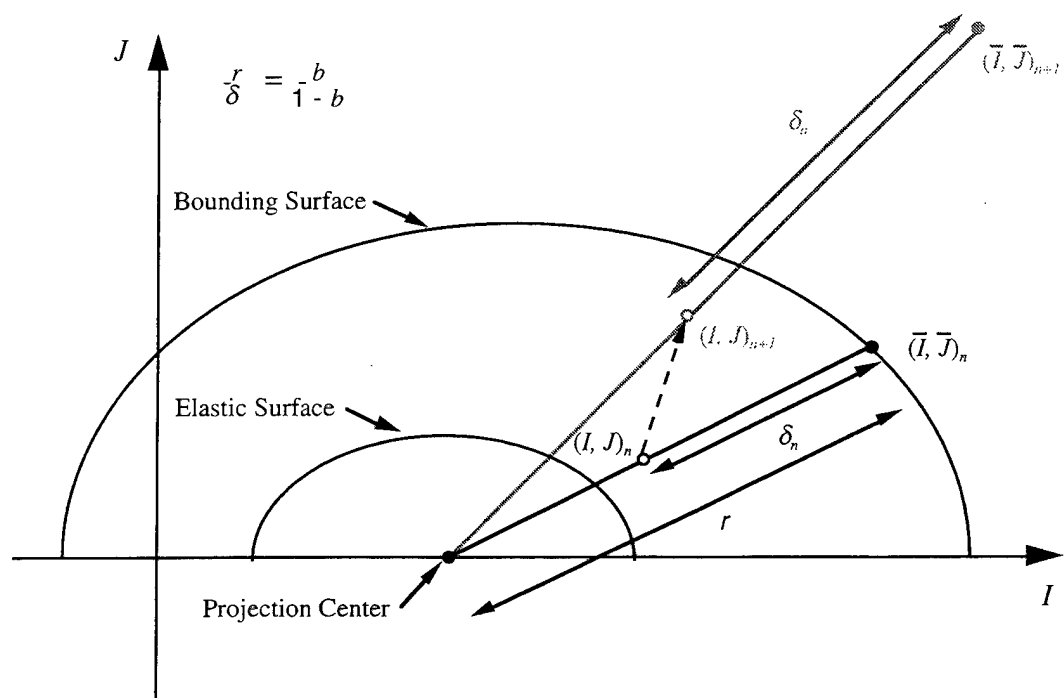Figure 2.3-1. Closest Point Projection - General Model.

Figure 2.6-1. Use of Internal Variable b for Determining Plasticity within the Bound.

3. Reduced Newton Method

The Reduced Newton method was developed by Leonard Herrmann for integrating the two-dimensional Cam-Clay model [Roscoe and Burland, 1968]. The method maps the stress rate equations and the consistency condition into a single nonlinear equation and integrates them with backwards Euler integration using Newton-Raphson iteration. The method incorporates uniform substepping and has been implemented into a steady-state finite element program [Herrmann, 1997].

For simplicity, the application of the method will be restricted to the case where there is no dependency on the "lode" angle (it is assumed that the results of compression and extension triaxial tests are approximately the same). This special case will be referred to as a two-invariant model.

Applying the Reduced Newton method to the two-invariant Bounding Surface Plasticity model for clays requires a second equation that determines the level of plasticity occurring within the Bounding Surface (Equation 1.2-4). This section describes the method applied to the two-invariant version of the clay model.

Section 3.1 simplifies the Bounding Surface model for clays to a two-invariant form. Section 3.2 describes elastic stress paths that begin inside the elastic nucleus and intersect with it. The elastic algorithmic consistent tangent moduli are developed in Section 3.3. Section 3.4 explains the "Reduced Newton" stress point algorithm for plastic calculations. The corresponding plastic algorithmic consistent tangent moduli are developed in Section 3.5. Finally, Section 3.6 discusses the handling of the unloading stress path.

3.1 Two Invariant-Bounding Surface Plasticity

Section 1 describes the Bounding Surface Plasticity model for clays when all three stress invariants are involved. The model can be simplified when it is only a function of two invariants. The Bounding Surface becomes in this case:

$$F = \frac{a_2}{a_1} \bar{J}^2 + \left(\bar{I} - \rho I_o \right)^2 - \frac{1}{a_1} I_o^2 = 0 \qquad (3.1\text{-}1)$$

where F = Bounding Surface function

$\bar{I} = b(I - I_c) + I_c$

I = first stress invariant = $(\sigma_{11} + \sigma_{22} + \sigma_{33})$

b = measure of distance between stress point and surface (> 1)

$I_c = CI_o$

C = material constant defining the projection center location

I_o = bound size (i.e., intersection of bound with volumetric axis)

$\bar{J} = bJ$

J = second stress invariant $\sqrt{\frac{1}{2} s_{ij} s_{ij}}$

$$a_1 = \frac{1}{(1-\rho)^2} \qquad a_2 = \frac{1}{N^2 \rho^2} \qquad \rho = \frac{1}{R} \qquad N = \frac{M}{\sqrt{27}}$$

M = slope of critical state line in triaxial space (assumed the same in extension and compression)

R = shape of ellipsoid.

This function uses the soil mechanics sign convention of compression as positive and tension as negative. The surface is shown in Figure 3.1-1.

3.2 Elastic Calculations

For stress paths starting within the elastic nucleus, a closed form solution can be found to predict the intersection of the path with the elastic nucleus. The beginning and end of the step are denoted by t_b and t_{elas} respectively. Therefore, $I(t_b) = I_b$ is used for the beginning of the step and $I(t_{elas}) = I_{elas}$ for the end of the step.

To find the results of an increment of strain with a beginning value and an assumed proportional strain history for $t = 0 \rightarrow 1$, a relative time scale is used since viscous effects are not present. The strains can be written as:

$$\varepsilon_{ij}(t) = \varepsilon_{ij_b} + \Delta\varepsilon_{ij}t \tag{3.2-1}$$

The rates of the total, deviatoric and volumetric strains are:

$$\dot{\varepsilon}_{ij} = \Delta\varepsilon_{ij}, \quad \dot{e}_{ij} = \Delta e_{ij}, \quad \dot{\theta} = \Delta\theta \tag{3.2-2}$$

The Bounding Surface Plasticity model for clays uses the log-linear relationship for the volumetric stress versus the void ratio for volumetric stresses greater than the transition stress (I_t) and a linear-linear relationship for stresses less than I_t. This is shown in Figure 3.2-1 and discussed more thoroughly in Section 1.3.

Now at some point, t in the interval Equation 1.3-8 can be written in the form:

$$I = I_b e^{\beta\left(\theta^e - \theta_b^e\right)} \qquad (I > I_t) \tag{3.2-3a}$$

$$I = \beta I_t \left(\theta^e - \theta_b^e\right) + I_b \qquad (I < I_t) \tag{3.2-3b}$$

It is assumed that the path from time t_b to t will be entirely elastic

(i.e., $\theta^e - \theta^e_b = \Delta\theta^e t$). Because this is an elastic step ($\Delta\theta^e = \Delta\theta$), however, the "e"

notation will be used to emphasize of the nature of the elastic step. The volumetric

expressions can be rewritten in terms of the strain increment as:

$$I = I_b e^{\beta\Delta\theta^e t} \qquad\qquad (I > I_l) \qquad (3.2\text{-}4a)$$

$$I = \beta I_l \Delta\theta^e t + I_b \qquad\qquad (I < I_l) \qquad (3.2\text{-}4b)$$

The tangent bulk modulus is a function of the pressure only and can be found by

taking the derivative of Equation 3.2-3 with respect to the volumetric strain:

$$B = \frac{1}{3}\frac{dI}{d\theta^e} = \frac{I}{3}\beta \qquad\qquad (I > I_l) \qquad (3.2\text{-}5a)$$

$$B = \frac{I_l}{3}\beta \qquad\qquad (I < I_l) \qquad (3.2\text{-}5b)$$

Writing the modulus in terms of the behavior at the beginning of the step, the

following is obtained:

$$B = B_b e^{\beta\Delta\theta^e t} \qquad\qquad (I > I_l) \qquad (3.2\text{-}6a)$$

$$B = B_b \qquad\qquad (I < I_l) \qquad (3.2\text{-}6b)$$

where B_b = tangent bulk modulus at the beginning of the step.

The shear modulus at time t can be expressed in terms of the bulk modulus as:

$$G = \eta B \qquad\qquad (3.2\text{-}7)$$

where $\eta = \dfrac{3(1-2\upsilon)}{2(1+\upsilon)}$.

Writing this in terms of the value at the beginning of the step, the following is obtained:

$$G = G_b e^{\beta \Delta \theta^e t} \qquad\qquad (I > I_l) \qquad (3.2\text{-}8a)$$

$$G = G_b \qquad\qquad (I < I_l) \qquad (3.2\text{-}8b)$$

where G_b = shear modulus at the beginning of the step.

The relationship between the deviatoric stress rate and the deviatoric strain rate is given as:

$$\dot{s}_{ij} = 2G \, \dot{e}^e_{ij} \qquad\qquad (3.2\text{-}9)$$

Substituting Equation 3.2-8 into 3.2-9, the deviatoric stress rate can be written as:

$$\dot{s}_{ij} = 2G_b e^{\beta \Delta \theta^e t} \, \dot{e}^e_{ij} \qquad\qquad (I > I_l) \qquad (3.2\text{-}10a)$$

$$\dot{s}_{ij_{n+1}} = 2G_b \, \dot{e}^e_{ij} \qquad\qquad (I < I_l) \qquad (3.2\text{-}10b)$$

Integrating the above expressions from 0 to t yields:

$$s_{ij}(t) = 2G_b \, \Delta e^e_{ij} f(t) + s_{ij_b} \qquad\qquad (3.2\text{-}11)$$

where $\quad f(t) = \dfrac{e^{\beta \Delta \theta^e t} - 1}{\beta \Delta \theta^e} \qquad (I > I_l)$

$$f(t) = t \qquad\qquad (I < I_l)$$

Using the definition for $f(t)$ in Equation 3.2-11, Equation 3.2-4 can be rewritten as:

$$I = \beta \Delta \theta^e f(t) g(I) + I_b \qquad\qquad (3.2\text{-}12)$$

where $\quad g(I) = I_b \qquad\qquad (I > I_l)$

$$g(I) = I_l \qquad\qquad (I < I_l)$$

The following definitions will be required for the development of this method:

$$I^2 = \left(\beta\Delta\theta^e f(t)g(I)\right)^2 + 2\beta\Delta\theta^e f(t)g(I)\, I_b + I_b^2 \qquad (3.2\text{-}13)$$

$$\bar{I} = bI + (1-b)I_c \qquad (3.2\text{-}14)$$

$$\bar{I}^2 = (bI)^2 + 2b(1-b)I_c I + (1-b)^2 I_c^2 \qquad (3.2\text{-}15)$$

$$J^2 = \tfrac{1}{2}s_{ij}s_{ij} = \left(2G_b f(t)\right)^2 \chi_1 + 2G_b f(t)\,\chi_2 + J_b^2 \qquad (3.2\text{-}16)$$

$$\bar{J} = b\, J \qquad (3.2\text{-}17)$$

where $\quad \chi_1 = \tfrac{1}{2}\Delta e_{ij}^e \Delta e_{ij}^e$

$$\chi_2 = s_{ij_b}\Delta e_{ij}^e.$$

Now the value of $t = t^*$ is defined where the stress path intersects the elastic surface. The equation for the elastic surface is given by Equation 3.1-1 using the value of b that defines the size of the elastic surface ($b_{elastic}$ in Equation 1.6-5). Replacing b with $b_{elastic}$ and t with t^* in Equations 3.2-13 through 3.2-17 and substituting these equations into Equation 3.1-1 gives:

$$F = q_2 f^2\left(t^*\right) + q_1 f\left(t^*\right) + q_0 = 0 \qquad (3.2\text{-}18)$$

where $\quad q_2 = \dfrac{a_2}{a_1}\left(2b_{elastic}\, G_b\right)^2 \chi_1 + \left(b_{elastic}\beta\Delta\theta^e g(I)\right)^2$

$$q_1 = \dfrac{a_2}{a_1}b_{elastic}^2 2G_b\chi_2 + 2b_{elastic}^2\beta\Delta\theta^e g(I)\, I_b$$

$$+ 2b_{elastic}\left((1 - b_{elastic})I_c - \rho I_o\right)\beta\Delta\theta^e g(I)$$

$q_0 = F$ evaluated at time t_b.

The above equation can be solved for f^* ($f^* = f(t^*)$) using the quadratic formula:

$$f^* = \frac{-q_1 \pm \sqrt{q_1^2 - 4q_2 q_0}}{2q_2}$$

(3.2-19)

Possibilities for these roots are shown in Figure 3.2-2. For a strain increment in a positive direction, the positive root is needed (shown in Figure 3.2-2a); hence the + sign is used in Equation 3.2-19. For a strain increment in a negative direction, the roots would reverse; hence, the + sign would still be used. For stress points close to the elastic surface and a strain increment in a positive direction, the root is near zero (as shown Figure 3.2-2b) and still requires using the + sign in Equation 3.2-19. It is important to note that round-off error could actually cause the root to become complex (i.e., the term in the radical may be negative). In that case, the root is then taken to be zero. For stress points close to the elastic surface and a strain increment in a negative direction, the positive root is needed (shown in Figure 3.2-2c) thus requiring the + sign. When the direction is tangent to the surface (as shown in Figure 3.2-2d) two zero roots are the result. In all cases, however, the + sign is used before the radical in order to ensure a positive root.

At this point, the length of the elastic step (s) is sought. The value of s will be equal to the value of t^* where the stress path intersects the elastic surface, or the upper limit of $t = 1$ when the step is entirely elastic. Thus, two questions must be considered in assigning the elastic step size:

    1) Is the indicated step greater than 1? (indicating that the strain step is

    entirely elastic, as in Equation 3.2-1)

    2) Is the transition stress crossed?

One approach is to evaluate I (from Equation 3.2-12) and test for the crossing of the transition stress. However when the indicated step size is very large, numerical problems could occur, especially for $I < 0$. Therefore, the step size tests are done on the variable f

where f is defined in Equation 3.2-11. The limit on the value of f for $s \le 1$ is:

$$f_1 = \frac{e^{\beta\Delta\theta} - 1}{\beta\Delta\theta} \qquad\qquad (I > I_t) \qquad (3.2\text{-}20a)$$

$$f_1 = 1 \qquad\qquad (I < I_t) \qquad (3.2\text{-}20b)$$

To determine whether the stress path has crossed the transition stress (I_t), the value of f when the transition stress line is crossed is found as follows:

$$f_t = \frac{I_t - I_b}{\beta\,\Delta\theta\,I_b} \qquad\qquad (I > I_t) \qquad (3.2\text{-}21a)$$

$$f_t = \frac{I_t - I_b}{\beta\,\Delta\theta\,I_t} \qquad\qquad (I < I_t) \qquad (3.2\text{-}21b)$$

If the path has crossed the transition stress, the elastic calculation is done as two steps (e.g., the first step is up to I_t and the second is beyond).

The quantity f^* is first found using Equation 3.2-19, then compared against Equations 3.2-20 and 3.2-21. The smallest value of f is taken:

$$f_{min} = \min\,[\,f^*, f_1, f_t\,] \qquad\qquad\qquad (3.2\text{-}22)$$

The elastic step size (s) is determined from Equation 3.2-11:

$$s = \frac{1}{\beta\Delta\theta^e}\ln\!\left(\beta\Delta\theta^e f_{min} + 1\right) \qquad\qquad (I > I_t) \qquad (3.2\text{-}23a)$$

$$s = f_{min} \qquad\qquad (I < I_t) \qquad (3.2\text{-}23b)$$

Once the value of s is found, t is set to s and this result is substituted into Equation 3.2.12 to find the value of the volumetric stress (I_{elas}). When $I > I_t$ and $\Delta\theta = 0$, the equations simplify to:

$$I_{elas} = I_b \qquad s_{ij_{elas}} = 2G_b\Delta e_{ij}s \qquad\qquad (3.2\text{-}24)$$

The stresses at the end of the elastic step are determined by:

$$\sigma_{ij_{elas}} = \sigma_{ij_b} + 2G_b \Delta e_{ij}^e \ f(s) + \tfrac{1}{3} \Delta I \delta_{ij} \tag{3.2-25}$$

where $\Delta I = \beta \ \Delta \theta^e \ f(s) g(I)$.

Once the stresses are calculated, the loading surface measure (b) is updated along with the stresses. If $s < 1.0$ then the remainder of the step (i.e., $t^* \le t \le 1$) is plastic. The updated values (I_{elas}, etc.) are now the beginning values for the start of the plastic step (or the beginning values of the second elastic step if the transition stress is crossed). The flow chart for the elastic evaluation is shown in Figure 3.2-3.

3.3 Elastic Contribution to the Global Jacobian

Once the length of the elastic step (s) is found, the elastic contribution to the global Jacobian matrix $\left(\dfrac{\partial \sigma_{ij}|_s}{\partial \Delta \varepsilon_{kl}} \right)$ must be calculated. Recalling the development of the elastic step in Section 3.2, the elastic Jacobian is also evaluated in terms of deviatoric and volumetric components. The decomposition of the stress tensor is given as:

$$\sigma_{ij} = s_{ij} + \tfrac{1}{3} I \delta_{ij} \tag{3.3-1}$$

where σ_{ij} = total stress

s_{ij} = deviatoric stress

I = volumetric stress ($\sigma_{11} + \sigma_{22} + \sigma_{33}$).

Differentiating the stress at s with respect to the increment of strain results in:

$$\frac{\partial \sigma_{ij}|_s}{\partial \Delta \varepsilon_{ij}} = \frac{\partial s_{ij}|_s}{\partial \Delta \varepsilon_{ij}} + \tfrac{1}{3} \delta_{ij} \frac{\partial I|_s}{\partial \Delta \varepsilon_{ij}} \tag{3.3-2}$$

The volumetric portion can be evaluated by differentiating Equation 3.2-4 with respect to the strain increment and setting $t = s$:

$$\frac{\partial I|_s}{\partial \Delta \varepsilon_{kl}} = \beta \, I \, s \delta_{kl} \qquad (I > I_t) \qquad (3.3\text{-}3a)$$

$$\frac{\partial I|_s}{\partial \Delta \varepsilon_{kl}} = I_t \, \beta \, s \delta_{kl} \qquad (I < I_t) \qquad (3.3\text{-}3b)$$

The deviatoric portion is evaluated by differentiating Equation 3.2-11 with respect to the strain increment:

$$\frac{\partial s_{ij}|_s}{\partial \Delta \varepsilon_{kl}} = 2G_b \left(\frac{\partial \Delta e^e_{ij}}{\partial \Delta \varepsilon_{kl}} \frac{e^{\beta \Delta \theta^e s} - 1}{\beta \Delta \theta^e} + \frac{\partial \Delta \theta^e}{\partial \Delta \varepsilon_{kl}} \frac{\Delta e^e_{ij}}{\Delta \theta^e} \left(s e^{\beta \Delta \theta^e s} - \frac{e^{\beta \Delta \theta^e s} - 1}{\beta \Delta \theta^e} \right) \right) \quad (I > I_t) \qquad (3.3\text{-}4a)$$

$$\frac{\partial s_{ij}|_s}{\partial \Delta \varepsilon_{kl}} = 2G_b s \frac{\partial \Delta e^e_{ij}}{\partial \Delta \varepsilon_{kl}} \qquad (I < I_t) \qquad (3.3\text{-}4b)$$

For stress paths that cross through the transition stress (I_t), the values on both sides of I_t contribute to the global Jacobian. In order to develop their respective contributions, consider the current stress which is a function of the previous stress and strain increment:

$$\sigma_{ij} = \sigma_{ij} \left(\sigma_{kl_b}, \Delta \varepsilon_{kl} \right) \qquad (3.3\text{-}5)$$

Now if two (or more) steps are taken (i.e., $\sigma_b \rightarrow \sigma_{s_1} \rightarrow \sigma_{s_2}$), the final stress can be written as a function of the intermediate stress and a portion of the strain increment:

$$\sigma_{ij_{s_2}} = \sigma_{ij} \left(\sigma_{kl_{s_1}}, (s_2 - s_1) \Delta \varepsilon_{kl} \right) \qquad (3.3\text{-}6)$$

where s_1 = length of first portion of the step

s_2 = length of second portion of the step.

Differentiating Equation 3.3-6 with respect to the strain increment and applying the chain rule results in the Jacobian matrix:

$$\frac{\partial \sigma_{ij}\big|_{s_2}}{\partial \Delta \varepsilon_{kl}} = S_{ijmn}\, s_1 \frac{\partial \sigma_{mn}\big|_{s_1}}{\partial \Delta \varepsilon_{kl}} + \left(s_2 - s_1\right)\frac{\partial \sigma_{ij}\big|_{s_2}}{\partial \Delta \varepsilon_{kl}} + \left\{ \frac{\partial \sigma_{ij}\big|_{s_2}}{\partial \Delta \varepsilon_{qr}} \Delta \varepsilon_{qr} \frac{\partial\left(s_2 - s_1\right)}{\partial \Delta \varepsilon_{kl}} \right\} \tag{3.3-7}$$

$$\text{where} \quad S_{ijmn} = \frac{\partial \sigma_{ij}\big|_{s_2}}{\partial \sigma_{mn}\big|_{s_1}}.$$

For simplicity, the last term in Equation 3.3-7 (the term in brackets { }) has been neglected.

Additional derivatives that will be required later in the calculation of the plastic contributions to the global Jacobian are:

1) derivatives with respect to the increment of strain of the square of the second stress invariant (J^2), and

2) the distance from the current stress point to the Bounding Surface (b) with respect to the increment of strain.

Differentiating the square of the second stress invariant (as defined in Equation 3.2-16) results in:

$$\frac{\partial J^2}{\partial \Delta \varepsilon_{kl}} = \frac{\partial s_{ij}}{\partial \Delta \varepsilon_{kl}} s_{ij} \tag{3.3-7}$$

The distance measure (b) is found by substituting Equations 3.2-14 through -18 into the Bounding Surface function (Equation 3.1-1) and solving the resulting quadratic equation. The equation for b is:

$$b = I_o \frac{-\left(C - \rho\right)\left(I - CI_o\right) \pm \frac{\sqrt{a_2}}{a_1} J}{\frac{a_2}{a_1} J^2 + \left(I - CI_o\right)} \tag{3.3-8}$$

For b to be positive (and knowing that a_1, a_2 and J are always positive), the $+$ sign is used before the radical. The derivative of b with respect to the increment in strain is given, noting that I_o is fixed for an elastic step:

$$\frac{\partial b}{\partial \Delta \varepsilon_{kl}} = \frac{-1}{\dfrac{a_2}{a_1}J^2 + \left(I - CI_o\right)} \left[\begin{array}{c} I_o \left((C-\rho)\dfrac{\partial I}{\partial \Delta \varepsilon_{kl}} - \dfrac{\sqrt{a_2}}{a_1}\dfrac{\partial J}{\partial \Delta \varepsilon_{kl}} \right) \\[2mm] +b \left(\dfrac{a_2}{a_1}\dfrac{\partial J^2}{\partial \Delta \varepsilon_{kl}} + \dfrac{\partial I}{\partial \Delta \varepsilon_{kl}} \right) \end{array} \right] \tag{3.3-9}$$

where $\dfrac{\partial J}{\partial \Delta \varepsilon_{kl}} = \dfrac{1}{2J}\dfrac{\partial J^2}{\partial \Delta \varepsilon_{kl}}$.

3.4 Plastic Calculations

The plastic part of the increment begins at the end of the elastic step. The stresses and strains are updated after the elastic step. The beginning of the plastic step is designated with a subscript b and treated as a new step with:

$$t_b = 0, \quad \varepsilon_{ij_b} \leftarrow \varepsilon_{ij_b} + \Delta \varepsilon_{ij} s, \quad \Delta \varepsilon_{ij} \leftarrow (1-s)\Delta \varepsilon_{ij}, \quad \Delta \theta \leftarrow (1-s)\Delta \theta \tag{3.4-1}$$

To assure accuracy, the plastic step will allow substepping. The strains are subdivided into N uniform substeps as follows:

$$\Delta \varepsilon_{ij_N} = \frac{\Delta \varepsilon_{ij}}{N} \tag{3.4-2}$$

The notation used throughout this section is $I(t_b) = I_b$ for the beginning of the step, $I(t_n) = I_n$ for the beginning of the substep, and $I(t_{n+1}) = I_{n+1}$ for the end of the substep. The plastic volumetric strain can be written in terms of the total strain and elastic strain as:

$$\theta^p(t) = \theta(t) - \theta^e(t) \tag{3.4-3}$$

Rewriting Equation 3.4-3 in terms of the strain increment gives:

$$\theta^P(t) = \theta_b + \Delta\theta(t - t_b) - \theta_b^e - \Delta\theta^e(t - t_b) \tag{3.4-4}$$

Solving Equation 3.2-4 in terms of the elastic strain increment and substituting into Equation 3.4-4 yields:

$$\theta^P(t) = \theta_b + \Delta\theta(t - t_b) - \frac{1}{\beta}\ln\left(\frac{I(t)}{I_b}\right) - \theta_b^e \qquad (I > I_l) \tag{3.4-5a}$$

$$\theta^P(t) = \theta_b + \Delta\theta(t - t_b) - \frac{1}{\beta}\left(\frac{I(t) - I_b}{I_l}\right) - \theta_b^e \qquad (I < I_l) \tag{3.4-5b}$$

Differentiating these equations with respect to time t_{n+1} (noting that the beginning values are fixed) results in the rate form relationship between the total, elastic and plastic volumetric strains. This relationship is written as follows:

$$\dot{\theta}_{n+1}^P = \Delta\theta - \frac{1}{\beta}\frac{\dot{I}_{n+1}}{I_{n+1}} \qquad (I > I_l) \tag{3.4-6a}$$

$$\dot{\theta}_{n+1}^P = \Delta\theta - \frac{1}{\beta}\frac{\dot{I}_{n+1}}{I_l} \qquad (I < I_l) \tag{3.4-6b}$$

The associative flow rule for the volumetric plastic strain rate in the Bounding Surface formulation is given as:

$$\dot{\theta}_{n+1}^P = 3\gamma_{n+1}\frac{\partial F}{\partial \bar{I}}\bigg|_{n+1} \tag{3.4-7}$$

where γ_{n+1} = plasticity parameter (loading index).

Using Equation 3.1-1, the derivative of F with respect to $\bar{I}$, taken at t_{n+1}, can be expressed as:

$$\left.\frac{\partial F}{\partial \bar{I}}\right|_{n+1} = 2\left(\bar{I}_{n+1} - \rho I_{o_{n+1}}\right) \tag{3.4-8}$$

where $\quad \bar{I}_{n+1} = b_{n+1}\left(I_{n+1} - CI_{o_{n+1}}\right) + CI_{o_{n+1}}$.

Combining Equations 3.4-6, 3.4-7 and 3.4-8 yields the volumetric differential equation that must be satisfied during plastic deformation (where $t = t_{n+1}$):

$$6\,\gamma_{n+1}\left(\bar{I}_{n+1} - \rho I_{o_n}\right) = \Delta\theta - \frac{1}{\beta}\frac{\dot{I}_{n+1}}{I_{n+1}} \qquad (I > I_l) \tag{3.4-9a}$$

$$6\,\gamma_{n+1}\left(\bar{I}_{n+1} - \rho I_{o_{n-1}}\right) = \Delta\theta - \frac{1}{\beta}\frac{\dot{I}_{n+1}}{I_l} \qquad (I < I_l) \tag{3.4-9b}$$

At this point, the unknowns in Equation 3.4-9 include the volumetric stress, the volumetric stress rate, the loading surface measure, the plastic parameter and the bound size ($I_{n+1}, \dot{I}_{n+1}, b_{n+1}, \gamma_{n+1}, I_{o_{n+1}}$, respectively). The evolution of the Bounding Surface size for clays (I_0) is described in Section 1.5 [Kaliakin, 1985; Dafalias and Herrmann, 1986]. Equation 1.5-8 written in terms of the strain at the beginning of the step is given as:

$$I_{o_{n+1}} = I_{o_b}e^{\xi\left(\theta^p_{n+1} - \theta^p_b\right)} \tag{3.4-10}$$

Noting that $\Delta\theta^p_{n+1} = \theta^p_{n+1} - \theta^p_b$ and $t_b = 0$, Equation 3.4-5 is now substituted into Equation 3.4-10 resulting in:

$$I_{o_{n+1}} = I_{o_b}e^{\xi\left(\Delta\theta t_{n+1} - \frac{1}{\beta}\ln\left(\frac{I_{n+1}}{I_b}\right)\right)} \qquad (I > I_l) \tag{3.4-11a}$$

$$I_{o_{n+1}} = I_{o_b}e^{\xi\left(\Delta\theta t_{n+1} - \frac{1}{\beta}\left(\frac{I_{n+1} - I_b}{I_l}\right)\right)} \qquad (I < I_l) \tag{3.4-11b}$$

For the special case of the volumetric stress (I) crossing the transition stress (I_t), the equations can be modified to incorporate the transition. This case requires adding the known distance (from the current stress point to the transition stress) to the unknown distance (the term in parentheses in Equation 3.4-11). For stress points originating in the log-linear region (Equation 3.4-11a), the known distance is in the log-linear portion and the unknown distance is in the linear-linear portion. For stress points originating in the linear-linear region, the reverse is true. The modification is given as:

$$I_{0_{n+1}} = I_{0_b} e^{\xi\left(\Delta\theta t_{n+1} - \frac{1}{\beta}\left[\ln\left(\frac{I_t}{I_b}\right) + \frac{I_{n+1} - I_b}{I_t}\right]\right)} \qquad (I_b > I_t \text{ and } I_{n+1} < I_t) \qquad (3.4\text{-}12\text{a})$$

$$I_{0_{n+1}} = I_{0_b} e^{\xi\left(\Delta\theta t_{n+1} - \frac{1}{\beta}\left[\frac{I_t - I_b}{I_t} + \ln\left(\frac{I_{n+1}}{I_b}\right)\right]\right)} \qquad (I_b < I_t \text{ and } I_{n+1} > I_t) \qquad (3.4\text{-}12\text{b})$$

The unknown volumetric stress rate $\left(\dot{I}_{n+1}\right)$ can be approximated with a backward differences formula:

$$\dot{I}_{n+1} \approx \frac{I_{n+1} - I_n}{\Delta t} \qquad (3.4\text{-}13)$$

Using Equations 3.4-11 through -13, the unknowns in Equation 3.4-9 are now reduced to just I_{n+1}, b_{n+1} and γ_{n+1}.

Similar to the volumetric strains, the deviatoric total, elastic and plastic strain rates at the end of the step are related via:

$$\dot{e}_{ij_{n+1}} = \dot{e}^e_{ij_{n+1}} + \dot{e}^p_{ij_{n+1}} \qquad (3.4\text{-}14)$$

The elastic deviatoric stress-strain rate relationship is given as:

$$\dot{e}^e_{ij_{n+1}} = \frac{\dot{s}_{ij_{n+1}}}{2G_{n+1}} \qquad (3.4\text{-}15)$$

It is important to note that the shear modulus (G_{n+1} defined in Equation 3.2-8) is a function of the bulk modulus (B_{n+1}) which, in turn, is a function of the volumetric stress (I_{n+1}). The associative flow rule for the deviatoric plastic strain rates in the Bounding Surface formulation is given as:

$$\dot{e}^p_{ij_{n+1}} = \gamma_{n+1} \left(\frac{\partial F}{\partial s_{ij}} \right)_{n+1} \tag{3.4-16}$$

The derivative of the Bounding Surface function (F) with respect to the deviatoric stresses can be expressed in terms of the invariants as:

$$\left(\frac{\partial F}{\partial s_{ij}} \right)_{n+1} = \left(\frac{\partial F}{\partial \bar{J}^2} \right)_{n+1} \left(\frac{\partial \bar{J}^2}{\partial s_{ij}} \right)_{n+1} \tag{3.4-17}$$

where $$\left(\frac{\partial F}{\partial \bar{J}^2} \right)_{n+1} = \frac{a_2}{a_1}$$

$$\left(\frac{\partial \bar{J}^2}{\partial s_{ij}} \right)_{n+1} = \bar{s}_{ij_{n+1}} = b_{n+1} s_{ij_{n+1}}.$$

An approximation for $\dot{s}_{ij_{n+1}}$ of Equation 3.4-15 is made by a backward difference formula resulting in:

$$\dot{s}_{ij_{n+1}} \approx \frac{s_{ij_{n+1}} - s_{ij_n}}{\Delta t} \tag{3.4-18}$$

where $$\Delta t = t_{n+1} - t_n = \frac{1}{N}.$$

Substituting Equations 3.4-15 though -18 into the strain rate equation (Equation 3.4-14), and recalling that the deviatoric strain rate is $\Delta e_{ij} = \dot{e}_{ij}$, yields:

$$\Delta e_{ij} = \frac{s_{ij_{n+1}} - s_{ij_n}}{2 G_{n+1} \Delta t} + \frac{a_2}{a_1} \gamma_{n+1} b_{n+1} s_{ij_{n+1}} \tag{3.4-19}$$

The expression can be solved for the deviatoric stresses at the end of the step as:

$$s_{ij_{n+1}} = \frac{2\,G_{n+1}\Delta t \Delta e_{ij} + s_{ij_n}}{1 + 2\,G_{n+1}\Delta t \dfrac{a_2}{a_1}\gamma_{n+1}b_{n+1}}$$

(3.4-20)

The square of the second invariant is:

$$J_{n+1}^2 = \tfrac{1}{2}\,s_{ij_{n+1}}s_{ij_{n+1}}$$

(3.4-21)

Substituting the deviatoric stress defined in Equation 3.4-20 into Equation 3.4-21 results in the deviatoric equation that must be satisfied during plastic deformation:

$$4G_{n+1}^2\Delta t^2\chi_1 + 2G_{n+1}\Delta t\chi_2 + J_n^2 = \left(1 + 2\,G_{n+1}\Delta t \frac{a_2}{a_1}\gamma_{n+1}b_{n+1}\right)^2 J_{n+1}^2$$

(3.4-22)

where $\quad \chi_1 = \tfrac{1}{2}\Delta e_{ij}\Delta e_{ij}$

$$\chi_2 = \Delta e_{ij}s_{ij_n}$$

$$J_n^2 = \tfrac{1}{2}\,s_{ij_n}s_{ij_n}\,.$$

The unknowns in these equations include the new shear modulus (which is a function of the volumetric stress), second stress invariant, loading surface measure, and the plastic parameter ($I_{n+1}, J_{n+1}^2, b_{n+1}$ and γ_{n+1}, respectively). The square of the second invariant can be solved for by rewriting the Bounding Surface equation (Equation 3.1-1) as:

$$J_{n+1}^2 = \frac{1}{a_2 b_{n+1}^2}\left[I_{o_{n+1}}^2 - a_1\left(\bar{I}_{n+1} - \rho I_{o_{n}}\right)^2\right]$$

(3.4-23)

This reduces the number of unknowns by defining J_{n+1}^2, but introduces $I_{o_{n+1}}$. Recall, however, that Equation 3.4-11 relates $I_{o_{n+1}}$ to I_{n+1}, thereby leaving the same three unknowns as in the volumetric equation (Equation 3.4-9): I_{n+1}, b_{n+1} and γ_{n+1}.

At this point, since there are two equations (Equation 3.4-9 and Equation 3.4-22) and three unknowns, a third equation is required. The obvious choice is an equation that relates the plasticity parameter to the amount of plasticity deformation occurring within the bound. The fundamental equation of the Bounding Surface Plasticity concept [Kaliakin, 1985; Dafalias and Herrmann, 1986] relates the plasticity to the current stress state. Equation 1.2-4 can be rewritten in terms of the invariants as:

$$\gamma_{n+1} = \frac{1}{K_{p_{n+1}}} \left(\left(\frac{\partial F}{\partial \bar{I}} \right)_{n+1} \dot{I}_{n+1} + \left(\frac{\partial F}{\partial \bar{J}^2} \right)_{n+1} b_{n+1} \dot{J}^2_{n+1} \right)$$
(3.4-24)

The definition of the hardening modulus $\left(K_{p_{n+1}} \right)$ is given in Equation 1.6-4 [Kaliakin, 1985; Dafalias and Herrmann, 1986]. The volumetric stress rate $\left(\dot{I}_{n+1} \right)$ is approximated in Equation 3.4-13, and the second invariant rate $\left(\dot{J}^2_{n+1} \right)$ is evaluated by taking the derivative of Equation 3.4-23 with respect to the current time (t_{n+1}):

$$\dot{J}^2_{n+1} = -\frac{2 \dot{b}_{n+1}}{b_{n+1}} J^2_{n+1} + \frac{1}{a_2 b^2_{n+1}} \left[I_{o_{n+1}} \dot{I}_{o_{n+1}} - a_1 \left(\bar{I}_{n+1} - \rho I_{o_{n+1}} \right) \left(\dot{\bar{I}}_{n+1} - \rho \dot{I}_{o_{n+1}} \right) \right]$$
(3.4-25)

The time derivatives of the Bounding Surface size are achieved by differentiating Equations 3.4-11:

$$\dot{I}_{o_{n+1}} = I_{o_{n+1}} \xi \left(\Delta \theta - \frac{1}{\beta} \frac{\dot{I}_{n+1}}{I_{n+1}} \right)$$
$(I > I_l)$ (3.4-26a)

$$\dot{I}_{o_{n+1}} = I_{o_{n+1}} \xi \left(\Delta \theta - \frac{1}{\beta} \frac{\dot{I}_{n+1}}{I_l} \right)$$
$(I < I_l)$ (3.4-26b)

For the special case of the volumetric stress crossing the transition stress (Equation 3.4-12), the "a" and "b" equations are reversed (i.e., Equation 3.4-25a is used for $I < I_l$ and Equation 3.4-25b is used for $I > I_l$).

The rate of the loading surface measure $\left(\dot{b}_{n+1}\right)$ is approximated with a backward difference formula as:

$$\dot{b}_{n+1} \approx \frac{b_{n+1} - b_n}{\Delta t} \tag{3.4-27}$$

Using Equations 3.4-25 through -27, the number of unknowns for Equation 3.4-24 is reduced to the same set of unknowns as in the volumetric and deviatoric equations (Equations 3.4-9 and 3.4-22), I_{n+1}, b_{n+1} and γ_{n+1}. The equation is purposely written so that the hardening modulus $\left(K_{p_{n+1}}\right)$ appears in the denominator. This is necessary because as the stress state approaches the elastic bound, the hardening modulus approaches infinity at a rapid rate. When the hardening modulus is in the denominator, the plasticity parameter approaches zero as the elastic bound is reached.

Since the equations are extremely complex, the solution for the three unknowns is achieved with Newton-Raphson iteration. The approach used in this study is to treat I and b as independent variables in the volumetric and deviatoric equations (Equations 3.4-9, 3.4-22). The Bounding Surface equation (Equation 3.4-24) is solved for the plasticity parameter (γ). Another approach that was used for the Cam-Clay model [Herrmann, 1997] is discussed in Appendix B. The residuals are defined as the error in the governing equations (Equations 3.4-9 and 3.4-22) and are given as:

$$R_1 = 6\,\gamma_{n+1}\left(\bar{I}_{n+1} - \rho I_{0_{n+1}}\right) - \Delta\theta + \frac{1}{\beta}\frac{\dot{I}_{n+1}}{I_{n+1}} \qquad (I > I_l) \tag{3.4-28a}$$

$$R_1 = 6\,\gamma_{n+1}\left(\bar{I}_{n+1} - \rho I_{0_{n+1}}\right) - \Delta\theta + \frac{1}{\beta}\frac{\dot{I}_{n+1}}{I_l} \qquad (I < I_l) \tag{3.4-28b}$$

$$R_2 = \left(1 + 2\,G_{n+1}\Delta t \frac{a_2}{a_1}\gamma_{n+1}b_{n+1}\right)^2 J_{n+1}^2 - 4G_{n+1}^2\Delta t^2 \chi_1 - 2G_{n+1}\Delta t\chi_2 - J_n^2 \qquad (3.4\text{-}29)$$

The Newton-Raphson method iterates on the independent variables in order to find the roots of the residuals. The general one-dimensional form is given as:

$$x_{i+1} = x_i - \frac{f(x_i)}{f'(x_i)} \qquad (3.4\text{-}30)$$

where i = iteration counter

x_{i+1} = improved value of x

x_i = previous value of x

$f(x_i)$ = residual (function of x)

$f'(x_i)$ = derivative of residual with respect to x.

The two-dimensional form involves matrices and matrix inversion and is given as:

$$\left\{\begin{matrix}I\\b\end{matrix}\right\}_{i+1,n+1} = \left\{\begin{matrix}I\\b\end{matrix}\right\}_{i,n+1} - \Psi_{i,n+1}^{-1}\left\{\begin{matrix}R_1\\R_2\end{matrix}\right\}_{i,n+1} \qquad (3.4\text{-}31)$$

where $\Psi = \begin{bmatrix}\dfrac{\partial R_1}{\partial I} & \dfrac{\partial R_1}{\partial b}\\[2mm] \dfrac{\partial R_2}{\partial I} & \dfrac{\partial R_2}{\partial b}\end{bmatrix}.$

The local Jacobian (Ψ) is defined by taking derivatives of the residuals with respect to the independent variables I and b (note that when taking derivatives with respect to one independent variable, the other independent variable is held constant). Dropping the

iteration counter (i) for clarity, these derivatives are given as:

$$\left(\frac{\partial R_1}{\partial I}\right)_{n+1} = 6\gamma_{n+1}\left(\left(\frac{\partial \bar{I}}{\partial I}\right)_{n+1} - \rho\left(\frac{\partial I_o}{\partial I}\right)_{n+1}\right) + 6\left(\bar{I}_{n+1} - \rho I_{o_{n+1}}\right)\left(\frac{\partial \gamma}{\partial I}\right)_{n+1}$$
$$+ \frac{1}{\beta I_{n+1}}\left(\frac{1}{\Delta t} - \frac{\dot{I}_{n+1}}{I_{n+1}}\right) \qquad (I > I_l)(3.4\text{-}32a)$$

$$\left(\frac{\partial R_1}{\partial I}\right)_{n+1} = 6\gamma_{n+1}\left(\left(\frac{\partial \bar{I}}{\partial I}\right)_{n+1} - \rho\left(\frac{\partial I_o}{\partial I}\right)_{n+1}\right) + 6\left(\bar{I}_{n+1} - \rho I_{o_{n+1}}\right)\left(\frac{\partial \gamma}{\partial I}\right)_{n+1}$$
$$+ \frac{1}{\beta \Delta t I_{n+1}} \qquad (I < I_l) \quad (3.4\text{-}32b)$$

$$\left(\frac{\partial R_1}{\partial b}\right)_{n+1} = 6\gamma_{n+1}\left(\frac{\partial \bar{I}}{\partial b}\right)_{n+1} + 6\left(\bar{I}_{n+1} - \rho I_{o_{n+1}}\right)\left(\frac{\partial \gamma}{\partial b}\right)_{n+1} \qquad (3.4\text{-}33)$$

$$\left(\frac{\partial R_2}{\partial I}\right)_{n+1} = 4\Delta t \frac{a_2}{a_1} b_{n+1}\left(1 + 2G_{n+1}\Delta t \frac{a_2}{a_1}\gamma_{n+1}b_{n+1}\right)\left(\gamma_{n+1}\left(\frac{\partial G}{\partial I}\right)_{n+1} + G_{n+1}\left(\frac{\partial \gamma}{\partial I}\right)_{n+1}\right)J_{n+1}^2$$
$$+ \left(1 + 2G_{n+1}\Delta t \frac{a_2}{a_1}\gamma_{n+1}b_{n+1}\right)^2\left(\frac{\partial J^2}{\partial I}\right)_{n+1} - 8G_{n+1}\Delta t^2 \chi_1\left(\frac{\partial G}{\partial I}\right)_{n+1} - 2\Delta t \chi_2\left(\frac{\partial G}{\partial I}\right)_{n+1} \qquad (3.4\text{-}34)$$

$$\left(\frac{\partial R_2}{\partial b}\right)_{n+1} = 4\Delta t \frac{a_2}{a_1} G_{n+1}\left(1 + 2G_{n+1}\Delta t \frac{a_2}{a_1}\gamma_{n+1}b_{n+1}\right)\left(\gamma_{n+1} + b_{n+1}\left(\frac{\partial \gamma}{\partial b}\right)_{n+1}\right)J_{n+1}^2$$
$$+ \left(1 + 2G_{n+1}\Delta t \frac{a_2}{a_1}\gamma_{n+1}b_{n+1}\right)^2\left(\frac{\partial J^2}{\partial b}\right)_{n+1} \qquad (3.4\text{-}35)$$

The derivatives of the plasticity parameter are given as:

$$\left(\frac{\partial \gamma}{\partial I}\right)_{n+1} = \frac{1}{K_p^2}\left(\left(\frac{\partial F}{\partial \bar{I}}\right)_{n+1}\dot{I}_{n+1} + \left(\frac{\partial F}{\partial J^2}\right)_{n+1}b_{n+1}\dot{J}_{n+1}^2\right)\left(\frac{\partial K_p}{\partial I}\right)_{n+1}$$
$$- \frac{1}{K_p}\left(\left(\frac{\partial^2 F}{\partial \bar{I}\partial I}\right)_{n+1}\dot{I}_{n+1} + \left(\frac{\partial F}{\partial \bar{I}}\right)_{n+1}\left(\frac{\partial \dot{I}}{\partial I}\right)_{n+1} + \left(\frac{\partial F}{\partial J^2}\right)_{n+1}b_{n+1}\left(\frac{\partial \dot{J}^2}{\partial I}\right)_{n+1}\right) \qquad (3.4\text{-}36)$$

$$\left(\frac{\partial \gamma}{\partial b}\right)_{n+1} = \frac{1}{K_p^2}\left(\left(\frac{\partial F}{\partial \bar{I}}\right)_{n+1} \dot{I}_{n+1} + \left(\frac{\partial F}{\partial \bar{J}^2}\right)_{n+1} b_{n+1}\dot{J}_{n+1}^2\right)\left(\frac{\partial K_p}{\partial b}\right)_{n+1}$$

$$-\frac{1}{K_p}\left(\left(\frac{\partial^2 F}{\partial \bar{I}\partial b}\right)_{n+1} \dot{I}_{n+1} + \left(\frac{\partial F}{\partial \bar{J}^2}\right)_{n+1} \dot{J}_{n+1}^2 + \left(\frac{\partial F}{\partial \bar{J}^2}\right)_{n+1} b_{n+1}\left(\frac{\partial \dot{J}^2}{\partial b}\right)_{n+1}\right) \tag{3.4-37}$$

The local Jacobian introduces a large number of derivatives. These are summarized below and are grouped by terms. Some of the terms were defined previously (and hence, their original equation numbers are used), but they are grouped here for clarity. The pertinent derivatives of the volumetric stress (I) are given as:

$$\dot{I}_{n+1} \approx \frac{I_{n+1} - I_n}{\Delta t} \tag{3.4-13}$$

$$\left.\frac{\partial \dot{I}}{\partial I}\right|_{n+1} = \frac{1}{\Delta t} \tag{3.4-38}$$

$$\bar{I}_{n+1} = b_{n+1}\left(I_{n+1} - C I_{o_{n+1}}\right) + C I_{o_{n+1}} \tag{3.4-39}$$

$$\left.\frac{\partial \bar{I}}{\partial I}\right|_{n+1} = b_{n+1} + \left(1 - b_{n+1}\right)C\left.\frac{\partial I_o}{\partial I}\right|_{n+1} \tag{3.4-40}$$

$$\left.\frac{\partial \bar{I}}{\partial b}\right|_{n+1} = I_{n+1} - C I_{o_{n+1}} \tag{3.4-41}$$

$$\dot{\bar{I}}_{n+1} = \dot{b}_{n+1}\left(I_{n+1} - C I_{o_{n+1}}\right) + b_{n+1}\left(\dot{I}_{n+1} - C \dot{I}_{o_{n+1}}\right) + C \dot{I}_{o_{n+1}} \tag{3.4-42}$$

$$\left.\frac{\partial \dot{\bar{I}}}{\partial I}\right|_{n+1} = \dot{b}_{n+1}\left(1 - C\left.\frac{\partial I_o}{\partial I}\right|_{n+1}\right) + b_{n+1}\left(\left.\frac{\partial \dot{I}}{\partial I}\right|_{n+1} - C\left.\frac{\partial \dot{I}_o}{\partial I}\right|_{n+1}\right) + C\left.\frac{\partial \dot{I}_o}{\partial I}\right|_{n+1} \tag{3.4-43}$$

$$\left.\frac{\partial \dot{\bar{I}}}{\partial b}\right|_{n+1} = \left.\frac{\partial \dot{b}}{\partial b}\right|_{n+1}\left(1 - C\left.\frac{\partial I_o}{\partial I}\right|_{n+1}\right) + \left(\dot{I}_{n+1} - C \dot{I}_{o_{n+1}}\right) \tag{3.4-44}$$

The derivatives of the other independent variable (b), the loading surface measure, are:

$$\dot{b}_{n+1} \approx \frac{b_{n+1} - b_n}{\Delta t} \tag{3.4-27}$$

$$\left. \frac{\partial \dot{b}}{\partial b} \right|_{n+1} = \frac{1}{\Delta t} \tag{3.4-45}$$

The derivation of the shear modulus (Equation 3.2-8) shows that for the log-linear range, the modulus is a function only of the volumetric stress. The derivative of the shear modulus with respect to the volumetric stress is given as:

$$\left(\frac{\partial G}{\partial I} \right)_{n+1} = \frac{G_b}{I_b} \qquad\qquad (I > I_l) \tag{3.4-46a}$$

$$\left(\frac{\partial G}{\partial I} \right)_{n+1} = 0 \qquad\qquad (I < I_l) \tag{3.4-46b}$$

The derivatives of the Bounding Surface function (F) are:

$$\left(\frac{\partial F}{\partial \bar{I}} \right)_{n+1} = 2\left(\bar{I}_{n+1} - \rho I_{o_{n+1}} \right) \tag{3.4-47}$$

$$\left(\frac{\partial F}{\partial \bar{J}^2} \right)_{n+1} = \frac{a_2}{a_1} \tag{3.4-48}$$

$$\left(\frac{\partial^2 F}{\partial \bar{I} \partial I} \right)_{n+1} = 2\left(\left(\frac{\partial \bar{I}}{\partial I} \right)_{n+1} - \rho \left(\frac{\partial I_o}{\partial I} \right)_{n+1} \right) \tag{3.4-49}$$

$$\left(\frac{\partial^2 F}{\partial \bar{I} \partial b} \right)_{n+1} = 2\left(\frac{\partial \bar{I}}{\partial b} \right)_{n+1} \tag{3.4-50}$$

The second invariant (J^2) and its derivatives are:

$$J_{n+1}^2 = \frac{1}{a_2 b_{n+1}^2}\left[I_{o_{n+1}}^2 - a_1\left(\bar{I}_{n+1} - \rho I_{o_{n+1}}\right)^2\right] \tag{3.4-23}$$

$$\left(\frac{\partial J^2}{\partial I}\right)_{n+1} = \frac{2}{a_2 b_{n+1}^2}\left[I_{o_{n+1}}\left(\frac{\partial I_o}{\partial I}\right)_{n+1} - a_1\left(\bar{I}_{n+1} - \rho I_{o_{n+1}}\right)\left(\left(\frac{\partial \bar{I}}{\partial I}\right)_{n+1} - \rho\left(\frac{\partial I_o}{\partial I}\right)_{n+1}\right)\right] \tag{3.4-51}$$

$$\left(\frac{\partial J^2}{\partial b}\right)_{n+1} = -\frac{2 J_{n+1}^2}{b_{n+1}} - \frac{2}{a_2 b_{n+1}^2}\left[a_1\left(\bar{I}_{n+1} - \rho I_{o_{n+1}}\right)\left(\frac{\partial \bar{I}}{\partial b}\right)_{n+1}\right] \tag{3.4-52}$$

$$\dot{J}_{n+1}^2 = -\frac{2\dot{b}_{n+1}}{b_{n+1}} J_{n+1}^2 + \frac{2}{a_2 b_{n+1}^2}\left[I_{o_{n+1}}\dot{I}_{o_{n+1}} - a_1\left(\bar{I}_{n+1} - \rho I_{o_{n+1}}\right)\left(\dot{\bar{I}}_{n+1} - \rho \dot{I}_{o_{n+1}}\right)\right] \tag{3.4-25}$$

$$\left(\frac{\partial \dot{J}^2}{\partial I}\right)_{n+1} = -\frac{2\dot{b}_{n+1}}{b_{n+1}}\left(\frac{\partial J^2}{\partial I}\right)_{n+1} + \frac{2}{a_2 b_{n+1}^2}\begin{bmatrix}\left(\frac{\partial I_o}{\partial I}\right)_{n+1}\dot{I}_{o_{n+1}} + I_{o_{n+1}}\left(\frac{\partial \dot{I}_o}{\partial I}\right)_{n+1} \\[2mm] -a_1\left(\left(\frac{\partial \bar{I}}{\partial I}\right)_{n+1} - \rho\left(\frac{\partial I_o}{\partial I}\right)_{n+1}\right)\left(\dot{\bar{I}}_{n+1} - \rho \dot{I}_{o_{n+1}}\right) \\[2mm] -a_1\left(\bar{I}_{n+1} - \rho I_{o_{n+1}}\right)\left(\left(\frac{\partial \dot{\bar{I}}}{\partial I}\right)_{n+1} - \rho\left(\frac{\partial \dot{I}_o}{\partial I}\right)_{n+1}\right)\end{bmatrix} \tag{3.4-53}$$

$$\left(\frac{\partial \dot{J}^2}{\partial b}\right)_{n+1} = -\frac{2}{\Delta t\, b_{n+1}} J_{n+1}^2 + \frac{2\dot{b}_{n+1}}{b_{n+1}^2} J_{n+1}^2 - \frac{2\dot{b}_{n+1}}{b_{n+1}}\left(\frac{\partial J^2}{\partial b}\right)_{n+1}$$

$$- \frac{4}{a_2 b_{n+1}^2}\left[I_{o_{n+1}}\dot{I}_{o_{n+1}} - a_1\left(\bar{I}_{n+1} - \rho I_{o_{n+1}}\right)\left(\dot{\bar{I}}_{n+1} - \rho \dot{I}_{o_{n+1}}\right)\right] \tag{3.4-54}$$

$$- \frac{2a_1}{a_2 b_{n+1}^2}\left[\left(\frac{\partial \bar{I}}{\partial b}\right)_{n+1}\left(\dot{\bar{I}}_{n+1} - \rho \dot{I}_{o_{n+1}}\right) + \left(\bar{I}_{n+1} - \rho I_{o_{n+1}}\right)\left(\frac{\partial \dot{\bar{I}}}{\partial b}\right)_{n+1}\right]$$

The Bounding Surface size (I_o) derivatives are:

$$I_{o_{n+1}} = I_{o_b} e^{\xi\left(\Delta\theta\, t_{n+1} - \frac{1}{\beta}\ln\left(\frac{I_{n+1}}{I_b}\right)\right)} \qquad (I > I_l) \qquad (3.4\text{-}11a)$$

$$I_{o_{n+1}} = I_{o_b} e^{\xi\left(\Delta\theta\, t_{n+1} - \frac{1}{\beta}\left(\frac{I_{n+1}-I_b}{I_l}\right)\right)} \qquad (I < I_l) \qquad (3.4\text{-}11b)$$

$$\left(\frac{\partial I_o}{\partial I}\right)_{n+1} = -\frac{\xi}{\beta}\frac{I_{o_{n+1}}}{I_{n+1}} \qquad (I > I_l) \qquad (3.4\text{-}55a)$$

$$\left(\frac{\partial I_o}{\partial I}\right)_{n+1} = -\frac{\xi}{\beta}\frac{I_{o_{n+1}}}{I_l} \qquad (I < I_l) \qquad (3.4\text{-}55b)$$

$$\dot{I}_{o_{n+1}} = I_{o_{n+1}}\xi\left(\Delta\theta - \frac{1}{\beta}\frac{\dot{I}_{n+1}}{I_{n+1}}\right) \qquad (I > I_l) \qquad (3.4\text{-}56a)$$

$$\dot{I}_{o_{n+1}} = I_{o_{n+1}}\xi\left(\Delta\theta - \frac{1}{\beta}\frac{\dot{I}_{n+1}}{I_l}\right) \qquad (I < I_l) \qquad (3.4\text{-}56b)$$

$$\left(\frac{\partial \dot{I}_o}{\partial I}\right)_{n+1} = \left(\frac{\partial I_o}{\partial I}\right)_{n+1}\xi\left(\Delta\theta - \frac{1}{\beta}\frac{\dot{I}_{n+1}}{I_{n+1}}\right) - \frac{\xi}{\beta}I_{o_{n+1}}\left(\frac{1}{\Delta t\, I_{n+1}} - \frac{\dot{I}_{n+1}}{I_{n+1}^2}\right)(I > I_l) \qquad (3.4\text{-}57a)$$

$$\left(\frac{\partial \dot{I}_o}{\partial I}\right)_{n+1} = \left(\frac{\partial I_o}{\partial I}\right)_{n+1}\xi\left(\Delta\theta - \frac{1}{\beta}\frac{\dot{I}_{n+1}}{I_l}\right) - \frac{\xi}{\beta}I_{o_{n+1}}\frac{1}{\Delta t\, I_l} \qquad (I < I_l) \qquad (3.4\text{-}57b)$$

For the special case of the volumetric stress crossing the transition stress, Equation 3.4-12 is used for I_0 and the time derivatives are reversed (i.e., Equation 3.4-56a is used for $I < I_l$ and 3.4-56b is used for $I > I_l$).

The Newton-Raphson method is set up using Equations 3.4-28 and -29 as the residuals and I_{n+1} and b_{n+1} as the independent variables. The method is begun by assigning I_{n+1} and b_{n+1} their current values and calculating a new estimate with Equation 3.4-31. The iteration continues until a convergence criterion is met. The criterion chosen for this study

is that the change in residuals be smaller than a user-defined percentage of the absolute value of the total strain increment. This is given as:

$$\|R\| = \frac{|R_1| + |R_2|}{\sum |\Delta \varepsilon|}$$

(3.4-58)

where $\|R\|$ = norm on the residuals.

This requires that the residuals are in terms of strains, or at least their magnitude is that of strain. Another advantage of having the residuals near the same magnitude is to prevent any numerical problems in the matrix inversion. Residual 1 (Equation 3.4-28) is already in terms of strain. Residual 2, however, (Equation 3.4-29) is in terms of stress. This residual is given the magnitude of strain by dividing it and its derivatives by the initial shear modulus. The new residual and derivatives are given as:

$$R_2^* = \frac{R_2}{G_b^2}, \qquad \frac{\partial R_2^*}{\partial I} = \frac{1}{G_b^2} \frac{\partial R_2}{\partial I}, \qquad \frac{\partial R_2^*}{\partial b} = \frac{1}{G_b^2} \frac{\partial R_2}{\partial b}$$

(3.4-59)

In order to add robustness, the plastic increment is uniformly substepped as described in Equation 3.4-2. First a single step is tried, then the strain increment is divided by two and the stress recalculated. This process continues until some convergence criterion is met or the maximum number of allowable substeps is exceeded. In order to compare the various methods, a criterion based upon terms that are present in each of the methods was chosen. The criterion used for the substepping evaluation is that the change of the Bounding Surface size (I_o) should be less than a user-defined tolerance. This is written as follows:

$$\left\{ \left[\left(I_{o_{n+1,m}} - I_{o_{n+1,m-1}} \right) < Toler_{I_o} \right] \quad OR \quad \left[It > It_{max} \right] \right\} \quad THEN: \quad EXIT$$

(3.4-60)

where $I_{o_{n+1,m}}$ = stress at end of step and substep level, m

$I_{o_{n+1,m-1}}$ = stress at end of step and substep level, $m-1$

m = substep level (i.e., number of substeps = 1, 2, 4, 8, 16, ...)

It = iteration counter

It_{max} = maximum number of iterations.

Another criterion considered involves the stress distance measure (b_{n+1}). The value of b_{n+1} is used during the iteration as an independent variable. It can also be calculated independently knowing the stress state and the Bounding Surface size (Equation 3.3-8). A convergence criterion can be defined as follows:

$$\left\{\left[\left(b_{n+1} - b_{calc}\right) < Toler_b\right] \quad OR \quad \left[It > It_{max}\right]\right\} \quad THEN: \quad EXIT \qquad (3.4\text{-}61)$$

where b_{calc} = b calculated from I_{n+1}, J^2_{n+1} and $I_{0_{n+1}}$.

This criterion is important for stress points near $I = 0$, $J = 0$ and $C = 0$ because the iteration residuals, and thus the iteration criterion (Equation 3.4-58), are near zero, but the variable b can vary significantly.

An important difference exists in the use of the subscripts b and n. Most of the equations for the method are defined in terms of the beginning of the plastic increment (e.g., I_b). Terms defined at the beginning are fixed, thus simplifying derivations (i.e., terms defined at time t_n do not contribute to derivatives taken at time t_{n+1}). The rate equations for the independent variables $\dot{I}$ and $\dot{b}$ (Equations 3.4-13 and 3.4-27), however, require information at the beginning of each substep (i.e., I_n and b_n). Therefore, the independent variables at the end of the substep must be reserved for calculating these rate equations and for eventual use in computing the algorithmic consistent moduli (Section 3.5). The algorithm is given in Box 3.4-1.

Box 3.4-1. Reduced Newton Algorithm for Plastic Steps.

1. **Set Substep Level:** $N = 1$

2. **Substep Level Loop:** $m = 1, m_{max}$

$$\Delta\varepsilon_{ij_m} = \frac{\Delta\varepsilon_{ij}}{N}$$

3. **Initialize to Beginning of Step:**

$$I_{n+1} = I_b, \; b_{n+1} = b_b$$

4. **Substep Loop:** $k = 1, N$

5. **Determine Volumetric Form:**

$(I > I_l)$ Linear-Linear $(I < I_l)$ Log-Linear

6. **Iteration Loop:** $It = 1, It_{max}$

7. **Calculate Residuals and Local Jacobian:** R_1, R_2, Ψ

8. **Solve for Increment in Variables:** ΔI_{n+1}, Δb_{n+1}

9. **Calculate and Test Norm:** IF $(\|R\| < Toler_{It})$

   TRUE: Go to step 11

   FALSE: Increment variables, I_{n+1}, b_{n+1}, Go to step 7

10. **Calculate Stresses and Check Substeps:** σ_{n+1}

    IF $(k < N)$ TRUE: Go to step 4   FALSE: Go to step 12

11. **Compare stresses with previous substep level:**

$$\left[\left(I_{o_{n+1,m}} - I_{o_{n+1,m-1}}\right) < Toler_{I_o}\right] \quad \text{OR} \quad \left[It > It_{max}\right]$$

   TRUE: EXIT   FALSE: $N = 2N$, Go to step 2

3.5 Plastic Contribution to the Global Jacobian

Once the plastic step has converged, the plastic contribution to the global Jacobian

matrix $\left(\dfrac{\partial \sigma_{ij}}{\partial \Delta \varepsilon_{kl}}\right)_{n+1}$ must be calculated. The local Jacobian will be evaluated in terms of the

deviatoric and volumetric components similar to the elastic Jacobian. The volumetric

component of the Jacobian can be obtained by noting that the residuals are a function of the

independent variables I and b which, in turn, are a function of the strain increment. The

derivatives can be obtained by an application of the chain rule: holding the independent

variables constant and then adding the derivatives with respect to the independent variables.

At convergence, the residual is equal to zero and the derivatives can be written as:

$$\left(\frac{\partial R_q}{\partial \Delta \varepsilon_{kl}}\right)_{n+1} = \frac{\partial R_q}{\partial \Delta \varepsilon_{kl}}\bigg|_{I_{n+1},b_{n+1}} + \frac{\partial R_q}{\partial I}\bigg|_{b_{n+1}}\left(\frac{\partial I}{\partial \Delta \varepsilon_{kl}}\right)_{n+1} + \frac{\partial R_q}{\partial b}\bigg|_{I_{n+1}}\left(\frac{\partial b}{\partial \Delta \varepsilon_{kl}}\right)_{n+1} = 0 \quad (3.5\text{-}1)$$

Expressed in matrix form:

$$\left\{\begin{array}{c} \dfrac{\partial R_1}{\partial \Delta \varepsilon_{kl}} \\[2mm] \dfrac{\partial R_2}{\partial \Delta \varepsilon_{kl}} \end{array}\right\}_{n+1} = \left\{\begin{array}{c} \dfrac{\partial R_1}{\partial \Delta \varepsilon_{kl}} \\[2mm] \dfrac{\partial R_2}{\partial \Delta \varepsilon_{kl}} \end{array}\right\}_{I_{n+1},b_{n+1}} + \Psi_{n+1}\left\{\begin{array}{c} \dfrac{\partial I}{\partial \Delta \varepsilon_{kl}} \\[2mm] \dfrac{\partial b}{\partial \Delta \varepsilon_{kl}} \end{array}\right\}_{n+1} = \left\{\begin{array}{c} 0 \\ 0 \end{array}\right\} \quad (3.5\text{-}2)$$

$$\text{where} \quad \Psi = \begin{bmatrix} \dfrac{\partial R_1}{\partial I} & \dfrac{\partial R_1}{\partial b} \\[3mm] \dfrac{\partial R_2}{\partial I} & \dfrac{\partial R_2}{\partial b} \end{bmatrix}.$$

Note that the matrix (Ψ) has been computed in the stress point algorithm (Equation

3.4-31). Equation 3.5-2 can be rearranged to solve for the derivatives of the independent

variables with respect to the strain increments. This is given as:

$$\left\{\begin{array}{c} \dfrac{\partial I}{\partial \Delta \varepsilon_{kl}} \\ \dfrac{\partial b}{\partial \Delta \varepsilon_{kl}} \end{array}\right\}_{n+1} = -\Psi_{n+1}^{-1}\left\{\begin{array}{c} \dfrac{\partial R_1}{\partial \Delta \varepsilon_{kl}} \\ \dfrac{\partial R_2}{\partial \Delta \varepsilon_{kl}} \end{array}\right\}_{I_{n+1},b_{n+1}}$$

(3.5-3)

The derivative of the first residual (Equation 3.4-28) with respect to the strain increment (holding the independent variables at the end of the step (I_{n+1}, b_{n+1}) constant) is given as:

$$\left.\frac{\partial R_1}{\partial \Delta \varepsilon_{kl}}\right|_{I_{n+1},b_{n+1}} = 6\gamma_{n+1}\left(\left.\frac{\partial \bar{I}_{n+1}}{\partial \Delta \varepsilon_{kl}}\right|_{I_{n+1},b_{n+1}} - \rho\left.\frac{\partial I_{o_{n+1}}}{\partial \Delta \varepsilon_{kl}}\right|_{I_{n+1},b_{n+1}}\right)$$
$$+ 6\left(\bar{I}_{n+1} - \rho I_{o_{n+1}}\right)\left.\frac{\partial \gamma_{n+1}}{\partial \Delta \varepsilon_{kl}}\right|_{I_{n+1},b_{n+1}} - \delta_{kl} - \frac{1}{\beta \Delta t I_{n+1}}\left.\frac{\partial I_n}{\partial \Delta \varepsilon_{kl}}\right|_{I_{n+1},b_{n+1}}$$

$(I > I_l)$(3.5-4a)

$$\left.\frac{\partial R_1}{\partial \Delta \varepsilon_{kl}}\right|_{I_{n+1},b_{n+1}} = 6\gamma_{n+1}\left(\left.\frac{\partial \bar{I}_{n+1}}{\partial \Delta \varepsilon_{kl}}\right|_{I_{n+1},b_{n+1}} - \rho\left.\frac{\partial I_{o_{n+1}}}{\partial \Delta \varepsilon_{kl}}\right|_{I_{n+1},b_{n+1}}\right)$$
$$+ 6\left(\bar{I}_{n+1} - \rho I_{o_{n+1}}\right)\left.\frac{\partial \gamma_{n+1}}{\partial \Delta \varepsilon_{kl}}\right|_{I_{n+1},b_{n+1}} - \delta_{kl} - \frac{1}{\beta \Delta t I_l}\left.\frac{\partial I_n}{\partial \Delta \varepsilon_{kl}}\right|_{I_{n+1},b_{n+1}}$$

$(I < I_l)$(3.5-4b)

The derivative of the second residual (Equation 3.4-29) is given as:

$$\left.\frac{\partial R_2}{\partial \Delta \varepsilon_{kl}}\right|_{I_{n+1},b_{n+1}} = 4G_{n+1}\Delta t\frac{a_2}{a_1}b_{n+1}\left(1 + 2G_{n+1}\Delta t\frac{a_2}{a_1}\gamma_{n+1}b_{n+1}\right)J_{n+1}^2\left.\frac{\partial \gamma_{n+1}}{\partial \Delta \varepsilon_{kl}}\right|_{I_{n+1},b_{n+1}}$$
$$+ \left(1 + 2G_{n+1}\Delta t\frac{a_2}{a_1}\gamma_{n+1}b_{n+1}\right)^2\left.\frac{\partial J_{n+1}^2}{\partial \Delta \varepsilon_{kl}}\right|_{I_{n+1},b_{n+1}}$$

(3.5-5)

$$- 4G_{n+1}^2\Delta t^2\left.\frac{\partial \chi_1}{\partial \Delta \varepsilon_{kl}}\right|_{I_{n+1},b_{n+1}} - 2G_{n+1}\Delta t\left.\frac{\partial \chi_2}{\partial \Delta \varepsilon_{kl}}\right|_{I_{n+1},b_{n+1}} - \left.\frac{\partial J_n^2}{\partial \Delta \varepsilon_{kl}}\right|_{I_{n+1},b_{n+1}}$$

The derivative of the plasticity parameter with respect to the strain increment is given by:

$$\left.\frac{\partial \gamma_{n+1}}{\partial \Delta \varepsilon_{kl}}\right|_{I_{n+1},b_{n+1}} = -\frac{1}{2J_{n+1}K_{p_{n+1}}^2}\left(\frac{\partial F}{\partial \bar{I}}\dot{I}_{n+1} + \frac{\partial F}{\partial \bar{J}^2}b_{n+1}\dot{J}_{n+1}^2\right)\frac{\partial K_{p_{n+1}}}{\partial J}\frac{\partial J_{n+1}^2}{\partial \Delta \varepsilon_{kl}}$$

$$+\frac{1}{K_{p_{n+1}}}\left(-\frac{1}{\Delta t}\frac{\partial F}{\partial \bar{I}}\left.\frac{\partial I_n}{\partial \Delta \varepsilon_{kl}}\right|_{I_{n+1},b_{n+1}} + \frac{\partial F}{\partial \bar{J}^2}b_{n+1}\left.\frac{\partial \dot{J}_{n+1}^2}{\partial \Delta \varepsilon_{kl}}\right|_{I_{n+1},b_{n+1}}\right) \qquad (3.5\text{-}6)$$

$$+\frac{2}{K_{p_{n+1}}}\left(\frac{\partial \bar{I}_{n+1}}{\partial \Delta \varepsilon_{kl}} - \rho\frac{\partial I_{0_{n+1}}}{\partial \Delta \varepsilon_{kl}}\right)\dot{I}_{n+1}$$

Additional derivatives required for Equations 3.5-4 through -6 are given as:

$$\left.\frac{\partial \bar{I}_{n+1}}{\partial \Delta \varepsilon_{kl}}\right|_{I_{n+1},b_{n+1}} = C(1 - b_{n+1})\left.\frac{\partial I_{0_{n+1}}}{\partial \Delta \varepsilon_{kl}}\right|_{I_{n+1},b_{n+1}} \qquad (3.5\text{-}7)$$

$$\left.\frac{\partial \dot{\bar{I}}_{n+1}}{\partial \Delta \varepsilon_{kl}}\right|_{I_{n+1},b_{n+1}} = -\frac{\left(I_{n+1} - CI_{0_{n+1}}\right)}{\Delta t}\left.\frac{\partial b_n}{\partial \Delta \varepsilon_{kl}}\right|_{I_{n+1},b_{n+1}} - \dot{b}_{n+1}\, C\left.\frac{\partial I_{0_{n+1}}}{\partial \Delta \varepsilon_{kl}}\right|_{I_{n+1},b_{n+1}}$$

$$-b_{n+1}\frac{1}{\Delta t}\left.\frac{\partial I_n}{\partial \Delta \varepsilon_{kl}}\right|_{I_{n+1},b_{n+1}} + C\,(1 - b_{n+1})\left.\frac{\partial \dot{I}_{0_{n+1}}}{\partial \Delta \varepsilon_{kl}}\right|_{I_{n+1},b_{n+1}} \qquad (3.5\text{-}8)$$

$$\left.\frac{\partial I_{0_{n+1}}}{\partial \Delta \varepsilon_{kl}}\right|_{I_{n+1},b_{n+1}} = I_{0_{n+1}}\xi t\,\delta_{kl} \qquad (3.5\text{-}9)$$

$$\left.\frac{\partial \dot{I}_{0_{n+1}}}{\partial \Delta \varepsilon_{kl}}\right|_{I_{n+1},b_{n+1}} = \xi\left(\Delta\theta - \frac{1}{\beta}\frac{\dot{I}_{n+1}}{I_{n+1}}\right)\left.\frac{\partial I_{0_{n+1}}}{\partial \Delta \varepsilon_{kl}}\right|_{I_{n+1},b_{n+1}}$$

$$\qquad\qquad (I > I_l) \qquad (3.5\text{-}10a)$$

$$+\xi I_{0_{n+1}}\left(\delta_{kl} + \frac{1}{\Delta t}\frac{1}{\beta}\frac{1}{I_{n+1}}\left.\frac{\partial I_n}{\partial \Delta \varepsilon_{kl}}\right|_{I_{n+1},b_{n+1}}\right)$$

$$\frac{\partial \dot{I}_{o_{n+1}}}{\partial \Delta \varepsilon_{kl}}\bigg|_{I_{n+1},b_{n+1}} = \xi \left(\Delta\theta - \frac{1}{\beta}\frac{\dot{I}_{n+1}}{I_l} \right) \frac{\partial I_o}{\partial \Delta \varepsilon_{kl}}\bigg|_{I_{n+1},b_{n+1}}$$

$$+ \xi I_{o_{n+1}} \left(\delta_{kl} + \frac{1}{\Delta t\, \beta\, I_l}\frac{\partial I_n}{\partial \Delta \varepsilon_{kl}}\bigg|_{I_{n+1},b_{n+1}} \right) \qquad\qquad (I < I_l) \qquad (3.5\text{-}10b)$$

$$\frac{\partial J_{n+1}^2}{\partial \Delta \varepsilon_{kl}}\bigg|_{I_{n+1},b_{n+1}} = \frac{2}{a_2 b_{n+1}^2} \left[\begin{array}{c} I_{o_{n+1}} \dfrac{\partial I_{o_{n+1}}}{\partial \Delta \varepsilon_{kl}}\bigg|_{I_{n+1},b_{n+1}} \\[2ex] -a_1\left(\bar{I}_{n+1} - \rho I_{o_{n+1}}\right)\left(\dfrac{\partial \bar{I}_{n+1}}{\partial \Delta \varepsilon_{kl}}\bigg|_{I_{n+1},b_{n+1}} - \rho\dfrac{\partial I_{o_{n+1}}}{\partial \Delta \varepsilon_{kl}}\bigg|_{I_{n+1},b_{n+1}} \right) \end{array} \right] \qquad (3.5\text{-}11)$$

$$\frac{\partial \dot{J}_{n+1}^2}{\partial \Delta \varepsilon_{kl}}\bigg|_{I_{n+1},b_{n+1}} = \frac{2 J_{n+1}^2}{\Delta t\, b_{n+1}}\frac{\partial b_n}{\partial \Delta \varepsilon_{kl}}\bigg|_{I_{n+1},b_{n+1}} - \frac{2\dot{b}}{b_{n+1}}\frac{\partial J_{n+1}^2}{\partial \Delta \varepsilon_{kl}}\bigg|_{I_{n+1},b_{n+1}}$$

$$+ \frac{2}{a_2 b_{n+1}^2} \left[\begin{array}{c} \dot{I}_{o_{n+1}} \dfrac{\partial I_{o_{n+1}}}{\partial \Delta \varepsilon_{kl}}\bigg|_{I_{n+1},b_{n+1}} + I_{o_{n+1}} \dfrac{\partial \dot{I}_{o_{n+1}}}{\partial \Delta \varepsilon_{kl}}\bigg|_{I_{n+1},b_{n+1}} \\[2ex] -a_1\left(\bar{I}_{n+1} - \rho I_{o_{n+1}}\right)\left(\dfrac{\partial \dot{\bar{I}}_{n+1}}{\partial \Delta \varepsilon_{kl}}\bigg|_{I_{n+1},b_{n+1}} - \rho\dfrac{\partial \dot{I}_{o_{n+1}}}{\partial \Delta \varepsilon_{kl}}\bigg|_{I_{n+1},b_{n+1}} \right) \\[2ex] -a_1\left(\dot{\bar{I}}_{n+1} - \rho \dot{I}_{o_{n+1}}\right)\left(\dfrac{\partial \bar{I}_{n+1}}{\partial \Delta \varepsilon_{kl}}\bigg|_{I_{n+1},b_{n+1}} - \rho\dfrac{\partial I_{o_{n+1}}}{\partial \Delta \varepsilon_{kl}}\bigg|_{I_{n+1},b_{n+1}} \right) \end{array} \right] \qquad (3.5\text{-}12)$$

$$\frac{\partial \chi_1}{\partial \Delta \varepsilon_{kl}}\bigg|_{I_{n+1},b_{n+1}} = \frac{\partial \chi_1}{\partial \Delta \varepsilon_{kl}} = e_{kl_{n+1}} \qquad\qquad (3.5\text{-}13)$$

$$\frac{\partial \chi_2}{\partial \Delta \varepsilon_{kl}}\bigg|_{I_{n+1},b_{n+1}} = \frac{\partial \chi_2}{\partial \Delta \varepsilon_{kl}} = s_{kl_n} + e_{kl_{n+1}}\left(\frac{\partial s_{ij}}{\partial \Delta \varepsilon_{kl}} \right)_n \qquad\qquad (3.5\text{-}14)$$

The derivative of the deviatoric stress at time t_n with respect to the increment in

strain $\left(\dfrac{\partial s_{ij}}{\partial \Delta \varepsilon_{kl}} \right)_n$ in Equation 3.5-14 is known from the previous substep. If the previous

substep was elastic, the derivative is calculated via Equation 3.3-4.

The derivative of the deviatoric stress at the end of the step (t_{n+1}) is obtained by differentiating Equation 3.4-20 by the strain increment. This derivative is given as:

$$\left(\frac{\partial s_{ij}}{\partial \Delta \varepsilon_{kl}}\right)_{n+1} = \frac{\begin{bmatrix} 2\Delta t \Delta e_{ij_{n+1}}\left(\frac{\partial G}{\partial I}\right)_{n+1}\left(\frac{\partial I}{\partial \Delta \varepsilon_{kl}}\right)_{n+1} + 2 G_{n+1}\Delta t \left(\frac{\partial \Delta e_{ij_{n+1}}}{\partial \Delta \varepsilon_{kl}}\right)_{n+1} + \left(\frac{\partial s_{ij}}{\partial \Delta \varepsilon_{kl}}\right)_{n} \\[2em] -2\Delta t \frac{a_2}{a_1} s_{ij_{n+1}} \begin{pmatrix} \gamma_{n+1} b_{n+1}\left(\frac{\partial G}{\partial I}\right)_{n+1}\left(\frac{\partial I}{\partial \Delta \varepsilon_{kl}}\right)_{n+1} + G_{n+1}\gamma_{n+1}\left(\frac{\partial b}{\partial \Delta \varepsilon_{kl}}\right)_{n+1} \\[1em] + G_{n+1}b_{n+1}\begin{pmatrix} \left.\frac{\partial \gamma_{n+1}}{\partial \Delta \varepsilon_{kl}}\right|_{I_{n+1},b_{n+1}} + \left(\frac{\partial \gamma}{\partial I}\right)_{n+1}\left(\frac{\partial I}{\partial \Delta \varepsilon_{kl}}\right)_{n+1} \\[1em] + \left(\frac{\partial \gamma}{\partial b}\right)_{n+1}\left(\frac{\partial b}{\partial \Delta \varepsilon_{kl}}\right)_{n+1} \end{pmatrix} \end{pmatrix} \end{bmatrix}}{1 + 2 G_{n+1}\Delta t \frac{a_2}{a_1}\gamma_{n+1}b_{n+1}} \quad (3.5\text{-}15)$$

Note that this derivative requires the derivatives $\left(\frac{\partial I}{\partial \Delta \varepsilon_{kl}}\right)_{n+1}$ and $\left(\frac{\partial b}{\partial \Delta \varepsilon_{kl}}\right)_{n+1}$ calculated in Equation 3.5-3. Also, a number of the derivatives are taken at time t_n (i.e., values found at the end of the previous substep and saved). When substepping is used in the stress point iteration, it also must be used in the evaluation of the local Jacobian. The same substep level is used for both the calculation of stress and the local Jacobian. As described in Section 3.4, the independent variables I and b are saved at the end of each substep. The local Jacobian is constructed by recalling these values to calculate the current substep t_{n+1} derivatives. These current values are reserved and used in the calculation of the derivatives at time t_{n+2}, etc. For steps that transition through the elastic zone, the first substep requires values calculated at the boundary of the elastic nucleus (Equations 3.3-4 and 3.3-9). At the end of the substepping, both the volumetric and deviatoric components are combined to provide the local contribution to the global Jacobian.

3.6 Unloading

For each global step, it must be determined whether the step is loading (elastic or plastic) or unloading (elastic). One common approach, especially useful when a predictor stress is calculated, is to cross the stress increment with the normal to the function surface (i.e., the loading index). A positive value indicates loading and a negative value indicates unloading. The loading index is given as:

$$L = \frac{\partial f}{\partial \sigma} \Delta \sigma \qquad (3.6\text{-}1)$$

where L = loading index ($L > 0$, loading; $L < 0$ unloading).

Another approach, similar to the elastic case, is to determine whether there are any positive roots when calculating the intercept to the loading surface. This approach additionally provides the terms necessary to calculate the length of the elastic unloading step. Equation 3.2-18 can be rewritten as:

$$F = q_2 f^2(t) + q_1 f(t) + q_0 = 0 \qquad (3.6\text{-}2)$$

where $q_2 = b^2 c_1$

$$c_1 = \frac{a_2}{a_1}(2\,G_b)^2 \chi_1 + (\beta\Delta\theta\,g(I))^2$$

$$q_1 = b^2 c_2 + b\,c_3$$

$$c_2 = \frac{a_2}{a_1} 2G_b\chi_2 + 2\beta\Delta\theta\,g(I)\,I_b - 2I_c\beta\Delta\theta\,g(I)$$

$$c_3 = 2\beta\Delta\theta\,g(I)\left(I_c - \rho I_{o_{n+1}}\right)$$

$$q_0 = b^2 c_4 + b\,c_5 + c_6$$

$$c_4 = \frac{a_1}{a_2} J_n^2 + \left(I_n - I_{o_{n+1}} \right)^2$$

$$c_5 = 2\left(I_c - \rho I_{o_{n+1}} \right) I_n - 2 I_c \left(I_c - \rho I_{o_{n+1}} \right)$$

$$c_6 = I_c^2 - 2\rho I_c I_{o_{n+1}} + \left(\rho^2 - \frac{1}{a_1} \right) I_{o_{n+1}}^2 .$$

Similar to the elastic case, assume that t in Equation 3.6-2 can take on any value ($t**$). The loading surface intercept is defined by using the current value of $b = b_n$ and solving for the value of f in Equation 3.6-2. Defining $f** = f(t**)$, the solution is:

$$f** = \frac{-q_1 \pm \sqrt{q_1^2 - 4q_2 q_0}}{2q_2} \tag{3.6-3}$$

One root is always near zero (since the current stress point is on the loading surface) and the other will be either positive (indicating an intercept with the loading surface and therefore unloading) or negative (which indicates loading). Therefore, the root with the larger absolute magnitude is tested for its sign:

$$n \supset f_n = \max \left(\left| f_1^{**} \right|, \left| f_2^{**} \right| \right) \tag{3.6-4}$$

where $f_n^{**} > 0 \Rightarrow$ unloading

$f_n^{**} < 0 \Rightarrow$ loading.

If the test determines that unloading is occurring, the length of the unloading step must be calculated. Consider an unloading stress path as shown in Figure 3.6-1. Initially the loading surface shrinks or unloads until the stress path becomes tangent with the surface. At this point the surface begins to grow and loading begins. Now if b is treated as an unknown in Equation 3.6-3, we can determine at what value of b the two roots will be the same, thus defining the loading surface just tangent to the stress path. The roots are

the same when the radical term in Equation 3.6-3 goes to zero (i.e., $q_1^2 - 4q_2q_0 = 0$). This yields an equation for b using the terms calculated in Equation 3.6-2:

$$b^2 \left[b^2 q_5 + b\, q_4 + q_3 \right] = 0 \qquad\qquad (3.6\text{-}5)$$

where $\quad q_3 = c_3^2 - 4c_1 c_6$

$$q_4 = 2c_2 c_3 - 4c_1 c_5$$

$$q_5 = c_2^2 - 4c_1 c_4.$$

Noting that the definition of b requires that it be greater than one, the two zero roots are discarded. The quadratic in the square brackets is solved for b_{min} where the loading surface is a minimum:

$$b_{min} = \frac{-q_4 \pm \sqrt{q_4^2 - 4q_5 q_3}}{2q_5} \qquad\qquad (3.6\text{-}6)$$

Because the loading surface is described in J^2 space (i.e., the square of the deviatoric stresses), one root will be positive and the other will be negative. Again, because the definition of b requires that it be greater than one, the positive root is taken. The value of b_{min} can be substituted for b into Equation 3.6-2 and a new f^{**} is determined (Equation 3.6-3) which yields the length of the unloading step (s_{unload}). The calculation of the behavior of the unloading step is the same as described for the elastic step calculation (Equations 3.2-26). Solving for b first is advantageous because if the minimum falls within the elastic surface (i.e., $b_{min} > b_{elastic}$), the elastic intercept can be easily calculated by substituting $b = b_{elastic}$. The flow chart for determining the elastic unloading step is shown in Figure 3.6-2.
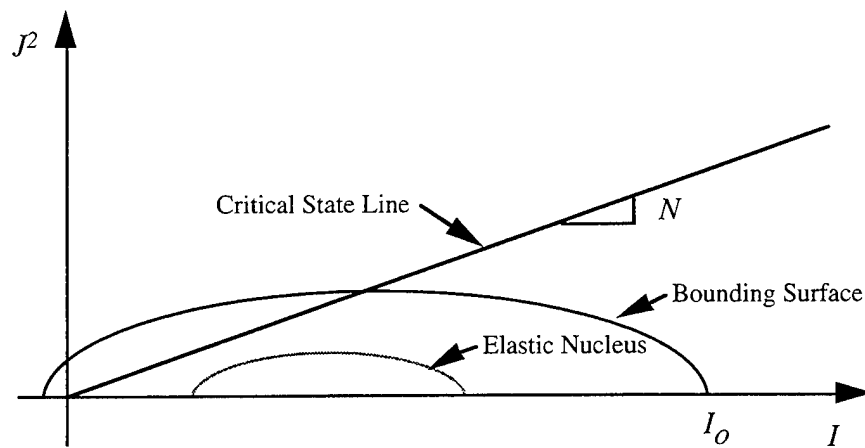
Figure 3.1-1. Bounding Surface in Two-Invariant Space.

First Effective Stress Invariant, I
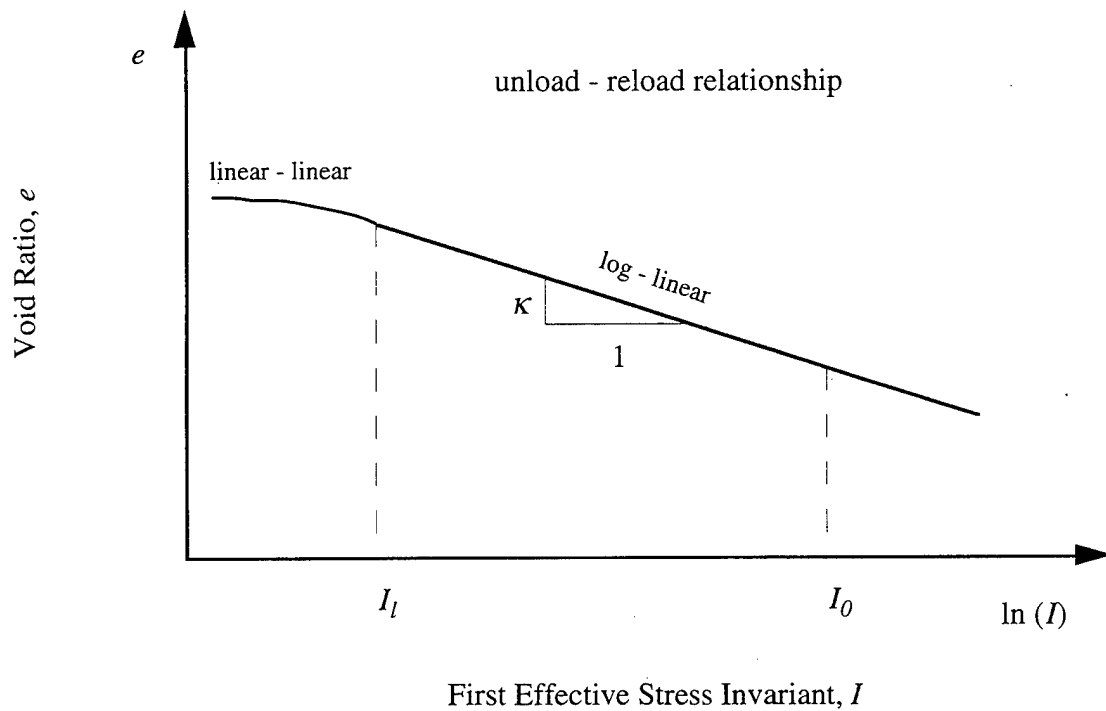
Figure 3.2-1. Volumetric Stress versus Void Ratio Relationship.
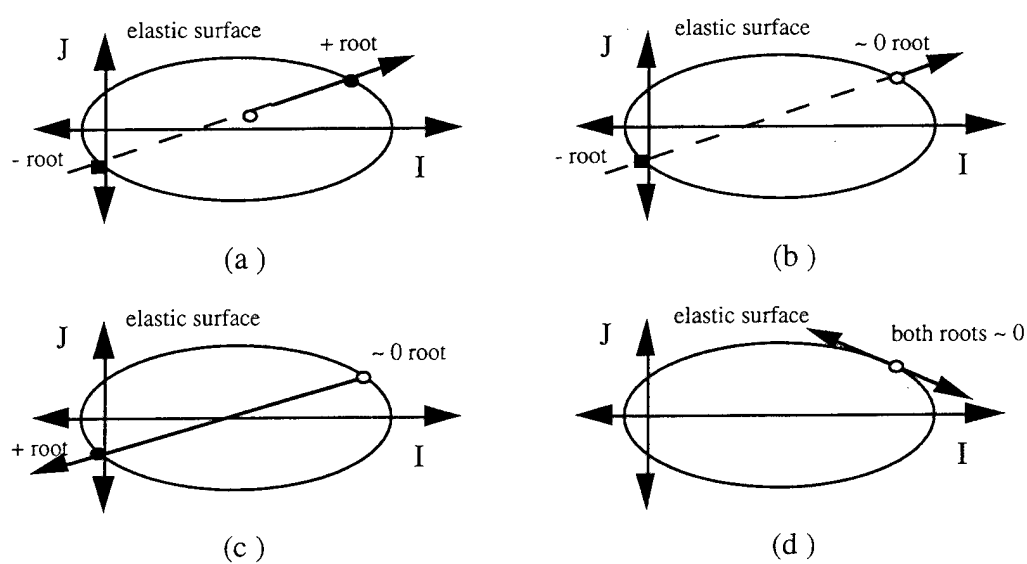
Figure 3.2-2. Possible Roots for the Intersections of the Elastic Surface.
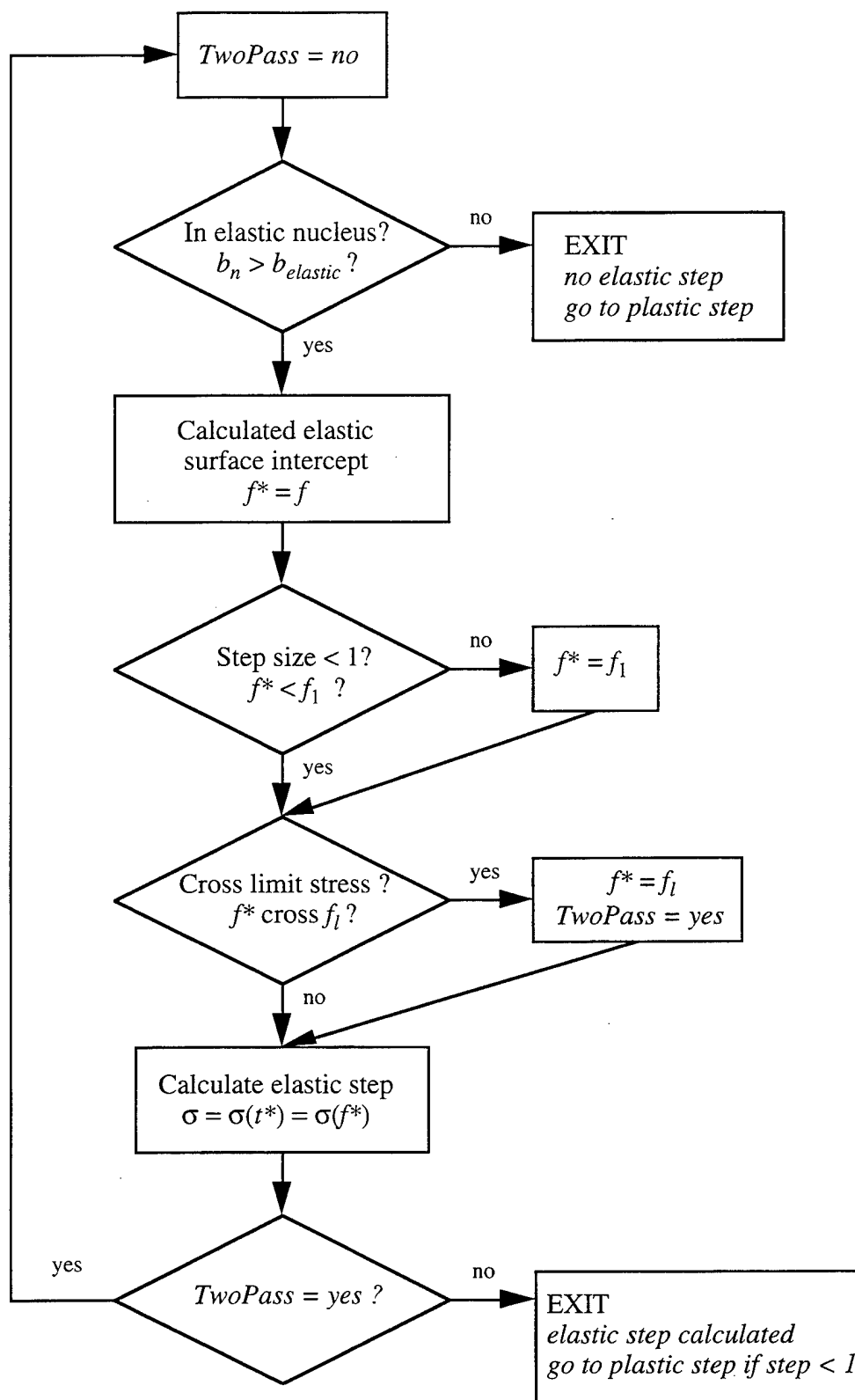
Figure 3.2-3. Elastic Step Flow Chart
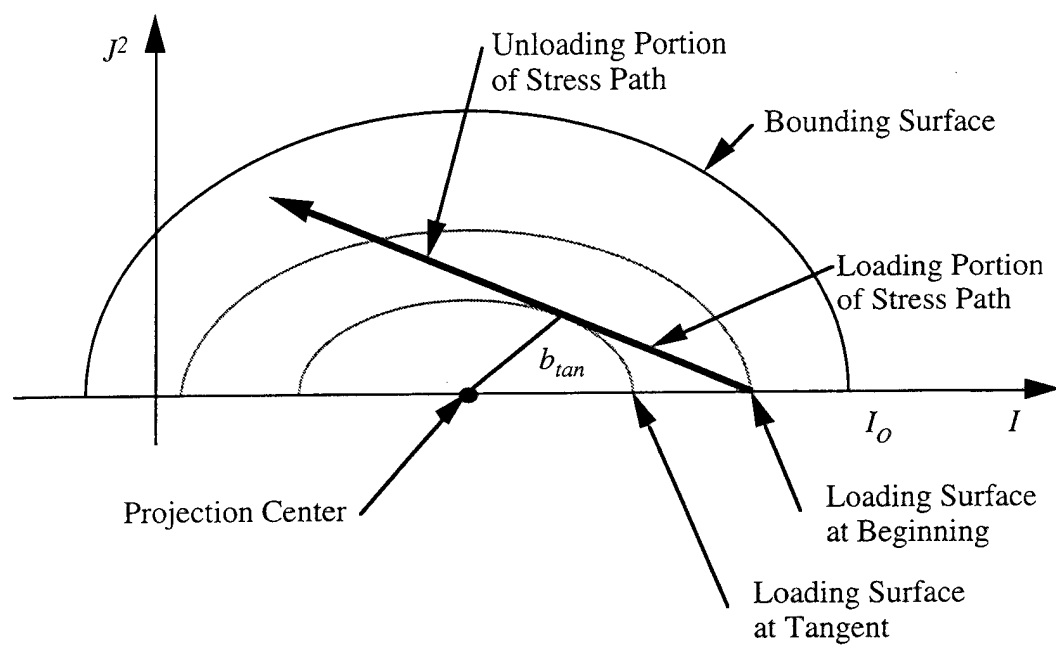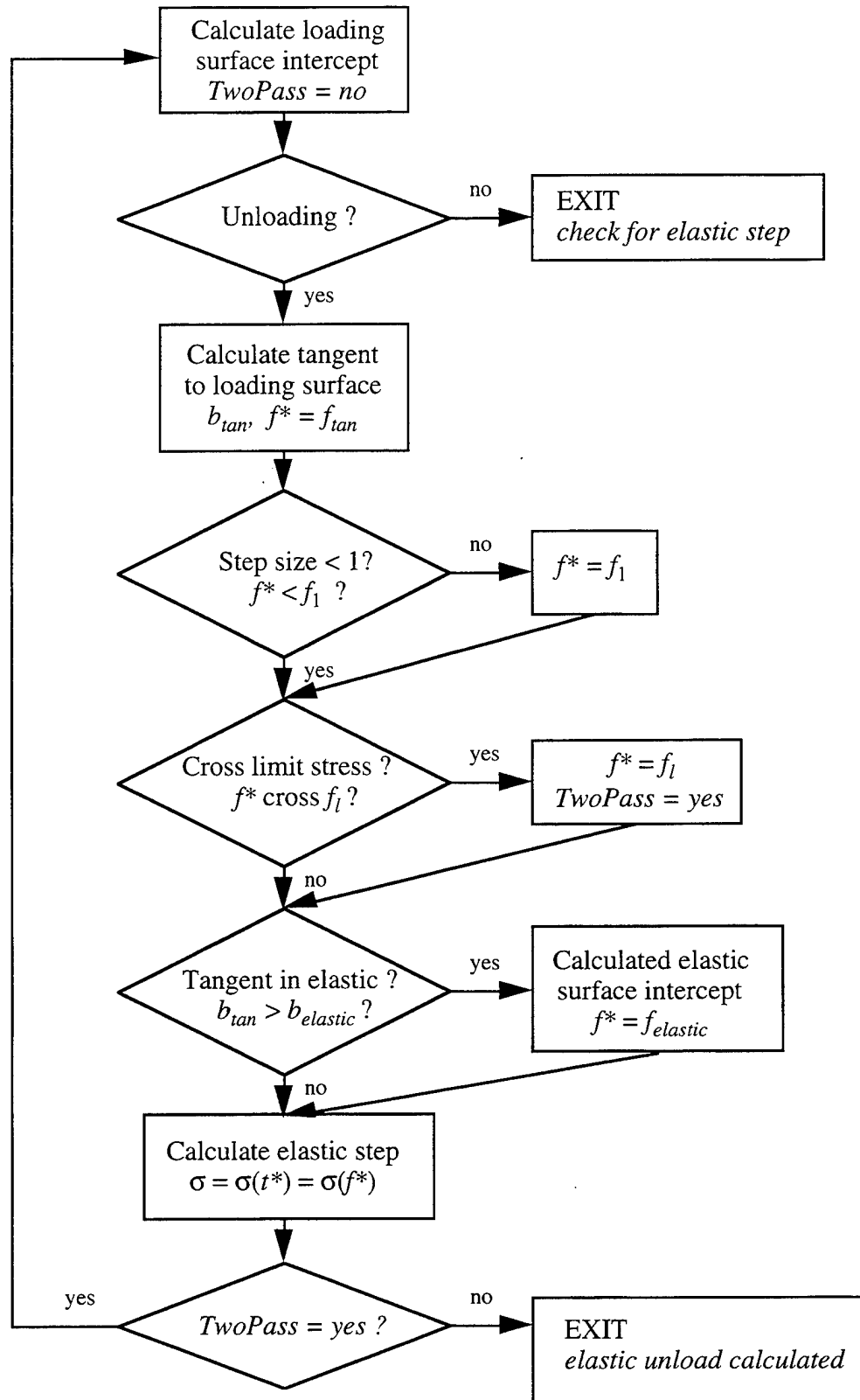
Figure 3.6-1. Typical Unloading Path.

Figure 3.6-2. Elastic Unloading Flow Chart

4. Example Calculations

4.1 Problem Descriptions

Comparisons of predictions for a number of sample problems were made using the three methods: 1) trapezoidal (Trap), 2) Closest Point (CP), and 3) Reduced Newton (RN), in order to determine their behavior. This comparison section is divided into three sections: 1) comparison of the methods without substepping starting on the bound, 2) comparison of the methods without substepping starting inside the bound and 3) comparison of the methods with substepping. Substepping involves uniformly subdividing the strain increment within the material model subroutine and solving for the stress as a cumulative sum of the incremental stresses from each substep.

Section 4.2 compares the methods without substepping and provides a general description of how each method behaves. Because the convergence criterion for the iterations of each of the methods is different, comparison of computational times is meaningless. The methods are compared at 1, 2, 4 and 100 global steps. There is a difference between taking N substeps across the interval as compared to taking N global steps. The histories of the various strain components are generally not proportional. When N global steps are used, this nonproportionality is taken into account $\left(\text{i.e., } \dot{\varepsilon}_{ij}/\dot{\varepsilon}_{kl} = f(t)\right)$. In contrast, the use of N substeps approximates the strain histories as proportional $\left(\text{i.e., } \dot{\varepsilon}_{ij}/\dot{\varepsilon}_{kl} = \text{constant}\right)$.

For points that start on the bound, the "exact" solutions are established by assigning an arbitrary change in state and calculating (using numerical integration with a very tight tolerance) the corresponding strains. The strains for the intermediate steps are also determined by integration. The strain calculations are given in Appendix C.

Section 4.3 considers stress points that start within the bound. Since no "exact" strains were calculated, an arbitrary strain increment was chosen. The trapezoidal solution for 100 uniform global steps is assumed to be nearly exact for comparison purposes.

Section 4.4 compares the methods with uniform substepping within the algorithm. A common convergence criterion is established for the substepping, therefore comparison of computational times is made possible. The criterion used is defined in Equation 3.4-59. A set of strain increments is chosen for each problem and the algorithm is allowed to uniformly substep as required to meet the substepping convergence criterion.

4.2 Comparison of Methods for Stress Points on the Bound (no substepping)

Several tests were performed to compare of the behavior of the methods for stress points initially on the bound. The Bounding Surface parameters used for these tests are given in Table 4.2-1. Discussion of the parameters is given in the references [Herrmann and Mish, 1983b and Kaliakin, 1985].

Table 4.2-1. Bounding Surface Parameters for Stress Points on the Bound.

λ	κ	M	υ	I_l	R
0.14	0.05	1.05	0.2	14.7 (psi)	2.6

4.2.1 Volumetric Compression Test 1

A simple compression test along the volumetric axis was analyzed using the three methods. The problem data is given in Table 4.2.1-1. The "exact", Trap, CP and RN results are given on Tables 4.2.1-2, 4.2.1-3, 4.2.1-4 and 4.2.1-5, respectively. The Trap method provides reasonable results at one step with a slight improvement as the number of

steps increases. Because the CP and RN methods treat the volumetric behavior separately, they achieve the exact answer within a few iterations.

4.2.2 Volumetric Tension Test

Similar to the compression test, a simple tension test along the volumetric axis was also performed. The problem data and the "exact" results are given in Table 4.2.2-1 and 4.2.2-2, respectively. The first attempt using the Trap method is shown in Table 4.2.2-3. The solution is wrong and does not improve, even with 100 steps. The problem lies in the implementation of the hardening rule (Section 1.5). In the previous work [Kaliakin, 1985], the hardening rule was broken into a linear-linear and log-linear section similar to the volumetric stress behavior (Section 1.3). As strain developed for a given stress path (Appendix C, Section C.1), the amount of tensile volumetric strain that this form of the hardening rule could tolerate was limited. Simplifying the hardening rule to the log-linear form improved the performance, although a large number of steps were required to achieve a reasonable answer (see Table 4.2.2-4). In contrast, the CP and RN methods exhibited accurate results with one step (see Tables 4.2.2-5 and 4.2.2-6).

4.2.3 Shear Test 1

A shear test was designed so that the stress is initially on the volumetric stress axis and travels in the direction of the second stress invariant (J) while keeping the first invariant (I) constant. The problem data is given in Table 4.2.3-1. The results for the Trap, CP and RN methods are shown in terms of J and the hardening (i.e., the bound size, I_o) in Figures 4.2.3-1, 4.2.3-2 and 4.2.3-3, respectively. The Trap method shows the largest error at the larger strain increments, which can be expected since the integration does not explicitly satisfy the consistency condition at the end of the step (i.e., maintaining $F = 0$). The error manifests itself in larger shear stresses and less hardening than the "exact" stress path. This behavior indicates that the final stress point is outside of the Bounding Surface. The

CP and RN methods show similar behavior because they both are Newton-Raphson methods that explicitly satisfy the consistency condition at the end of the step. Although there is some error for the larger strain increments, the stress points fall close to the "exact" stress path. The convergence from below the "exact" path indicates points falling within the bound.

4.2.4 Shear Test 2

Shear Test 1 is now modified so that the stress begins some distance from the volumetric axis (i.e., $J = 0$), but still on the bound. This data is given in Table 4.2.4-1. The Trap (Figure 4.2.4-1) again shows larger shear stresses and less hardening than the "exact" stress path for large strain increments. For smaller strain steps, however, the Trap method exhibits somewhat better accuracy. The CP and RN methods (Figures 4.2.4-2 and 4.2.4-3) show virtually the same behavior and converge from the opposite side than the Trap method.

4.3 Comparison of Methods for Stress Points inside the Bound (no substepping)

Several tests were conducted for comparison of the behaviors of the methods for stress points initially inside the bound. The Bounding Surface parameters used for these tests include those for points on the bound (given in Table 4.2-1) and the parameters defining behavior within the bound (given in Table 4.3-1). Discussion of these parameters is given in the references [Herrmann and Mish, 1983b and Kaliakin, 1985].

Table 4.3-1. Bounding Surface Parameters for Stress Points within the Bound.

p_{atm}	C	s_p	m	H_c	H_o	a	w
14.7 psi	0.28	0	0.02	4.0	4.0	1.2	5.0

4.3.1 Volumetric Compression Test 2

A simple strain-controlled compression test along the volumetric axis is described in Table 4.3.1-1. No "exact" solution was calculated (i.e., a stress path is assumed and the corresponding strains calculated) so the Trap solution using 100 steps was assumed to be the actual answer. The Trap, CP and RN results are given in Tables 4.3.1-2, 4.3.1-3 and 4.3.1-4, respectively. All of the methods provided reasonable results at one step and a slight improvement as the number of steps increased.

4.3.2 Shear Test 3

A shear test was analyzed that starts the stress on the volumetric axis and moves mostly in the second stress invariant (J) direction. The problem data is given in Table 4.3.2-1. The results for the Trap, CP and RN methods are shown in terms of J and I_o in Figures 4.3.2-1, 4.3.2-2 and 4.3.2-3, respectively. The Trap method shows greater shear stress and less hardening for the larger strain increments. The CP and RN methods, while having significant error for the large strain increments, show end points that fall on the actual stress path.

4.3.3 Shear Test 4

Shear Test 3 is now modified so that the stress begins some distance from the volumetric axis (i.e., $J = 0$). This data is given in Table 4.3.3-1. The Trap method (Figure 4.3.3-1) for this test actually shows the best behavior converging on the "exact" stress path within two steps. The CP and RN methods (Figures 4.2.4-2 and 4.2.4-3) show poorer accuracy and converge to the "exact" answer from the opposite side than the Trap method.

4.4 Comparison of Methods with Substepping

The Bounding Surface parameters used for the substepping tests are given in Tables 4.2-1 and 4.4-1. The only difference from the solutions inside the bound (Section 4.3) is that a small elastic nucleus has been introduced (e.g., $s_p = 3.0$).

Table 4.4-1. Bounding Surface Parameters used for Substepping Tests.

p_{atm}	C	s_p	m	H_c	H_o	a	w
14.7 psi	0.28	3.0	0.02	4.0	4.0	1.2	5.0

The substepping used for this study is a linear subdivision of the strain increment (i.e., dividing the strain increments by two) up to a level of 32 (i.e., 2^5) equal substeps. The substepping levels and number of steps are given in Table 4.4-2.

Table 4.4-2. Substep Levels versus Number of Substeps.

Substep Level, m	1	2	3	4	5	6
Number of Equal Substeps	1	2	4	8	16	32

The convergence criterion used to stop substepping in this study is the percentage of change in the predicted final Bounding Surface size. This was defined in Equation 3.4-60 and is given by:

$$\left\{\left[\left(I_{o_{n+1,m}} - I_{o_{n+1,m-1}}\right) < Toler_{I_o}\right] \quad OR \quad \left[It > It_{\max}\right]\right\} \quad THEN: \quad EXIT \qquad (3.4\text{-}60)$$

The methods iterate on the solution for each strain level produced by the substepping until the iteration criterion is satisfied. At the end of each substepping process, the Bounding Surface size (I_o) is compared to the value found with the previous

substepping. When the change in the bound size is below the specified tolerance, the results are printed. The tolerance used for this study was 0.001 psi.

4.4.1 Nearly Elastic Compression and Shear

A test was designed to start within the elastic nucleus and project out into the plastic realm. The initial stress is located on the volumetric axis (i.e., $J = 0$) near the projection center so a large part of the path is elastic. This data is given in Table 4.4.1-1. The stress path in I - J space is shown in Figure 4.4.1-1. The "exact" solution uses the Trap method and 100 linearly interpolated global strain increments.

The Trap and RN methods show nearly identical results and nearly give the "exact" solution. The CP method shows significant error in the stress path. This error is caused by the inaccuracy of the rate equation for the stress distance measure (b) near the elastic surface.

The computational time of the methods were compared with the codes compiled with Language Systems FORTRAN on a Macintosh Centris 650. The times are compared on a relative scale with the Trap method time used as the base (i.e., the Trap method is always one). The relative speeds and substepping are shown in Figure 4.4.1-2. Although the Trap and RN methods show nearly identical results, the Trap method shows the best behavior converging on the "exact" solution in less time and fewer substeps. This is to be expected since it is a second order method and is most appropriate for nearly elastic calculations. Also, the RN and CP methods converge in the same number of substeps, but the CP method takes significantly longer. This is a result of the second order derivatives that need to be calculated every iteration. In addition, each iteration of the CP method must solve nine simultaneous equations while the RN method only solves two. Another difficulty with the CP method is the use of the rate equation for b (Equation 1.7-11) which is a function of the hardening modulus (K_p). As the hardening modulus approaches the elastic surface it rapidly goes to infinity (see Equation 1.6-4). The behavior of the

hardening modulus and the *b* rate equation is shown in Figure 4.4.1-3. For stress points near the elastic surface, the use of Equation 1.7-11 actually slows convergence because of the large gradient.

4.4.2 Plastic Compression and Shear

A plasticity test was designed to start near the bound and project out into the plastic realm. The initial stress is located off the volumetric axis (i.e., $J = -3.6$ psi) near the bound so a significant portion of the path is on the Bounding Surface. This data is given in Table 4.4.2-1. The stress path in $I - J$ space is shown in Figure 4.4.2-1.

All of the methods show results close to the "exact" solution. The CP method shows slightly more error than the other methods.

The relative times are shown in Figure 4.4.2-2, and for the Trap and RN methods they are almost the reverse of what was observed in Section 4.4.1. The RN method shows about a 50% decrease from the Trap method. The CP and RN methods were developed to account for plasticity and show improved performance by converging in fewer substeps. Again, because of the calculation of the second order derivatives in the CP method, the relative time is significantly higher.

4.4.3 Shear Softening

A shear test in the softening realm was designed to start on the bound. Volumetric strains were prescribed to keep the volumetric stress nearly constant. This data is given in Table 4.4.3-1. The stress path in $I - J$ space is shown in Figure 4.4.3-1.

All of the methods show results close to the "exact" solution. The CP and RN methods show slightly more error than the Trap method, but this is small (note the scale of the I-axis).

The computational times are shown in Figure 4.4.3-2. The CP and RN show a larger number of substeps for convergence, yet the RN method took less time than the Trap

method with fewer substeps. Again, because of the calculation of the second order derivatives in the CP method, the relative time is significantly higher.

Table 4.2.1-1. Compression Test 1-Parameters.

$I_o = 81$ (psi), $e_o = 0.94$

$\sigma_{11} = \sigma_{22} = \sigma_{33} = -27$ psi, $\sigma_{12} = \sigma_{13} = \sigma_{23} = 0$

$\Delta\varepsilon_{11} = \Delta\varepsilon_{22} = \Delta\varepsilon_{33} = -2.80025 \times 10^{-3}$, $\Delta\varepsilon_{12} = \Delta\varepsilon_{13} = \Delta\varepsilon_{23} = 0$

Table 4.2.1-2. Compression "Exact" Results.

I	I_o	b
91	91	1

Table 4.2.1-3. Compression Test 1-Trapezoidal Results.

Number of Steps	I	I_o	b
1	90.9799	91.0101	0.9996
2	90.9894	91.0012	0.9997
4	90.9968	90.9980	1.0000

Table 4.2.1-4. Compression Test 1-Closest Point Results.

Number of Steps	I	I_o	b
1	91.0000	91.0000	1.0000

Table 4.2.1-5. Compression Test 1-Reduced Newton Results.

Number of Steps	I	I_o	b
1	91.0000	91.0000	1.0000

Table 4.2.2-1. Tension Test Parameters.

$I_o = 0.9$ psi, $e_o = 0.94$

$\sigma_{11} = \sigma_{22} = \sigma_{33} = -6.92308\text{x } 10^{-2}$ psi, $\sigma_{12} = \sigma_{13} = \sigma_{23} = 0$

$\Delta\varepsilon_{11} = \Delta\varepsilon_{22} = \Delta\varepsilon_{33} = 9.15692\text{x}10^{-3}$, $\Delta\varepsilon_{12} = \Delta\varepsilon_{13} = \Delta\varepsilon_{23} = 0$
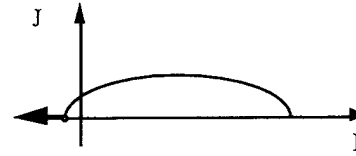
Table 4.2.2-2. Tension "Exact" Results.

I	I_o	b
$-2.07692\text{x}10^{-2}$	0.5	1

Table 4.2.2-3. Tension Test Trapezoidal Results before I_o Fix.

Number of Steps	I	I_o	b
1	2.0965	0.0010	~ 0

Table 4.2.2-4. Tension Test Trapezoidal Results with I_o Fix.

Number of Steps	I	I_o	b
1	2.0965	0.6408	~ 0
2	-3.0007	0.6413	0.0493
4	-1.6303	0.6161	0.0872
100	-0.1629	0.5048	1.0000

Table 4.2.2-5. Tension Test Closest Point Results.

Number of Steps	I	I_o	b
1	-0.1145	0.4961	1.0000

Table 4.2.2-6. Tension Test Reduced Newton Results.

Number of Steps	I	I_o	b
1	-0.1145	0.4961	1.0000

Table 4.2.3-1. Shear Test 1-Parameters.

$I_o = 81$ psi, $e_o = 0.94$

$\sigma_{11} = \sigma_{22} = \sigma_{33} = -27$ psi, $\sigma_{12} = \sigma_{13} = \sigma_{23} = 0$

$\Delta\varepsilon_{11} = \Delta\varepsilon_{22} = \Delta\varepsilon_{33} = -1.80016\times10^{-3}$, $\Delta\varepsilon_{12} = -1.14129\times10^{-2}$, $\Delta\varepsilon_{13} = \Delta\varepsilon_{23} = 0$
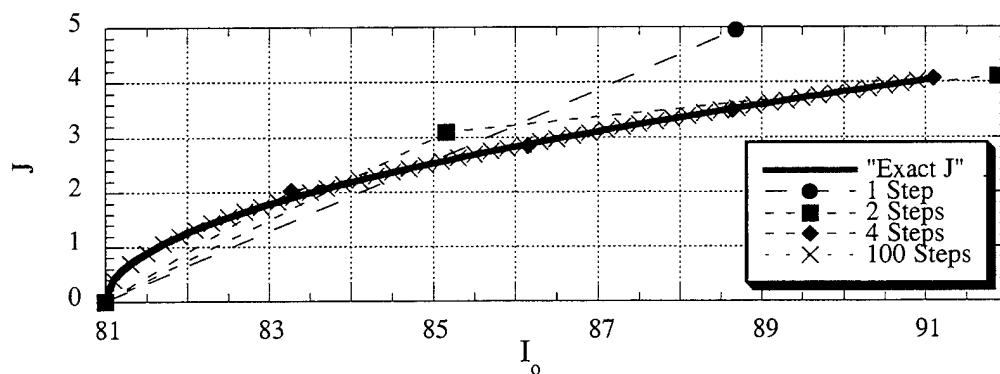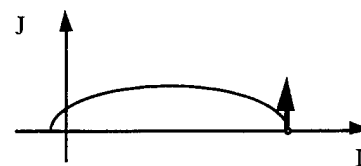
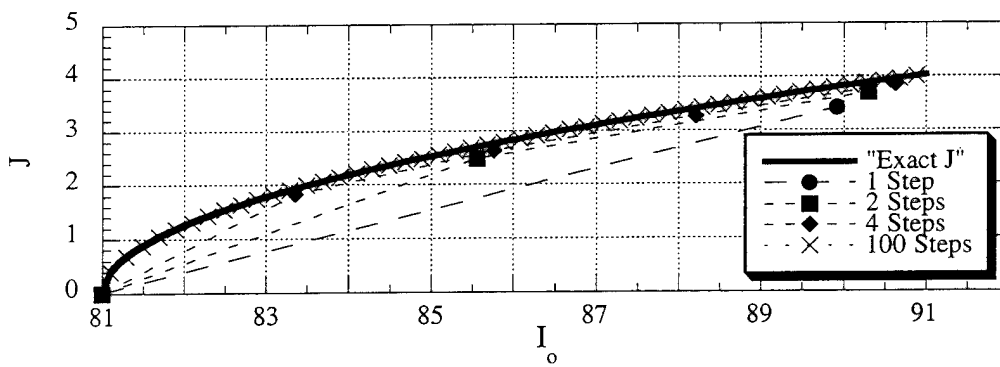Figure 4.2.3-1. Trapezoidal Shear Test 1-Results.
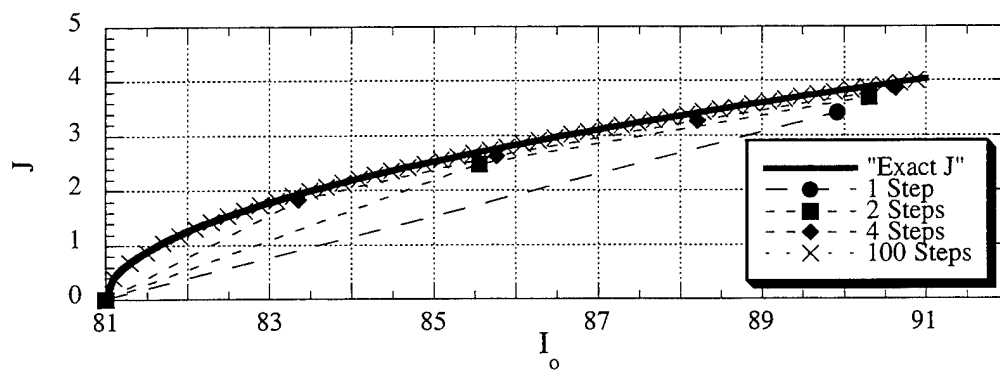
Figure 4.2.3-2. Closest Point Shear Test 1-Results.
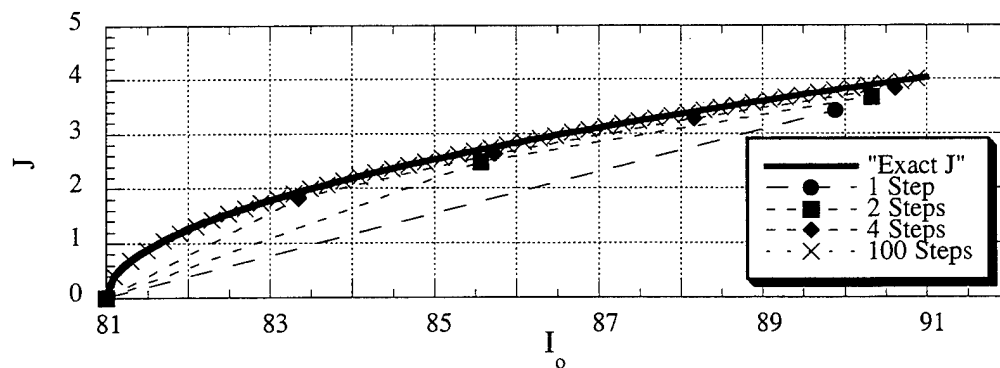
Figure 4.2.3-3. Reduced Newton Shear Test 1-Results.

Table 4.2.4-1. Shear Test 2-Parameters.

$I_o = 60$ psi, $e_o = 0.94$

$\sigma_{11} = \sigma_{22} = \sigma_{33} = -18$ psi, $\sigma_{12} = 3.63731$ psi, $\sigma_{13} = \sigma_{23} = 0$

$\Delta\varepsilon_{11} = \Delta\varepsilon_{22} = \Delta\varepsilon_{33} = -2.38377 \times 10^{-3}$, $\Delta\varepsilon_{12} = -1.77091 \times 10^{-2}$, $\Delta\varepsilon_{13} = \Delta\varepsilon_{23} = 0$
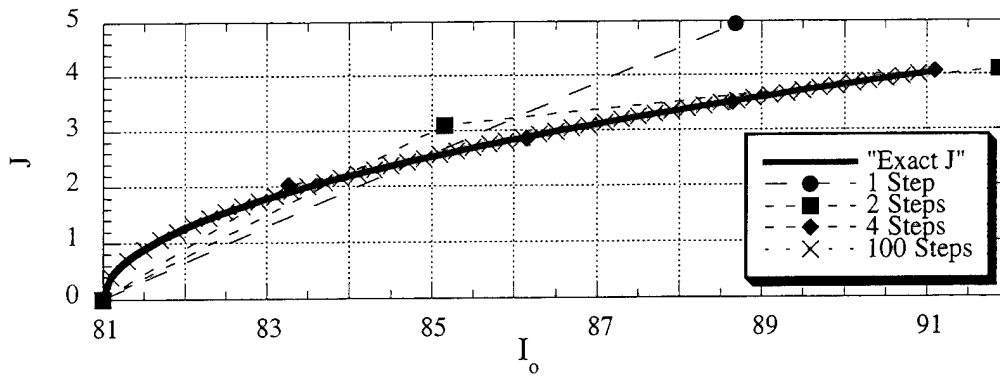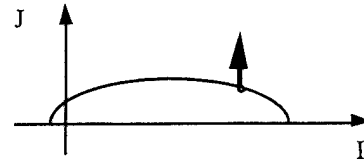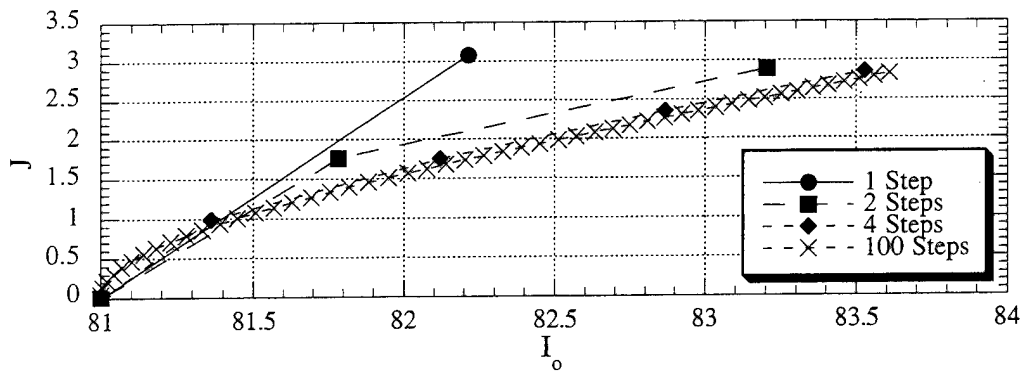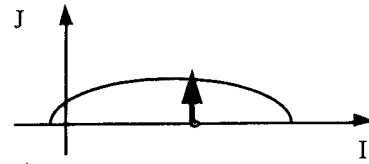

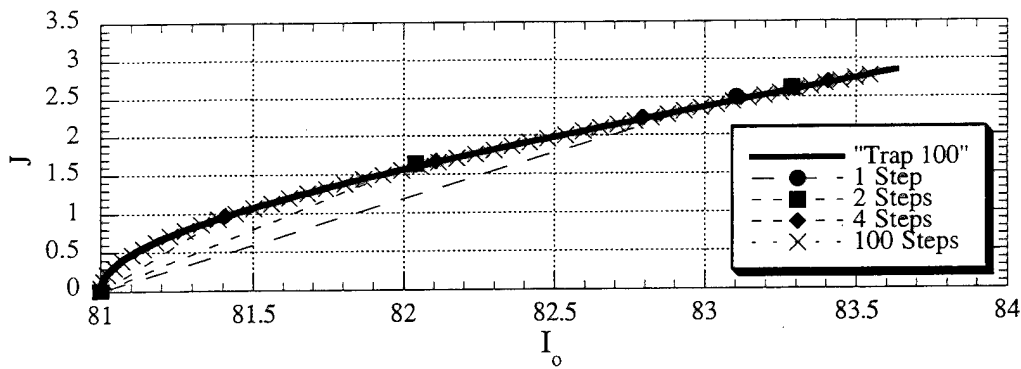Figure 4.2.4-1. Trapezoidal Shear Test 2-Results.
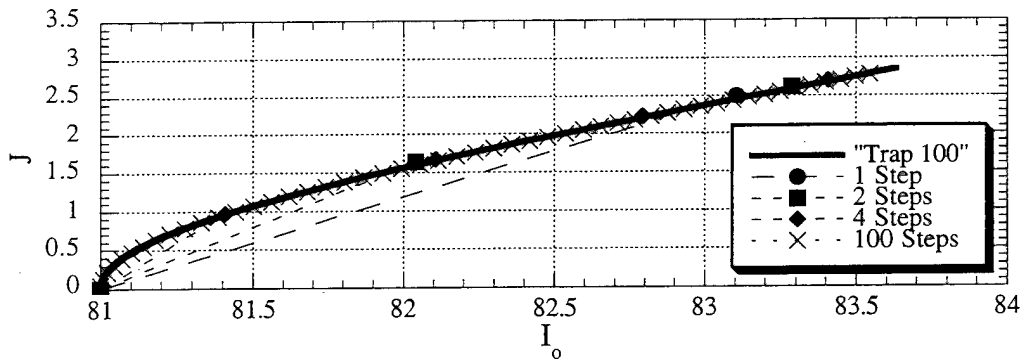

Figure 4.2.4-2. Closest Point Shear Test 2-Results.
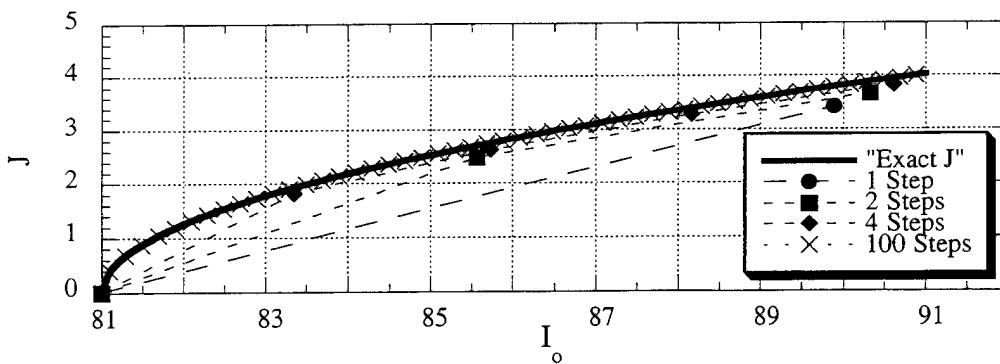
Figure 4.2.4-3. Reduced Newton Shear Test 2-Results.

Table 4.3.1-1. Compression Test 2-Parameters.

$I_o = 81$ (psi), $e_o = 0.94$

$\sigma_{11} = \sigma_{22} = \sigma_{33} = -15$ psi, $\sigma_{12} = \sigma_{13} = \sigma_{23} = 0$

$\Delta\varepsilon_{11} = \Delta\varepsilon_{22} = \Delta\varepsilon_{33} = -1.0 \times 10^{-3}$, $\Delta\varepsilon_{12} = \Delta\varepsilon_{13} = \Delta\varepsilon_{23} = 0$
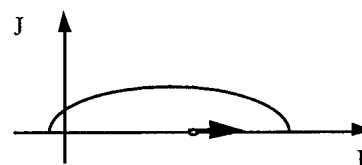
Table 4.3.1-2. Compression Test 2-Trapezoidal Results.

Number of Steps	I	I_o	b
1	48.8177	82.5852	2.3143
2	48.8186	82.5874	2.3143
4	48.8188	82.5878	2.3143
100	48.8188	82.5879	2.3143

Table 4.3.1-3. Compression Test 2-Closest Point Results.

Number of Steps	I	I_o	b
1	48.6779	82.7207	2.3342
2	48.7452	82.6572	2.3245
4	48.7855	82.6193	2.3193
100	48.8173	82.5894	2.3145

Table 4.3.1-4. Compression Test 2-Reduced Newton Results.

Number of Steps	I	I_o	b
1	48.7494	82.6532	2.3240
2	48.7877	82.6172	2.3186
4	48.8017	82.6040	2.3167
100	48.8182	82.5885	2.3144

Table 4.3.2-1. Shear Test 3-Parameters.

$I_o = 81$ psi, $e_o = 0.94$

$\sigma_{11} = \sigma_{22} = \sigma_{33} = -15$ psi, $\sigma_{12} = \sigma_{13} = \sigma_{23} = 0$

$\Delta\varepsilon_{11} = \Delta\varepsilon_{22} = \Delta\varepsilon_{33} = 0$, $\Delta\varepsilon_{12} = -1.0\times10^{-2}$, $\Delta\varepsilon_{13} = \Delta\varepsilon_{23} = 0$
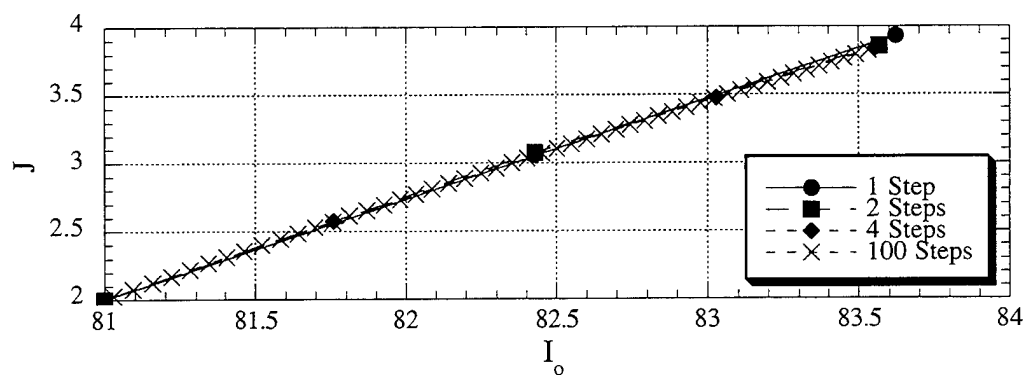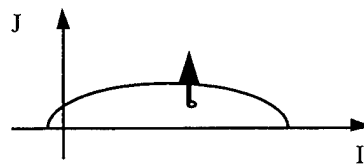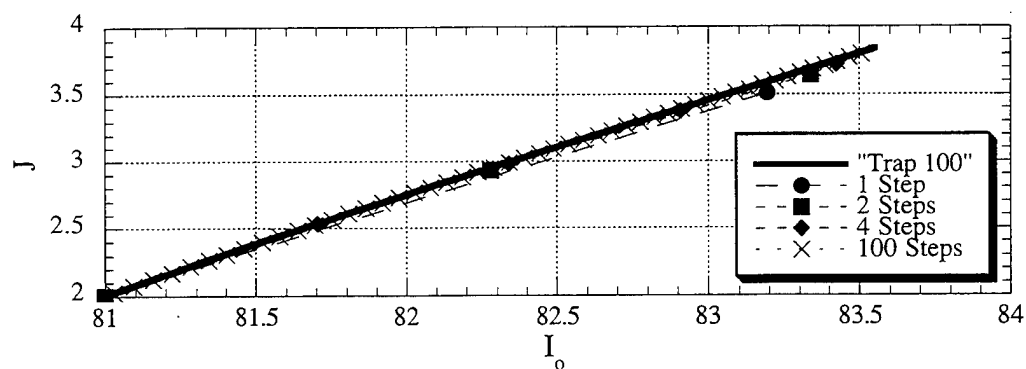

Figure 4.3.2-1. Trapezoidal Shear Test 3-Results.

Figure 4.3.2-2. Closest Point Shear Test 3-Results.

Figure 4.3.2-2. Reduced Newton Shear Test 3-Results.

Table 4.3.3-1. Shear Test 4-Parameters.

$I_o = 81$ psi, $e_o = 0.94$

$\sigma_{11} = \sigma_{22} = \sigma_{33} = -15$ psi, $\sigma_{12} = -2.0$ psi, $\sigma_{13} = \sigma_{23} = 0$

$\Delta\varepsilon_{11} = \Delta\varepsilon_{22} = \Delta\varepsilon_{33} = 0$, $\Delta\varepsilon_{12} = -1.0\times10^{-2}$, $\Delta\varepsilon_{13} = \Delta\varepsilon_{23} = 0$

Figure 4.3.3-1. Trapezoidal Shear Test 4-Results.
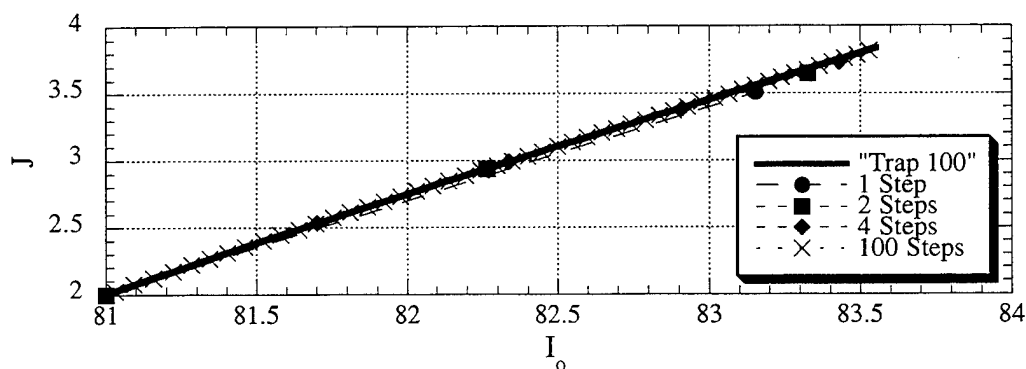

Figure 4.3.3-2. Closest Point Shear Test 4-Results.

Figure 4.3.3-3. Reduced Newton Shear Test 4-Results.

Table 4.4.1-1. Nearly Elastic Compression and Shear Test-Parameters.

$I_o = 81$ psi, $e_o = 0.94$

$\sigma_{11} = \sigma_{22} = \sigma_{33} = -10$ psi, $\sigma_{12} = \sigma_{13} = \sigma_{23} = 0$

$\Delta\varepsilon_{11} = \Delta\varepsilon_{22} = \Delta\varepsilon_{33} = -1.0 \times 10^{-2}$, $\Delta\varepsilon_{12} = 1.0 \times 10^{-2}$, $\Delta\varepsilon_{13} = \Delta\varepsilon_{23} = 0$
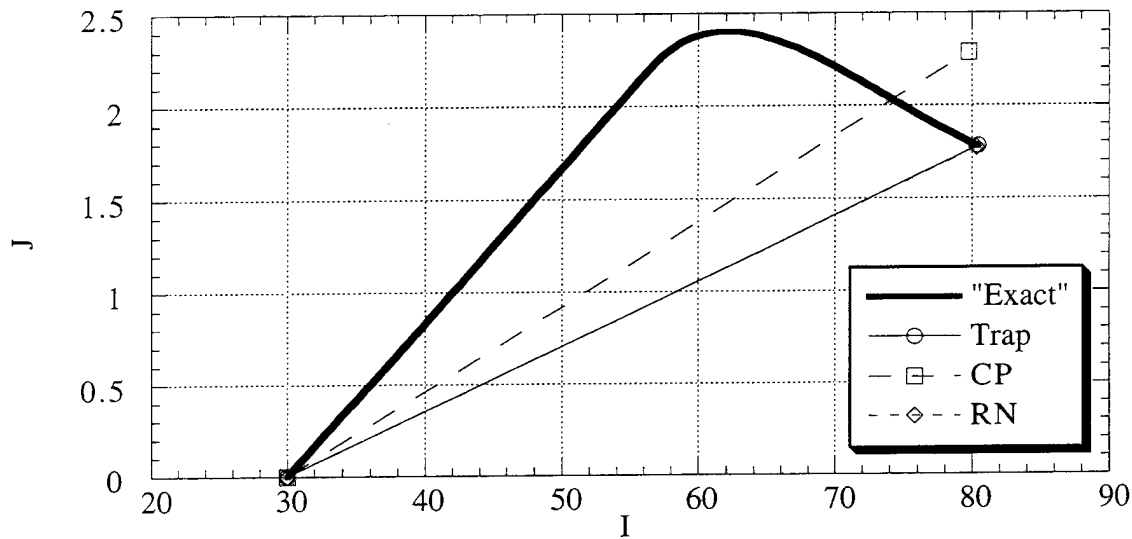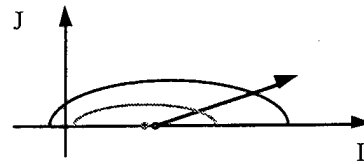

Figure 4.4.1-1. Nearly Elastic Test Stress Path.

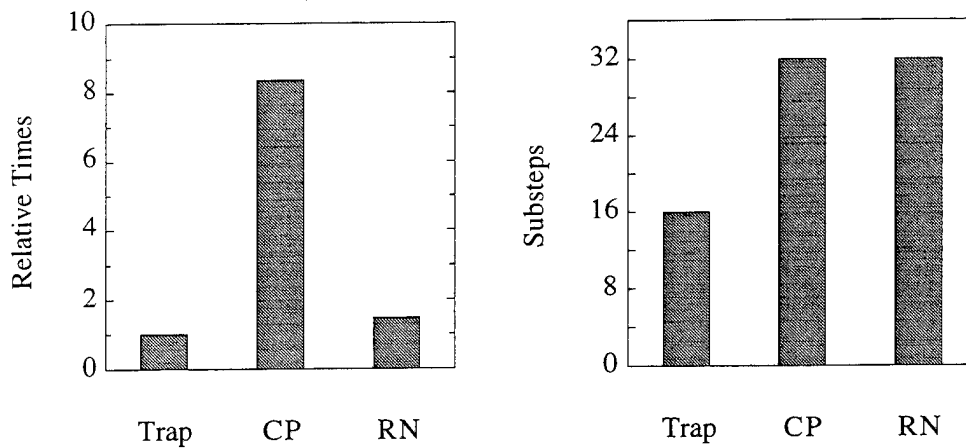

Figure 4.4.1-2. Nearly Elastic Test-Relative Times and Substeps.

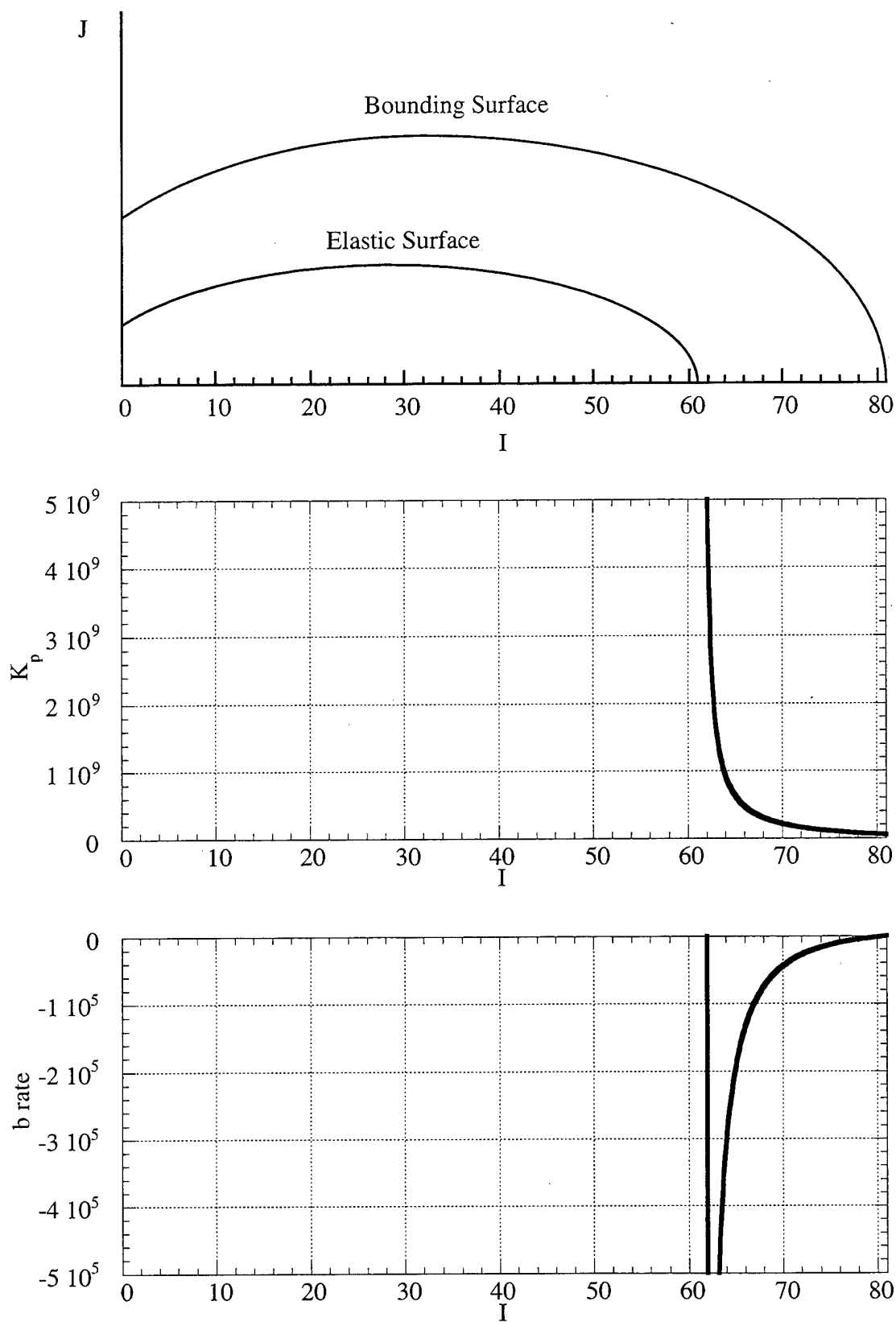Figure 4.4.1-3. Hardening Modulus and b Rate Behavior Along I-Axis.

Table 4.4.2-1. Plastic Compression and Shear Test-Parameters.

$I_o = 60$ psi, $e_o = 0.94$

$\sigma_{11} = \sigma_{22} = \sigma_{33} = -15$ psi, $\sigma_{12} = -3.6$ psi, $\sigma_{13} = \sigma_{23} = 0$

$\Delta\varepsilon_{11} = 2.0\times10^{-2}$, $\Delta\varepsilon_{22} = -4.0\times10^{-2}$, $\Delta\varepsilon_{33} = -1.0\times10^{-2}$,

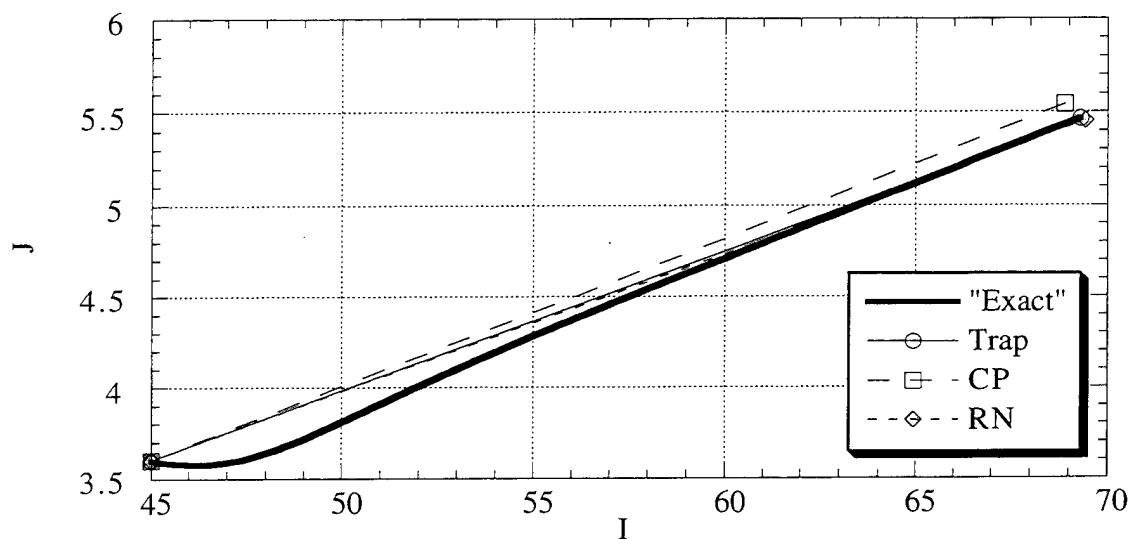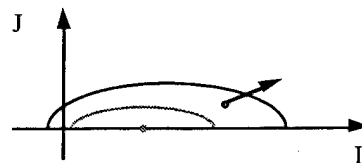$\Delta\varepsilon_{12} = -3.0\times10^{-2}$, $\Delta\varepsilon_{13} = \Delta\varepsilon_{23} = 0$

Figure 4.4.2-1. Plastic Test-Stress Path.
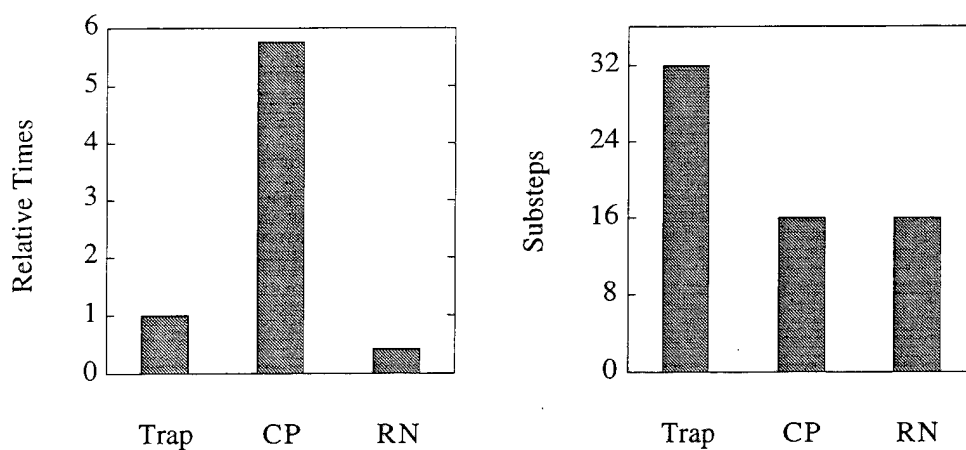
Figure 4.4.2-2. Plastic Test-Relative Times and Substeps.

Table 4.4.3-1. Softening Shear Test-Parameters.

$I_o = 81$ psi, $e_o = 0.94$

$\sigma_{11} = \sigma_{22} = \sigma_{33} = -4$ psi, $\sigma_{12} = -5.81202$ psi, $\sigma_{13} = \sigma_{23} = 0$

$\Delta\varepsilon_{11} = \Delta\varepsilon_{22} = \Delta\varepsilon_{33} = -2.03767 \times 10^{-3}$, $\Delta\varepsilon_{12} = -3.632453 \times 10^{-2}$,

$\Delta\varepsilon_{13} = \Delta\varepsilon_{23} = 0$
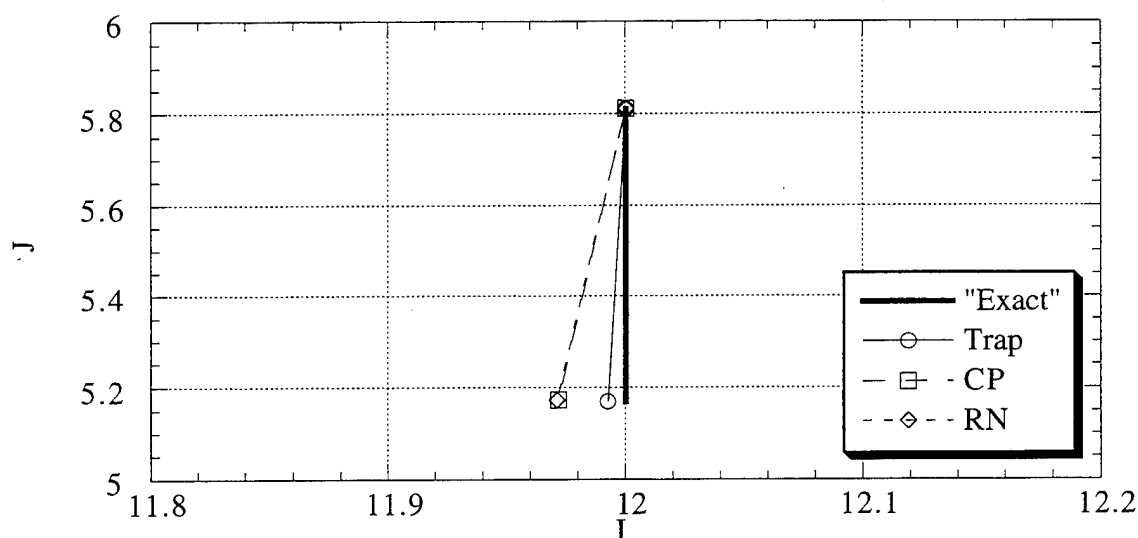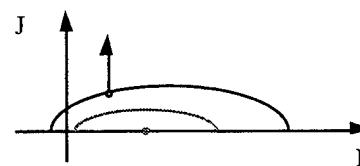

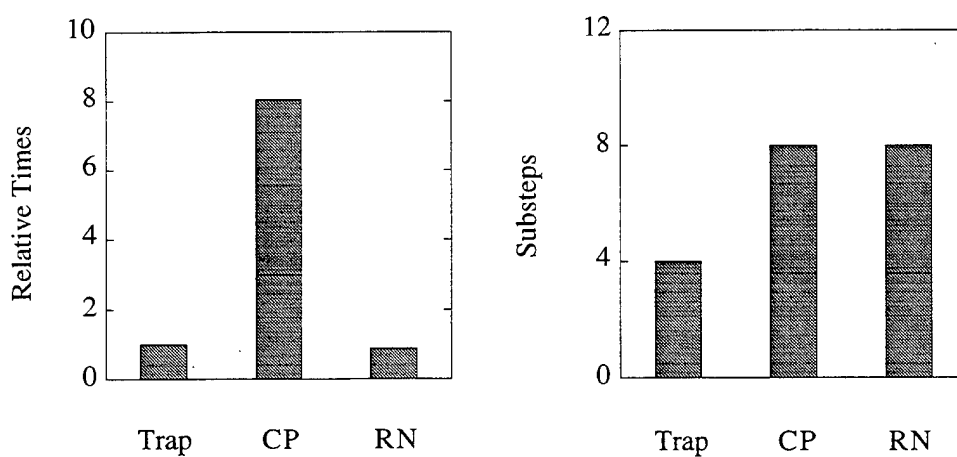Figure 4.4.3-1. Softening Shear-Test Stress Path.

Figure 4.4.3-2. Softening Shear-Test Relative Times and Substeps.

5. Constitutive Model Implementation

Constitutive models are generally designed to be implemented within finite element programs. The manner in which these programs solve the global nonlinear problem dictates the requirements of the constitutive model. For this study, the implementation will be in a program which uses the Newton-Raphson method for nonlinear solutions. The DYSAC2 finite element computer program is a dynamic analysis code for soils and was written at the University of California at Davis [Muraleetharan, et. al., 1991].

This section will be divided into two parts:

1) discussion of the issues of interfacing a constitutive model into a typical finite element program that uses the Newton-Raphson method, and

2) results of implementing the Bounding Surface model for clays into the DYSAC2 program.

5.1 Standard Interface

The development of a "standard" interface for constitutive models creates a conflict between modular programming and the means for convenient debugging (for an analyst to debug a "bad" solution as opposed to the debugging required for implementing a constitutive model). These two opposing philosophies dictate the level of information that should be provided through the constitutive model interface. Modular programming requires the minimum amount of information in the interface, whereas debugging often requires more.

Modular programming is based on a "need-to-know" philosophy and provides only the information required to perform its function. The benefit of this minimal interface is that it prevents additional information (especially in weakly-typed languages, such as FORTRAN) from being corrupted. It also provides the easiest means for adding new constitutive models to existing programs because the user is not required to track the meaning of extraneous variables.

Convenient debugging, on the other hand, requires a great deal of information that is never used within the constitutive model. The information is needed for tracking the cause of the problem in the event of a numerical failure within the model. When a constitutive model fails (e.g., does not converge) the user can extract information (such as the integration point, element, iteration and time step numbers) to determine whether an input parameter was specified wrongly or simply that the mesh was not detailed enough in a particular area. This information, however, is not required for the execution of the constitutive model.

In order to provide the best of both philosophies, two interfaces are proposed:

1) the constitutive branching routine, and

2) the standard constitutive model.

The constitutive branching routine is generally called from the integration point routine and contains the logic for deciding which material set belongs to the element. The constitutive model can be called from five separate areas in the program during the analysis phase (depending on the program's architecture):

1) reading of constitutive properties,

2) initialization of internal variables,

3) stresses and tangent moduli calculation during the Newton-Raphson iteration,

4) updating internal variables, and

5) stress reporting.

Often the updating is merely the swapping of a temporary and permanent internal variable array, and stress reporting is accessing the stored stresses. At this level, sufficient debugging information should exist to track a numerical problem in the constitutive array. The branching routine is proposed to have both debugging and constitutive information

with an interface defined as:

> ***branching routine*** **(analysis phase, time step number, iteration number, element number, integration point number, *constitutive information*)**

The constitutive properties and the initial values of the internal variables are obtained during the reading phase. This step is done once for each separate material type and often doesn't go through the branching routine (since element information is not required for debugging). A typical read routine interface is defined as:

> ***read routine*** **(properties, internal variables)**

> ***output:***
>> **properties** = constitutive property array
>>
>> **internal variables** = internal variable array.

The constitutive information required will be defined by the initialization and Newton-Raphson iteration requirements. A typical initialization routine interface is:

> ***initialization routine*** **(properties, initial stresses, internal variables, external variables)**

> ***input:***
>> **properties** = constitutive property array
>>
>> **initial stresses** = initial stress state array
>>
>> **external variables** = external variable array

output:

> **internal variables** = internal variable array.

During the Newton-Raphson iteration, the constitutive routine should produce the change in stress, tangent moduli and the change in internal variables given, the constitutive model properties, initial stresses, existing strains, internal and external variables and the increment in strain. The routine should be written so that when numerical errors occur (or are about to occur) they are trapped and it exits to the branching routine where the error and necessary debugging information can be reported. This is known as defensive programming and prevents the code from crashing within the constitutive routine where no debugging information is available. A typical constitutive routine interface is defined as:

> *constitutive routine* **(properties, strains, strain increment,**
>
> > **stresses, internal variables, external variables,**
> >
> > **tangent moduli, error, convergence information)**

input:

> **properties** = constitutive property array
>
> **strains** = existing strain array
>
> **strain increment** = new strain increment array

input and output:

> **stresses** = previous stress state array (overwritten with the new stresses)
>
> **internal variables** = internal variable array (overwritten with new array)
>
> **external variables** = external variable array (possibly overwritten)

output:

tangent moduli = the stress - strain gradient, $\left(\dfrac{\partial\sigma}{\partial\varepsilon}\right)_{n+1}$ matrix

error = convergence errors

convergence information = whether or not convergence occurred.

The external variables (e.g., temperature, T) are often input only. If the analysis is coupled with these variables, the main program might also require additional gradients associated with them to be defined $\left(\text{e.g.,}\ \dfrac{\partial(flux)}{\partial\varepsilon}\ \text{and}\ \dfrac{\partial\sigma}{\partial T}\right).$

As shown above, the stress and internal variable arrays are overwritten. Often a temporary array is maintained for both the stresses and internal variables. Once the global solution has converged, then the updating simply consists of copying the temporary array into the permanent array. If the temporary arrays need to be maintained at the global level, separate arrays of the previous and new values can be specified at the interface. This allows for faster global updating (i.e., a single loop over all of the update arrays without going down to the element level) and easier restart capabilities. The constitutive routine interface can now be defined as:

> *constitutive routine* **(properties, strains, strain increment,**
> **previous stresses, previous internal variables,**
> **previous external variables, new stresses,**
> **new internal variables, new external variables**
> **tangent moduli, error, convergence information)**

input:

> **previous stresses** = previous stress state array
>
> **previous internal variables** = previous internal variable array
>
> **previous external variables** = previous external variable array

output:

> **new stresses** = new stress state array
>
> **new internal variables** = new internal variable array
>
> **new external variables** = new external variable array

When temporary arrays are used, stress reporting at the integration points becomes a matter of simply printing the stress array. Calculation of stresses at other points within the element (e.g., node points) is generally done at a global/element level (i.e., curve fitting) in order of average element contributions to common points. A graphical representation of this interface is given in Figure 5.1-1. The dotted lines indicate calls that the main program can make directly without going through the branching routine.

5.2 Application of the DYSAC2 Program to an Embankment Subjected to an Earthquake

In order to evaluate the performance of the Reduced Newton version of the Bounding Surface clay model (Section 3), the model was implemented into the DYSAC2 finite element computer program [Muraleetharan, et. al., 1991]. DYSAC2 is a dynamic soil analysis code for two-dimensional plane strain problems that fully couples the governing equations of a saturated porous media (two phase). The implementation was made in accordance with the "standard interface" discussed in the previous section.

The problem chosen for the evaluation of the numerical model involves an earthen clay embankment subjected to an earthquake. The embankment was previously analyzed

using DYSAC2 (with base shaking) using the three-surface clay model with trapezoidal integration and comparing the results to the centrifuge results [Muraleetharan, et. al., 1994]. For this study, the single-surface model (ellipse) was used with the properties given in Table 5.2-1 using both the trapezoidal and Reduced Newton integrations. A more detailed description of the parameters is given in an earlier publication [Herrmann and Mish, 1983b]. The interest here is not to compare the results to the centrifuge test results (although a direct comparison to the experimental results indicates a slight improvement in accuracy), but to compare the performance of the Reduced Newton integration to the trapezoidal integration. The finite element dicretization is shown in Figure 5.2-1.

The centrifuge model was spun up to 80g, allowed to consolidate and then subjected to base motion. The initial stresses (created by the centrifuge spin up) in the finite element model were calculated using SAC2 [Herrmann and Mish, 1983c; Herrmann and Kaliakin., 1987b]. Since the current version of DYSAC2 does not have this capability, the initial stresses were graciously provided by Dr. Muraleetharan. DYSAC2 is then used to calculate the embankment response to the base motion. The input base acceleration is shown in Figure 5.2-2.

The comparison of the embankment predictions using the trapezoidal and Reduced Newton methods can be evaluated by looking at various nodal and element responses. The analysis used 1,008 time steps with a time increment of 1.5625×10^{-4} seconds. An additional analysis was performed using the trapezoidal method, but with twice the number of steps (Trapezoidal x2), for accuracy comparisons. The horizontal and vertical accelerations and displacements are shown in Figures 5.2-3 and 5.2-4, respectively. The accelerations of all three analyses match extremely well. The displacements show a slight discrepancy near the end of the analysis, with the Reduced Newton method closely following the more accurate trapezoidal run. Excess pore water pressure histories for selected elements are shown in Figure 5.2-5, and show a similar variation with the Reduced Newton being more accurate. Contour plots of the excess pore water pressure for

both methods are shown in Figure 5.2-6 and indicate little difference between the two

methods. The times as recorded on a PowerMac 8100/100 are given in Table 5.2-2 and

shows the Reduced Newton method slightly faster. The global iterations per step are

shown in Figure 5.2-7 and the results are quite similar.

5.3 Application of the DYSAC2 Program to an Embankment Subjected to a Shock

Another analysis was conducted of the clay embankment with a shock applied at the

base. The same material properties were used and are given in Table 5.2-1. The model

was analyzed at the same 80g level (created by the centrifuge) so that the same initial

conditions could be used. The base shock is shown in Figure 5.3-1.

The analysis used 5,000 time steps with a time increment of 5.0×10^{-5} seconds.

Similar to the earthquake study, an additional analysis was performed using the trapezoidal

method, but with twice the number of steps (Trapezoidal x2), for accuracy comparisons.

The horizontal and vertical accelerations and displacements are shown in Figures 5.3-2 and

5.3-3, respectively. The accelerations are shown for the first 0.1 second for clarity and all

of the methods match extremely well. The displacements show a slight divergence near the

end with the trapezoidal and Reduced Newton methods drifting slightly from the more

accurate Trapezoidal x2 analysis. Excess pore water pressure histories for selected

elements are shown in Figure 5.3-4 and show results similar to the displacements.

Contour plots of the excess pore water pressure for both methods are shown in Figure 5.3-

5 and indicate little difference between the methods. The times as recorded on a PowerMac

8100/100 are given in Table 5.3-1 and show the Reduced Newton method to be slightly

faster.

Table 5.2-1. Bounding Surface Model Parameters.

Parameter	Description	Value
λ	Slope of virgin compression line	0.25
κ	Slope of swell/compression line	0.05
M_c	Slope of critical state (triaxial space)	0.88
M_e/M_c	Ratio of CSL slopes extension to compression (3D only)	1.0
ν	Poisson's ratio or shear modulus	0.3
I_l	Transition I for log to linear	101.4 kPa
p_{atm}	Atmospheric pressure	30.4 kPa
R	Shape of bounding surface	2.4
C	Projection center parameter	0.0
s_p	Elastic zone parameter	1.0
m	Exponent for shape hardening function	0.02
H_c	Hardening parameter associated with compression	3.0
H_e/H_c	Ratio of hardening parameters, ext/ comp (3D only)	1.0
H_0	Hardening parameter associated with I axis	2.0
a	Parameter controlling magnitude of hardening	1.2
w	Parameter controlling decrease of hardening	5.0

Table 5.2-2. Embankment Subjected to an Earthquake Timing Results.

Method	Time (sec)	Time (min)
Trapezoidal	3252	54.2
Reduced Newton	3223	53.7

Table 5.3-1. Embankment Subjected to a Shock Timing Results.

Method	Time (sec)	Time (min)
Trapezoidal	12052	200.9
Reduced Newton	11789	196.5

main program

main program

branching routine
(global information available here)

constitutive model interface
(information limited to what constitutive routines need)

stress reporting

print

stresses
internal variables?
convergence
information?

update *

previous ← new

stresses
internal variables
external variables

* (could be done
at global level)

constitutive

in
properties
strains
strain increment
previous stresses
previous internal variables
previous external variables

out
new stresses
new internal variables
new external variables
tangent moduli
other gradients (if needed)
error and convergence?

initialization

in
properties
initial stresses
external variables

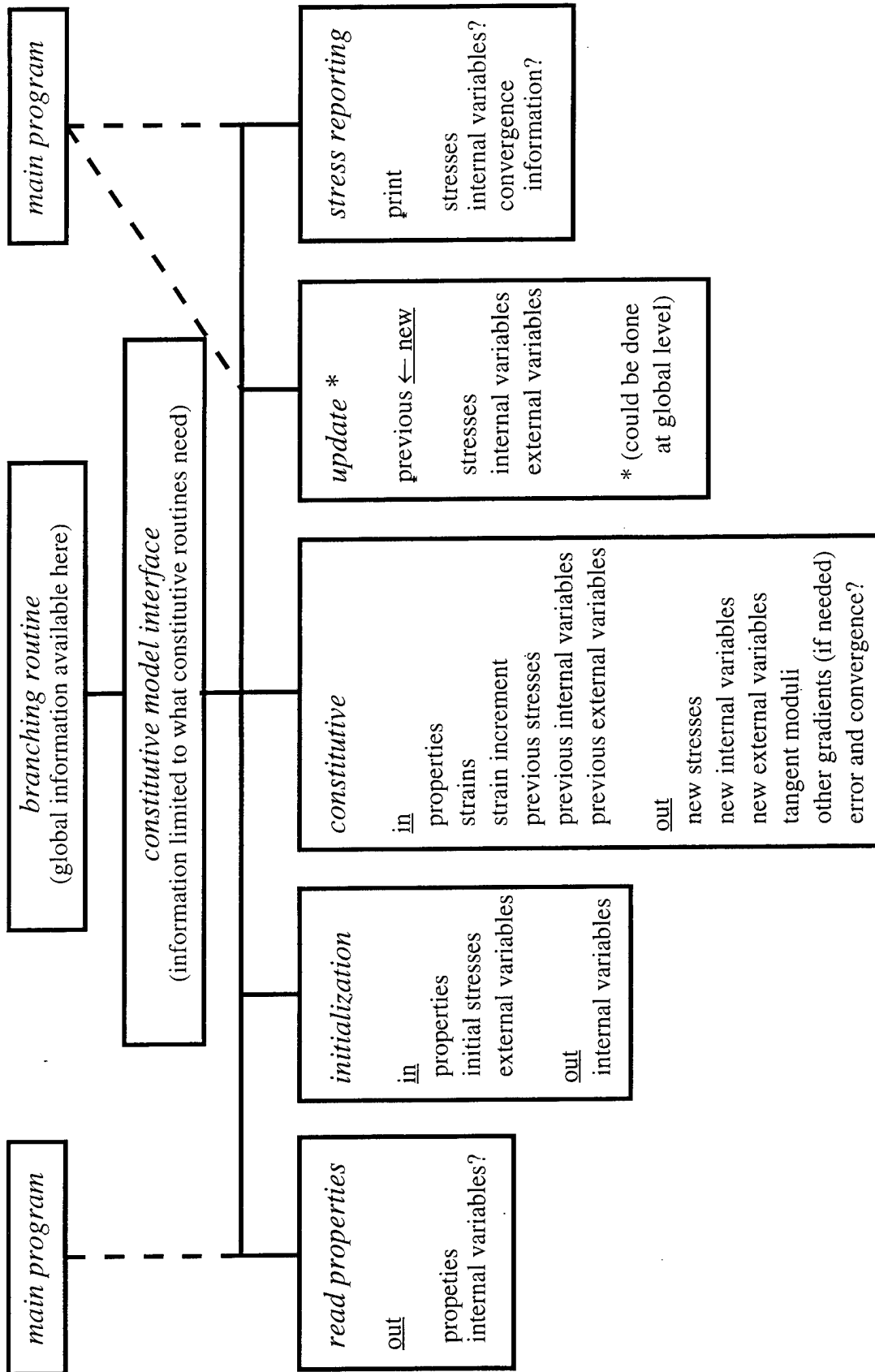out
internal variables

read properties

out

propeties
internal variables?

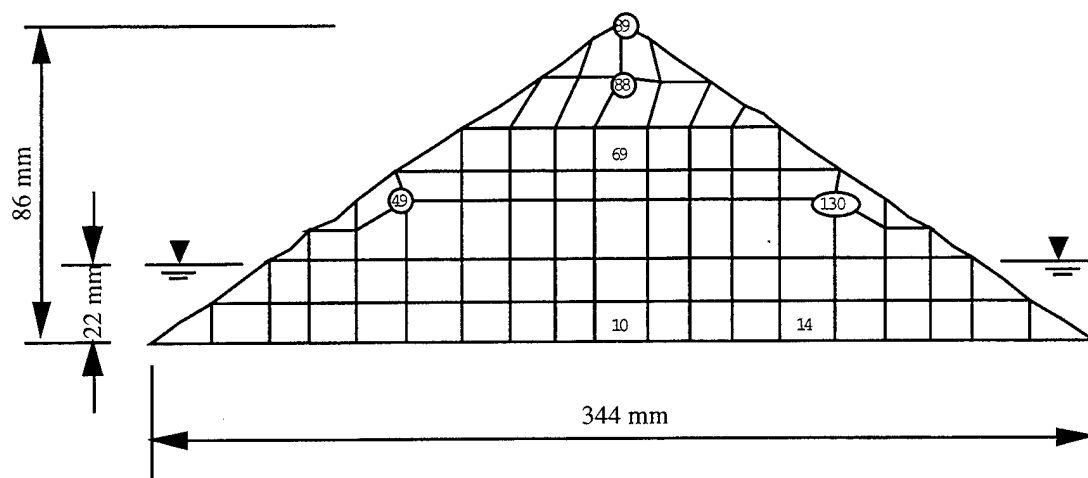FIgure 5.1-1. Constitutive Model Interface

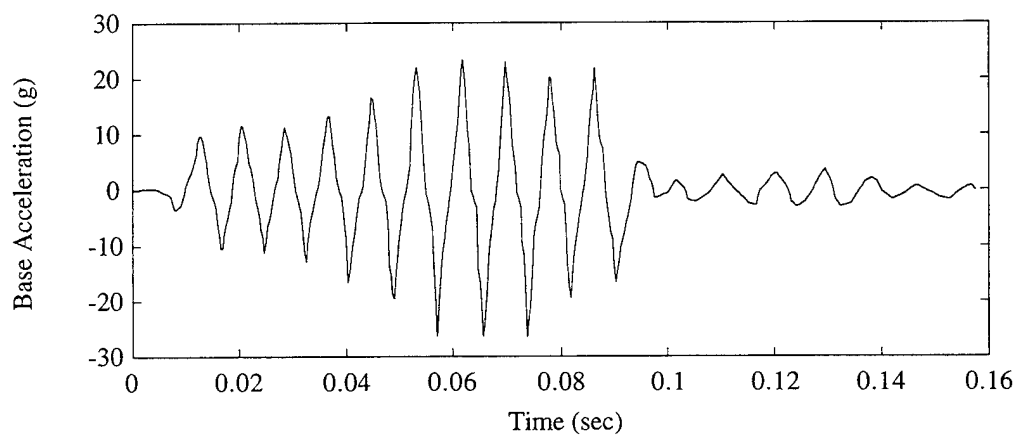Figure 5.2-1. Finite Element Discretization of Embankment.

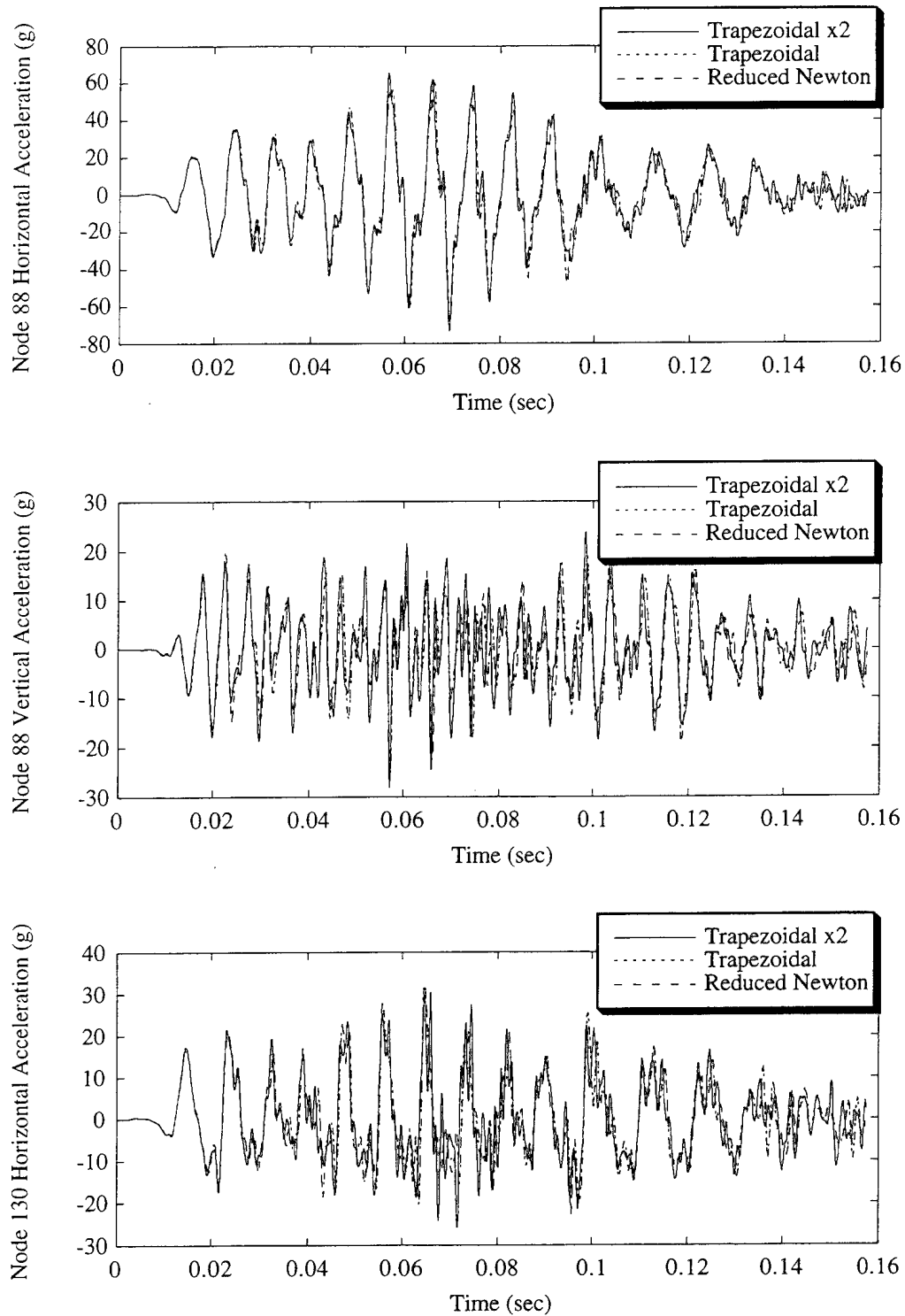Figure 5.2-2. Input Base Acceleration for Earthquake.

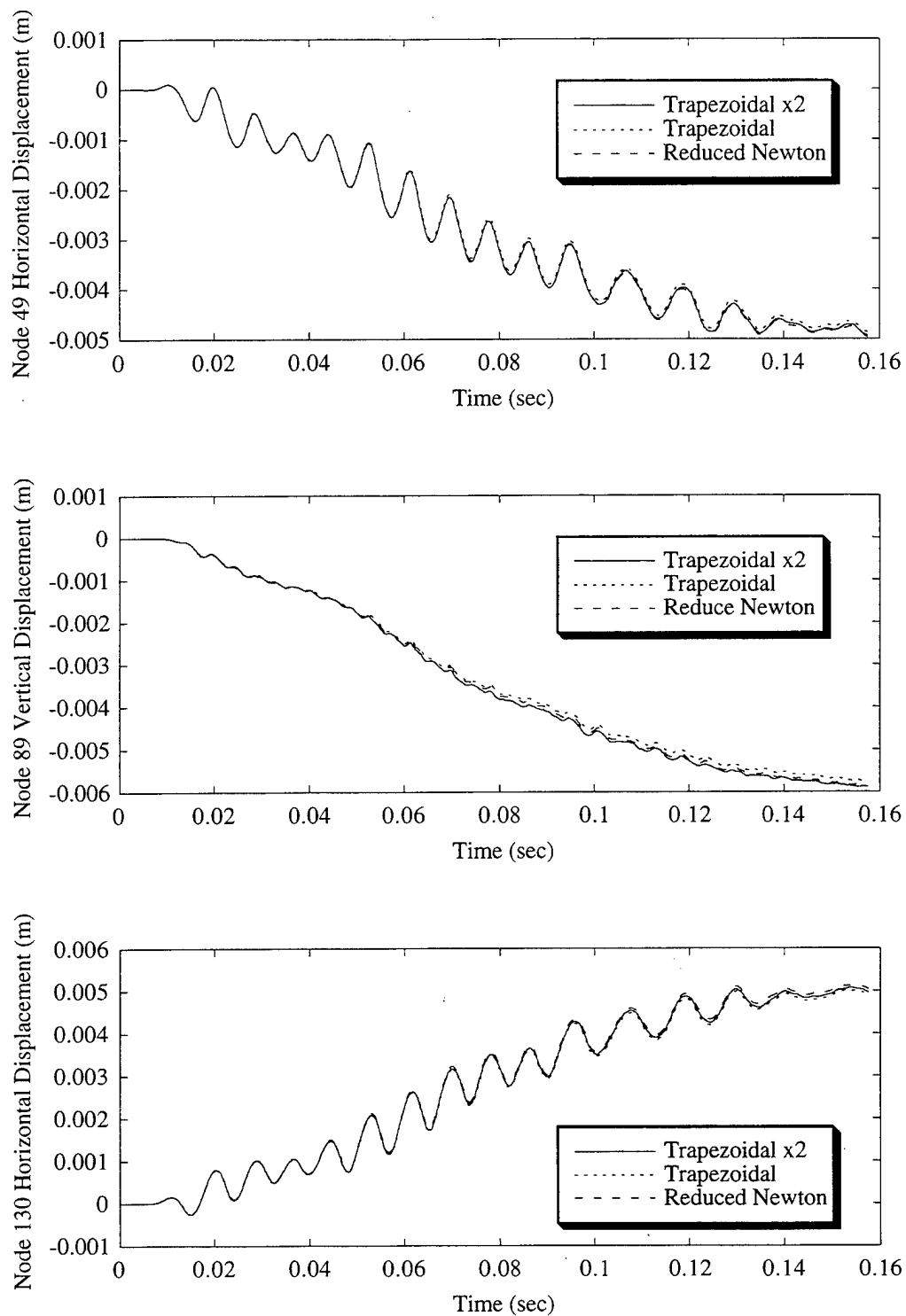Figure 5.2-3. Comparison of Acceleration Histories of Various Nodes Due to Earthquake.

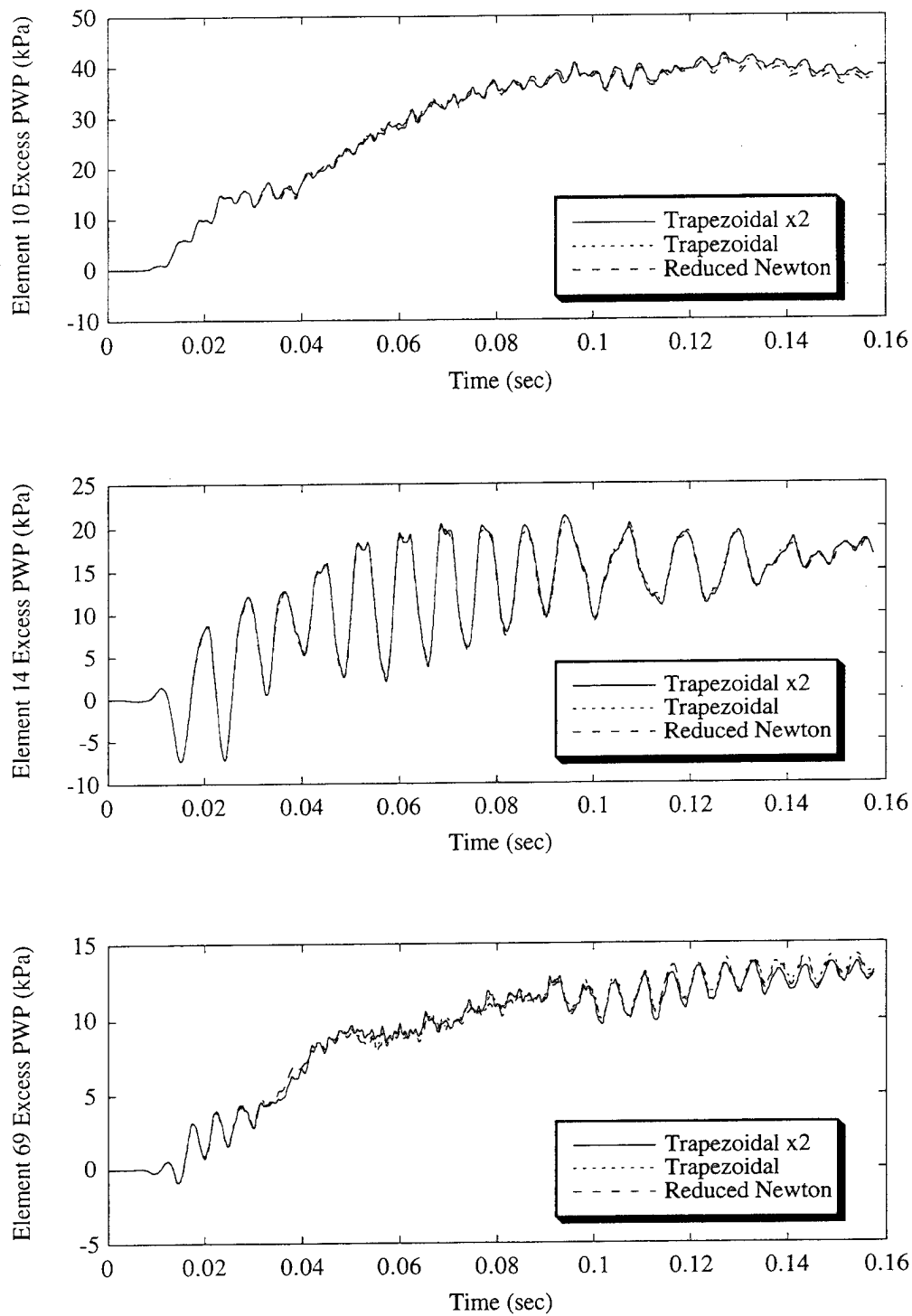Figure 5.2-4. Comparison of Displacement Histories of Various Nodes Due to Earthquake.

Figure 5.2-5. Comparison of Excess Pore Water Pressure Histories of Various Nodes Due

to Earthquake.

min -1.7748E+01

max 4.1338E+01

A	45
B	39
C	33
D	27
E	21
F	15
G	9
H	3
I	-3
J	-9
K	-15
L	-21

Figure 5.2-6a. Contours of Excess Pore Water Pressure Due to Earthquake, Trapezoidal
Method.

min -1.8270E+01

max 4.0975E+01

A	45
B	39
C	33
D	27
E	21
F	15
G	9
H	3
I	-3
J	-9
K	-15
L	-21
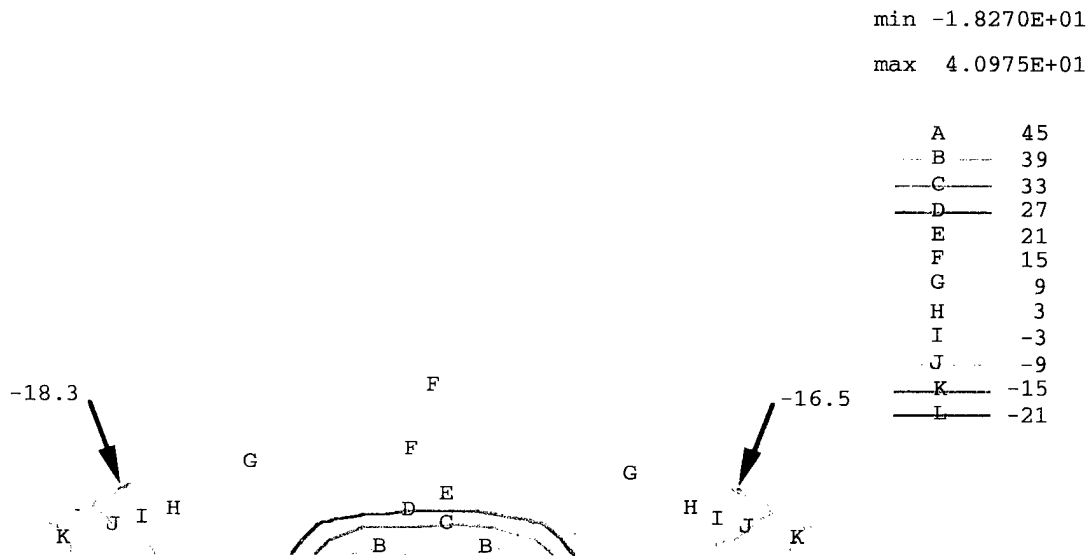
Figure 5.2-6b. Contours of Excess Pore Water Pressure Due to Earthquake, Reduced
Newton Method.

Figure 5.2-7. Global Iterations per Step.

Figure 5.3-1. Input Base Acceleration for Shock Calculation.
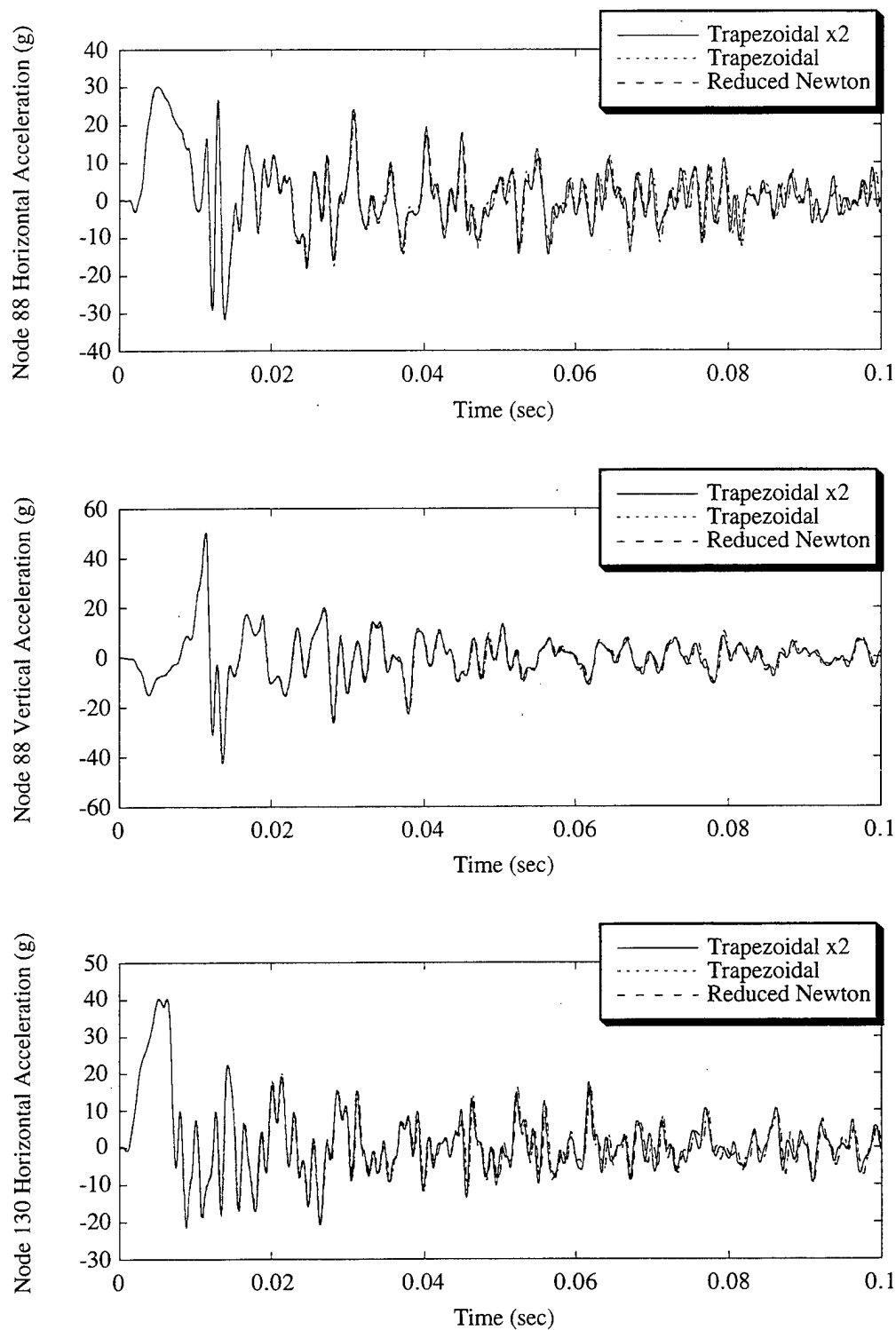
Figure 5.3-2. Comparison of Acceleration Histories of Various Nodes Due to Shock.
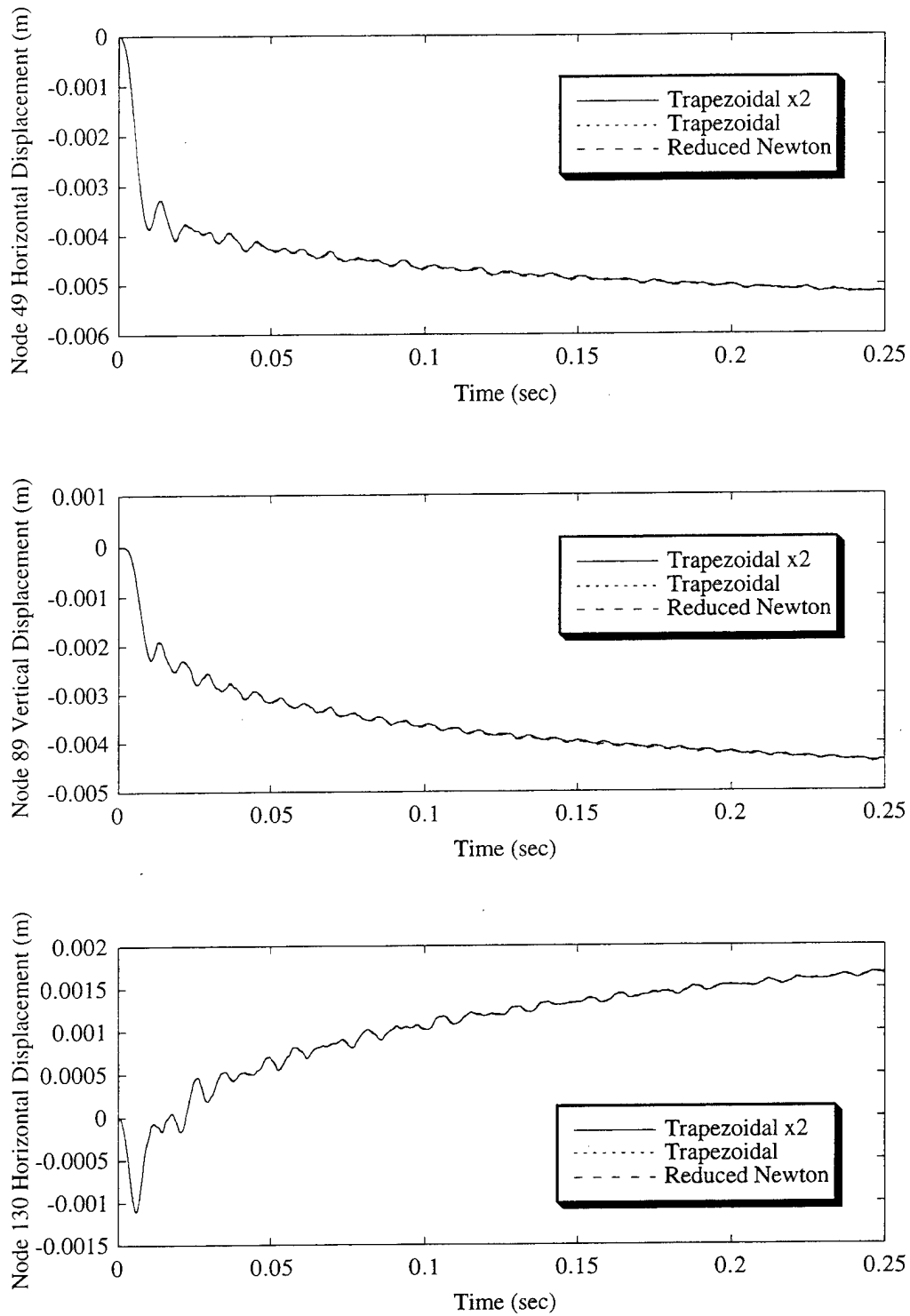
Figure 5.3-3. Comparison of Displacement Histories of Various Nodes Due to Shock.
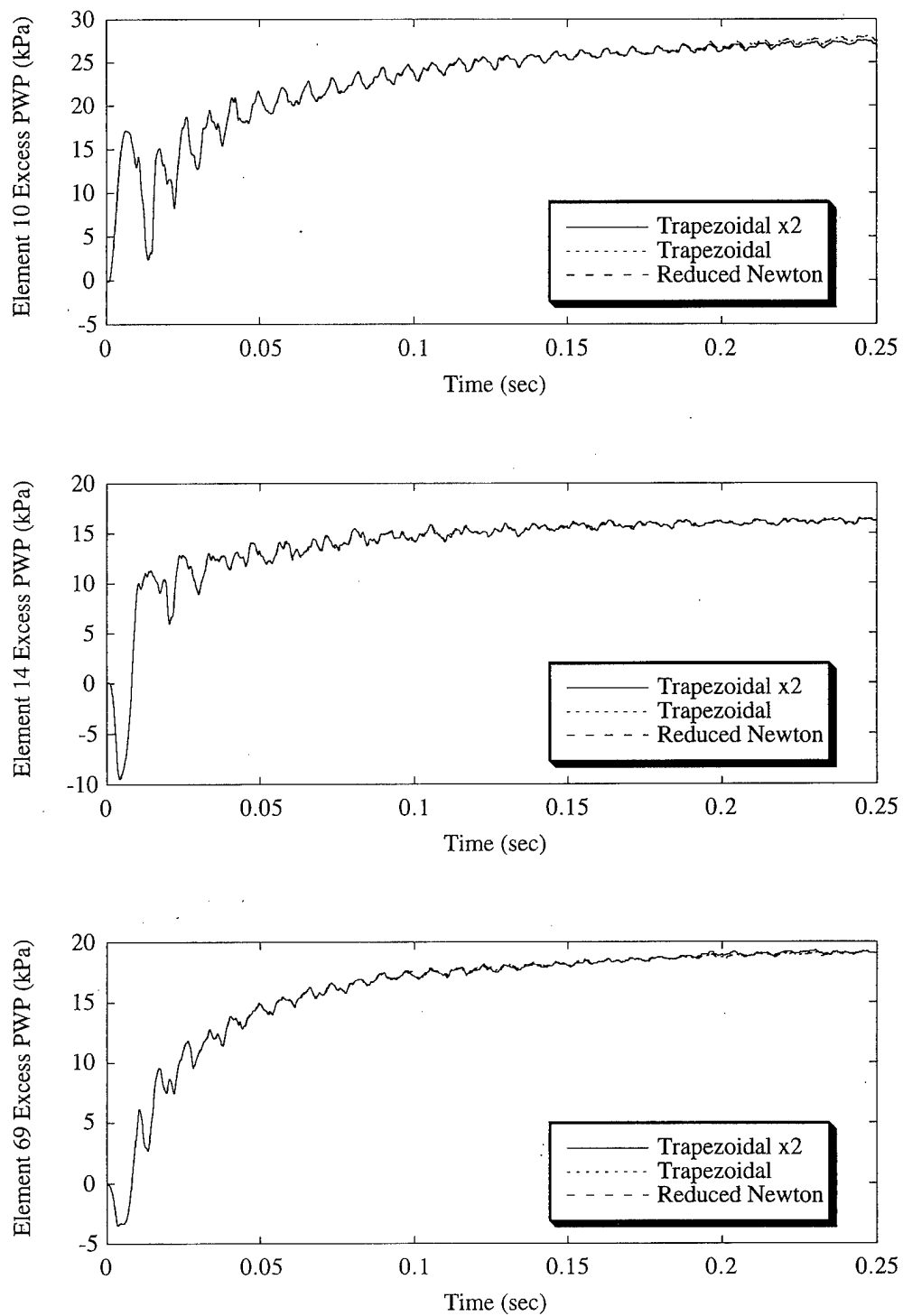
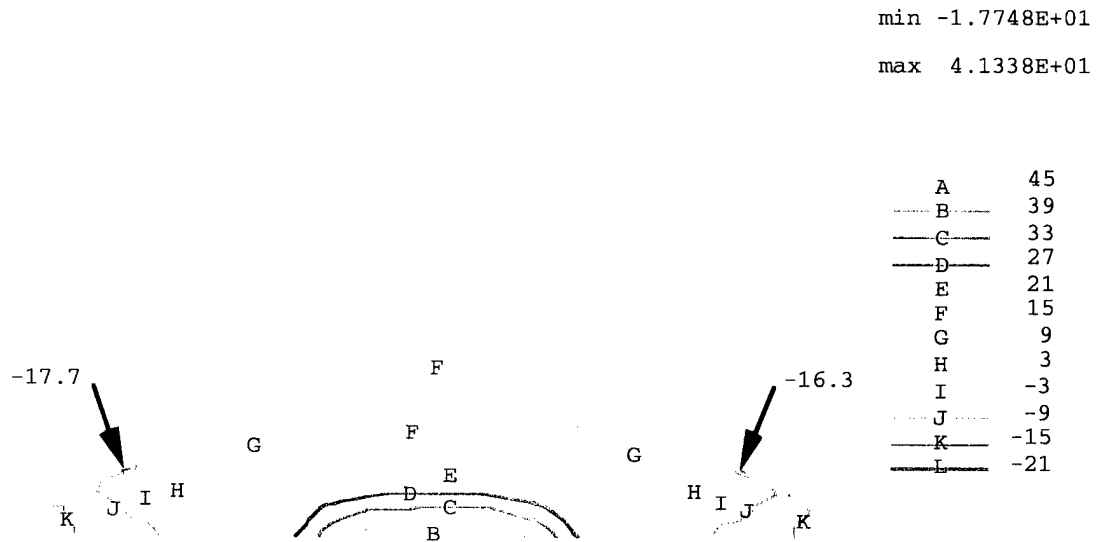Figure 5.3-4. Comparison of Excess Pore Water Pressure Histories of Various Nodes Due to Shock.

min -1.6148E+01

max   3.2504E+01

A	37.5
B	32.5
C	27.5
D	22.5
E	17.5
F	12.5
G	7.5
H	2.5
I	-2.5
J	-7.5
K	-12.5
L	-17.5
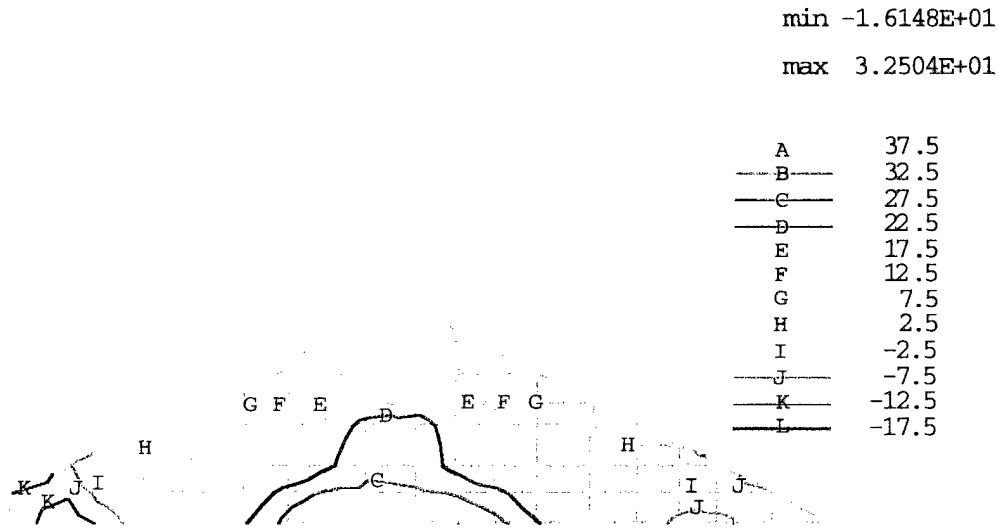
Figure 5.3-5a. Contours of Excess Pore Water Pressure Due to Shock, Trapezoidal

Method.

min -1.6103E+01

max   3.2438E+01

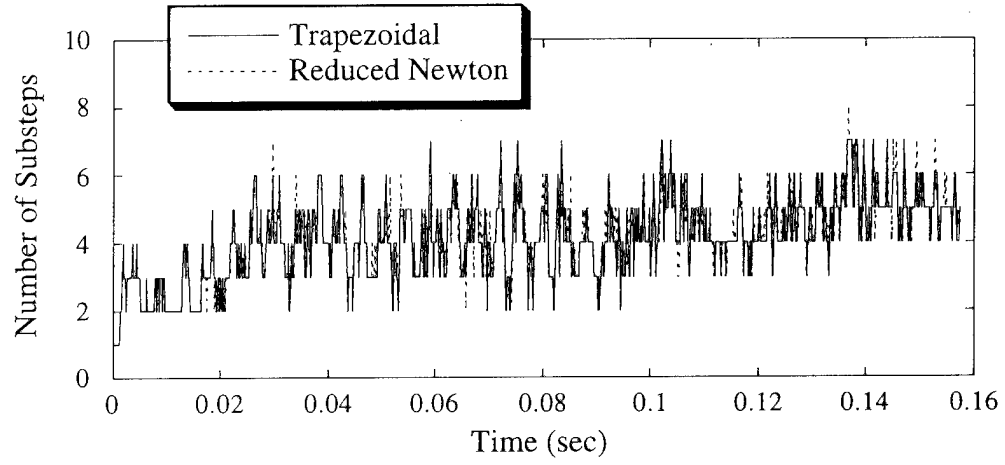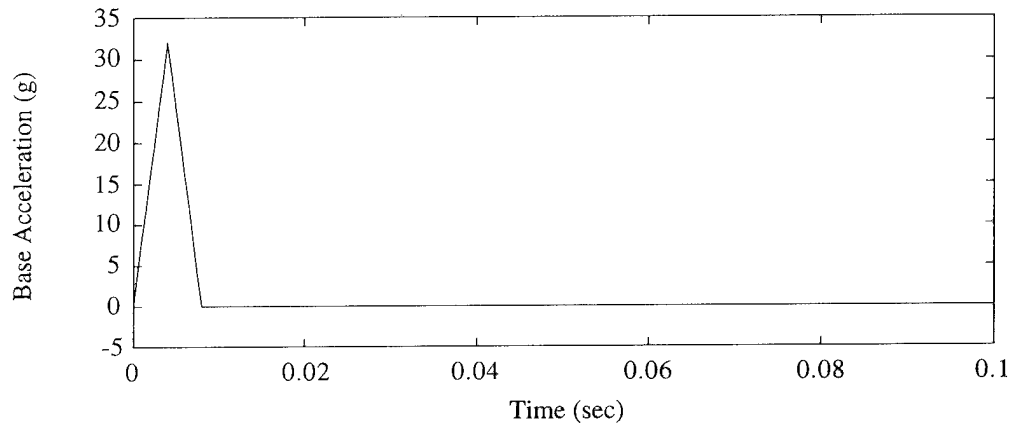|	
A	37.5
B	32.5
C	27.5
D	22.5
E	17.5
F	12.5
G	7.5
H	2.5
I	-2.5
J	-7.5
K	-12.5
L	-17.5

Figure 5.3-5b. Contours of Excess Pore Water Pressure Due to Shock, Reduced Newton

Method.

6. Conclusions and Recommendations

6.1 Conclusions

The Bounding Surface Plasticity theory provides a means to gradually transition from elastic to plastic behavior within a plasticity setting. Other approaches using multi-surface plasticity have been proposed to achieve the same behavior [Mróz, 1967; Krieg, 1975; Eisenberg and Phillips, 1971]. This capability is especially useful in cyclic loading cases where the change in volume occurs gradually over a number of cycles. Classical plasticity models consist of a yield surface defined in stress space where stress paths within the surface are 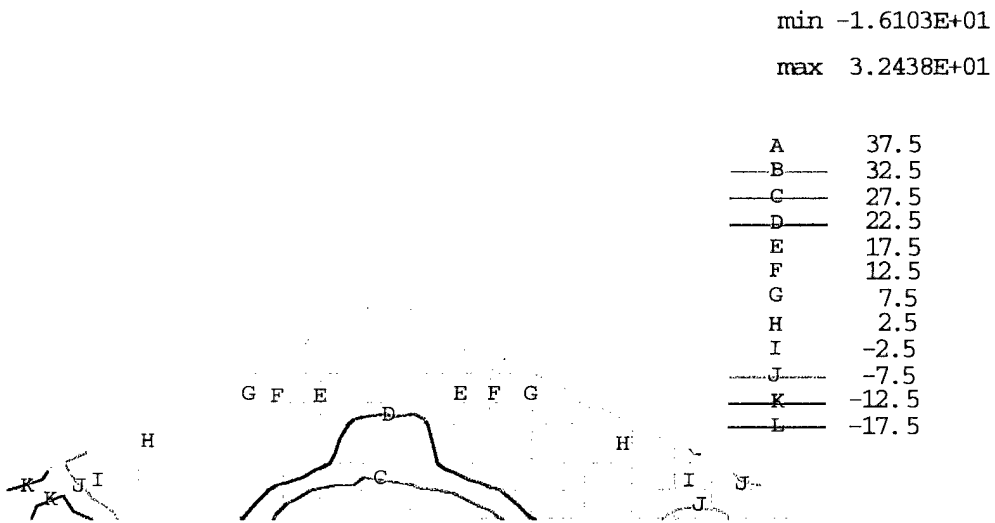elastic and paths on the surface are plastic. Cyclic behavior that occurs within the surface is elastic and can never generate the observed plastic behavior. Unlike classical plasticity models, the surface defined in a Bounding Surface model is a bound rather than a yield surface and therefore allows plasticity to occur within the surface, not just when the stress path reaches it. This feature presents difficulties when trying to implement the model using conventional numerical techniques which were developed for yield surface models.

This study investigates numerical techniques for specifically implementing the Bounding Surface model for clays. The first goal was to lay out the Bounding Surface theory in a framework that would allow implementation using conventional numerical methods. Section 1.7 describes an approach that explicitly defines the loading surface in terms of an additional internal variable so that the model fits the conventional plasticity framework.

The Closest Point Projection method (Section 2) is one of the modern techniques for numerically evaluating conventional plasticity models. The use of an elastic predictor and a plastic corrector makes it very well suited for yield surface plasticity that has distinct elastic and plastic zones. Adding an additional internal variable and the loading surface rate equation allows a direct application of this method to the Bounding Surface model. Since

the method explicitly satisfies the consistency condition, it often provides a more accurate answer than the trapezoidal method (used previously with the Bounding Surface model for clays) in fewer steps. However, it requires solving for and inverting a nonsymmetric matrix (8x8 Jacobian) in every iteration at the material point level. This Jacobian is eventually used to construct the consistent tangent moduli, so the tangent moduli are effectively being calculated in every iteration. Also, since the hardening modulus (K_p) grows rapidly near the elastic surface or projection point, the loading surface rate equation becomes ill-behaved and requires substepping for nearly elastic steps.

The Reduced Newton method was developed from some of the concepts in the Closest Point Projection method. It maps the stresses, strains and consistency condition into invariant space and employs the Newton-Raphson method to solve the reduced set of equations. The loading surface relationship developed in Section 1.7 is still used, but in a more general form that avoids having the numerical stability problems. The method also has the advantage of solving for the stress increment first, then calculating the tangent moduli only for the converged stress solution.

Both the Reduced Newton and the Closest Point Projection methods show the same behavior in terms of accuracy (Section 4). In addition, both methods tend to be more accurate than the trapezoidal method for integration of large plastic strains, because they explicitly include the consistency condition. For robustness, both methods (like the trapezoidal method) employ uniform substepping within the global strain increment, which assures a consistent level of accuracy within the global finite element mesh.

The Reduced Newton method calculates a nearly exact Jacobian (i.e., "consistent tangent stiffness matrix"), while the trapezoidal method uses a tangent stiffness approximation. In light of this fact, is somewhat surprising that the two methods require substantially the same number of global iterations. This is most likely due to the fact that the dynamic analysis required very small time steps.

The development of the Reduced Newton method requires extensive mathematical manipulations and computer coding. The method is best suited for well established models for which reducing computational time is desired. On the other hand, the Closest Point Projection method is easier to implement and is ideal for testing constitutive models under development.

From both an accuracy and cost standpoint, the trapezoidal method compared more favorably to the other two methods than expected. As a consequence, it may be desirable to attempt to correct the problem of straying outside the bound by strictly enforcing the consistency condition within the trapezoidal method.

6.2 Recommendations for Future Research

This study has suggested a number of possibilities for future research and improvements on the Bounding Surface model for clays and its numerical implementation.

Recommendations for additional research in the numerical implementation of Bounding Surface models are as follows:

a) Investigate a trapezoidal algorithm that explicitly satisfies the consistency condition.

b) Investigate a Closest Point Projection algorithm where the interval is divided into N substeps, the first N-1 of equal length and the last with half of the spacing. For the first N-1 substeps, the finite difference equations would be written at the center of the substep (in an attempt to improve accuracy), while for the last substep a backward formula would be used so consistency at the end point is exactly satisfied. It is expected that this method might demonstrate the favorable convergence characteristics of the trapezoidal method.

c) Extend the Reduced Newton method to three invariants.

d) Further improve robustness of the methods by computationally efficient techniques, such as, variable substepping.

Specific recommendations for additional research on the existing clay model include the following:

e) Determine a more computationally efficient expression for the hardening modulus inside the bound. The modulus described in Section 1.6 is extremely complicated and requires finite difference approximations for its derivatives. A simpler, computationally efficient modulus would improve the speed significantly. This simpler form would come from one or more of the following recommendations.

f) Define a bounding shape that more closely follows the critical state line. Part of the reason for the complicated hardening modulus is that the elliptical shape extends far beyond the critical state line. Other shapes in the various regions have been tried with some success, but they have significantly increased both the complexity and the computational time of the model.

g) Recast the consolidation law to eliminate the two solution regions defined by the transitional volumetric stress (I_t).

h) Consider a model without a purely elastic region. This type of model would be more appropriate for clays and would eliminate the two separate solution regions.

i) Consider treating the unloading implicitly (as was done for the Closest Point algorithm) instead of explicitly (i.e., calculation of the intersections). It is assumed that the global step sizes would be sufficiently small that this approximation would be valid (which is often the case in earthquake analyses).

j) Incorporate inherent and induced anisotropy into the model.

7. References

[ABAQUS, 1994] ABAQUS 5.4 Theory Manual. Hibbitt, Karlsson and Sorensen, Inc., Pawtucket, RI, pp. 4.4.3-1,10, 1994.

[Dafalias and Popov, 1975] Dafalias, Y.F. and Popov, E.P., "A Model of Nonlinearly Hardening Materials for Complex Loading," Acta Mechanica, 21, pp. 173-192, 1975.

[Dafalias and Herrmann, 1980a] Dafalias, Y.F. and Herrmann, L.R., "A Bounding Surface Soil Plasticity Model," Proceedings of the International Symposium on Soils Under Cyclic and Transient Loading, Swansea, pp. 335-345, January, 1980.

[Dafalias et. al. 1980b] Dafalias, Y.F., Herrmann, L.R. and DeNatale, J.S., "Prediction of the Response of the Natural Clays X and Y Using the Bounding Surface Model," ASCE publication of Proceedings on the North American Workshop on Limit Equilibrium, Plasticity and Generalized Stress-Strain in Geotechnical Engineering, jointly sponsored by NSF/NSERC, McGill University, Montreal, pp. 402-415, May, 1980.

[Dafalias et. al., 1980c] Dafalias, Y.F., Herrmann, L.R. and DeNatale, J.S., "Description of Natural Clay Behavior by a Simple Bounding Surface Plasticity Formulation," ASCE publication of Proceedings on the North American Workshop on Limit Equilibrium, Plasticity and Generalized Stress-Strain in Geotechnical Engineering, jointly sponsored by NSF/NSERC, McGill University, Montreal, pp. 711-744, May, 1980.

[Dafalias 1980d] Dafalias, Y.F., "The Concept and Application of the Bounding Surface in Plasticity Theory," Proceedings of the IUTAM Symposium on Physical Non-Linearities in Structural Analysis, Senlis, France, May, 1980.

[Dafalias and Herrmann, 1980e] Dafalias, Y.F. and Herrmann, L.R., "A Generalized Bounding Surface Model for Clays," Proceedings of the ASCE Convention and Exposition, Florida, pp. 78-95, October, 1980.

[Dafalias et. al., 1981] Dafalias, Y.F., Herrmann, L.R. and Anandarajah, A., "Cyclic Loading Response of Cohesive Soils Using a Bounding Surface Plasticity Model," Proceedings of the International Conference on Recent Advances in Geotechnical Earthquake Engineering and Soils Dynamics, pp. 139-144, April 1981.

[Dafalias, 1986] Dafalias, Y.F., "Bounding Surface Plasticity. I: Mathematical Foundation and Hypoplasticity," Journal of Engineering Mechanics, Vol. 112, No. 9, September, 1986.

[Dafalias and Herrmann, 1986] Dafalias, Y.F. and Herrmann, L.R., "Bounding Surface Plasticity. II: Application to Isotropic Cohesive Soils," Journal of Engineering Mechanics, Vol. 112, No. 12, December, 1986.

[Dafalias, 1990] Dafalias, Y.F., Class notes for Plasticity (ECI 203) and Viscoplasticity (ECI 204), University of California at Davis, 1990.

[Dafalias, 1992] Personal communications with Y.F. Dafalias.

[DeNatale, et. al. 1983] DeNatale, J.S., Herrmann, L.R., and Dafalias, Y.F., "User's Manual for Modcal - Bounding Surface Soil Plasticity Model Calibration and Prediction Code (Volume I)," Naval Civil Engineering Laboratory, Pt. Hueneme, CA, CR 83.011, February, 1983.

[DeNatale, et. al. 1983] DeNatale, J.S., "On the Calibration of Constitutive Models by Multivariate Optimization. A Case Study: The Bounding Surface Plasticity Model," dissertation presented to the University of California, Davis, in 1983 in partial fulfillment of the requirements for the degree of Doctor of Philosophy.

[Eisenberg and Phillips, 1971] Eisenberg, M.A. and Phillips, A., "A Theory of Plasticity with Non-Coicident Yield and Loading Surfaces," Acta Mechanica, Vol. 11, pp. 247-260, 1971.

[Herrmann, et. al., 1982] Herrmann, L.R., Dafalias, Y.S. and DeNatale, J.S., "Numerical Implementation of a Bounding Surface Soil Plasticity Model," International Symposium on Numerical Models in Geomechanics, Zurich, September, 1982.

[Herrmann, et. al. 1983a] Herrmann, L.R., DeNatale, J.S., Dafalias, Y.F. and Chen, W.P., "Numerical Implementation of the Cohesive Soil Bounding Surface Plasticity Model (Volume I)," Naval Civil Engineering Laboratory, Pt. Hueneme, CA, CR 83.010, February, 1983.

[Herrmann and Mish, 1983b] Herrmann, L.R. and Mish, K.D. "Finite Element Analysis for Cohesive Soil, Stress and Consolidation Problems Using Bounding Surface Plasticity Theory," Naval Civil Engineering Laboratory, Pt. Hueneme, CA, CR 84.006, December, 1983.

[Herrmann, et. al. 1983c] Herrmann, L.R., Kaliakin, V.N. and Dafalias, Y.F, "Computer Implementation of the Bounding Surface Plasticity Model for Cohesive Soils," Naval Civil Engineering Laboratory, Pt. Hueneme, CA, CR 84.007, December, 1983.

[Herrmann and Mish, 1983d] Herrmann, L.R., and Mish, K.D, "User's Manual for SAC-2: A Two-Dimensional Nonlinear, Time Dependent Soil Analysis Code Using the Bounding Surface Plasticity Model," Naval Civil Engineering Laboratory, Pt. Hueneme, CA, CR 84.008, December, 1983.

[Herrmann and Mish, 1983e] Herrmann, L.R., and Mish, K.D, "User's Manual for SAC-3: A Three-Dimensional Nonlinear, Time Dependent Soil Analysis Code Using the Bounding Surface Plasticity Model," Naval Civil Engineering Laboratory, Pt. Hueneme, CA, CR 84.009, December, 1983.

[Herrmann, et. al., 1985] Herrmann, L.R., Kaliakin, V.N. and Shen, C.K., "Improved Numerical Implementation of Plasticity Model for Cohesive Soils," Naval Civil Engineering Laboratory, Pt. Hueneme, CA, CR 85.009, November, 1985.

[Herrmann, et. al., 1987a] Herrmann, L.R., Kaliakin, V.N., Shen, C.K., Mish, K.D. and Zhu, Z.Y., "Numerical Implementation of Plasticity Model for Cohesive Soils," Journal of Engineering Mechanics, Vol. 113, No. 4, April, 1987.

[Herrmann and Kaliakin, 1987b] Herrmann, L.R., Kaliakin, V.N., "User's Manual for SAC-2: A Two-Dimensional Nonlinear, Time Dependent, Soil Analysis Code Using the Bounding Surface Elastoplasticity-Viscoplasticity Model (Revised)," Department of Civil Engineering, University of California, Davis, 1987.

[Herrmann, 1997] Herrmann, L.R., "Reduced Newton Method for the Cam-Clay Model," to be published.

[Kaliakin, 1985] Kaliakin, V.N., "Bounding Surface Elastoplasticity-Viscoplasticity for Clays," dissertation presented to the University of California, as Davis, in 1985 in partial fulfillment of the requirements for the degree of Doctor of Philosophy.

[Krieg, 1975] Krieg, R.D., "A Practical Two Surface Plasticity Theory," Journal of Applied Mechanics, Transactions of the ASME, Vol. 42, pp. 641-646, September, 1975.

[Mróz, 1967] Mróz, Z., "On the Description of Anisotropic Workhardening," Journal of Mechanics and Physics of Solids, Vol. 15, pp. 163-175, 1967.

[Muraleetharan, et. al., 1991] Muraleetharan, K.K., Mish, K.D., Yogachandran, C. and Arulanandan, K., "User's Manual for DYSAC2: A Dynamic Soil Analysis Code for 2-Dimensional Problems," Department of Civil Engineering, University of California, Davis, 1991.

[Muraleetharan, et. al., 1994] Muraleetharan, K.K., Mish, K.D. and Arulanandan, K., "A Fully Coupled Non-Linear Dynamic Analysis Procedure and Its Verification Using Centrifuge Test Results," International Journal for Numerical Methods in Geomechanics, Vol. 18, pp. 305-325, 1994.

[Ortiz and Simo, 1986] Ortiz, M. and Simo, J.C., "An Analysis of a New Class of Integration Algorithms for Elastoplastic Constitutive Relations," International Journal for Numerical Methods in Engineering, Vol. 23, pp. 353-366, 1986.

[Roscoe and Burland, 1968] Roscoe, K.H. and Burland, J.B., "On the Generalized Stress-Strain Behaviour of 'Wet' Clay," Engineering Plasticity, edited by Heyman, J. and Leckie, F.A., Cambridge University Press, Cambridge, U.K., pp. 535-609, 1968.

[Shen, et. al., 1986] Shen, C.K., Zhu, Z.Y., Herrmann, L.R. and Kaliakin, V.N.,

"Validation of Bounding Surface Plasticity Theory Using Preliminary Geotechnical

Centrifuge Experiments," Naval Civil Engineering Laboratory, Pt. Hueneme, CA,

CR 86.011, July, 1986.

[Simo and Taylor, 1985] Simo, J.C. and Taylor, R.L., "Consistent Tangent Operators for

Rate-Independent Elastoplasticity," Computer Methods in Applied Mechanics and

Engineering, 48, pp. 101-118, 1985.

[Simo and Hughes, 1990] Elastoplasticity and Viscoplasticity: Computational Aspects,

Simo, J.C. and Hughes T.J.R., book to be published, 1990.

[Simo and Meschke, 1993] Simo, J.C., and Meschke, G., "A New Class of Algorithms

for Classical Plasticity Extended to Finite Strains. Application to Geomaterials,"

Computational Mechanics, 11, pp. 253-278, 1993.

Appendix A. Derivatives for Single Ellipse Bounding Surface

The Bounding Surface function for a single ellipse model is described in Section 1.4 [Kaliakin, 1985; Herrmann, et. al., 1985; Herrmann, et. al., 1987]. The function is given as:

$$F = \bar{I}^2 + (R-1)^2\left(\frac{\bar{J}}{N}\right)^2 - \frac{2}{R}I_o\bar{I} + \frac{2-R}{R}I_o^2 \tag{A-1}$$

As described in Section 1.8, the Bounding Surface function is differentiated with respect to the "image" stress using the chain rule and the invariants. This can be written as:

$$\frac{\partial F}{\partial \bar{\sigma}_{ij}} = \frac{\partial F}{\partial \bar{I}}\frac{\partial \bar{I}}{\partial \bar{\sigma}_{ij}} + \frac{\partial F}{\partial \bar{J}}\frac{\partial \bar{J}}{\partial \bar{\sigma}_{ij}} + \frac{\partial F}{\partial \mu}\frac{\partial \mu}{\partial \bar{\sigma}_{ij}} \tag{A-2}$$

where $\mu = \sin(3\alpha)$.

The first derivatives are given as:

$$\frac{\partial F}{\partial \bar{I}} = 2\bar{I} - \frac{2}{R}I_o \tag{A-3}$$

$$\frac{\partial F}{\partial \bar{J}} = 2(R-1)^2\frac{\bar{J}}{N^2} \tag{A-4}$$

$$\frac{\partial F}{\partial \mu} = -2(R-1)^2\frac{\bar{J}^2}{N^3}\frac{\partial N}{\partial \mu} \tag{A-5}$$

$$\frac{\partial N}{\partial \alpha} = \frac{3N^2(1-N_{ec})}{2N_e} \tag{A-6}$$

$$\frac{\partial \alpha}{\partial \bar{\sigma}_{ij}} = \frac{3\sqrt{3}}{2J}\left[\frac{s_{ik}s_{kj}}{J^2} - 3\left(\frac{S}{J}\right)^3\frac{s_{ij}}{2J} - \frac{2}{3}\delta_{ij}\right] \tag{A-7}$$

The second partial derivative of F with respect to the "image" and current stresses is given as:

$$\frac{\partial^2 F}{\partial \overline{\sigma}_{ij} \partial \sigma_{kl}} = \frac{\partial^2 F}{\partial \overline{I} \partial \sigma_{kl}} \frac{\partial \overline{I}}{\partial \overline{\sigma}_{ij}} + \frac{\partial F}{\partial \overline{I}} \frac{\partial^2 \overline{I}}{\partial \overline{\sigma}_{ij} \partial \sigma_{kl}} + \frac{\partial^2 F}{\partial \overline{J} \partial \sigma_{kl}} \frac{\partial \overline{J}}{\partial \overline{\sigma}_{ij}} + \frac{\partial F}{\partial \overline{J}} \frac{\partial^2 \overline{J}}{\partial \overline{\sigma}_{ij} \partial \sigma_{kl}}$$
$$+ \frac{\partial^2 F}{\partial \mu \partial \sigma_{kl}} \frac{\partial \mu}{\partial \overline{\sigma}_{ij}} + \frac{\partial F}{\partial \mu} \frac{\partial^2 \mu}{\partial \overline{\sigma}_{ij} \partial \sigma_{kl}}$$

$$(A-8)$$

The terms for the second derivative are found to be:

$$\frac{\partial^2 F}{\partial \overline{I} \partial \sigma_{kl}} = 2b\delta_{ij} \tag{A-9}$$

$$\frac{\partial^2 \overline{I}}{\partial \overline{\sigma}_{ij} \partial \sigma_{kl}} = 0 \tag{A-10}$$

$$\frac{\partial^2 F}{\partial \overline{J} \partial \sigma_{kl}} = \frac{2(R-1)^2}{N^2} \left(b \frac{\partial \overline{J}}{\partial \sigma_{kl}} - \frac{2\overline{J}}{N} \frac{\partial N}{\partial \mu} \frac{\partial \mu}{\partial \sigma_{kl}} \right) \tag{A-11}$$

$$\frac{\partial^2 \overline{J}}{\partial \overline{\sigma}_{ij} \partial \sigma_{kl}} = \frac{1}{2J} \frac{\partial s_{ij}}{\partial \sigma_{kl}} - \frac{s_{ij}}{2J^2} \frac{\partial J}{\partial \sigma_{kl}} \tag{A-12}$$

$$\frac{\partial^2 F}{\partial \mu \partial \sigma_{kl}} = -\frac{(1-N_{ec})(R-1)^2}{N_e} \left[\frac{2b\overline{J}}{N} \frac{\partial \overline{J}}{\partial \sigma_{kl}} - \left(\frac{\overline{J}}{N} \right)^2 \frac{\partial N}{\partial \mu} \frac{\partial \mu}{\partial \sigma_{kl}} \right] \tag{A-13}$$

$$\frac{\partial^2 \mu}{\partial \overline{\sigma}_{ij} \partial \sigma_{kl}} = \frac{\partial X}{\partial \sigma_{kl}} Y - X \frac{\partial Y}{\partial \sigma_{kl}} \tag{A-14}$$

where $\quad \dfrac{\partial^2 s_{ij}}{\partial \sigma_{kl}} = \delta_{ik}\delta_{jl} - \tfrac{1}{3}\delta_{in}\delta_{jn}\delta_{kl}$

$$X = \frac{3\sqrt{3}}{2J}$$

$$Y = \frac{s_{im} s_{mj}}{J^2} - 3\left(\frac{S}{J}\right)^3 \frac{s_{ij}}{2J} - \frac{2}{3}\delta_{ij}$$

$$\frac{\partial X}{\partial \sigma_{kl}} = -\frac{3\sqrt{3}}{2J^2} \frac{\partial J}{\partial \sigma_{kl}}$$

$$\frac{\partial Y}{\partial \sigma_{kl}} = \frac{1}{2J^6}\left[\begin{array}{l} 6S^3 s_{ij} s_{kl} - 2s_{im} s_{mj} s_{kl} - 9S^2 s_{ij} \dfrac{\partial S}{\partial \sigma_{kl}} \\[4mm] -3S^3 \dfrac{\partial s_{ij}}{\partial \sigma_{kl}} + 2J^2 s_{mj} \dfrac{\partial s_{im}}{\partial \sigma_{kl}} + 2J^2 s_{ip} \dfrac{\partial s_{pj}}{\partial \sigma_{kl}} \end{array}\right]$$

$$\frac{\partial S}{\partial \sigma_{kl}} = s_{km} s_{ml} - \tfrac{2}{3}\delta_{kl} J^2 .$$

It is especially important that the above definition of the invariants that involve μ be

used to form the second derivatives. In the previous form (see Section 1.8), the term

cos (α) appears several times in the denominator within these second derivatives. This

creates numeric problems as cos (α) approaches zero.

Appendix B. Plastic Algorithms B and C

Another approach for the plastic algorithm was developed originally for the Cam-Clay model [Herrmann, 1997]. This method solved a single nonlinear differential equation to evaluate the material behavior. Because of numerical problems near the volumetric stress axis (i.e., $J = 0$) and the apex of the ellipse ($J = $ maximum), different forms of the equation were used in these two regions. The first section of this appendix discusses the two separate equations that need to be solved when using this approach for the stress point algorithm. The second section describes the calculation of the consistent tangent moduli.

Appendix B.1 Stress Point Algorithm

Section 3.4 develops the nonlinear differential equations that describe the material behavior. The volumetric equations are given as:

$$6\,\gamma_{n+1}\left(\overline{I}_{n+1} - \rho I_{o_{n+1}}\right) = \Delta\theta - \frac{1}{\beta}\frac{\dot{I}_{n+1}}{I_{n+1}} \qquad (I > I_l) \qquad \text{(B.1-1a)}$$

$$6\,\gamma_{n+1}\left(\overline{I}_{n+1} - \rho I_{o_{n+1}}\right) = \Delta\theta - \frac{1}{\beta}\frac{\dot{I}_{n+1}}{I_l} \qquad (I < I_l) \qquad \text{(B.1-1b)}$$

The deviatoric equation is given as:

$$4G_{n+1}^2\Delta t^2\chi_1 + 2G_{n+1}\Delta t\chi_2 + J_n^2 = \left(1 + 2\,G_{n+1}\Delta t\frac{a_2}{a_1}\gamma_{n+1}b_{n+1}\right)^2 J_{n+1}^2 \qquad \text{(B.1-2)}$$

The above equations are sufficient for the Cam-Clay model. For the Bounding Surface plasticity model, an additional equation is required to describe the plasticity behavior within the surface. The equation used is:

$$\gamma_{n+1} = \frac{1}{K_{p_{n+1}}}\left(\left.\frac{\partial F}{\partial \overline{I}}\right|_{n+1}\dot{I}_{n+1} + \left.\frac{\partial F}{\partial J^2}\right|_{n+1}b_{n+1}\dot{J}_{n+1}^2\right) \qquad \text{(B.1-3)}$$

The current algorithm described in Section 3.4 solves for I and J using the two nonlinear Equations B.1-1 and B.1-2 and then Equation B.1-3 to solve for the plasticity parameter (γ). The original implementation, which is consistent with the Cam-Clay model implementation [Herrmann, 1997], solved Equation B.1-3 and either Equation B.1-1 or B.1-2 for I and b. The equation not used in this process was used to find the plasticity parameter. The choice of Equation B.1-1 or B.1-2 is based upon numerical considerations and is described later in this section.

In both cases, the first equation is Equation B.1-3 and gives the Newton-Raphson residual:

$$R_1 = \gamma_{n+1} - \frac{1}{K_{p_{n+1}}} \left(\left. \frac{\partial F}{\partial \bar{I}} \right|_{n+1} \dot{I}_{n+1} + \left. \frac{\partial F}{\partial J^2} \right|_{n+1} b_{n+1} \dot{J}_{n+1}^2 \right) = 0 \qquad \text{(B.1-4)}$$

Algorithm B uses Equation B.1-2 for the second equation. Equation B.1-1 is then used to solve for the plasticity parameter. Residual 2 is defined as:

$$R_2 = \left(1 + 2 G_{n+1} \Delta t \frac{a_2}{a_1} \gamma_{n+1} b_{n+1} \right)^2 J_{n+1}^2 - 4 G_{n+1}^2 \Delta t^2 \chi_1 - 2 G_{n+1} \Delta t \chi_2 - J_n^2 = 0 \qquad \text{(B.1-5)}$$

$$\gamma_{n+1} = \frac{\Delta\theta - \frac{1}{\beta} \frac{\dot{I}_{n+1}}{I_{n+1}}}{6 \left(\bar{I}_{n+1} - \rho I_{o_{n+1}} \right)} \qquad (I > I_l) \qquad \text{(B.1-6a)}$$

$$\gamma_{n+1} = \frac{\Delta\theta - \frac{1}{\beta} \frac{\dot{I}_{n+1}}{I_l}}{6 \left(\bar{I}_{n+1} - \rho I_{o_{n+1}} \right)} \qquad (I < I_l) \qquad \text{(B.1-6b)}$$

Numerical problems arise in this algorithm near the apex of the Bounding Surface (J = maximum) because the denominator of Equation B.1-6 approaches zero. To resolve this problem, Algorithm C exchanges the second residual and the plasticity parameter

equations. Residual 2 and the plasticity parameter for Algorithm C are defined as:

$$R_2 = 6\,\gamma_{n+1}\left(\bar{I}_{n+1} - \rho I_{o_{n+1}}\right) - \Delta\theta + \frac{1}{\beta}\frac{\dot{I}_{n+1}}{I_{n+1}} = 0 \qquad (I > I_l) \qquad \text{(B.1-7a)}$$

$$R_2 = 6\,\gamma_{n+1}\left(\bar{I}_{n+1} - \rho I_{o_{n+1}}\right) - \Delta\theta + \frac{1}{\beta}\frac{\dot{I}_{n+1}}{I_l} = 0 \qquad (I < I_l) \qquad \text{(B.1-7b)}$$

$$\gamma_{n+1} = \frac{-1 + \sqrt{\dfrac{1}{J_{n+1}^2}\left(4G_{n+1}^2\Delta t^2\chi_1 + 2G_{n+1}\Delta t\chi_2 + J_n^2\right)}}{2\,G_{n+1}\Delta t\,\dfrac{a_2}{a_1}\,b_{n+1}} \qquad \text{(B.1-8)}$$

The plus sign before the radical is required to assure a positive plasticity parameter. Numerical problems arise in this algorithm, however, near the volumetric axis (i.e., $J = 0$). Solving for the plasticity parameter using Equation B.1-8 results in inaccurate estimates because of the division by small values of J (the J^2 divisor within the radical).

Because of the nature of these equations, the solution realm is broken into two zones:

1) Algorithm B is used for solutions in the bottom half of the Bounding Surface (near the hydrostatic axis), and

2) Algorithm C is used for solutions in the top half of the Bounding Surface (near the apex).

The dividing point for the algorithms is arbitrarily taken as the half point and is based upon the second invariant value at the beginning of the step:

$$\text{Algorithm B:}\quad J_b^2 \le \frac{\rho}{2}N\frac{I_{o_b}}{b_b} \qquad \text{Algorithm C:}\quad J_b^2 > \frac{\rho}{2}N\frac{I_{o_b}}{b_b} \qquad \text{(B.1-9)}$$

$$\text{where}\quad N = \frac{M}{\sqrt{27}}\,(\text{angle of the critical state line in } I\text{-}J \text{ space})$$

$$M = \text{angle of the critical state line in } p\text{-}q \text{ space.}$$

Similar to Section 3.4, the independent variables I and b are chosen. The Newton-Raphson method requires derivatives of the residuals with respect to the independent variables. The derivatives of the first residual (Equation B.1-4) with respect to I_{n+1} and b_{n+1} are given as:

$$
\begin{aligned}
\left(\frac{\partial R_1}{\partial I}\right)_{n+1} &= \left(\frac{\partial \gamma}{\partial I}\right)_{n+1} + \frac{1}{K_p^2}\left(\left(\frac{\partial F}{\partial \bar{I}}\right)_{n+1} \dot{I}_{n+1} + \left(\frac{\partial F}{\partial J^2}\right)_{n+1} b_{n+1} \dot{J}_{n+1}^2\right)\left(\frac{\partial K_p}{\partial I}\right)_{n+1} \\
&\quad - \frac{1}{K_p}\left(\left(\frac{\partial^2 F}{\partial \bar{I} \partial I}\right)_{n+1} \dot{I}_{n+1} + \left(\frac{\partial F}{\partial \bar{I}}\right)_{n+1}\left(\frac{\partial \dot{I}}{\partial I}\right)_{n+1} + \left(\frac{\partial F}{\partial J^2}\right)_{n+1} b_{n+1}\left(\frac{\partial \dot{J}^2}{\partial I}\right)_{n+1}\right)
\end{aligned}
\tag{B.1-10}
$$

$$
\begin{aligned}
\left(\frac{\partial R_1}{\partial b}\right)_{n+1} &= \left(\frac{\partial \gamma}{\partial b}\right)_{n+1} + \frac{1}{K_p^2}\left(\left(\frac{\partial F}{\partial \bar{I}}\right)_{n+1} \dot{I}_{n+1} + \left(\frac{\partial F}{\partial J^2}\right)_{n+1} b_{n+1} \dot{J}_{n+1}^2\right)\left(\frac{\partial K_p}{\partial b}\right)_{n+1} \\
&\quad - \frac{1}{K_p}\left(\left(\frac{\partial^2 F}{\partial \bar{I} \partial b}\right)_{n+1} \dot{I}_{n+1} + \left(\frac{\partial F}{\partial J^2}\right)_{n+1} \dot{J}_{n+1}^2 + \left(\frac{\partial F}{\partial J^2}\right)_{n+1} b_{n+1}\left(\frac{\partial \dot{J}^2}{\partial b}\right)_{n+1}\right)
\end{aligned}
\tag{B.1-11}
$$

The derivatives of the second residual (Equation B.1-5) and the plasticity parameter (Equation B.1-6) for Algorithm B are given as:

$$
\begin{aligned}
\left(\frac{\partial R_2}{\partial I}\right)_{n+1} &= 4\Delta t \frac{a_2}{a_1} b_{n+1}\left(1 + 2 G_{n+1}\Delta t \frac{a_2}{a_1}\gamma_{n+1} b_{n+1}\right)\left(\gamma_{n+1}\left(\frac{\partial G}{\partial I}\right)_{n+1} + G_{n+1}\left(\frac{\partial \gamma}{\partial I}\right)_{n+1}\right) J_{n+1}^2 \\
&\quad + \left(1 + 2 G_{n+1}\Delta t \frac{a_2}{a_1}\gamma_{n+1} b_{n+1}\right)^2\left(\frac{\partial J^2}{\partial I}\right)_{n+1} - \left(8 G_{n+1}\Delta t^2 \chi_1 + 2\Delta t \chi_2\right)\left(\frac{\partial G}{\partial I}\right)_{n+1}
\end{aligned}
\tag{B.1-12}
$$

$$
\begin{aligned}
\left(\frac{\partial R_2}{\partial b}\right)_{n+1} &= 4\Delta t \frac{a_2}{a_1} G_{n+1}\left(1 + 2 G_{n+1}\Delta t \frac{a_2}{a_1}\gamma_{n+1} b_{n+1}\right)\left(\gamma_{n+1} + b_{n+1}\left(\frac{\partial \gamma}{\partial b}\right)_{n+1}\right) J_{n+1}^2 \\
&\quad + \left(1 + 2 G_{n+1}\Delta t \frac{a_2}{a_1}\gamma_{n+1} b_{n+1}\right)^2\left(\frac{\partial J^2}{\partial b}\right)_{n+1}
\end{aligned}
\tag{B.1-13}
$$

$$\left(\frac{\partial \gamma}{\partial I}\right)_{n+1} = \frac{1}{\left(\bar{I}_{n+1} - \rho I_{o_{n+1}}\right)} \left[\begin{array}{c} -\frac{1}{6\beta}\left(\frac{1}{\Delta t I_{n+1}} - \frac{\dot{I}_{n+1}}{I_{n+1}^2}\right) \\ -\gamma_{n+1}\left(\left(\frac{\partial \bar{I}}{\partial I}\right)_{n+1} - \rho\left(\frac{\partial I_o}{\partial I}\right)_{n+1}\right) \end{array} \right] \quad (I > I_l) \qquad \text{(B.1-14a)}$$

$$\left(\frac{\partial \gamma}{\partial I}\right)_{n+1} = \frac{1}{\left(\bar{I}_{n+1} - \rho I_{o_{n+1}}\right)} \left[-\frac{1}{6\beta\Delta t I_l} - \gamma_{n+1}\left(\left(\frac{\partial \bar{I}}{\partial I}\right)_{n+1} - \rho\left(\frac{\partial I_o}{\partial I}\right)_{n+1}\right) \right] (I < I_l) \text{(B.1-14b)}$$

$$\left(\frac{\partial \gamma}{\partial b}\right)_{n+1} = -\frac{\gamma_{n+1}}{\left(\bar{I}_{n+1} - \rho I_{o_{n+1}}\right)}\left(\frac{\partial \bar{I}}{\partial b}\right)_{n+1} \qquad \text{(B.1-15)}$$

The derivatives of the second residual (Equation B.1-7) and the plasticity parameter (Equation B.1-8) for Algorithm C are given as:

$$\left(\frac{\partial R_2}{\partial I}\right)_{n+1} = 6\gamma_{n+1}\left(\left(\frac{\partial \bar{I}}{\partial I}\right)_{n+1} - \rho\left(\frac{\partial I_o}{\partial I}\right)_{n+1}\right) + 6\left(\bar{I}_{n+1} - \rho I_{o_{n+1}}\right)\left(\frac{\partial \gamma}{\partial I}\right)_{n+1}$$
$$+\frac{1}{\beta I_{n+1}}\left(\frac{1}{\Delta t} - \frac{\dot{I}_{n+1}}{I_{n+1}}\right) \qquad (I > I_l) \text{(B.1-16a)}$$

$$\left(\frac{\partial R_2}{\partial I}\right)_{n+1} = 6\gamma_{n+1}\left(\left(\frac{\partial \bar{I}}{\partial I}\right)_{n+1} - \rho\left(\frac{\partial I_o}{\partial I}\right)_{n+1}\right) + 6\left(\bar{I}_{n+1} - \rho I_{o_{n+1}}\right)\left(\frac{\partial \gamma}{\partial I}\right)_{n+1}$$
$$+\frac{1}{\beta\Delta t I_{n+1}} \qquad (I < I_l) \text{(B.1-16b)}$$

$$\left(\frac{\partial R_2}{\partial b}\right)_{n+1} = 6\gamma_{n+1}\left(\frac{\partial \bar{I}}{\partial b}\right)_{n+1} + 6\left(\bar{I}_{n+1} - \rho I_{o_{n+1}}\right)\left(\frac{\partial \gamma}{\partial b}\right)_{n+1} \qquad \text{(B.1-17)}$$

$$\left(\frac{\partial \gamma}{\partial I}\right)_{n+1} = \frac{\left[\begin{array}{c}\left(8G_{n+1}\Delta t^2\chi_1 + 2\Delta t\chi_2\right)\left(\dfrac{\partial G}{\partial I}\right)_{n+1} \\[2mm] -\left(1 + 2G_{n+1}\Delta t\dfrac{a_2}{a_1}b_{n+1}\gamma_{n+1}\right)^2\left(\dfrac{\partial J^2}{\partial I}\right)_{n+1}\end{array}\right]}{4G_{n+1}\Delta t\dfrac{a_2}{a_1}b_{n+1}J_{n+1}^2\left(1 + 2G_{n+1}\Delta t\dfrac{a_2}{a_1}b_{n+1}\gamma_{n+1}\right)} - \frac{\gamma_{n+1}}{G_{n+1}}\left(\frac{\partial G}{\partial I}\right)_{n+1} \quad \text{(B.1-18)}$$

$$\left(\frac{\partial \gamma}{\partial b}\right)_{n+1} = -\frac{\left(1 + 2G_{n+1}\Delta t\dfrac{a_2}{a_1}b_{n+1}\gamma_{n+1}\right)^2\left(\dfrac{\partial J^2}{\partial b}\right)_{n+1}}{4G_{n+1}\Delta t\dfrac{a_2}{a_1}b_{n+1}J_{n+1}^2} - \frac{\gamma_{n+1}}{b_{n+1}} \quad \text{(B.1-19)}$$

The convergence criterion chosen for this study is that the change in residuals must be smaller than a user-defined percentage of absolute value of the total strain increment. The first residual is in terms of the plasticity parameter. In order to compare its value at the magnitude of strain, the residual and its derivatives are multiplied by the following:

$$R_1^* = z\,R_1, \qquad \frac{\partial R_1^*}{\partial I} = z\,\frac{\partial R_1}{\partial I}, \qquad \frac{\partial R_1^*}{\partial b} = z\,\frac{\partial R_1}{\partial b} \qquad \text{(B.1-20)}$$

where $\quad z = 3\left(\dfrac{\partial F}{\partial \overline{I}}\right)_b.$

Algorithm C uses the volumetric Equation B.1-7 for the second nonlinear equation, which is already in terms of strain. Algorithm B, however, uses the deviatoric Equation B.1-5, which is in terms of stress. Its residual is scaled to the magnitude of strain by dividing it and its derivatives by the initial shear modulus. The new residual and derivatives are given as:

$$R_2^* = \frac{R_2}{G_b^2}, \qquad \frac{\partial R_2^*}{\partial I} = \frac{1}{G_b^2}\frac{\partial R_2}{\partial I}, \qquad \frac{\partial R_2^*}{\partial b} = \frac{1}{G_b^2}\frac{\partial R_2}{\partial b} \qquad \text{(Algorithm B)} \qquad \text{(B.1-21)}$$

The norm as described in Section 3.4 is based upon a percentage of the input strains and is defined as:

$$\|R\| = \frac{|R_1| + |R_2|}{\sum |\Delta\varepsilon|}$$

(B.1-22)

where $\|R\|$ = norm on the residuals.

The Newton-Raphson algorithm is the same as described in Section 3.4 and is given as:

$$\begin{Bmatrix} I \\ b \end{Bmatrix}_{i+1,n+1} = \begin{Bmatrix} I \\ b \end{Bmatrix}_{i,n+1} - \Psi^{-1}_{i,n+1} \begin{Bmatrix} R_1 \\ R_2 \end{Bmatrix}_{i,n+1}$$

(B.1-23)

where $\Psi = \begin{bmatrix} \left.\dfrac{\partial R_1}{\partial I}\right|_{b_{i,n+1}} & \left.\dfrac{\partial R_1}{\partial b}\right|_{I_{i,n+1}} \\ \left.\dfrac{\partial R_2}{\partial I}\right|_{b_{i,n+1}} & \left.\dfrac{\partial R_2}{\partial b}\right|_{I_{i,n+1}} \end{bmatrix}$.

Residual 2 in the Jacobian (Ψ) is dependent on the algorithm being used. The algorithm is shown in Box B.1-1.

Box B.1-1. Algorithms B and C for Plastic Steps.

---

1. Set Substep Level: $N = 1$

2. Substep Level Loop: $m = 1, m_{max}$

$$\Delta \varepsilon_{ij_m} = \frac{\Delta \varepsilon_{ij}}{N}$$

3. Initialize to Beginning of Step:

$$I_{n+1} = I_b, \; b_{n+1} = b_b$$

4. Substep Loop: $k = 1, N$

5. Determine Volumetric Form:

$(I > I_l)$ Linear-Linear $(I < I_l)$ Log-Linear

6. Determine Algorithm:

$J_b^2 \leq \dfrac{\rho}{2} N \dfrac{I_{o_b}}{b_b}$ Algorithm B $J_b^2 > \dfrac{\rho}{2} N \dfrac{I_{o_b}}{b_b}$ Algorithm C

7. Iteration Loop: $It = 1, It_{max}$

8. Calculate Residuals and Local Jacobian: R_1, R_2, Ψ

9. Solve for Increment in Variables: $\Delta I_{n+1}, \Delta b_{n+1}$

10. Calculate and Test Norm: IF $(\|R\| < Toler_{It})$

   TRUE: Go to step 11

   FALSE: Increment variables, I_{n+1}, b_{n+1}, Go to step 7

11. Calculate Stresses and Check Substeps: σ_{n+1}

   IF $(k < N)$ TRUE: Go to step 4   FALSE: Go to step 12

12. Compare stresses with previous substep level:

$\left[\left(I_{o_{n+1,m}} - I_{o_{n+1,m-1}} \right) < Toler_{I_o} \right]$ OR $\left[It > It_{max} \right]$

   TRUE: EXIT   FALSE: $N = 2N$, Go to step 2

Appendix B.2 Plastic Contribution to the Global Jacobian

Once the stress algorithm has converged, the plastic contribution $\left(\dfrac{\partial \sigma_{ij}}{\partial \Delta \varepsilon_{kl}}\right)_{n+1}$ to the

global Jacobian matrix must be calculated. The local Jacobian will be evaluated in terms of

the deviatoric and volumetric components, similar to the elastic Jacobian. The volumetric

component can be obtained by noting that the residuals are a function of the independent

variables (I, b) which, in turn, are a function of the strain increment. The derivatives can

be obtained by an application of the chain rule (i.e., holding the independent variables

constant and then adding the derivatives with respect to the independent variables). At

convergence, the residual is equal to zero and the derivatives can be written as:

$$\left(\frac{\partial R_i}{\partial \Delta \varepsilon_{kl}}\right)_{n+1} = \frac{\partial R_i}{\partial \Delta \varepsilon_{kl}}\bigg|_{I_{n+1},b_{n+1}} + \frac{\partial R_i}{\partial I}\bigg|_{b_{n+1}} \frac{\partial I}{\partial \Delta \varepsilon_{kl}}\bigg|_{n+1} + \frac{\partial R_i}{\partial b}\bigg|_{I_{n+1}} \frac{\partial b}{\partial \Delta \varepsilon_{kl}}\bigg|_{n+1} = 0 \qquad \text{(B.2-1)}$$

Expressed in matrix form:

$$\begin{Bmatrix} \dfrac{\partial R_1}{\partial \Delta \varepsilon_{kl}} \\[2mm] \dfrac{\partial R_2}{\partial \Delta \varepsilon_{kl}} \end{Bmatrix}_{n+1} = \begin{Bmatrix} \dfrac{\partial R_1}{\partial \Delta \varepsilon_{kl}} \\[2mm] \dfrac{\partial R_2}{\partial \Delta \varepsilon_{kl}} \end{Bmatrix}_{I_{n+1},b_{n+1}} + \Psi \begin{Bmatrix} \dfrac{\partial I}{\partial \Delta \varepsilon_{kl}} \\[2mm] \dfrac{\partial b}{\partial \Delta \varepsilon_{kl}} \end{Bmatrix}_{n+1} = \begin{Bmatrix} 0 \\ 0 \end{Bmatrix} \qquad \text{(B.2-2)}$$

$$\text{where} \quad \Psi = \begin{bmatrix} \dfrac{\partial R_1}{\partial I}\bigg|_{b_{n+1}} & \dfrac{\partial R_1}{\partial b}\bigg|_{I_{n+1}} \\[4mm] \dfrac{\partial R_2}{\partial I}\bigg|_{b_{n+1}} & \dfrac{\partial R_2}{\partial b}\bigg|_{I_{n+1}} \end{bmatrix}_{n+1}.$$

The local Jacobian (Ψ) is the same as that required in the local Newton-Raphson

iteration (B.1-23). The derivatives of the independent variables with respect to the strain

increments can be found by solving Equation B.2-2:

$$
\left\{ \begin{array}{c} \dfrac{\partial I}{\partial \Delta \varepsilon_{kl}} \\[2mm] \dfrac{\partial b}{\partial \Delta \varepsilon_{kl}} \end{array} \right\}_{n+1} = -\Psi^{-1} \left\{ \begin{array}{c} \dfrac{\partial R_1}{\partial \Delta \varepsilon_{kl}} \\[2mm] \dfrac{\partial R_2}{\partial \Delta \varepsilon_{kl}} \end{array} \right\}_{I_{n+1}, b_{n+1}}
$$

(B.2-3)

The derivatives of the residuals with respect to the strain increments are calculated holding the independent variables at the end of the step (I_{n+1}, b_{n+1}) constant. It is important to note that the shear modulus (G_{n+1}) is a function only of the current volumetric stress (I_{n+1}), and therefore is also fixed. For both algorithms, the derivative of the first residual is given as:

$$
\left.\frac{\partial R_1}{\partial \Delta \varepsilon_{kl}}\right|_{I_{n+1}, b_{n+1}} = \left.\frac{\partial \gamma_{n+1}}{\partial \Delta \varepsilon_{kl}}\right|_{I_{n+1}, b_{n+1}} + \frac{1}{K_p^2}\left(\frac{\partial F}{\partial \bar{I}} \dot{I} + \frac{\partial F}{\partial \bar{J}^2} b \dot{j}^2 \right)
$$
$$
- \frac{1}{K_p}\left(-\frac{1}{\Delta t}\frac{\partial F}{\partial \bar{I}} \left.\frac{\partial I_n}{\partial \Delta \varepsilon_{kl}}\right|_{I_{n+1}, b_{n+1}} + \frac{\partial F}{\partial \bar{J}^2} b \left.\frac{\partial \dot{j}^2}{\partial \Delta \varepsilon_{kl}}\right|_{I_{n+1}, b_{n+1}} \right)
$$

(B.2-4)

The derivatives of the second residual for Algorithm B and that of the plasticity parameter are given as:

$$
\left.\frac{\partial R_2}{\partial \Delta \varepsilon_{kl}}\right|_{I_{n+1}, b_{n+1}} = 4 G_{n+1} \Delta t \frac{a_2}{a_1} b_{n+1}\left(1 + 2 G_{n+1}\Delta t \frac{a_2}{a_1}\gamma_{n+1} b_{n+1} \right) J_{n+1}^2 \left.\frac{\partial \gamma_{n+1}}{\partial \Delta \varepsilon_{kl}}\right|_{I_{n+1}, b_{n+1}}
$$
$$
+ \left(1 + 2 G_{n+1}\Delta t \frac{a_2}{a_1}\gamma_{n+1} b_{n+1} \right)^2 \left.\frac{\partial J_{n+1}^2}{\partial \Delta \varepsilon_{kl}}\right|_{I_{n+1}, b_{n+1}}
$$

(B.2-5)

$$
-4 G_{n+1}^2 \Delta t^2 \left.\frac{\partial \chi_1}{\partial \Delta \varepsilon_{kl}}\right|_{I_{n+1}, b_{n+1}} - 2 G_{n+1}\Delta t \left.\frac{\partial \chi_2}{\partial \Delta \varepsilon_{kl}}\right|_{I_{n+1}, b_{n+1}} - \left.\frac{\partial J_n^2}{\partial \Delta \varepsilon_{kl}}\right|_{I_{n+1}, b_{n+1}}
$$

$$\left.\frac{\partial \gamma_{n+1}}{\partial \Delta \varepsilon_{kl}}\right|_{I_{n+1},b_{n+1}} = \frac{1}{\left(\bar{I}_{n+1} - \rho I_{o_{n+1}}\right)} \left[\begin{array}{c} \frac{1}{6}\left(\delta_{kl} - \frac{1}{\beta \Delta t I_{n+1}} \left.\frac{\partial I_n}{\partial \Delta \varepsilon_{kl}}\right|_{I_{n+1},b_{n+1}}\right) \\ -\gamma_{n+1}\left(\left.\frac{\partial \bar{I}_n}{\partial \Delta \varepsilon_{kl}}\right|_{I_{n+1},b_{n+1}} - \rho \left.\frac{\partial I_{o_{n+1}}}{\partial \Delta \varepsilon_{kl}}\right|_{I_{n+1},b_{n+1}}\right) \end{array} \right] (I > I_l) \text{ (B.2-6a)}$$

$$\left.\frac{\partial \gamma_{n+1}}{\partial \Delta \varepsilon_{kl}}\right|_{I_{n+1},b_{n+1}} = \frac{1}{\left(\bar{I}_{n+1} - \rho I_{o_{n+1}}\right)} \left[\begin{array}{c} \frac{1}{6}\left(\delta_{kl} - \frac{1}{\beta \Delta t I_l} \left.\frac{\partial I_n}{\partial \Delta \varepsilon_{kl}}\right|_{I_{n+1},b_{n+1}}\right) \\ -\gamma_{n+1}\left(\left.\frac{\partial \bar{I}_n}{\partial \Delta \varepsilon_{kl}}\right|_{I_{n+1},b_{n+1}} - \rho \left.\frac{\partial I_{o_{n+1}}}{\partial \Delta \varepsilon_{kl}}\right|_{I_{n+1},b_{n+1}}\right) \end{array} \right] (I < I_l) \text{ (B.2-6b)}$$

For Algorithm C, the derivatives of the second residual and the plasticity parameter are given as:

$$\left.\frac{\partial R_2}{\partial \Delta \varepsilon_{kl}}\right|_{I_{n+1},b_{n+1}} = 6\gamma_{n+1}\left(\left.\frac{\partial \bar{I}_{n+1}}{\partial \Delta \varepsilon_{kl}}\right|_{I_{n+1},b_{n+1}} - \rho \left.\frac{\partial I_{o_{n+1}}}{\partial \Delta \varepsilon_{kl}}\right|_{I_{n+1},b_{n+1}}\right)$$
$$+ 6\left(\bar{I}_{n+1} - \rho I_{o_{n+1}}\right)\left.\frac{\partial \gamma_{n+1}}{\partial \Delta \varepsilon_{kl}}\right|_{I_{n+1},b_{n+1}} - \delta_{kl} - \frac{1}{\beta \Delta t I_{n+1}} \left.\frac{\partial I_n}{\partial \Delta \varepsilon_{kl}}\right|_{I_{n+1},b_{n+1}} \qquad (I > I_l) \text{(B.2-7a)}$$

$$\left.\frac{\partial R_2}{\partial \Delta \varepsilon_{kl}}\right|_{I_{n+1},b_{n+1}} = 6\gamma_{n+1}\left(\left.\frac{\partial \bar{I}_{n+1}}{\partial \Delta \varepsilon_{kl}}\right|_{I_{n+1},b_{n+1}} - \rho \left.\frac{\partial I_{o_{n+1}}}{\partial \Delta \varepsilon_{kl}}\right|_{I_{n+1},b_{n+1}}\right)$$
$$+ 6\left(\bar{I}_{n+1} - \rho I_{o_{n+1}}\right)\left.\frac{\partial \gamma_{n+1}}{\partial \Delta \varepsilon_{kl}}\right|_{I_{n+1},b_{n+1}} - \delta_{kl} - \frac{1}{\beta \Delta t I_l} \left.\frac{\partial I_n}{\partial \Delta \varepsilon_{kl}}\right|_{I_{n+1},b_{n+1}} \qquad (I < I_l) \text{(B.2-7b)}$$

$$\left.\frac{\partial \gamma_{n+1}}{\partial \Delta \varepsilon_{kl}}\right|_{I_{n+1},b_{n+1}} = \frac{\left[\begin{array}{c} -\left(1 + 2G_{n+1}\Delta t \frac{a_2}{a_1} b_{n+1}\gamma_{n+1}\right)^2 \left.\frac{\partial J_{n+1}^2}{\partial \Delta \varepsilon_{kl}}\right|_{I_{n+1},b_{n+1}} + 4G_{n+1}^2 \Delta t^2 \left.\frac{\partial \chi_1}{\partial \Delta \varepsilon_{kl}}\right|_{I_{n+1},b_{n+1}} \\ +2G_{n+1}\Delta t \left.\frac{\partial \chi_2}{\partial \Delta \varepsilon_{kl}}\right|_{I_{n+1},b_{n+1}} + \left.\frac{\partial J_n^2}{\partial \Delta \varepsilon_{kl}}\right|_{I_{n+1},b_{n+1}} \end{array} \right]}{4G_{n+1}\Delta t \frac{a_2}{a_1} b_{n+1} J_{n+1}^2 \left(1 + 2G_{n+1}\Delta t \frac{a_2}{a_1} b_{n+1}\gamma_{n+1}\right)} \qquad \text{(B.2-8)}$$

The derivatives in Equations B.2-5 through B.2-8 are as follows:

$$\left.\frac{\partial \bar{I}}{\partial \Delta \varepsilon_{kl}}\right|_{I_{n+1},b_{n+1}} = C(1-b_{n+1})\left.\frac{\partial I_o}{\partial \Delta \varepsilon_{kl}}\right|_{I_{n+1},b_{n+1}} \tag{B.2-9}$$

$$\left.\frac{\partial \dot{\bar{I}}}{\partial \Delta \varepsilon_{kl}}\right|_{I_{n+1},b_{n+1}} = -\frac{(I-CI_o)}{\Delta t}\left.\frac{\partial b_n}{\partial \Delta \varepsilon_{kl}}\right|_{I_{n+1},b_{n+1}} - \dot{b}\, C\left.\frac{\partial I_o}{\partial \Delta \varepsilon_{kl}}\right|_{I_{n+1},b_{n+1}}$$
$$-b\,\frac{1}{\Delta t}\left.\frac{\partial I_n}{\partial \Delta \varepsilon_{kl}}\right|_{I_{n+1},b_{n+1}} + C\,(1-b)\left.\frac{\partial \dot{I}_o}{\partial \Delta \varepsilon_{kl}}\right|_{I_{n+1},b_{n+1}} \tag{B.2-10}$$

$$\left.\frac{\partial I_o}{\partial \Delta \varepsilon_{kl}}\right|_{I_{n+1},b_{n+1}} = I_{o_b}\,\xi\, t\,\delta_{kl} \tag{B.2-11}$$

$$\left.\frac{\partial \dot{I}_o}{\partial \Delta \varepsilon_{kl}}\right|_{I_{n+1},b_{n+1}} = \xi\left(\Delta\theta - \frac{1}{\beta}\frac{\dot{I}}{I_{n+1}}\right)\left.\frac{\partial I_o}{\partial \Delta \varepsilon_{kl}}\right|_{I_{n+1},b_{n+1}}$$
$$+\xi I_{o_{n+1}}\left(\delta_{kl} + \frac{1}{\Delta t\,\beta\,I_{n+1}}\left.\frac{\partial I_n}{\partial \Delta \varepsilon_{kl}}\right|_{I_{n+1},b_{n+1}}\right) \qquad (I>I_l) \tag{B.2-12a}$$

$$\left.\frac{\partial \dot{I}_o}{\partial \Delta \varepsilon_{kl}}\right|_{I_{n+1},b_{n+1}} = \xi\left(\Delta\theta - \frac{1}{\beta}\frac{\dot{I}}{I_l}\right)\left.\frac{\partial I_o}{\partial \Delta \varepsilon_{kl}}\right|_{I_{n+1},b_{n+1}}$$
$$+\xi I_{o_{n+1}}\left(\delta_{kl} + \frac{1}{\Delta t\,\beta\,I_l}\left.\frac{\partial I_n}{\partial \Delta \varepsilon_{kl}}\right|_{I_{n+1},b_{n+1}}\right) \qquad (I<I_l) \tag{B.2-12b}$$

$$\left.\frac{\partial J^2}{\partial \Delta \varepsilon_{kl}}\right|_{I_{n+1},b_{n+1}} = \frac{2}{a_2 b_{n+1}^2}\left[I_{o_{n+1}}\left.\frac{\partial I_o}{\partial \Delta \varepsilon_{kl}}\right|_{I_{n+1},b_{n+1}}\right.$$
$$\left. -a_1\left(\bar{I}_{n+1}-\rho I_{o_{n+1}}\right)\left(\left.\frac{\partial \bar{I}}{\partial \Delta \varepsilon_{kl}}\right|_{I_{n+1},b_{n+1}} - \rho\left.\frac{\partial I_o}{\partial \Delta \varepsilon_{kl}}\right|_{I_{n+1},b_{n+1}}\right)\right] \tag{B.2-13}$$

$$\left.\frac{\partial \dot{J}^2}{\partial \Delta \varepsilon_{kl}}\right|_{I_{n+1},b_{n+1}} = \frac{2J_{n+1}^2}{\Delta t\, b_{n+1}}\left.\frac{\partial b_n}{\partial \Delta \varepsilon_{kl}}\right|_{I_{n+1},b_{n+1}} - \frac{2\dot{b}}{b_{n+1}}\left.\frac{\partial J^2}{\partial \Delta \varepsilon_{kl}}\right|_{I_{n+1},b_{n+1}}$$

$$+ \frac{2}{a_2 b_{n+1}^2}\left[\begin{array}{c} \dot{I}_{o_{n+1}}\left.\dfrac{\partial I_o}{\partial \Delta \varepsilon_{kl}}\right|_{I_{n+1},b_{n+1}} + I_{o_{n+1}}\left.\dfrac{\partial \dot{I}_o}{\partial \Delta \varepsilon_{kl}}\right|_{I_{n+1},b_{n+1}} \\[2ex] -a_1\left(\bar{I}_{n+1}-\rho I_{o_{n+1}}\right)\left(\left.\dfrac{\partial \dot{\bar{I}}}{\partial \Delta \varepsilon_{kl}}\right|_{I_{n+1},b_{n+1}} - \rho\left.\dfrac{\partial \dot{I}_o}{\partial \Delta \varepsilon_{kl}}\right|_{I_{n+1},b_{n+1}}\right) \\[2ex] -a_1\left(\dot{\bar{I}}_{n+1}-\rho \dot{I}_{o_{n+1}}\right)\left(\left.\dfrac{\partial \bar{I}}{\partial \Delta \varepsilon_{kl}}\right|_{I_{n+1},b_{n+1}} - \rho\left.\dfrac{\partial I_o}{\partial \Delta \varepsilon_{kl}}\right|_{I_{n+1},b_{n+1}}\right) \end{array}\right] \tag{B.2-14}$$

$$\left.\frac{\partial \chi_1}{\partial \Delta \varepsilon_{kl}}\right|_{I_{n+1},b_{n+1}} = \frac{\partial \chi_1}{\partial \Delta \varepsilon_{kl}} = e_{kl_{n+1}} \tag{B.2-15}$$

$$\left.\frac{\partial \chi_2}{\partial \Delta \varepsilon_{kl}}\right|_{I_{n+1},b_{n+1}} = \frac{\partial \chi_2}{\partial \Delta \varepsilon_{kl}} = s_{kl_n} + e_{kl_{n+1}}\left(\frac{\partial s_{ij}}{\partial \Delta \varepsilon_{kl}}\right)_n \tag{B.2-16}$$

The derivative of the deviatoric stress with respect to the increment in strain

$\left(\dfrac{\partial s_{ij}}{\partial \Delta \varepsilon_{kl}}\right)_n$ in Equation B.2-16 is evaluated at the beginning of the step or substep. If the

initial portion of the step was elastic, then this derivative is calculated using Equation 3.3-4.

If, on the other hand, the initial portion of the step was plastic, then the derivative comes from the previous plastic step. The deviatoric stress derivative at the end of the step is defined as:

$$\left(\frac{\partial s_{ij}}{\partial \Delta \varepsilon_{kl}}\right)_{n+1} = \frac{\left[\begin{array}{l} 2\,\Delta t \Delta e_{ij_{n+1}}\left(\frac{\partial G}{\partial I}\right)_{n+1}\left(\frac{\partial I}{\partial \Delta \varepsilon_{kl}}\right)_{n+1} + 2\,G_{n+1}\Delta t\left(\frac{\partial \Delta e_{ij}}{\partial \Delta \varepsilon_{kl}}\right)_{n+1} + \left(\frac{\partial s_{ij}}{\partial \Delta \varepsilon_{kl}}\right)_{n} \\[2em] -2\,\Delta t \frac{a_2}{a_1} s_{ij_{n+1}}\left(\begin{array}{l} \gamma_{n+1}b_{n+1}\left(\frac{\partial G}{\partial I}\right)_{n+1}\left(\frac{\partial I}{\partial \Delta \varepsilon_{kl}}\right)_{n+1} + G_{n+1}\gamma_{n+1}\left(\frac{\partial b}{\partial \Delta \varepsilon_{kl}}\right)_{n+1} \\[1.5em] +G_{n+1}b_{n+1}\left(\begin{array}{l}\left.\frac{\partial \gamma_{n+1}}{\partial \Delta \varepsilon_{kl}}\right|_{I_{n+1},b_{n+1}} + \left(\frac{\partial \gamma}{\partial I}\right)_{n+1}\left(\frac{\partial I}{\partial \Delta \varepsilon_{kl}}\right)_{n+1} \\[1.5em] +\left(\frac{\partial \gamma}{\partial b}\right)_{n+1}\left(\frac{\partial b}{\partial \Delta \varepsilon_{kl}}\right)_{n+1}\end{array}\right)\end{array}\right)\end{array}\right]}{1+2\,G_{n+1}\Delta t \frac{a_2}{a_1}\gamma_{n+1}b_{n+1}} \quad (B.2\text{-}17)$$

This derivative requires the derivatives $\left(\frac{\partial I}{\partial \Delta \varepsilon_{kl}}\right)_{n+1}$ and $\left(\frac{\partial b}{\partial \Delta \varepsilon_{kl}}\right)_{n+1}$, which are given by Equation B.2-3.

Appendix C. Strain Calculations for "Exact" Solutions

Appendix C.1 Volumetric Problems

In order to verify that the numerical implementation of the Bounding Surface models are calculating the correct results, several "exact" solutions were constructed. Exact is in quotes because in some cases (such as the volumetric tests) the exact solution can be found. In general, however, numerical integration is required. The "exact" solutions are constructed by starting with a stress point on the Bounding Surface, giving the surface and the stress point a known movement together and calculating the strains required to achieve the movement. Since the stress point starts on the surface, this solution could also be used to test a Cam-Clay model.

The "exact" solution is constructed by assuming a linear expansion with time (t) of the Bounding Surface size (I_o):

$$I_o(t) = I_{o_i} + t \tag{C.1-1}$$

where I_{o_i} = initial Bounding Surface size.

The derivative of this Bounding Surface expression with respect to time is:

$$\dot{I}_o = 1 \tag{C.1-2}$$

The previously defined rate equation for the Bounding Surface hardening [Kaliakin, 1985] is given as:

$$\dot{I}_o = \frac{3\,\upsilon_o}{\lambda - \kappa} \left(\langle I_o(t) - I_I \rangle + I_I \right) \gamma\; \frac{\partial F}{\partial \bar{I}} \tag{C.1-3}$$

where $\upsilon_o = 1 + e_o$ = initial specific volume

e_o = initial void ratio

λ = normal consolidation line

κ = elastic load-reload line

I_l = Limit stress for linear relationship

γ = plasticity parameter (loading index).

Consider the case when the value of I_0 is less than the transition stress (I_l). The Bounding Surface relationship reduces to:

$$\dot{I}_o = \frac{3\,\upsilon_o\,I_l}{\lambda-\kappa}\,\gamma\,\frac{\partial F}{\partial \bar{I}}$$

(C.1-4)

where $\quad \bar{I} = b(I - I_c) + I_c$

b = measure of distance between stress point and surface

$I_c = CI_o$

C = material constant defining the projection center location.

The single ellipse Bounding Surface function is defined [Kaliakin, 1985] as:

$$F = \bar{I}^2 + (R+1)^2 \left(\frac{\bar{J}}{N}\right)^2 - \frac{2}{R}\,I_o\,\bar{I} + \frac{2-R}{R}\,I_o^2$$

(C.1-5)

The intercepts of the Bounding Surface with the volumetric axis (I axis) are:

$$I = \left(\frac{2}{R}-1\right)I_o,\quad I_o$$

(C.1-6)

The derivative of the Bounding Surface function (Equation 1.4-1) with $\bar{I}$ is:

$$\frac{\partial F}{\partial \bar{I}} = 2\bar{I} - \frac{2}{R}\,I_o$$

(C.1-7)

Substituting Equation C.1-7 into Equation C.1-4 and recalling Equation C.1-2:

$$\dot{I}_o(t) = \frac{3\,\upsilon_o\,I_l}{\lambda - \kappa}\,\gamma\left(2\bar{I} - \frac{2}{R}\,I_o(t)\right) = 1 \tag{C.1-8}$$

Equation C.1-8 can now be solved for the plastic parameter (γ):

$$\gamma = \left(\frac{\lambda - \kappa}{3\,\upsilon_o\,I_l}\right)\frac{1}{2\bar{I} - \dfrac{2}{R}\,I_o(t)} \tag{C.1-9}$$

The rate equation for the plastic volumetric strain ($\dot{\theta}^p$) is given by the volumetric

form of Equation 1.2-2 [Kaliakin, 1985]:

$$\dot{\theta}^p = 3\,\gamma\,\frac{\partial F}{\partial \bar{I}} \tag{C.1-10}$$

Substituting in the expressions for the plastic parameter and derivative (Equations

C.1-7 and C.1-9) yields:

$$\dot{\theta}^p = \frac{\lambda - \kappa}{\upsilon_o\,I_l} \tag{C.1-11}$$

The plastic volumetric strain can be obtained by integrating the rate with respect to t:

$$\theta^p(t) = \frac{\lambda - \kappa}{\upsilon_o I_l}\,t + C \tag{C.1-12}$$

where C = constant of integration.

The constant of integration is evaluated by noting that $\theta^p = 0$ at $t = 0$, and therefore

$C = 0$. Thus the equation for the plastic volumetric strain is:

$$\theta^p(t) = \left(\frac{\lambda - \kappa}{\upsilon_o\,I_l}\right)t \tag{C.1-13}$$

The total volumetric strain consists of both the plastic and elastic strain. This relationship is given by the familiar decomposition of strains written in volumetric form:

$$\theta(t) = \theta^e(t) + \theta^p(t) \tag{C.1-14}$$

In order to determine the elastic volumetric strain, the stress history is required. For volumetric stresses (I) less than the transition stress (I_l), the bulk modulus (K) is constant:

$$K = \frac{v_o \, I_l}{3 \, \kappa} \tag{C.1-15}$$

The volumetric stress rate is defined as:

$$\dot{I}(t) = 3K \, \dot{\theta}^e(t) \tag{C.1-16}$$

Equation C.1-16 can be integrated for the elastic volumetric strain (θ^e). This is a straightforward integration since the bulk modulus is constant. The constant of integration is zero since $I = 0$ at $\theta^e = 0$. Substituting the elastic strain, the plastic volumetric strain (θ^p in Equation C.1-13) and the bulk modulus (K in Equation C.1-15) into Equation C.1-14, the total strain can be written as:

$$\theta(t) = \frac{\kappa \, I(t)}{v_o \, I_l} + \left(\frac{\lambda - \kappa}{v_o \, I_l} \right) t \tag{C.1-17}$$

Consider a volumetric tension test. The stress point originates on the volumetric axis intercept of the Bounding Surface on the tension side (for $R > 0$) and remains there throughout the test. $I(t)$ can be defined by the tension side intercept of the bounding surface (first term of Equation C.1-6). Substituting this into Equation C.1-17 results in the

volumetric strain as a function of the Bounding Surface size only:

$$\theta(t) = \frac{\kappa\left(\frac{2}{R}-1\right)}{v_o\,I_l}\left(I_{o_i}+t\right)+\left(\frac{\lambda-\kappa}{v_o\,I_l}\right)t \tag{C.1-18}$$

This equation for strain highlights a problem with the Bounding Surface rate relationship given in Equation C.1-3. When considering the case where the Bounding Surface collapses to zero (i.e., $I_o \rightarrow 0$), t cannot be less than $-I_{o_i}$. Therefore the total tensile volumetric strain in this limit cannot exceed:

$$\theta\left(-I_{o_i}\right) = -\left(\frac{\lambda-\kappa}{v_o\,I_l}\right)I_{o_i} \tag{C.1-19}$$

Tensile strains exceeding this value will cause the model to have numeric difficulties. In order to avoid this problem, one approach is to reconsider the Bounding Surface rate (Equation C.1-3). Since there was no experimental evidence cited for the transition from a log to linear rate form, the linear portion is dropped. The rate equation for I_o (previously defined in Equation C.1-3) is now defined:

$$\dot{I}_o = \frac{3\,v_o}{\lambda-\kappa}\,I_o(t)\,\gamma\,\frac{\partial F}{\partial \bar{I}} \tag{C.1-20}$$

Note that this form of the rate equation is valid on either side of the transition stress. The plastic parameter is now solved for:

$$\gamma = \left(\frac{\lambda-\kappa}{3\,v_o}\right)\frac{1}{2\bar{I}\,I_o(t)-\frac{2}{R}\,I_o^2(t)} \tag{C.1-21}$$

Substituting the plasticity parameter into the rate equation for the plastic volumetric

strain (θ^p) (Equation C.1-10) results in:

$$\dot{\theta}^p = \left(\frac{\lambda - \kappa}{\upsilon_o}\right)\frac{1}{I_o(t)}$$

(C.1-22)

Integrating to get the plastic volumetric strain gives:

$$\theta^p(t) = \left(\frac{\lambda - \kappa}{\upsilon_o}\right)\ln\left(I_o(t)\right) + C$$

(C.1-23)

The constant of integration is obtained, noting that $\theta^p = 0$ at $t = 0$:

$$C = -\left(\frac{\lambda - \kappa}{\upsilon_o}\right)\ln\left(I_o(t)\right)$$

(C.1-24)

The equation for the plastic volumetric strain as a function of time is:

$$\theta^p(t) = \left(\frac{\lambda - \kappa}{\upsilon_o}\right)\left(\ln\left(\frac{I_o(t)}{I_{o_i}}\right)\right)$$

(C.1-25)

Substituting this relationship into the equation for the total volumetric strain (Equation C.1-14) for tensile tests results in:

$$\theta(t) = \frac{\kappa}{\upsilon_o I_l}\left(\frac{2}{R} - 1\right)\left(I_{o_i} + t\right) + \frac{\lambda - \kappa}{\upsilon_o}\ln\left(\frac{I_{o_i} + t}{I_{o_i}}\right)$$

(C.1-26)

When considering the case where the Bounding Surface collapses to zero (i.e., $I_o \rightarrow 0$), $t = -I_{o_i}$. The total tensile volumetric strain is now given as:

$$\theta\left(-I_{o_i}\right) = -\infty$$

(C.1-27)

Now in order to collapse the Bounding Surface to zero, an infinite value of tensile volumetric strain is required. Although the precision of the machine will limit this strain, the formulation will avoid the numerical difficulties of the previous formula.

For volumetric stresses (I) greater than the transition stress (I_l), the bulk modulus(K) is now a function of the volumetric stress:

$$K = \frac{v_o\, I(t)}{3\,\kappa}$$

(C.1-28)

The integration of the elastic volumetric strain (Equation C.1-16) results in a slightly more complex expression:

$$\theta(t) \;=\; \frac{\kappa}{v_o}\; \ln\left(I(t)\right) + C$$

(C.1-29)

Solving for the constant of integration results in:

$$\theta(t) \;=\; \frac{\kappa}{v_o}\; \ln\left(\frac{I(t)}{I(0)}\right)$$

(C.1-30)

Consider a volumetric compression test. The volumetric stress (I) would originate on the compression side, intercept with the Bounding Surface and remain on the surface as the bound expands. Substituting for the volumetric stress (i.e., second term of Equation C.1-6), the total strain becomes a function of the Bounding Surface size:

$$\theta(t) \;=\; \frac{\lambda}{v_o}\; \ln\left(\frac{I_{o_i} + t}{I_{o_i}}\right)$$

(C.1-31)

The volumetric compression test in Section 4.2.1 used Equation C.1-30 to calculate the strains. The Bounding Surface parameters are given in Table C.1-1. The void ratio was given as $e_o = 0.94$. The problem definitions are given in Table C.1-2.

The volumetric tension test in Section 4.2.2 used Equation C.1-26 to calculate the strains. The Bounding Surface parameters and the void ratio are the same as the

compression test. The parameters defining the problem definitions for the tension tests are given in Table C.1-3.

Table C.1-1. Bounding Surface Model Parameters

Traditional Model Parameters	Surface Configuration Parameters
$\lambda = 0.14$ $\kappa = 0.05$ $M_c = 1.05$ $\nu = 0.2$	$R = 2.6$

Table C.1-2. Volumetric Compression Problem Definitions

	Bound Size, I_o	Volumetric Stress, I	Volumetric Strain, θ
Beginning	81	81	0
Final	91	91	-0.00840075

Table C.1-3. Volumetric Tension Problem Definitions

	Bound Size, I_o	Volumetric Stress, I	Volumetric Strain, θ
Beginning	0.9	0.207692	0
Final	0.5	0.115385	0.0274708

Appendix C.2 Shear Problem

A problem is designed to test the behavior of the model in shear. In order to make finding the exact solutions tractable, some simplifying assumptions are made:

1) the first invariant remains constant (i.e., $I_{n+1} = I_n$), and

2) the third invariant is zero ($S = 0$).

Similar to the volumetric cases, a linear variation in I_o is assumed:

$$I_o(t) = I_{o_i} + t \tag{C.2-1}$$

As derived in the previous section (Equation C.1-21), the plastic parameter (γ) is given as:

$$\gamma = \left(\frac{\lambda - \kappa}{3\, v_o} \right) \frac{1}{2\bar{I}\, I_o(t) - \dfrac{2}{R}\, I_o^2(t)} \tag{C.2-2}$$

The plastic volumetric strain (Equation C.1-25) is given:

$$\theta^p(t) \;=\; \left(\frac{\lambda - \kappa}{v_o} \right) \left(\ln \left(\frac{I_o(t)}{I_{o_i}} \right) \right) \tag{C.2-3}$$

Since the volumetric stress (I) is assumed to remain constant, the total volumetric strain can be expressed:

$$\theta(t) \;=\; \theta^p(t) \tag{C.2-4}$$

The second image stress invariant ($\bar{J}$) is obtained as a function of time by recalling the equation for the Bounding Surface (Equation C.1-5) and noting that $F = 0$:

$$\bar{J}(t) = \frac{N}{(R-1)} \sqrt{ -\bar{I}^2 + \frac{2}{R}\, I_o(t)\bar{I} - \frac{2-R}{R}\, I_o^2(t) } \tag{C.2-5}$$

The equation for N is defined as:

$$N = \frac{2N_e}{1 + \dfrac{N_e}{N_c} - \left(1 - \dfrac{N_e}{N_c}\right)\dfrac{3\sqrt{3}}{2}\left(\dfrac{S}{J}\right)^3}$$

(C.2-6)

Noting that the third invariant is assumed to be zero (i.e., $S = 0$), the equation for N becomes constant and can be written as:

$$N = \frac{2\, N_e}{1 + \dfrac{N_e}{N_c}}$$

(C.2-7)

For tests originating and remaining on the surface, the first and second invariants can be simplified to:

$$\bar{I} = I \qquad \bar{J} = J$$

(C.2-8)

In order to ensure that I = constant and $S = 0$, the following assumption on the deviatoric stresses is made:

$$s_{11} = s_{22} = s_{33} = s_{13} = s_{23} = 0, \qquad s_{12} \neq 0$$

(C.2-9)

The shear stress (σ_{12}) can be written as:

$$\sigma_{12}(t) = s_{12}(t) = J(t)$$

(C.2-10)

The rate equations for the plastic deviatoric strains are defined as:

$$\dot{e}^p_{ij} = \gamma\,\frac{\partial F}{\partial s_{ij}}$$

(C.2-11)

The derivatives of the Bounding Surface function (F in Equation C.1-5) with respect to the deviatoric stresses are given as:

$$\frac{\partial F}{\partial s_{ij}} = \frac{\partial F}{\partial J}\frac{\partial J}{\partial s_{ij}} + \frac{\partial F}{\partial \mu}\frac{\partial \mu}{\partial s_{ij}}$$

(C.2-12)

where $\mu = \sin(3\alpha)$.

Specific derivatives of the Bounding Surface function are given as:

$$\frac{\partial F}{\partial J} = 2\,(R-1)^2\,\frac{J}{N^2}$$

(C.2-13)

$$\frac{\partial F}{\partial \mu} = -2\,(R-1)^2\,\frac{J^2}{N^3}\frac{\partial N}{\partial \mu}$$

(C.2-14)

$$\frac{\partial N}{\partial \mu} = \frac{N^2\left(1-\dfrac{N_e}{N_c}\right)}{2N_e}$$

(C.2-15)

$$\frac{\partial F}{\partial \mu} = -\,(R-1)^2\,\frac{\left(1-\dfrac{N_e}{N_c}\right)}{N_e}\frac{J^2}{N}$$

(C.2-16)

The derivatives of the invariants with respect to the deviatoric stresses are:

$$\frac{\partial J}{\partial s_{11}} = \frac{\partial J}{\partial s_{22}} = \frac{\partial J}{\partial s_{33}} = \frac{\partial J}{\partial s_{13}} = \frac{\partial J}{\partial s_{23}} = 0$$

(C.2-17)

$$\frac{\partial J}{\partial s_{12}} = \frac{1}{2}$$

(C.2-18)

$$\frac{\partial \mu}{\partial s_{11}} = \frac{\partial \mu}{\partial s_{22}} = \frac{\sqrt{3}}{2J}$$

(C.2-19)

$$\frac{\partial \mu}{\partial s_{33}} = -\frac{\sqrt{3}}{J} \tag{C.2-20}$$

$$\frac{\partial \mu}{\partial s_{12}} = \frac{\partial \mu}{\partial s_{13}} = \frac{\partial \mu}{\partial s_{23}} = 0 \tag{C.2-21}$$

Upon combining these terms, the derivatives of the Bounding Surface function with respect to the deviatoric stresses are defined as:

$$\frac{\partial F}{\partial s_{11}} = \frac{\partial F}{\partial s_{22}} = -\frac{\sqrt{3}}{2} (R-1)^2 \frac{\left(1-\dfrac{N_e}{N_c}\right)}{N\,N_e} J(t) \tag{C.2-22}$$

$$\frac{\partial F}{\partial s_{33}} = \sqrt{3}\,(R-1)^2 \frac{\left(1-\dfrac{N_e}{N_c}\right)}{N\,N_e} J(t) \tag{C.2-23}$$

$$\frac{\partial F}{\partial s_{12}} = 2\,(R-1)^2 \frac{1}{N^2} J(t) \tag{C.2-24}$$

$$\frac{\partial F}{\partial s_{13}} = \frac{\partial F}{\partial s_{23}} = 0 \tag{C.2-25}$$

Substituting in the plastic parameter (Equation C.2-2), the second invariant (Equation C.2-5), and the derivatives (Equations C.2-22 through C.2-25) into the deviatoric strain rate (Equation C.2-11), the rates can be written as:

$$\dot{e}_{11}^p = \dot{e}_{22}^p = -\frac{\sqrt{3}}{12} (R-1)\left(\frac{\lambda-\kappa}{\upsilon_o}\right) \frac{\left(1-\dfrac{N_e}{N_c}\right)}{N_e} \frac{\sqrt{-I^2 + \dfrac{2}{R} I_o(t)I - \dfrac{2-R}{R} I_o^2(t)}}{I\,I_o(t) - \dfrac{1}{R} I_o^2(t)} \tag{C.2-26}$$

$$\dot{e}_{33}^p = -2\,\dot{e}_{11}^p \tag{C.2-27}$$

$$\dot{e}_{12}^p = \frac{1}{3}(R-1)\left(\frac{\lambda-\kappa}{v_o}\right)\frac{1}{N}\frac{\sqrt{-I^2 + \frac{2}{R}I_o(t)I - \frac{2-R}{R}I_o^2(t)}}{II_o(t) - \frac{1}{R}I_o^2(t)} \tag{C.2-28}$$

To obtain the plastic deviatoric strains, these rates must be integrated thus requiring numerical evaluation of the last term. With this approximation, the deviatoric plastic strains can be expressed as a function of time. The total deviatoric strains are obtained by recalling that:

$$s_{ij} = G\left(e_{ij} - e_{ij}^p\right) \tag{C.2-29}$$

The shear modulus (G) is a function of the bulk modulus (K) which, in turn, is a function of the first stress invariant (I). Assuming that I = constant, the shear modulus is also constant. From Equation C.2-9, the total deviatoric strains are obtained:

$$e_{11} = e_{11}^p \quad e_{22} = e_{22}^p \quad e_{33} = e_{33}^p \tag{C.2-30}$$

$$e_{12}(t) = \frac{s_{12}(t)}{G} + e_{12}^p(t) \tag{C.2-31}$$

Finally the total strain histories are calculated using Equation C.2-4:

$$\varepsilon_{ii}(t) = e_{ii}(t) + \frac{1}{3}\theta(t) \qquad \text{(no sum)} \tag{C.2-32}$$

$$\varepsilon_{ij}(t) = e_{ij}(t) \tag{C.2-33}$$

The Shear Test 1 in Section 4.2.3 used the Bounding Surface parameters given in Table C.1-1. The void ratio was given as $e_o = 0.94$ and the volumetric stress was set to $I = 81$ psi. The parameters defining the problem are given in Table C.2-1.

Shear Test 2 in Section 4.2.4 also uses the Bounding Surface parameters given in Table C.1-1. The void ratio was given as $e_o = 0.94$, the volumetric stress was set to

$I = 60$ psi and the initial shear stress was given as $\sigma_{12} = 3.63731$ psi. The parameter

definitions are given in Table C.2-2.

Table C.2-1. Shear Test 1 Definitions

	Bound Size, I_o	Volumetric Strain, θ	Shear Strain, ε_{12}
Beginning	81	0	0
Final	91	0.00540048	-0.0114129

Table C.2-2. Shear Test 2 Definitions

	Bound Size, I_o	Volumetric Strain, θ	Shear Strain, ε_{12}
Beginning	81	0	0
Final	91	0.00715132	-0.0177091